DISSERTATION

INTEGRATED STATISTICAL MODELS IN ECOLOGY

Submitted by

Justin Van Ee

Department of Statistics

In partial fulfillment of the requirements

For the Degree of Doctor of Philosophy

Colorado State University

Fort Collins, Colorado

Fall 2023

Doctoral Committee:

Advisor: Mevin Hooten
Co-Advisor: Matthew Koslovsky

Kayleigh Keller
Andee Kaplan
Larissa Bailey

ABSTRACT

INTEGRATED STATISTICAL MODELS IN ECOLOGY

The number of endangered and vulnerable species continues to grow globally as a result of habitat destruction, overharvesting, invasive species, and climate change. Understanding the drivers of population decline is pivotal for informing species conservation. Many datasets collected are restricted to a limited portion of the species range, may not include observations of other organisms in the community, or lack temporal breadth. When analyzed independently, these datasets often overlook drivers of population decline, muddle community responses to ecological threats, and poorly predict population trajectories. Over the last decade, thanks to efforts like The Long Term Ecological Research Network and National Ecological Observatory Network, citizen science surveys, and technological advances, ecological datasets that provide insights about collections of organisms or multiple characteristics of the same organism have become prevalent. The conglomerate of datasets has the potential to provide novel insights, improve predictive performance, and disentangle the contributions of confounded factors, but specifying joint models that assimilate all the available data sources is both intellectually daunting and computationally prohibitive.

I develop methodology for specifying computationally efficient integrated models. I discuss datasets frequently collected in ecology, objectives common to many analyses, and the methodological challenges associated with specifying joint models in these contexts. I introduce a suite of model building and computational techniques I used to facilitate inference in three applied analyses of ecological data. In a case study of the joint mammalian response to the bark beetle epidemic in Colorado, I describe a restricted regression approach to deconfounding the effects of environmental factors and community structure on species distributions. I highlight that fitting certain joint species distribution models in a restricted parameterization improves sampling efficiency. To improve abundance estimates for a federally protected species, I specify an integrated

model for analyzing independent aerial and ground surveys. I use a Markov melding approach to facilitate posterior inference and construct the joint distribution implied by the prior information, assumptions, and data expressed across a chain of submodels. I extend the integrated model by assimilating additional demographic surveys of the species that allow abundance estimates to be linked to annual variability in population vital rates. To reduce computation time, both models are fit using a multi-stage Markov chain Monte Carlo algorithm with parallelization. In each applied analysis, I uncover associations that would have been overlooked had the datasets been analyzed independently and improve predictive performance relative to models fit to individual datasets.

ACKNOWLEDGEMENTS

I thank my committee, Dr. Kayleigh Keller, Dr. Larissa Bailey, and Dr. Andee Kaplan for devoting your time to my professional development.

I thank my co-advisor Dr. Matthew Koslovsky for his collaboration and guidance. His enthusiasm for computational statistics inspired much of the work in my dissertation.

I thank my cohort, and especially Gray Stanton, for their insightful comments in class and their willingness to help me through the most challenging courses of my academic career.

I thank the Hooten Lab: Dr. Lucy Lu, Dr. Clint Leach, Dr. Ann Raiho, Abbey Feuka, Hanna McCaslin, Wilson Wright, and Michael Schwob. They have reviewed my manuscripts, critiqued my presentations, and helped me become a better Bayesian.

I thank Dr. Jacob Ivan, Dr. Christian Hagen, Dr. David Pavlacky, Kent Fricke, Liza Rossi, Russell Martin, Kurt Kuklinski, Grant Beauprez, Dr. Dave Haukos, Dr. Andy Lawrence, Dr. Ashley Tanner, and Dr. Blake Grisham, Jonathan Reitz, Troy Rintz, Dana Peterson, and Elisabeth Teige. The zeal of my collaborators for wildlife conservation is unmatched, and I am proud of the work we accomplished together.

I thank my parents, Verlan and Rebecca, for treating the outdoors like a subject as core to education as mathematics, reading, and writing, but also valuing the traditional subjects so that completing a dissertation in statistics someday was possible. I thank my four older siblings Noelle, Nathan, Nicholas, and Noah who inspired my love for the natural world and encouraged me to pursue an advanced degree in statistics. I thank my patient and loving wife Rachel who has faithfully supported me.

I thank my advisor, Dr. Mevin Hooten. You have fostered my passion for statistics and ecology and given me the tools to tackle any research question. Thank you for supporting me throughout my studies and seeking collaboration opportunities catered to my career goals.

DEDICATION

All glory be to the Creator, may I be a good steward of His great earth.

TABLE OF CONTENTS

LIST OF TABLES

LIST OF FIGURES

Chapter 1

Introduction

Human population growth coupled with technological advancement since the mid-20th century have elevated human impact on the earth to unprecedented levels [7]. Some argue for a new geological epoch called the Anthropocene in which human activity is a primary driver of the earth's ecosystems and climate [8]. The Anthropocene may also mark Earth's biota entering a sixth "mass extinction" where extinction rates are estimated at 100 times greater than their historical and prehistoric averages [9]. Biodiversity underpins ecosystem services such as flood control, pollination, soil enrichment, disease control, and air and water purification [10], and the loss of biodiversity may reduce the productivity of these services with detrimental impacts to human well being [11]. With species declining and disappearing at accelerated rates [12], the need to document and understand drivers of biodiversity loss are greater than ever before.

Documenting the decline of biodiversity is challenging because many species experienced the most precipitous declines prior to human monitoring. Population trajectories inferred from recently collected data often show stability or even improvement [13], but can overlook long-term declines that preceded data collection [14]. Declines may also be spatially heterogeneous, and spatially restricted monitoring programs can wrongly conclude population stability while a subpopulation heads to extirpation [15]. When subpopulations are genetically distinct, extirpation of a subpopulation reduces diversity and the species capacity to adapt to environmental changes thereby increasing susceptibility to extinction [16]. Lastly, species are interdependent [17], and accessing the health of species in isolation has the potential to overlook disruption of vital symbioses [18].

Determining the factors influencing biodiversity loss face similar hurdles. A short-term study may fail to identify a driver of decline if the driver is constant over the period of observation or if interannual fluctuations in population size swamp the signal of a weak yet persistent long-term effect [14, 19]. Likewise, species phenology and morphology can vary spatially, and observed resiliency to an ecological threat in one region may not accurately represent susceptibility in the

larger population [20, 16]. Species responses to environmental stimuli are also mediated by their community, which implies species-environment association should be examined in conjunction with the species community [21, 22]. It follows that documenting and understanding declines of biodiversity relies on spatially broad surveys of multiple species over long periods of observation [23]. Rarely can such data be procured from one source.

Ecological data collection has proliferated over the last two decades [24]. Multi-agency monitoring efforts like Long Term Ecological Research Network and National Ecological Observatory Network are increasingly common where thousands of scientists coordinate comprehensive surveys over long time periods [25]. Data collection has been facilitated by technological advancements such as data loggers, camera traps, telemetry, and environmental DNA [26, 27]. Publicly collected data sources have also expanded with an increase in citizen science surveys [28].

When analyzed independently, the eclectic datasets can be insufficient for understanding population dynamics and informing conservation practices [29, 30]. Integrated models assimilate multiple datasets in a cohesive framework and have been applied in econometrics, biostatistics, meteorology, and oceanography [31, 32, 33, 34, 35]. In an integrated model, multiple datasets are conditioned on common latent parameters. By simultaneously analyzing all the available data sources, integrated models can compensate for deficiencies in the individual datasets [36, 37] and have been shown to increase parameter precision, improve predictive performance, and provide novel insights into population dynamics [38].

Integrated models pose one of the most promising avenues for capitalizing on the wealth of data collected in the past few decades. Developing integrated models is challenging, and Zipkin et al. [36] highlighted four commonly encountered difficulties in ecology:

1. Resolving mismatches in spatial and temporal scales of available data sources.

2. Addressing unbalanced data: uneven quantities and information content.

3. Accounting for sampling biases in one or more data source(s).

4. Optimizing model development and assessment when incorporating multiple data sources.

In this dissertation, I discuss methods for addressing the methodological challenges discussed in (1)-(3), and briefly comment on future work for addressing (4). I also address the computational burden of fitting integrated models [39, 40], and describe a suite of methods I use for decreasing runtimes.

I develop methodology for integrated models in the context of Bayesian hierarchical modeling. Hierarchical models decompose complex problems into tractable components that can collectively account for uncertainty in the data, underlying processing, and parameters [41]. The ability to explicitly model the mechanistic processes which generated the observed data is one of the main features that popularized hierarchical models among ecologists [42], and the prevalence of Bayesian methods in ecology today is epitomized by the number of books published on the subject [43, 44, 45, 46, 47, 48, 49, 50, 42]. The Bayesian approach also admits mechanisms for incorporating previous scientific findings into the model [51], which can be especially useful in ecology where observations of certain phenomenon are limited and additional prior information is needed for facilitating inference [52]. The hierarchical framework partitions the variability in the process under study from the error resulting from imperfect observations of the process [53]. Most pertinent to my work, Bayesian methodology accommodates a joint analysis of multiple datasets.

Across three analyses of multi-source ecological data, I specify Bayesian hierarchical models (BHMs) for inferring trends in population dynamics while accounting for errors in the observational process. In Chapter 2, I specify a multispecies occupancy model for learning about the joint mammalian response to the bark beetle epidemic in Colorado. Fueled by favorable climatic conditions, bark beetle outbreaks have increased in range and severity in the subalpine forest of Colorado's Rocky Mountains in recent decades [2]. The loss of billions of trees situated on hundreds of millions of acres is unmatched in recorded history [54] and understanding how species are responding to this ecological catastrophe is vital to informing conservation. Ivan et al. [2] fit independent models to assess the response of 13 mammals to regions impacted by bark beetle infestation. I discuss how an independent analysis of each species has the potential to misidentify species-environment associations and propose a model for understanding joint patterns in species

distributions. I introduce the notion of community confounding where environmental factors and species interdependence compete to explain patterns in species distributions and discuss its implications for model fitting and inference.

I develop two integrated models for facilitating joint inference from multiple surveys of lesser prairie-chicken (*Tympanuchus pallidicinctus*; hereafter LEPC) in Chapters 3 and 4. The LEPC is a federally endangered species [55] threatened by habitat destruction, degradation and climate change [56, 57, 58, 59]. LEPC inhabitat four ecoregions across their range [60], and genetic evidence suggests the populations inhabiting each ecoregion are genetically distinct [20]. In some ecoregions, populations have been decimated [57, 61, 58], while in others, populations are growing and home ranges expanding [62]. Another challenge is that LEPC populations have large interannual fluctuations in abundance that make identifying trends difficult [6, 63]. Effective conservation strategies rely on understanding ecoregional heterogeneity in LEPC demography [15, 16], and quantifying species vulnerability depends on accurate assessment of long term trends [60].

I develop an integrated model for assimilating observations from independent aerial and ground surveys into a common model that provides joint inference on spatio-temporal trends in LEPC abundance. Using recently proposed chained Markov melding [64], I show how to construct the joint distribution of all inferential quantities implied by the specifications made across a chain of submodels. The approach preserves the observational uncertainty of each survey and assimilates surveys of varying spatial and temporal scales with possible sampling biases into a common framework. By specifying an integrated model for both data sources, the abundance of LEPC in unsampled regions and in years preceding aerial surveys could be inferred. I extend the previous framework by linking the aerial and ground surveys to additional demographic surveys of LEPC in population model for describing fluctuations in abundance driven by ecoregional and temporal variability in survival and productivity. I highlight discrepancies in LEPC demography that would have been overlooked had I not assimilated all the available data sources.

The remainder of Chapter 1 is split into three sections. In Section 1, I discuss including mechanistic processes in BHMs, a common approach for Bayesian analysis of ecology data and feature of

the BHMs presented in Chapters 2-4. Section 2 gives a brief history of the rise of integrated models in ecology and describes adaptations relevant to my work. I conclude with a suite of computational aides used to facilitate model fitting in Section 3.

1.1 Modeling Mechanistic Processes

Hierarchical models can be specified to reflect mechanisms in the system under study [65, 42]. Bayesian models are lauded for their ability to incorporate preexisting sources of information. If the mechanisms of a social, economic, ecological, or physical system are well studied, it would be remiss to ignore all the previous literature when designing a model [66, 67, 68]. Mechanisms may also pertain to the sampling process, and the Bayesian framework accommodates the unique observational errors arising from different survey methods. Mechanistic models incorporate prior information into model design and are distinct from phenomenological models that infer the association among variables based solely on the fit to observed data (i.e., linear regression [69]).

Phenomenological models often suffer from confounding where multiple effects compete to explain the same signal [70]. Because phenomenological models are naive to the system under study, they can produce posterior inference that is scientifically untenable or counter-intuitive. By prespecifying the known mechanisms in the system, it is often easier to discover novel mechanisms [71, 72]. Furthermore, restricting or penalizing a model to adhere to certain mechanisms can also improve prediction, reduce variance, and stabilize computation [73]. Mechanistic modeling facilitated my dissertation work and has been more broadly useful in hierarchical modeling of ecological datasets. I, first, introduce differential equation models, which have become a common approach for incorporating mechanisms into BHMs. Next, I provide examples from my dissertation work where taking a mechanistic approach was inferentially or computationally fruitful.

1.1.1 Differential Equation Models

Classic mathematical models in ecology such as Lotka–Volterra, Malthusian growth, logistical growth, ecological diffusion are rooted in differential equations, but only in the past decade have

statistical models that account for uncertainty in differential equation parameters been proposed in ecology [42, 65]. Statistical models that incorporate differential equations can better mimic the system while still accounting for and propagating uncertainty. For example, the Malthusian growth model describes the increase of a population over time when it is not influenced by carrying capacity or density dependent interactions. The model depends on the population growth rate and initial population size both of which are generally unknown and must be estimated with the available data. Accounting for the uncertainty of these parameters in the differential equation model properly propagates the uncertainty into the inferred population trajectories.

Differential equation models have been particularly useful for systems with well-structured dependence across space and time. For example, Hooten and Wikle [74] used a reaction-diffusion partial differential equation (PDE) to model the invasion of Eurasian Collared-Dove *Streptopelia decaocto* in the United States from 1986-2003. Williams et al. [75] and Lu et al. [76] used Reaction-diffusion PDEs to model the recolonization of Glacier Bay, Alaska by sea otters. Characterizing these systems with a phenomenological model would require a massive number of parameters to capture complex spatio-temporal interactions. By specifying the structure of those interactions with a PDE, Williams et al. [75] and Lu et al. [76] reduced the number of estimated parameters improving computation and prediction.

Mechanistic BHMs also facilitate posterior inference. By mimicking the data generating process, mechanistic models can provide inference for quantities that the observed data may not directly speak too. For example, Wilson et al. [77] specified a mechanistic spatial model for understanding heavy metal pollution. By including an advection-diffusion (PDE) for atmospheric dispersion in their BHM, Wilson et al. were able to learn about temporal dynamics in mental pollution, despite the fact that the data analyzed were only collected at one time point.

1.1.2 Royle-Nichols Occupancy Model

Mechanisms can also be incorporated in the sampling process. The Royle-Nichols occupancy model [78] includes mechanisms governing species occupancy to improve inference. At first

glance, it may sound dubious to learn about spatial heterogeneity in abundance from vectors of binary data, but this is exactly what the Royle-Nichols occupancy model achieves. I introduce the site-structured binary data commonly collected in ecology studies and present the standard models used for drawing inference before describing the Royle-Nichols model.

In Chapter 2, I specify a joint species distribution model (JSDM) [21], for mammals in the subalpine forest of Colorado. The data consists of binary vectors $\boldsymbol{y}_{ik}$ of length J_i, where $i = 1, \ldots, n$ and $k = 1, \ldots, K$ index sites and species, respectively. For simplicity, I will consider a single species, (i.e., $K = 1$). Each datum, y_{ij}, corresponds to whether the species was detected at site i during occasion $j = 1, \ldots, J_i$. A popular model for analyzing such data is as follows:

$$y_{ij} \sim \begin{cases} \text{Bern}(p_{ij}), & z_i = 1 \\ 0, & z_i = 0 \end{cases}, \tag{1.1}$$

$$z_i \sim \text{Bern}(\psi_i), \tag{1.2}$$

$$h(p_{ij}) = \boldsymbol{w}_{ij}'\boldsymbol{\alpha}, \tag{1.3}$$

$$g(\psi_i) = \boldsymbol{x}_i'\boldsymbol{\beta}, \tag{1.4}$$

$$\boldsymbol{\alpha} \sim \mathcal{N}(\boldsymbol{\mu}_{\boldsymbol{\alpha}}, \boldsymbol{\Sigma}_{\boldsymbol{\alpha}}), \tag{1.5}$$

$$\boldsymbol{\beta} \sim \mathcal{N}(\boldsymbol{\mu}_{\boldsymbol{\beta}}, \boldsymbol{\Sigma}_{\boldsymbol{\beta}}). \tag{1.6}$$

Hoeting et al. [79] and Mackenzie et al. [80] called equations (1.1)-(1.6) an occupancy model because it partitions the observed 0s across an occupancy, equation (1.2), and detection, equation (1.1), process. A surveyor may record a 0 (i.e., non-detection) at a site because either the species does not the occupy the site or the species occupies the site but the surveyor failed to detect it.

The function $g(\cdot)$ relates $\boldsymbol{x}_i$, a p-dimensional vector of observed covariates for the ith observation including an intercept term, to the species latent probability of occupancy ψ_i and is often referred to as a link function. Link functions transform the linear predictor to match the support of the parameter. In the case of occupancy probability, the link function $g(\cdot)$ ensures that the transformed linear predictor is bounded between 0 and 1, the support of ψ_i. Likewise, $h(\cdot)$ relates

site and occasion specific covariates $\boldsymbol{w}_{ij}$ to the probability of detecting the species on occasion j conditional on the species occupying site i.

Any function that maps the real number line to $(0, 1)$ is suitable for $h(\cdot)$ and $g(\cdot)$, but in the occupancy literature there is precedent for using the Probit link function [81, 82, 83]. Albert and Chib [84] introduced a data augmentation scheme that simplifies fitting the occupancy model, equations (1.1)-(1.6), using Probit link functions. Ease of implementation has popularized the Probit link in the occupancy modeling literature [85, 86, 87, 88, 89, 90] but other computationally efficient methods for fitting similar models exist [91, 92] (Section 1.3.3).

Royle and Nichols [78] considered an occupancy model that accounted for heterogeneity in detection induced by variation in abundance. For a survey of site i on occasion j, the probability of detecting any particular individual in the group of N_i individuals at site i is r_{ij}. Assuming individuals are detected independently of one another, the probability of detecting at least one of these individuals is

$$p_{ij} = 1 - (1 - r_{ij})^{N_i}. \tag{1.7}$$

Equation (1.7) reflects that the species is more likely to be detected at sites where it is more prevalent, (i.e., N_i larger implies larger p_{ij}). Royle and Nichols [78] recommended a Poisson model for N_i with the linear predictor latent mean $\log(\lambda_i) = \boldsymbol{x}_i'\boldsymbol{\beta}$.

By mimicking the mechanism of the sampling process (1.7), Royle and Nichols [78] could measure the association between site level covariates $\boldsymbol{x}_i$ and the species latent mean abundance λ_i. The traditional occupancy model, equations (1.1)-(1.6), provides inference on the association between $\boldsymbol{x}_i$ and the species latent probability of occupancy ψ_i. Species abundance and occupancy may be governed by different mechanisms, and inference from an intensity model can be distinct from that provided by an occupancy model [93, 94, 95]. In Chapter 2, I discuss the inferential implications of the two specifications when fitting occupancy data.

1.1.3 Mixture Models

A mixture model represents a probability distribution as a weighted sum of K other probability distributions,

$$[\theta] = \sum_{k=1}^{K} w_k [\theta]_k, \tag{1.8}$$

where $\sum_{k=1}^{K} w_k = 1$, and I use the bracket notation $[\theta]_k$ to represent the probability distribution of θ_k [96]. If each component distribution $[\theta]_k$ is specified to be normal, then equation (1.8) is a Gaussian mixture model which has diverse applications in cluster analysis, anomaly detection, and data augmentation [97, 98, 99]. Specification of mixture models is often motivated by the context. Consider, for example, a model for adult heights. A Gaussian mixture can account for bimodality in the observed heights induced by biological sex. Mixture models have also been used to model highly complex distributions that do not follow any common parametric form (e.g., infinite mixture models in a Dirichlet process [100, 101]).

In Chapter 3, I consider a mixture model for counts of LEPCs that was both biologically motivated and accommodated bimodality in the distribution of the counts. The data are counts of LEPC groups during the breeding season, during which, male LEPCs congregate into groups of 4-100 individuals called leks to collectively attract females. Females will temporarily visit leks but forage and travel in smaller groups. Occasionally, leks of less than 4 individuals are observed as well as groups of multiple females. These observations blur the distinctions between lek and non-lek observations and make it difficult to decipher whether a lek or non-lek is being observed.

I specified a mixture model for LEPC counts N_l with latent labels ω_l:

$$N_l \sim \begin{cases} \text{ZTP}(\lambda_1), & \omega_l = 1 \\ \text{ZTP}(\lambda_0), & \omega_l = 0 \end{cases}, \tag{1.9}$$

$$\omega_l \sim \text{Bern}(p), \tag{1.10}$$

where l indexes LEPC groups, ZTP is an abbreviation for zero-truncated Poisson, and I have omitted priors for λ_1, λ_0, and p for simplicity. Note that N_l is necessarily zero-truncated because if a group exists it must contain at least one individual. I also evaluated a simpler model by specifying $N_l \sim \text{ZTP}(\lambda)$ but found that the unimodel distribution was unable to characterize variability in the observed counts and resulted in poor model fit. To account for the overdispersed counts, I also considered a zero-truncated negative binomial model for N_l with overdispersion parameter θ. I had difficulty implementing the negative binomial model because of convergence issues with the overdispersion parameter θ. I did not have any issues with convergence fitting the ZTP mixture model, equations (1.9)-(1.10). As I discussed with differential equation models, a mechanistically motivated modeling approach can also improve computation.

1.2 Integrated Models

The Bayesian framework can assimilate multiple data sources into one cohesive model. I define integrated models as models that condition at least 2 datasets on common parameters, but the framework has also been described as integrated analysis [31], integrated distribution models [102], shared parameter models [32], joint models [33], Markov combination [103], Bayesian melding [104], data assimilation [34], data reconciliation [105], and data fusion [35]. The Bayesian framework allows the total error in a model to be split across uncertainties in the data, process, and parameters [41]. In many analyses, a single data source may be incapable of disentangling process from observation error in the model specified [36]. By assimilating multiple data sources, the uncertainty from each component of the model can be estimated with more precision [38].

The earliest applications of integrated modeling frameworks in the context of wildlife management arose in fisheries science [106]. Fournier and Archibald [106] described a general model for catch at age data in fisheries. A difficulty with analyzing these data is that variability in the number of fish caught annually is both influenced by demographic processes as well as fishing effort. Traditional approaches for analyzing the observed counts muddled effort with demography and poorly predicted the size of the fishery (i.e., stock assessment). Fournier and Archibald showed how to

include data on fishing effort and the age of fish at harvest in a common model to improve stock assessments. Integrated modeling frameworks have been adapted for other fields, and I describe adaptations pertinent to my research.

1.2.1 Joint Species Distribution Models

Ecologists study how organisms interact with each other and their physical surroundings. Species distributions are shaped by both environmental factors and their interactions with other species [17]. Pulliam [107] proposed that the distribution of species is governed by three forces: abiotic tolerance, dispersal, and biotic interactions. Abiotic tolerance refers to the set of environmental conditionals across which a species can exist and is called the fundamental niche [17]. Species rarely occupy their entire fundamental niche because of geographic isolation or biotic interactions. A species may not have dispersed to an environmentally habitable region or were out-competed by other organisms in a subregion of their fundamental niche. The region a species occupies is referred to as the realized niche [17]. Figure 1.1 illustrates this process for two competiting species A and B. Based on physiological tolerances, species A and B have fundamental niches across an environmental gradient that partially overlap. Assuming dispersal across the gradient for both species, only the niche of species A is fully realized as it outcompetes species B [17]. Biotic interactions can truncate a species realized niche to a subset of the fundamental niche but mutualistic relationships can also expand species ranges relative to their fundamental niches. For example, mutualistic relationships between algae, cyanobacteria, and fungi, known as lichen, allow the species to survive in environments that they could not inhabit individually.

Because of limitations in data collection and computational power, statistical models have lagged theory in the modeling of species distributions. Understanding the abiotic factors which govern species distributions is a long standing objective of ecological research [108], and applications of species distribution modeling can be found as early as the 1920s [109]. Modern statistical models for individual species distributions came in the 1970s [110] but only in the last decade, have methods been proposed for the joint prediction and analysis of species distributions [22].

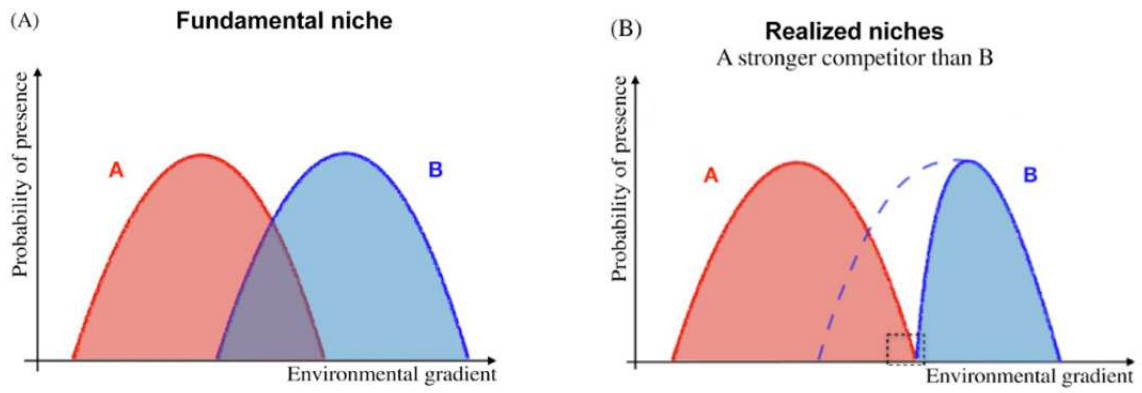

Figure 1.1: Illustration of fundamental versus realized niche for a simple community of two competing species across an environmental gradient.

JSDMs account for co-occurrence patterns in species distributions beyond what is explained by shared environmental preferences [17]. Multiple frameworks have been proposed to account for interdependence in species distributions [111, 89, 112], but most commonly a covariance matrix is specified to explain additional structure in the residuals [22, 21]:

$$g(\boldsymbol{z}_i) = \boldsymbol{x}_i'\boldsymbol{\beta} + \boldsymbol{\epsilon}_i, \tag{1.11}$$

$$\boldsymbol{\epsilon}_i \sim \mathcal{N}(\mathbf{0}, \boldsymbol{\Sigma}), \tag{1.12}$$

where $\boldsymbol{z}_i$ is a measure of prevalence (occupancy, density, abundance, etc.) for the K species in the community at site i, $\boldsymbol{x}_i$ is a P-dimensional vector of environmental covariates including an intercept, and $\boldsymbol{\Sigma}$ is a $K \times K$ species covariance matrix. Generally, the true state of ecological interest $\boldsymbol{z}_i$ is unobservable, and JSDMs may include another hierarchy to account for the observed data collected at site i conditional on the true state $\boldsymbol{z}_i$. The off-diagonals of the species covariance matrix, $\boldsymbol{\Sigma}$, provide inference for patterns in co-occurrence. JSDMs exploit patterns in co-occurrence to improve prediction [113]. In Chapter 2, I develop a JSDM for describing the joint mammalian response to the bark beetle epidemic. I also describe confounding in JSDMs and its consequences for inference and modeling fitting.

1.2.2 Integrated Population Models

Besbeas et al. [114] introduced integrated population models (IPMs) for assimilating population counts with demographic surveys to provide inference on population dynamics. IPMs are popular in ecology [115] and especially for avian conservation [38]. A typical IPM assimilates annual indices of population abundance, capture-recapture or telemetry data for learning about survival, and productivity data to infer the number of new individuals born each year. A directed acyclic graph (DAG) of an IPM is shown in Figure 1.2. In the IPM, survival, ϕ, and productivity, ρ, rates (possibly age and sex specific) are linked to an index of population abundance N. Information about the vital rates ϕ and ρ are primarily in the datasets $\boldsymbol{R}$, $\boldsymbol{J}$, and $\boldsymbol{m}$, but counts of the population size, $\boldsymbol{y}$, also facilitate inference.

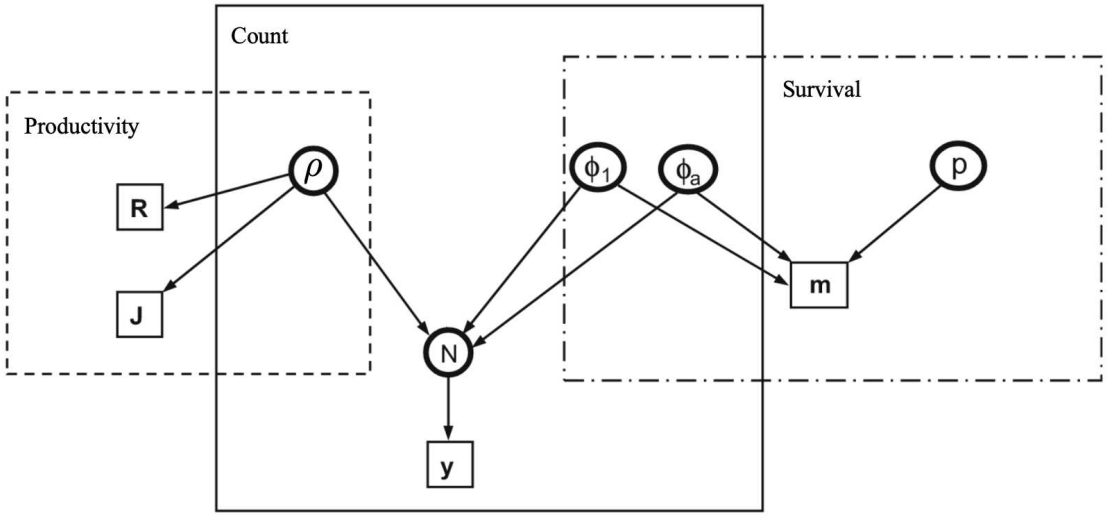

Figure 1.2: Directed acyclic graph of example integrated population model.

IPMs generally follow a state-space framework in which the latent demographic rates and abundances are informed by observations indexed in time [38]. For each data source, a distribution is assumed that relates the latent quantity of interest to the data collected. All latent quantities are then joined in one cohesive model for demography. One populatar choice is the Leslie matrix

model [116],

$$\begin{bmatrix} N_1 \\ \vdots \\ N_A \end{bmatrix}_{t+1} = \begin{bmatrix} \rho_1 & \cdots & \cdots & \cdots & \rho_A \\ \phi_1 & 0 & \cdots & \cdots & 0 \\ 0 & \phi_2 & 0 & \cdots & 0 \\ \vdots & \vdots & \vdots & \vdots & \vdots \\ 0 & \cdots & 0 & \phi_{A-1} & \phi_A \end{bmatrix}_t \begin{bmatrix} N_1 \\ \vdots \\ N_A \end{bmatrix}_t , \tag{1.13}$$

where $\boldsymbol{N}_t = (N_{1t}, \ldots, N_{At})'$ is the vector of female abundances in age classes $a \in \{1, \ldots, A\}$ in year t and ρ_{at} and ϕ_{at} are the age specific productivity and survival in year t. The Leslie matrix model is deterministic, and the predicted number of individuals in age class N_A in year $t + 1$, for example, is $N_A\phi_A + N_{A-1}\phi_{A-1}$. In practice, a distributional assumption is made for each row of the matrix to account for demographic stochasticity.

IPMs have been widely applied in conservation biology [63, 37, 117, 118, 119] because they link changes in population size to annual fluctuations in productivity and survival and can decipher which vital rate is more correlated with population growth [120, 121]. Wildlife managers use the inference provided by IPMs to develop strategies that explicitly target boosting survival or productivity. A phenomenological model can estimate the association between the observed counts $\boldsymbol{y}$ and a set of covariates but cannot identify whether the association is related to changes in productivity or survival. This is problematic in cases where an environmental factor has conflicting effects on productivity and survival. Inference from a phenomenological model may suggest the environmental factor has no influence on population growth even though it profoundly shapes demography. In Chapter 4, I specify an IPM for LEPC.

1.2.3 Markov Melding

The previous two sections included examples of modeling frameworks for assimilating multiple data sources. In this section, I describe a general technique for deriving joint inference from a set of submodels linked by common quantities. The need to infer the posterior distribution im-

plied by several separate analyses can arise in many contexts [122]. For example, suppose several laboratories are conducting experiments on the same phenomenon but use different equipment or suppose several researchers are studying unique sub-components of a larger object (i.e., genes on a chromosome, subplots in a field, species in a community, etc.). Goudie et al. [123] introduced Markov melding as a generic approaching for deriving the joint posterior distribution of all quantities expressed across a collection of analyses.

Markov melding is an extension of Markov combination [103], a formula for calculating the joint distribution implied by joining two or more other submodels. Dawid and Lauritzen [103] proved Markov combination in a more general context, but I will define it in the context of BHMs. Suppose there are M submodels with parameters $\psi_1, \ldots, \psi_M$ and data $Y_1, \ldots, Y_M$ and all models share the common quantity θ. If the marginal distribution of θ is consistent across all submodels, that is $[\theta] = [\theta]_1 = \cdots = [\theta]_M$, the Markov combination of all submodels is

$$[\theta, \boldsymbol{\psi}, \boldsymbol{Y}]_{\text{comb}} = [\theta] \prod_{m=1}^{M} [\psi_m, Y_m | \theta], \tag{1.14}$$

where $\boldsymbol{\psi} = (\psi_1, \ldots, \psi_M)'$, $\boldsymbol{Y} = (Y_1, \ldots, Y_M)'$, and Dawid and Lauritzen assumed the m submodels are independent conditional on θ.

Goudie et al. [123] relaxed the assumption of marginal consistency to introduce Markov melding. The method involves replacing the marginal distribution of θ in each submodel with a common marginal denoted by $[\theta]_{\text{pool}}$. Instituting a common marginal of $[\theta]_{\text{pool}}$ across all submodels, the joint melded distribution is formed as

$$[\theta, \boldsymbol{\psi}, \boldsymbol{Y}]_{\text{meld}} = [\theta]_{\text{pool}} \prod_{m=1}^{M} [\psi_m, Y_m | \theta]_m \tag{1.15}$$

$$= [\theta]_{\text{pool}} \prod_{m=1}^{M} \frac{[\psi_m, Y_m, \theta]_m}{[\theta]_m}, \tag{1.16}$$

where $[\psi_m, Y_m, \theta]_m$ and $[\theta]_m$ denote the joint and marginal distributions of θ in submodel m, respectively. Unlike Markov combination, which forms the exact joint distribution of all parameters,

Markov melding introduces a novel joint distribution by constraining each submodel to admit the same marginal for θ. Goudie et al. [123] proved that the modified submodel joint distributions, $[\psi_m, Y_m|\theta]_m[\theta]_{\text{pool}}$, minimize the Kullback-Leibler divergence between their original submodel joint distributions $[\psi_m, Y_m|\theta]_m[\theta]_m$ under that constraint that $[\theta]_m = [\theta]_{\text{pool}}$ for $m = 1, \ldots, M$. Thus, $[\psi_m, Y_m|\theta]_m[\theta]_{\text{pool}}$ is interpreted as the minimally modified submodel joint distribution that admits $[\theta]_{\text{pool}}$ as its marginal distribution for θ. Goudie et al. [123] proposed a number of options for forming the pooled prior $[\theta]_{\text{pool}}$ such that it summarizes the prior information expressed across all M submodels.

Manderson and Goudie [64] extended Markov melding to scenarios where a chain of submodels is linked by multiple parameters. Let $\theta_{m-1\cap m}$ denote a parameter common to the $m-1$ and mth submodels. Manderson and Goudie [64] introduced a chained melded joint distribution for the vector of $M-1$ quantities $\boldsymbol{\theta} = (\theta_{1\cap 2}, \theta_{2\cap 3}, \ldots, \theta_{M-1\cap M})'$, data $\boldsymbol{Y}$, and submodel parameters $\boldsymbol{\psi}$,

$$[\boldsymbol{\theta}, \boldsymbol{\psi}, \boldsymbol{Y}]_{\text{meld}} = [\boldsymbol{\theta}]_{\text{pool}} \frac{[\theta_{1\cap 2}, \psi_1, Y_1]_1}{[\theta_{1\cap 2}]_1} \frac{[\theta_{M-1\cap M}, \psi_M, Y_M]_M}{[\theta_{M-1\cap M}]_M} \tag{1.17}$$

$$\times \prod_{m=2}^{M-1} \left(\frac{[\theta_{m-1\cap m}, \theta_{m\cap m+1}, \psi_m, Y_m]_m}{[\theta_{m-1\cap m}, \theta_{m\cap m+1}]_m} \right). \tag{1.18}$$

Observe, equation (1.18), implies there may be prior dependence between the parameters $\theta_{m-1\cap m}$ and $\theta_{m\cap m+1}$. The chained melded joint distribution captures prior dependence between common quantities within a submodel and reconciles differences in priors for the same common quantity between two adjacent submodels [64]. Obtaining samples from $[\boldsymbol{\theta}, \boldsymbol{\psi}, \boldsymbol{Y}]_{\text{meld}}$ is non-trivial and relies on a multistage Markov Chain monte Carlo (MCMC) algorithm (see Section 1.3.5).

The IPM introduced in Section 1.2.2 falls under the chained Markov melding framework [64]. Although the model can be fit using conventional Bayesian methodology, the IPM can also be split into three submodels for the productivity, count, and survival data as illustrated by the boxes in Figure 1.2. Benefits of this approach include more flexibility in the prior specification for ϕ_1, ϕ_A, and ρ and decreased runtime through fitting a subset of the submodels in parallel (Section 1.3.5).

In other contexts, chained Markov melding can facilitate joint inference from a sequence of submodels for which specification of unified integrated model is non-obvious. For example, suppose the population counts, $\boldsymbol{y}$, in Figure 1.2 are not observed but can be inferred from submodel derived quantities. Previous approaches approximated the distribution of the derived quantity by matching its first two moments to some parametric distribution [124, 117]. The joint distribution implied by this approach is unclear, and minimizing the approximation error can be difficult for derived quantities with complex distributions. The chained Markov melding approach forms a unified joint distribution accounting for the contribution of each submodel and obviates approximation of the submodel derived quantities.

In Chapters 3 and 4, I developed two integrated models for learning about trends in LEPC abundance. In both analyses, counts of LEPC at the desired spatio-temporal scale are not observed, and I derive counts at the desired unit from independent aerial and ground surveys. Using chained Markov melding, I form the joint melded distribution for all parameters accounting for the data, prior specifications, and assumptions across all submodels.

1.3 Computational Methods and Aides

BHMs give tremendous flexibility for specifying models that mimic natural phenomenon and accommodate multiple data sources. Unfortunately, many models expressed in the previous sections are difficult to fit in practice. Common difficulties of fitting hierarchical models with MCMC include computation time, convergence, and mixing. In this section, I discuss computational aides for fitting BHMs with MCMC.

1.3.1 Restricted Regression

Consider the model

$$\boldsymbol{y} \sim [\boldsymbol{y}|\boldsymbol{\mu}, \boldsymbol{\psi}], \tag{1.19}$$

$$g(\boldsymbol{\mu}) = \boldsymbol{X}\boldsymbol{\beta} + \boldsymbol{\eta}, \tag{1.20}$$

$$\boldsymbol{\eta} \sim \mathcal{N}(\boldsymbol{0}, \boldsymbol{\Sigma}), \tag{1.21}$$

$$\boldsymbol{\beta} \sim \mathcal{N}(\boldsymbol{\mu}_{\boldsymbol{\beta}}, \boldsymbol{\Sigma}_{\boldsymbol{\beta}}), \tag{1.22}$$

where $g(\cdot)$ is a link function, $\boldsymbol{\psi}$ are additional parameters for the data model, and $\boldsymbol{\Sigma}$ is a covariance matrix. In the model, $\boldsymbol{\beta}$ are referred to as the fixed effects and $\boldsymbol{\eta}$ the random effects. The fixed effects $\boldsymbol{\beta}$ explain variation in the transformed latent mean $g(\boldsymbol{\mu})$ that is in the direction of the design matrix $\boldsymbol{X}$, and the random effect, $\boldsymbol{\eta}$, explains additional variation in $g(\boldsymbol{\mu})$ that is residual to the variation explained by $\boldsymbol{X}$. Reich et al. [125] showed that $\boldsymbol{\eta}$ is able to explain variation in $\boldsymbol{\mu}$ that is colinear to $\boldsymbol{X}$ which allows for confounding between $\boldsymbol{\eta}$ and $\boldsymbol{\beta}$.

Hodges and Reich [126] suggested the non-confounded GLM

$$\boldsymbol{y} \sim [\boldsymbol{y}|\boldsymbol{\mu}, \boldsymbol{\psi}], \tag{1.23}$$

$$g(\boldsymbol{\mu}) = \boldsymbol{X}\boldsymbol{\beta} + (\boldsymbol{I} - \boldsymbol{P}_{\boldsymbol{X}})\boldsymbol{\eta}, \tag{1.24}$$

$$\boldsymbol{\eta} \sim \mathcal{N}(\boldsymbol{0}, \boldsymbol{\Sigma}), \tag{1.25}$$

$$\boldsymbol{\beta} \sim \mathcal{N}(\boldsymbol{\mu}_{\boldsymbol{\beta}}, \boldsymbol{\Sigma}_{\boldsymbol{\beta}}), \tag{1.26}$$

where $\boldsymbol{I}$ is the identity matrix and $\boldsymbol{P}_{\boldsymbol{X}} = \boldsymbol{X}(\boldsymbol{X}'\boldsymbol{X})^{-1}\boldsymbol{X}'$ is the projection matrix onto the column space of $\boldsymbol{X}$. Model (1.23)-(1.26) restricts the random effect $\boldsymbol{\eta}$ to explain variation that is orthogonal or residual to $\boldsymbol{X}$ and is called restricted regression. Orthogonalizing the fixed and random effects reduces dependence in the Markov chain and generally improves mixing.

Over the past decade, restricted regression has garnered substantial attention in spatial statistics, and some have cautioned against its application. Paciorek [127] highlighted that, if confounding

exists, it may be inappropriate to attribute all contested variability in the latent mean $\boldsymbol{\mu}$ to the fixed effects. More recently, concerns regarding the coverage properties of the fixed effects estimator under restricted regression have been expressed [128, 129]. For example, Zimmerman and Ver Hoef [129] showed that applying any restricted regression method to a spatial general linear mixed model (SGLMM) leads to frequentist coverage of the fixed effects that is lower than the corresponding non-spatial model. Similarly, Khan and Calder [128] found that when fitting a restricted version of the SGLMM with an intrinsic conditional autoregressive prior, credible intervals of the fixed effects from the restricted model were generally nested inside those yielded by the non-spatial model. Given these results, both Zimmerman and Ver Hoef [129] and Khan and Calder [128] recommended reverting to inference from the non-spatial model, rather than that of the restricted SGLMM, when, based on the scientific context, inference from the unrestricted SGLMM was infeasible or counter-intuitive.

Hanks et al. [130] suggested a hybrid approach where the fixed effects, $\boldsymbol{\beta}$, are derived from the restricted SGLMM. This is possible because the restricted SGLMM is a reparameterization of the unrestricted SGLMM. The hybrid approach provides improved computational stability but yields the more conservative parameter estimates. While the above results regarding restricted regression have all been in the context of spatial statistics, the results hold more broadly for general GLMs as expressed in equations (1.19)-(1.22). In Chapter 2, I consider a model for describing the joint response of mammals in the subalpine forest of Colorado to the bark beetle epidemic. I employ restricted regression methods to orthogonalize the fixed and random effects to improve parameter mixing and convergence.

1.3.2 Tobit Model

Tobit models were first proposed for handling censored data [131] and are commonly employed in the context of nutrient monitoring. Dissolved phosphorus is an important indicator of health in aquatic ecosystems but can be difficult to monitor because the concentration can be as low as 0.01 milligram per liter (mg/L). Many instruments are unable to discriminate concentrations below

0.01 milligram per liter (mg/L) and will round any observations below the threshold to 0.01. A vector of measurements of dissolved phosphorous across $n = 7$ sites on one stream could be $\boldsymbol{y} = (0.01, 0.12, 0.17, 0.01, 0.01, 0.05, 0.01)'$.

Consider estimating the posterior distribution of the true mean concentration of dissolved phosphorous in the stream, denoted by μ. A naive model would be

$$y_i \sim \mathcal{N}(\mu, \sigma^2), \tag{1.27}$$

$$\mu \sim \mathcal{N}(\mu_0, \sigma_0^2), \tag{1.28}$$

$$\sigma^2 \sim \mathcal{IG}(q, r). \tag{1.29}$$

Model (1.27)-(1.29) does not account for the censoring of observations below the detection threshold and will result in a posterior distribution of μ that is both biased high and optimistic.

Let $\boldsymbol{y}^O$ and $\boldsymbol{y}^L$ denote the vectors of observed and latent measurements, respectively. The quantities are related as follows:

$$y_i^O = \begin{cases} y_i^L, & y_i^L > \xi \\ \xi, & y_i^L \leq \xi \end{cases}, \tag{1.30}$$

where ξ is the detection limit of the instrument. A tobit model in this context is

$$y_i^O = \begin{cases} y_i^L, & y_i^L > \xi \\ \xi, & y_i^L \leq \xi \end{cases}, \tag{1.31}$$

$$y_i^L \sim \mathcal{N}(\mu, \sigma^2), \tag{1.32}$$

$$\mu \sim \mathcal{N}(\mu_0, \sigma_0^2), \tag{1.33}$$

$$\sigma^2 \sim \mathcal{IG}(q, r). \tag{1.34}$$

For $y_i^O < \xi$, the latent measurement y_i^L is unobserved, and thus must be sampled. Conveniently, the full-conditional distribution of y_i^L is a zero-truncated normal distribution with upper bound ξ, mean μ, and variance σ^2. By accounting for the censoring induced by the detection limit of the instrument in the observational process, the tobit model corrects for the bias and optimism in the posterior of μ.

The tobit model may be computationally appealing more broadly. In Chapters 3 and 4, I describe a model for densities of LEPC at $n = 21$ sites. At site i, the surveyor recorded the count of birds N_{il} at each of L_i leks on the survey route. The density for route i was then calculated as $D_i = \sum_{l=1}^{L_i} N_i/A_i$, where A_i is the area of site i. Assuming $L_i > 0$ and $N_{i1}, \dots N_{iL_i}$ are independently and identically distributed with finite variance, the distribution of D_i is approximately normal by the central limit theorem when L_i is large. I considered the simple spatial linear regression model

$$\boldsymbol{D} \sim \mathcal{N}(\boldsymbol{X}\boldsymbol{\beta}, \boldsymbol{\Sigma}), \tag{1.35}$$

$$\boldsymbol{\beta} \sim \mathcal{N}(\boldsymbol{\mu}_{\boldsymbol{\beta}}, \boldsymbol{\Sigma}_{\boldsymbol{\beta}}), \tag{1.36}$$

$$\sigma^2 \sim \mathcal{IG}(q, r), \tag{1.37}$$

where $\boldsymbol{\Sigma} = \sigma^2 \boldsymbol{R}$ and $\boldsymbol{R}$ is a known correlation matrix that accounts for spatial dependence.

Model (1.36)-(1.37) is easy to implement via MCMC since both $\boldsymbol{\beta}$ and σ^2 have conjugate full-conditional distributions. A normal model for $\boldsymbol{D}$ was not appropriate because at some routes $L_i = 0$ and thus $D_i = 0$. To account for the mixture of discrete and continuous support, I considered the

following tobit model:

$$D_i = \begin{cases} \zeta_i, & \zeta_i > 0 \\ 0, & \zeta_i \leq 0 \end{cases}, \tag{1.38}$$

$$\boldsymbol{\zeta} \sim \mathcal{N}(\boldsymbol{X}\boldsymbol{\beta}, \boldsymbol{\Sigma}), \tag{1.39}$$

$$\boldsymbol{\beta} \sim \mathcal{N}(\boldsymbol{\mu}_{\boldsymbol{\beta}}, \boldsymbol{\Sigma}_{\boldsymbol{\beta}}), \tag{1.40}$$

$$\sigma^2 \sim \mathcal{IG}(q, r), \tag{1.41}$$

where $\boldsymbol{\Sigma} = \sigma^2 \boldsymbol{R}$ as before. The introduced parameter $\boldsymbol{\zeta}$, like $\boldsymbol{y}^L$ in the previous example, is partially unobserved. Unlike $\boldsymbol{y}^L$, $\boldsymbol{\zeta}$ does not have meaningful interpretation. All densities, D_i, were perfectly observed, and there was no censoring of the response. The tobit model accommodated the mixture of a discrete and continuous support while still retaining the conjugacy of $\boldsymbol{\beta}$ and σ^2.

To implement the tobit, I needed to sample $\boldsymbol{\zeta}_{\mathcal{S}}$, where $\mathcal{S}$ is the collection of sites at which $D_i = 0$. The full-conditional distribution of $\boldsymbol{\zeta}_{\mathcal{S}}$ is a truncated multivariate normal with upper bound $\mathbf{0}$, conditional mean $\boldsymbol{\mu}_{\mathcal{S}}$, and conditional variance $\boldsymbol{\Sigma}_{\mathcal{S}}$ defined as follows:

$$\boldsymbol{\mu}_{\mathcal{S}} = \boldsymbol{X}_{\mathcal{S}}\boldsymbol{\beta} + \boldsymbol{\Sigma}_{\mathcal{S},-\mathcal{S}}\boldsymbol{\Sigma}^{-1}_{-\mathcal{S},-\mathcal{S}}(\boldsymbol{\zeta}_{-\mathcal{S}} - \boldsymbol{X}_{-\mathcal{S}}\boldsymbol{\beta}), \tag{1.42}$$

$$\boldsymbol{\Sigma}_{\mathcal{S}} = \sigma^2 \left(\boldsymbol{\Sigma}_{\mathcal{S},\mathcal{S}} - \boldsymbol{\Sigma}_{\mathcal{S},-\mathcal{S}}\boldsymbol{\Sigma}^{-1}_{-\mathcal{S},-\mathcal{S}}\boldsymbol{\Sigma}_{-\mathcal{S},\mathcal{S}}\right), \tag{1.43}$$

where $\boldsymbol{\Sigma}_{\mathcal{S},-\mathcal{S}}$, for example, denotes the submatrix of $\boldsymbol{\Sigma}$ with rows in $\mathcal{S}$ but excluding columns in $\mathcal{S}$. Because $\boldsymbol{\Sigma}$ is known, I calculated all matrix inverses and products *a priori*, and sampling $\boldsymbol{\zeta}^{\mathcal{S}}$ was computationally inexpensive. For modeling LEPC densities, the improved mixing and convergence rate induced by conjugacy of $\boldsymbol{\beta}$ and σ^2 outweighed the burden of sampling $\boldsymbol{\zeta}_{\mathcal{S}}$.

1.3.3 Pólya-Gamma Data Augmentation

Ecologists often analyze binary data (e.g., species presence-absence, breeding success, survival analysis, etc.) [132], and are interested in the associations between covariates and quantities like

probability of occupancy, reproduction, or survival motivating the binary regression model

$$y_i \sim \text{Bern}(\psi_i), \tag{1.44}$$

$$\text{logit}(\psi_i) = \boldsymbol{x}_i'\boldsymbol{\beta}, \tag{1.45}$$

$$\boldsymbol{\beta} \sim \mathcal{N}(\boldsymbol{\mu}_{\boldsymbol{\beta}}, \boldsymbol{\Sigma}_{\boldsymbol{\beta}}), \tag{1.46}$$

where $i = 1, \ldots, n$ indexes observations. The logit link function induces a non-tractable full-conditional distribution for $\boldsymbol{\beta}$ that makes it difficult to fit the model with MCMC especially when there are many covariates.

Polson et al. [91] introduced a data augmentation scheme that induces conjugacy of the regression coefficients $\boldsymbol{\beta}$. Like the tobit model, Pólya-Gamma data augmentation involves introducing auxiliary parameters. The auxiliary parameters must be sampled but the extra computational cost is usually worth the improved mixing and convergence of $\boldsymbol{\beta}$.

Pólya-Gamma data augmentation derives its name from the distribution of the auxiliary variables. Let $\omega \sim \text{PG}(b, c)$, then

$$\omega \overset{\mathcal{D}}{=} \frac{1}{2\pi^2} \sum_{k=1}^{\infty} \frac{\gamma_k}{(k - \frac{1}{2})^2 + c^2/(4\pi^2)} \tag{1.47}$$

where the $\gamma_k \sim \mathcal{G}(b, 1)$ are independent gamma random variables and "$\overset{\mathcal{D}}{=}$" indicates equality in distribution. Pólya-Gamma data augmentation induces the following posteriors for the regression coefficients and auxiliary variables

$$\omega_i | \boldsymbol{\beta} \sim \text{PG}(1, \boldsymbol{x}_i'\boldsymbol{\beta}), \tag{1.48}$$

$$\boldsymbol{\beta} | \boldsymbol{y}, \boldsymbol{\omega} \sim \mathcal{N}(\boldsymbol{V}_{\boldsymbol{\omega}}\boldsymbol{m}_{\boldsymbol{\omega}}, \boldsymbol{V}_{\boldsymbol{\omega}}), \tag{1.49}$$

where

$$\boldsymbol{V}_{\boldsymbol{\omega}} = (\boldsymbol{X}'\boldsymbol{\Omega}\boldsymbol{X} + \boldsymbol{\Sigma}_{\boldsymbol{\beta}}^{-1})^{-1}, \tag{1.50}$$

$$\boldsymbol{m}_{\boldsymbol{\omega}} = \boldsymbol{X}'\boldsymbol{\kappa} + \boldsymbol{\Sigma}_{\boldsymbol{\beta}}^{-1}\boldsymbol{\mu}_{\boldsymbol{\beta}}, \tag{1.51}$$

$$\boldsymbol{\Omega} = \text{diag}(\omega_1, ..., \omega_n), \tag{1.52}$$

$$\boldsymbol{\kappa} = (y_1 - 1/2, \ldots, y_n - 1/2)'. \tag{1.53}$$

In Chapter 3, I use Pólya-Gamma data augmentation to facilitate model fitting for a Binomial regression model estimating the effect of land cover covariates on the number of LEPC groups in a region.

1.3.4 PX-DA for Abundance Estimation

Ecologists are often interested in counts such as clutch sizes, parasite loads, and local abundance. Abundance estimation is a heavily researched topic in ecology and many survey methods have been proposed [133]. Three popular survey methods for estimating abundance are capture-recapture, N-mixture, and distance sampling [42]. Models for analyzing each of these surveys leverages information about observed or captured individuals to make inference about the number of unobserved/uncaptured individuals.

Consider a distance sampling model for observations of a single species along a transect. The data consist of n distances $\boldsymbol{d}$ where n is itself a random quantity. The object of inference is N, the true number of individuals in the survey region. Following Royle et al. [134] and Hooten and

Hefley [42], consider the model

$$y_i \sim \begin{cases} \text{Bern}(p_i), & z_i = 1 \\ 0, & z_i = 0 \end{cases}, \tag{1.54}$$

$$\log(p_i) = -\frac{d_i^2}{\sigma^2}, \tag{1.55}$$

$$z_i \sim \text{Bern}(\psi), \tag{1.56}$$

$$\psi \sim \text{Beta}(a, b), \tag{1.57}$$

where $i = 1, \ldots, n$ indexes individuals. Analogous to the occupancy model, equations (1.1)-(1.6), the observational component, equation (1.54), accommodates zero-inflation where $y_i = 0$ because either the individual does not occupy the survey region or the individual does occupy the survey region but went undetected. The probability of detection for individual i is modeled as a function of d_i, the distance the individual was observed from the transect at the time of survey. In addition to distance, other traits might also impact detectability. For example, in Chapter 3, I consider a distance sampling model for aerial surveys of LEPC groups. I found that the count of birds in the group was an important predictor of detectability.

The crux of fitting model (1.54)-(1.57) is that the data only include observations for the detected individuals (i.e., $\boldsymbol{y} = \mathbf{1}$). Royle et al. [134] introduced parameter expanded data augmentation (PX-DA) and inflating the dataset, $\boldsymbol{y}$, with $M - n$ pseudo-individuals where $y_i = 0$ for $i = n + 1, \ldots, M$. Because the pseudo-individuals are unobserved, a prior distribution is specified for the unknown individual distances d_i for $i = n + 1, \ldots, M$. Assuming individuals are randomly distributed in the survey region, a reasonable prior for the unknown distances is $d_i \sim \mathcal{U}(0, \nu_d)$ for $i = n + 1, \ldots, M$, where ν_d is an upper detection limit.

Royle et al. [134] referred to M as the superpopulation size and interpreted z_i to be the indicator on whether individual i of the superpopulation occupied the survey area. The true number of individuals in the survey region can be calculated as the derived quantity $N = \sum_{i=1}^{n} z_i$. A heuristic for the PX-DA distance sampling model is that characteristics of the observed individuals help

to decipher whether it is more likely that a psuedo-individual did not occupy the survey region, $z_i = 0$, or the psuedo-individual did occupy the survey region, $z_i = 1$, but went undetected $y_i = 0$. Psuedo-individuals with characteristics similar to those of detected indivudals are more likely to be classified as not occupying the survey region because if these psuedo-individuals did occupy the region, they likely would have been detected.

Both hyperparameters M and ν_d must be specified *a priori*. The superpopulation size M should be chosen large enough to capture variability in N but not so large as to impose an unnecessary computational burden. Likewise, ν_d should be larger than any of the observed distances, but larger values of ν_d require larger M and hence more computation. Increasing ν_d enlarges the survey area and will increase both the posterior variance and mean of N. Because inference on N depends on ν_d, it is preferable to consider inference on the derived quantity density $D = N/2\nu_d\nu_l$, where ν_l is the length of the survey transect. The derived density D is generally unaffected by choice of ν_d.

1.3.5 Multistage MCMC Algorithms

Due to dependence in the Markov chain, MCMC algorithms are difficult to parallelize [135, 136, 137]. Lack of parallelization often precludes MCMC from being competitive with other methods for drawing inference from Bayesian models such as The EM algorithm [138] and Integrated Nested Laplace Approximation (INLA) [139]. A variety of multistage MCMC algorithms including Recursive Bayes (RB), Proposal-RB, Sequential Monte Carlo (SMC), and Markov melding have been proposed to alleviate the computation burden of MCMC [140, 141, 142, 143, 144, 64].

The computational benefits offered by these multistage algorithms are diverse [145]. For example, Lunn et al. [141] used Proposal-RB to fit a hierarchical model for a meta-analysis in two stages. By splitting the MCMC algorithm into stages, the first stage could be parallelized across the J studies in the meta-analysis resulting in shorter computation time overall. Hooten et al. [143] considered a hierarchical point process model for animal telemetry data. The observational component point process model required calculation of computationally expensive integral. Using Proposal-RB, Hooten et al. [143] obviated calculation of the integral in the 2nd stage of the

MCMC algorithm. Taylor et al. [146] developed a multistage algorithm for recursively updating posterior quantities in a record linkage model for streaming data.

Another potential benefit of fitting a hierarchical model in stages is that conjugacy of certain parameters may be preserved or induced. For example, McCaslin et al [147] introduced Transformation-assisted Recursive Bayes (TARB) that induces conjugacy at one stage of the algorithm by transforming the parameter of interest and specifying a temporary prior. In Chapters 3 and 4, I develop integrated models for LEPC abundance that are linked on submodel derived quantities. I implement a multistage MCMC algorithm that allows several of the submodels to be fit in parallel. The multistage algorithm also dodges costly Metropolis-Hastings updates for parameters with low acceptance rates.

1.3.6 `Rcpp`

The computational methods described have wide applicability and aide fitting complex models for multiple data sources. Nonetheless, even after employing the suite of methods described above, the computation time required to fit a MCMC algorithm undesirable may be undesirable. One solution is to transition our MCMC algorithm to a higher-level computer language.

In 2011, Eddelbuettel and Francois [148] launched `Rcpp`, an `R` package for incorporating `C++` objects and code into the `R` environment. Using `Rcpp`, programmers can seamlessly export functions and code from `C++`. Programmers implementing novel MCMC algorithms in `R` can code computationally burdensome portions of their MCMC algorithm in `C++`. Because `R` is a interpreted language, rather than compiled, its memory allocation routines are not suited for large, nested "`for`" loops, and the largest computation gains often result from coding the entire MCMC algorithm in `Rcpp`.

I code several of the MCMC algorithms presented in Chapter 3 and 4 using `Rcpp` and find the resulting algorithms to be orders of magnitude faster than those coded in `R`. For example, in Chapter 3, I implement an extension of the tobit model, equations (1.39)-(1.41), to infer spatio-temporal variability in LEPC density. Fitting the model via MCMC with an algorithm coded in `R`

required over 300 minutes per $100,000$ MCMC iterations. Fitting the analogous MCMC algorithm coded in `Rcpp` took only 30 minutes per $100,000$ iterations.

Chapter 2

Community Confounding in Joint Species Distribution Models

2.1 Introduction

Historically, species distributions have been modeled independently from each other due to unavailability of multispecies datasets and computational restraints. However, ecological datasets that provide insights about collections of organisms have become prevalent over the last decade thanks to efforts like The Long Term Ecological Research Network (LTER), National Ecological Observatory Network (NEON), and citizen science surveys [149]. In addition, technology has improved our ability to fit modern statistical models to these datasets that account for both species environmental preferences and interspecies dependence. These advancements have allowed for the development of joint species distribution models (JSDMs) [150, 21, 89] that can model dependence among species simultaneously with environmental drivers of occurrence and/or abundance.

Species distributions are shaped by both interspecies dynamics and environmental preferences [17, 151, 152, 153]. JSDMs integrate both sources of variability and adjust uncertainty to reflect that multiple confounded factors can contribute to similar patterns in species distributions. Some have proposed that JSDMs not only account for biotic interactions but also correct estimates of association between species distributions and environmental drivers [154, 21], while others claim JSDMs cannot disentangle the roles interspecies dependence and environmental drivers [17]. We address why JSDMs can provide inference distinct from their concomitant independent SDMs, how certain parameterizations of a JSDM induce confounding between the environmental and random species effects, and when deconfounding these effects may be appealing for computation and interpretation.

Because of the prevalence of occupancy data for biomonitoring in ecology, we focus our discussion of community confounding in JSDMs on occupancy models, although we also consider a JSDM for species density data in the simulation study. The individual species occupancy model was first formulated by MacKenzie et al. [80] and has several joint species extensions [155, 156, 86, 157, 87, 158, 89]. We chose to investigate the impacts of community confounding on the probit model since it has been widely used in the analysis of occupancy data [83, 86, 89]. We also developed a joint species extension to the Royle-Nichols model [78] and consider community confounding in that model.

We use the probit and Royle-Nichols occupancy models to improve our understanding of montaine mammal communities in what follows. We show that including unstructured random species effects in either occupancy model induces confounding between the fixed environmental and random species effects. We demonstrate how to orthogonalize these effects in the model and compare the resulting inference compared to models where species are treated independently.

Unlike previous approaches that have applied restricted regression techniques similar to ours, we use it in the context of well-known ecological models for species occupancy and intensity. While such approaches have been discussed in spatial statistics and environmental science, they have not been adopted in settings involving the multivariate analysis of community data. We draw parallels between restricted spatial regression and restricted JSDMs but also highlight where the methods differ in goals and outcomes. We find that the computational benefits conferred by performing restricted spatial regression also hold for some joint species distribution models.

2.1.1 Royle-Nichols Joint Species Distribution Model

We present a JSDM extension to the Royle-Nichols model [78]. The Royle-Nichols model accounts for heterogeneity in detection induced by the species' latent intensity, a surrogate related to true species abundance. Abundance, density, and occupancy estimation often requires an explicit spatial region that is closed to emmigration and immigration. In our model, the unobservable intensity variable helps us explain heterogeneity in the frequencies we observe a species at different

sites without making assumptions about population closure. In the *Model* section, we further discuss the distinctions between abundance and intensity in the Royle-Nichols model.

The Royle-Nichols model utilizes occupancy survey data but provides inference distinct from the basic occupancy model [80]. In the Royle-Nichols model, we estimate individual detection probability for homogeneous members of the population, whereas in an occupancy model, we estimate probability of observing at least one member of the population given that the site is occupied. Furthermore, the Royle-Nichols model allows us to relate environmental covariates to the latent intensity associated with a species at a site, while in an occupancy model, environmental covariates are associated with the species latent probability of occupancy at a site. Species intensity and occupancy may be governed by different mechanisms, and inference from an intensity model can be distinct from that provided by an occupancy model [93, 94, 95]. Cingolani et al. [94] proposed that, in plant communities, certain environmental filters preclude species from occupying a site and an additional set of filters may regulate if a species can flourish. Hence, certain covariates that were unimportant in an occupancy model may improve predictive power in an intensity model.

2.1.2 Community Confounding

Species distributions are shaped by environment as well as competition and mutualism within the community [159, 160, 153]. Community confounding occurs when species distributions are explained by a convolution of environmental and interspecies effects and can lead to inferential differences between a joint and single species distribution model as well as create difficulties for fitting JSDMs. Former studies have incorporated interspecies dependence into an occupancy model [155, 156, 86, 157, 87, 158, 89], and others have addressed spatial confounding [92, 161, 83, 149], but none of these explicitly addressed community confounding. However, all Bayesian joint occupancy models naturally attenuate the effects of community confounding due to the prior on the regression coefficients. The prior, assuming it is proper, induces regularization on the regression coefficients [162] that can lessen the inferential and computational impacts of confounding [70]. Furthermore, latent factor models like that described by Tobler et al. [89] restrict the dimension-

ality of the random species effect which should also reduce confounding with the environmental effects.

We address community confounding by formulating a version of our model that orthogonalizes the environmental effects and random species effects. Orthogonalizing the fixed and random effects is common practice in spatial statistics and often referred to as restricted spatial regression [125, 126, 163, 130, 70]. Restricted regression has been applied to spatial generalized linear mixed models (SGLMM) for observations $\boldsymbol{y}$, which can be expressed as

$$\boldsymbol{y} \sim [\boldsymbol{y}|\boldsymbol{\mu}, \boldsymbol{\psi}], \tag{2.1}$$

$$g(\boldsymbol{\mu}) = \boldsymbol{X}\boldsymbol{\beta} + \boldsymbol{\eta}, \tag{2.2}$$

$$\boldsymbol{\eta} \sim \mathcal{N}(\mathbf{0}, \boldsymbol{\Sigma}), \tag{2.3}$$

where $g(\cdot)$ is a link function, $\boldsymbol{\psi}$ are additional parameters for the data model, and $\boldsymbol{\Sigma}$ is the covariance matrix of the spatial random effect. In the SGLMM, prior information facilitates the estimation of $\boldsymbol{\eta}$, which would not be estimable otherwise due to its shared column space with $\boldsymbol{\beta}$ [163]. This is analogous to applying a ridge penalty to $\boldsymbol{\eta}$, which stabilizes the likelihood. Another method for fitting the confounded SGLMM is to specify a restricted version:

$$\boldsymbol{y} \sim [\boldsymbol{y}|\boldsymbol{\mu}, \boldsymbol{\psi}], \tag{2.4}$$

$$g(\boldsymbol{\mu}) = \boldsymbol{X}\boldsymbol{\delta} + (\boldsymbol{I} - \boldsymbol{P}_X)\boldsymbol{\eta}, \tag{2.5}$$

$$\boldsymbol{\eta} \sim \mathcal{N}(\mathbf{0}, \boldsymbol{\Sigma}), \tag{2.6}$$

where $\boldsymbol{P}_X = \boldsymbol{X}(\boldsymbol{X}\boldsymbol{X})^{-1}\boldsymbol{X}'$ is the projection matrix onto the column space of $\boldsymbol{X}$. In the unrestricted SGLMM, the regression coefficients $\boldsymbol{\beta}$ and random effect $\boldsymbol{\eta}$ in (2.1) compete to explain variability in the latent mean $\boldsymbol{\mu}$ in the direction of $\boldsymbol{X}$ [70]. In the restricted model, however, all

variability in the direction of $\boldsymbol{X}$ is explained solely by the regression coefficients $\boldsymbol{\delta}$ in equation (2.4) [130], and $\boldsymbol{\eta}$ explains residual variation that is orthogonal to $\boldsymbol{X}$. We refer to $\boldsymbol{\beta}$ as the conditional effects because they depend on $\boldsymbol{\eta}$, and $\boldsymbol{\delta}$ as the unconditional effects.

Restricted regression, as specified in equation (2.4), was proposed by Reich et al.[125]. Reich et al. [125] described a disease-mapping example in which the inclusion of a spatial random effect rendered one covariate effect unimportant that was important in the non-spatial model. Spatial maps indicated an association between the covariate and response, making inference from the spatial model appear untenable. Reich et al. [125] proposed restricted spatial regression as a method for recovering the posterior expectations of the non-spatial model and shrinking the posterior variances which tend to be inflated for the unrestricted SGLMM.

Several modifications of restricted spatial regression have been proposed [163, 164, 165, 166, 167]. All restricted spatial regression methods seek to provide posterior means $\mathrm{E}\left(\delta_j|\boldsymbol{Y}\right)$ and marginal posterior variances $\mathrm{Var}\left(\delta_j|\boldsymbol{Y}\right)$, $j = 1, ..., p$ that satisfy the following two conditions [128]:

1. $\mathrm{E}\left(\boldsymbol{\delta}|\boldsymbol{Y}\right) = \mathrm{E}\left(\boldsymbol{\beta}_{\mathrm{NS}}|\boldsymbol{Y}\right)$ and,

2. $\mathrm{Var}\left(\beta_{\mathrm{NS},j}|\boldsymbol{Y}\right) \leq \mathrm{Var}\left(\delta_j|\boldsymbol{Y}\right) \leq \mathrm{Var}\left(\beta_{\mathrm{Spatial},j}|\boldsymbol{Y}\right)$ for $j = 1, ..., p$,

where $\boldsymbol{\beta}_{NS}$ and $\boldsymbol{\beta}_{Spatial}$ are the regression coefficients corresponding to the non-spatial and unrestricted spatial models, respectively.

The inferential impacts of spatial confounding on the regression coefficients has been debated. Hodges and Reich [126] outlined five viewpoints on spatial confounding and restricted regression in the literature and refuted the two following views:

1. Adding the random effect $\boldsymbol{\eta}$ corrects for bias in $\boldsymbol{\beta}$ resulting from missing covariates.

2. Estimates of $\boldsymbol{\beta}$ in a SGLMM are shrunk by the random effect and hence conservative.

The random effect $\boldsymbol{\eta}$ can increase or decrease the magnitude of $\boldsymbol{\beta}$, and the change may be galvanized by mechanisms not related to missing covariates. Therefore, we cannot assume the regression coefficients in the SGLMM will exceed those of the restricted model, nor should we regard the

estimates in either model as biased due to misspecification. Confounding in the SGLMM causes $\text{Var}\left(\beta_j|\boldsymbol{Y}\right) \geq \text{Var}\left(\delta_j|\boldsymbol{Y}\right), j = 1, ..., p$, because of the shared column space of the fixed and random effects. Thus, we refer to the conditional coefficients as conservative with regard to their credible intervals, not their posterior expectations.

Reich et al. [125] argued that restricted spatial regression should always be applied because the spatial random effect is generally added to improve predictions and/or correct the fixed effect variance estimate. While it may be inappropriate to orthogonalize a set of fixed effects in an ordinary linear model, orthogonalizing the fixed and random effect in a spatial model is permissible because the random effect is generally not of inferential interest. Paciorek [127] provided the alternative perspective that, if confounding exists, it is inappropriate to attribute all contested variability in $\boldsymbol{y}$ to the fixed effects. Hanks et al. [130] discussed factors for deciding between the unrestricted and restricted SGLMM on a continuous spatial support. The restricted SGLMM leads to improved computational stability, but the unconditional effects are less conservative under model misspecification and more prone to type-S errors: The Bayesian analogue of Type I error. Fitting the unrestricted SGLMM when the fixed and random effects are truly orthogonal does not introduce bias, but it will increase the fixed effect variance. Given these considerations, Hanks et al. [130] suggested a hybrid approach where the conditional effects, $\boldsymbol{\beta}$, are extracted from the restricted SGLMM. This is possible because the restricted SGLMM is a reparameterization of the unrestricted SGLMM. This hybrid approach leads to improved computational stability but yields the more conservative parameter estimates. We describe how to implement this hybrid approach for joint species distribution models in the *Community Confounding* section.

Restricted regression has also been applied in time series applications. Dominici et al. [168] debiased estimates of fixed effects confounded by time using restricted smoothing splines. Without the temporal random effect, Dominici et al. [168] asserted all temporal variation in the response would be wrongly attributed to temporally correlated fixed effects. Houseman et al. [169] used restricted regression to ensure identifiability of a nonparametric temporal effect and highlighted certain covariate effects that were more evident in the restricted model (i.e., the unconditional ef-

fects' magnitude was greater). Furthermore, restricted regression is implicit in restricted maximum likelihood estimation (REML). REML is often employed for debiasing the estimate of the variance of $\boldsymbol{Y}$ in linear regression and fitting linear mixed models that are not estimable in their unrestricted format [170]. Because REML is generally applied in the context of variance and covariance estimation, considerations regarding the effects of REML on inference for the fixed effects are lacking in the literature.

In ecological science, JSDMs often include an unstructured random effect like $\boldsymbol{\eta}$ in equation (2.1) to account for interspecies dependence, and hence can also experience community confounding between $\boldsymbol{X}$ and $\boldsymbol{\eta}$ analogous to spatial confounding. Unlike a spatial or temporal random effect, we consider random species effects to be inferentially important, rather than a tool solely for improving predictions or catch-all for missing covariates. An orthogonalization approach in a JSDM attributes contested variation between the fixed effects (environmental information) and random effect (community information) to the fixed effect.

We describe how to orthogonalize the fixed and random species effects in a suite of JSDMs and present a method for detecting community confounding. In the simulation study, we test the efficacy of our method for detecting confounding, show that community confounding can lead to computational difficulties similar to those caused by spatial confounding [130], and highlight that, for some models, restricted regression can improve model fitting. We also investigate the inferential implications of community confouding and restricted regression in JSDMs by comparing outputs from the SDM, unrestricted JSDM, and restricted JSDM of the Royle-Nichols and probit occupancy models fit to mammalian camera trap data. Lastly, we discuss other inferential and computational methods for confounded models and consider their appropriateness for joint species distribution modeling.

2.2 Model

2.2.1 Data Model

The probit and Royle-Nichols occupancy models were developed for analyzing multispecies binary detection data, y_{ijk}, arising from a zero-inflated Bernoulli process with probability of success p_{ijk}, where $i = 1, \ldots, n$, $j = 1, \ldots, J_i$, and $k = 1, \ldots, K$ correspond to sites, occasions, and species, respectively. Occupancy data of this form have traditionally been analyzed in a latent variable framework [79, 80, 171]. In what follows, we let $z_{ik} \sim \text{Bern}(\psi_{ik})$ be an indicator on whether species k occupies site i. Given a site is occupied, we detect species k on occasion j with some probability p_{ijk}, such that $(y_{ijk}|z_{ik} = 1) \sim \text{Bern}(p_{ijk})$, but if species k is absent from the site, we have zero probability of detecting it, $P(y_{ijk} = 0|z_{ik} = 0) = 1$.

The probit occupancy model is so named because it links ψ_{ik} and p_{ijk} to occupancy and detection covariates $\boldsymbol{x}_{ik}$ and $\boldsymbol{w}_{ijk}$, respectively, with the standard normal CDF Φ. The probit link function can be paired with data augmentation [84, 81, 82, 83] to yield efficient Gibbs samplers for the occupancy and detection regression coefficients $\boldsymbol{\beta}$ and $\boldsymbol{\alpha}$, respectively.

Royle and Nichols [78] introduced a method for analyzing occupancy data that explicitly modeled the probability of detecting species k at a site as a function of a surrogate related to the true species abundance. Assuming there are N_{ik} individuals of species k in sample region i and that all individuals in species k on the sample unit have identical detection probabilities and are detected independently of other individuals, the probability of detecting at least one of these individuals can be expressed as

$$\rho_{ijk} = 1 - (1 - r_{jk})^{N_{ik}}, \tag{2.7}$$

where r_{jk} is a binomial sampling probability that a particular individual of species k is detected on occasion j. While the Royle-Nichols model facilitates inference on number of individuals of species k, N_{ik}, at each site when all the assumptions are met, we do not interpret them as such

because sites are not necessarily closed in camera trap studies due to mobile species with home ranges larger than the sampling radius of the camera. Note that ρ_{ijk} in equation (2.7) corresponds to the species probability of detection conditional on an intensity process. This is distinct from p_{ijk} in the probit model that is conditional on an occupancy process.

The nonlinear function of r_{jk} and N_{ik} in equation (2.7) involves more parameters than would be identifiable in a typical occupancy model, especially when the individual detection probability is heterogeneous across occasions (e.g., r_{jk} are heterogeneous). In the heterogeneous case, r_{jk} is connected to covariates with the logit link function:

$$\text{logit}(r_{jk}) = f(\boldsymbol{w}_{jk}, \boldsymbol{\alpha}_k), \tag{2.8}$$

where $f(\boldsymbol{w}_{ijk}, \boldsymbol{\alpha}_k)$ is a linear function of the detection covariates $\boldsymbol{w}_{ijk}$ and regression parameters $\boldsymbol{\alpha}_k$.

2.2.2 Modeling Interspecies Dependence

We extend both occupancy models to account for interspecies dependence by including random species effects in their process models. Following Royle and Nichols [78], we assume $N_{ik} \sim \text{Pois}(\lambda_{ik})$, where λ_{ik} is mean intensity of species k at site i. We let $\boldsymbol{\lambda}$ denote the vector of site specific intensities stacked across the K species in the community. To model interspecies dependence, we specify the conditional multivariate normal distribution:

$$\log(\boldsymbol{\lambda}) \sim \mathcal{N}(\boldsymbol{X}\boldsymbol{\beta} + \boldsymbol{\eta}, \boldsymbol{\Sigma}_{\boldsymbol{\lambda}}), \tag{2.9}$$

$$\boldsymbol{\eta} \sim \mathcal{N}(\boldsymbol{0}, \boldsymbol{\Sigma}_{spp} \otimes \boldsymbol{I}_n), \tag{2.10}$$

where $\boldsymbol{X}$ is a block-diagonal matrix of the K species design matrices, $\boldsymbol{\beta} = (\boldsymbol{\beta}_1', \ldots, \boldsymbol{\beta}_K')'$ is a stacked vector of species specific regression coefficients, $\boldsymbol{\eta}$ represents the random species effects,

and $\boldsymbol{\Sigma}_{spp}$ is a species covariance matrix, and $\boldsymbol{\Sigma}_{\boldsymbol{\lambda}}$ is a matrix that allows for additional covariance structures such as spatial dependence. For our purposes of comparing the SDM, unrestricted JSDM, and restricted JSDM for differences galvanized by community confounding, we assumed a simple independent structure for $\log(\boldsymbol{\lambda})$ and set $\boldsymbol{\Sigma}_{\boldsymbol{\lambda}} = \tau \boldsymbol{I}$.

In the probit model, we include a random species effect in the latent probability of occupancy: $\Phi(\boldsymbol{\psi}) = \boldsymbol{X}\boldsymbol{\beta} + \boldsymbol{\eta}$, where $\boldsymbol{\psi}$ is a vector of site specific occupancy probabilities stacked across the K species in the community and $\boldsymbol{X}$, $\boldsymbol{\beta} = (\boldsymbol{\beta}_1', \ldots, \boldsymbol{\beta}_K')'$, and $\boldsymbol{\eta}$ are defined as above.

In both occupancy models, $\boldsymbol{\eta}$ allows for dependence between all K species in the community at each site. In the probit model, $\boldsymbol{\eta}$ characterizes interspecies dependence in the probability of occupancy, whereas in the Royle-Nichols model interspecies dependence is characterized in the species latent intensities. Just as certain environmental features may not preclude species occupancy but can curb intensity, some species may coexist in a region but not be able to jointly flourish [172]. Hence, interspecies dependence on latent intensity is conceptually distinct from interspecies dependence on probability of occupancy and may lead to inferential differences in $\boldsymbol{\eta}$ in the two occupancy models.

Tobler et al. [89] developed a joint occupancy model that accounts for community structure using a latent variable approach. They express the latent probability of occupancy of species k at site i as

$$\Phi(\psi_{ik}) = \boldsymbol{x}_i'\boldsymbol{\beta}_k + \boldsymbol{l}_i'\boldsymbol{\theta}_k, \tag{2.11}$$

where $\boldsymbol{l}_i'$ is a vector of length T of latent variables, and $\boldsymbol{\theta}_k$ are species specific regression coefficients. The latent variable model (LVM) is a computationally efficient and implicitly accounts for community structure. Other occupancy models have included interspecies dependence in the structure of the regression coefficients. Known as multispecies models, these models assume the species specific regression coefficients $\boldsymbol{\beta}_k$ stem from a common multivariate normal distribution $\boldsymbol{\beta}_k \sim \mathcal{N}(\boldsymbol{\mu}, \boldsymbol{\Sigma}_{\boldsymbol{\beta}})$ where $\boldsymbol{\mu}$ is the typical response of a species to covariates $\boldsymbol{x}$ and $\boldsymbol{\Sigma}_{\boldsymbol{\beta}}$ allows for

dependence in different species response to the same covariates [173]. In our study of mammalian camera trap data, each species is modeled with unique covariates, and we do not consider shared environmental responses.

Scheffe [174] stipulated that the levels of a random effect are draws from a population, and the draws are not of interest in themselves but only as samples from the larger population, which is of interest. In more recent literature, the term random effect is used more broadly. Hodges and Clayton [175] categorized modern definitions of a random effect into three different varieties. The definition commonly used in spatial statistics is, the levels of the effect arise from a meaningful population, but they are the whole population and these particular levels are of interest. We adopt this definition for the random species effects in equation (2.9). In practice, some levels of the population will likely not be included in the random species effects. For example, in Ivan et al. [2], cameras were baited and arranged to capture all members of the mammalian community, but several species were excluded from the random species effects due to a lack of detections.

2.2.3 Priors

We specified normal priors for the regression coefficients, $\boldsymbol{\beta}$, in the intensity and occupancy processes of the Royle-Nichols and probit models, respectively to facilitate comparison with the occupancy and spatial confounding literature. We also specified normal priors for the detection coefficients, $\boldsymbol{\alpha}$, in the observation model and the conjugate Inverse-Wishart prior for the species covariance matrix $\boldsymbol{\Sigma}_{spp}$. A more general alternative to the Inverse-Wishart prior is to apply a Cholesky decomposition, $\boldsymbol{\Sigma}_{spp} = \boldsymbol{L}\boldsymbol{D}^{-1}\boldsymbol{L}'$, where $\boldsymbol{L}$ is lower diagonal with ones along the diagonal and $\boldsymbol{D}$ is diagonal with positive diagonal elements, and specify priors for the lower diagonal elements of $\boldsymbol{L}$ and diagonal elements of $\boldsymbol{D}$ [176]. We found the Inverse-Wishart prior suitable for our inferential goals, but see Chan and Jeliazkov [176] for alternative covariance matrix priors. The joint posterior distribution associated with our model is

$$[\boldsymbol{\alpha}, \boldsymbol{\beta}, \boldsymbol{\lambda}, \boldsymbol{N}, \boldsymbol{\Sigma}_{spp} | \boldsymbol{Y}] \propto$$
$$\prod_{k=1}^{K} \left(\prod_{i=1}^{n} \left(\prod_{j=1}^{J_i} \left([y_{ijk} | N_{ik}, \boldsymbol{\alpha}_k] \right) [N_{ik} | \lambda_{ik}] \right) [\boldsymbol{\alpha}_k] [\boldsymbol{\beta}_k] \right) [\boldsymbol{\lambda} | \boldsymbol{\beta}_1, \cdots, \boldsymbol{\beta}_K, \boldsymbol{\Sigma}_{spp}] [\boldsymbol{\Sigma}_{spp}]. \tag{2.12}$$

See Appendix A.1 for the full statements of both the joint probit and Royle-Nichols occupancy models.

2.3 Community Confounding

2.3.1 Restricted Regression Approach

We fit a restricted version of the each JSDM that orthogonalizes the fixed and random species effects. In the Royle-Nichols model, we express the species latent intensity and occupancy process conditionally as

$$\log(\boldsymbol{\lambda}) \sim \mathcal{N}(\boldsymbol{X}\boldsymbol{\delta} + (\boldsymbol{I} - \boldsymbol{P}_X)\boldsymbol{\eta}, \tau^2 \boldsymbol{I}), \tag{2.13}$$

$$\boldsymbol{\eta} \sim \mathcal{N}(\boldsymbol{0}, \boldsymbol{\Sigma}_{spp} \otimes \boldsymbol{I}_n), \tag{2.14}$$

where $\boldsymbol{P}_X$ is the projection matrix onto the column space of $\boldsymbol{X}$. Likewise, in the probit model we specify $\Phi(\boldsymbol{\psi}) = \boldsymbol{X}\boldsymbol{\delta} + (\boldsymbol{I} - \boldsymbol{P}_X)\boldsymbol{\eta}$ and retain the same prior for $\boldsymbol{\eta}$ as in (2.14). This specification forces the random species effects to explain patterns in the community that are orthogonal to the fixed effects. The latent variables and fixed effects in the LVM can also be orthogonalized. Writing equation (2.11) in matrix form, we have

$$\Phi(\boldsymbol{\psi}_k) = \boldsymbol{X}'\boldsymbol{\delta}_k + \boldsymbol{L}\boldsymbol{\theta}_k, \tag{2.15}$$

where $\boldsymbol{X}$ and $\boldsymbol{L}$ are the matrices of covariates and latent variables vertically stacked across sites, respectively. If we assume common covariates across all K species, we can specify a restricted LVM as follows:

$$\Phi(\boldsymbol{\psi}_k) = \boldsymbol{X}'\boldsymbol{\delta}_k + (\boldsymbol{I} - \boldsymbol{P}_{\boldsymbol{X}})\boldsymbol{L}\boldsymbol{\theta}_k. \tag{2.16}$$

However, if covariates differ by species, i.e., $\boldsymbol{X} = \boldsymbol{X}_k$, then the posterior distribution of latent variables will differ by species. To retain a common posterior distribution of latent variables across all species, the latent variables need to be orthogonalized against all covariates among the k species,

$$\boldsymbol{L}^R = \prod_{k=1}^{K}(\boldsymbol{I} - \boldsymbol{P}_{\boldsymbol{X}_k})\boldsymbol{L}. \tag{2.17}$$

The specification of equation (2.17) is more restrictive than the orthogalization in the Royle-Nichols and probit model, and so we omit the LVM from our case study.

Hanks et al. [130] showed that the restricted, equation (2.13), and unrestricted, equation (2.9), generalized linear mixed models GLMM are reparameterizations of the same model and derived the following relationship between the unconditional $\boldsymbol{\delta}$ and conditional $\boldsymbol{\beta}$ fixed effects:

$$\boldsymbol{\delta} \equiv \boldsymbol{\beta} + (\boldsymbol{X}'\boldsymbol{X})^{-1}\boldsymbol{X}'\boldsymbol{\eta}. \tag{2.18}$$

Using equation (2.18), one can easily sample both sets of fixed effects by fitting either the restricted or unrestricted parameterization. We can also sample the covariance structure of the restricted random species effect from either model fit by drawing samples from the distribution

$$\boldsymbol{\Sigma}_{spp,R}^{-1} \sim \text{Wishart}(\boldsymbol{S}\nu + \boldsymbol{\eta}'(\boldsymbol{I} - \boldsymbol{P}_{\boldsymbol{X}})\boldsymbol{\eta}, \nu + n). \tag{2.19}$$

Hence, regardless of which model is fit, we can obtain both the unconditional and conditional habitat effects as well as the unrestricted and restricted species covariance matrices.

2.3.2 Measuring Confounding

Hefley et al. [70] showed how to assess confounding in SGLMM models by computing the Pearson correlation coefficient between each pair of covariates and eigenvectors from the spectral decomposition of the spatial covariance matrix. Likewise, Prates et al. [167] proposed a test for spatial confounding that can be calculated prior to model fitting. We propose another approach relevant to our method that aids in interpretation. We compute the coefficient of determination of each covariate for species k regressed on the estimated random species effects. Because the latent intensities are unknown, the coefficents of determination of all covariates are derived quantities and can be computed at each iteration of the MCMC algorithm:

$$R^{2^{(l)}}(\boldsymbol{x}_k) = \frac{SSR^{(l)}(\boldsymbol{x}_k)}{SST(\boldsymbol{x}_k)} = \frac{\left(\boldsymbol{\Delta}^{(l)}\hat{\boldsymbol{\theta}}^{(l)} - \bar{\boldsymbol{x}}_k\right)'\left(\boldsymbol{\Delta}^{(l)}\hat{\boldsymbol{\theta}}^{(l)} - \bar{\boldsymbol{x}}_k\right)}{(\boldsymbol{x}_k - \bar{\boldsymbol{x}}_k)'(\boldsymbol{x}_k - \bar{\boldsymbol{x}}_k)}, \tag{2.20}$$

where $\bar{\boldsymbol{x}}_k = (\bar{x}_k, \ldots, \bar{x}_k)'$ is the mean of the covariate $\boldsymbol{x}_k$ for species k repeated n times, $\boldsymbol{\Delta}^{(l)} = \left(\boldsymbol{\eta}_1^{(l)}, \ldots, \boldsymbol{\eta}_K^{(l)}\right)$ is a matrix of the random species effects sampled for MCMC iteration l, and $\hat{\boldsymbol{\theta}}^{(l)}$ are estimated regression coefficients relating the estimated species intensities at iteration l to $\boldsymbol{x}_k$. The posterior mean $\text{E}\left(R^2(\boldsymbol{x}_k)|\boldsymbol{Y}\right)$ provides a measure of community confounding for the covariate $\boldsymbol{x}_k$ and can help identify which fixed effects will vary between the unrestricted and restricted models. Furthermore, we can use the global F-test of the linear relationship between $\boldsymbol{x}_k$ and $\boldsymbol{\Delta}$ to determine if confounding exists.

2.4 Simulation Study

We performed a simulation study to investigate the effects of community confounding and orthogonalization of the fixed and random species effects on model fitting. Specifically, we compared the effective sample sizes of $\boldsymbol{\beta}$ and $\boldsymbol{\eta}$ for three different models for confounded and unconfounded data with unrestricted and restricted parameterizations. The effective sample size (ESS) is the number of independent MCMC samples of a quantity and is a metric for measuring the sampling efficiency of an MCMC algorithm. Higher ESS are preferable as posterior distributions of quantities of interest can be obtained in fewer iterations.

We considered three models: The joint probit occupancy model, joint Royle-Nichols model, and joint normal model, which is derived from the scenario where $\boldsymbol{\lambda}$ in the Royle-Nichols is known (e.g., species density data). For each model, 150 datasets were generated with the fixed and random species effects independent and another 150 datasets were generated with confounding between the fixed and random species effects. To induce confounding between the fixed and random species effect, we expressed one covariate of the first species as a linear combination of the random species effects (i.e., $\boldsymbol{x}_1 = \boldsymbol{\Delta\theta}$).

Because the ratio of the random effects and random error magnitude is known to affect the severity of confounding in the spatial context [126, 130, 167], we varied the magnitude of the random species effect in each model while holding the random error magnitude constant. Specifically, each dataset was subdivided into thirds with 50 datasets simulated to have small, medium, and large random species effects relative to the random error.

All 900 simulated datasets across models and confounding levels were for $K = 2$ species across $n = 50$ sites with $J = 10$ occasions per site for the occupancy models. The correlation between the two species was allowed to vary for each dataset. Each habitat design matrix included an intercept and one continuous covariate. Each MCMC algorithm was run for a burn-in period of $L = 10000$ to ensure convergence. The next $L = 10000$ iterations were used to calculate the posterior quantities in Table 2.1. Code for performing the simulation study in `R` is available in the supplementary electronic files.

Table 2.1: Summary of simulations results. All results are averaged across 3 magnitudes of random species effects and 50 simulated datasets. ESS Ratio is the effective sample size of the restricted parameterizations over the unrestricted and the mean ESS is the average of the two. E $\left(R^2(\boldsymbol{x}_1)|\boldsymbol{Y}\right)$ is the posterior mean R^2 of confounding for species 1 continuous habitat covariate. Rejection rate is the portion of times the the posterior mean p-value from overall F-test of a linear relationship between $\boldsymbol{x}_1$ and $\boldsymbol{\Delta}$ was below 0.05.

Model	Data	$\boldsymbol{\beta}$ ESS Ratio	$\boldsymbol{\beta}$ Mean ESS	$\boldsymbol{\eta}$ ESS Ratio	$\boldsymbol{\eta}$ Mean ESS	E $(R^2(\boldsymbol{x}_1)|\boldsymbol{Y})$	Rejection Rate
Normal	Unconfounded	18.69	5143	6.20	5670	0.04	0.01
Normal	Confounded	8.67	4219	5.79	4800	0.51	0.87
Probit	Unconfounded	1.73	959	1.08	534	0.04	0.00
Probit	Confounded	1.96	444	1.23	293	0.19	0.63
Royle-Nichols	Unconfounded	0.81	232	0.98	307	0.04	0.00
Royle-Nichols	Confounded	0.80	186	0.98	301	0.18	0.51

For both $\boldsymbol{\beta}$ and $\boldsymbol{\eta}$, ESS was lower on average for the confounded data than the unconfounded data for all three models demonstrating the negative impacts confounding can have on model fitting. For all three models, the computational impact of fitting the restricted parameterization did not differ depending on whether confounding exists or not. In the case of the normal and probit models, fitting the restricted parameterization improved ESS for both $\boldsymbol{\beta}$ and $\boldsymbol{\eta}$, although the gains were much greater for the normal model. On the other hand, the restricted parameterization of the Royle-Nichols model did not improve ESS for $\boldsymbol{\beta}$ or $\boldsymbol{\eta}$. The success of our method for detecting community confounding differed across models. The method was most powerful for the normal model followed by the probit and Royle-Nichols models.

2.5 Camera Trap Survey

2.5.1 Study Area

We analyzed data arising from a study area comprised of subalpine forests in the state of Colorado between 2590 and 3660 m elevation (Figure 2.1). Sites were restricted to public lands managed by the United States Forest Service, National Park Service, Bureau of Land Management, and Colorado State Forest Service. Forests in our study area were primarily composed of Lodgepole pine (*Pinus contorta*), Engelmann spruce (*Picea engelmannii*), and subalpine fir (*Abies lasiocarpa*). Lodgepole pine was dominant at lower elevations as well as higher elevations that were drier and/or on south-facing slopes; high elevation regions that had cool north-facing slopes

were co-dominated by Engelmann spruce and subalpine fir. Lodgepole pine is restricted to the northern two-thirds of Colorado, so all sites in the southern region of the study area were Engelmann spruce, subalpine fir co-dominated. Quaking aspen (*Populus tremuloides*), Douglas-fir (*Pseudotsuga menziesii*), bristlecone pine (*Pinus aristata*), limber pine (*Pinus flexilis*), and blue spruce (*Picea pungens*) were also present at some sites. Mean July and January temperature across the study area were 14°C and -6.1°C respectively. All camera data were collected during summers 2013-2014.

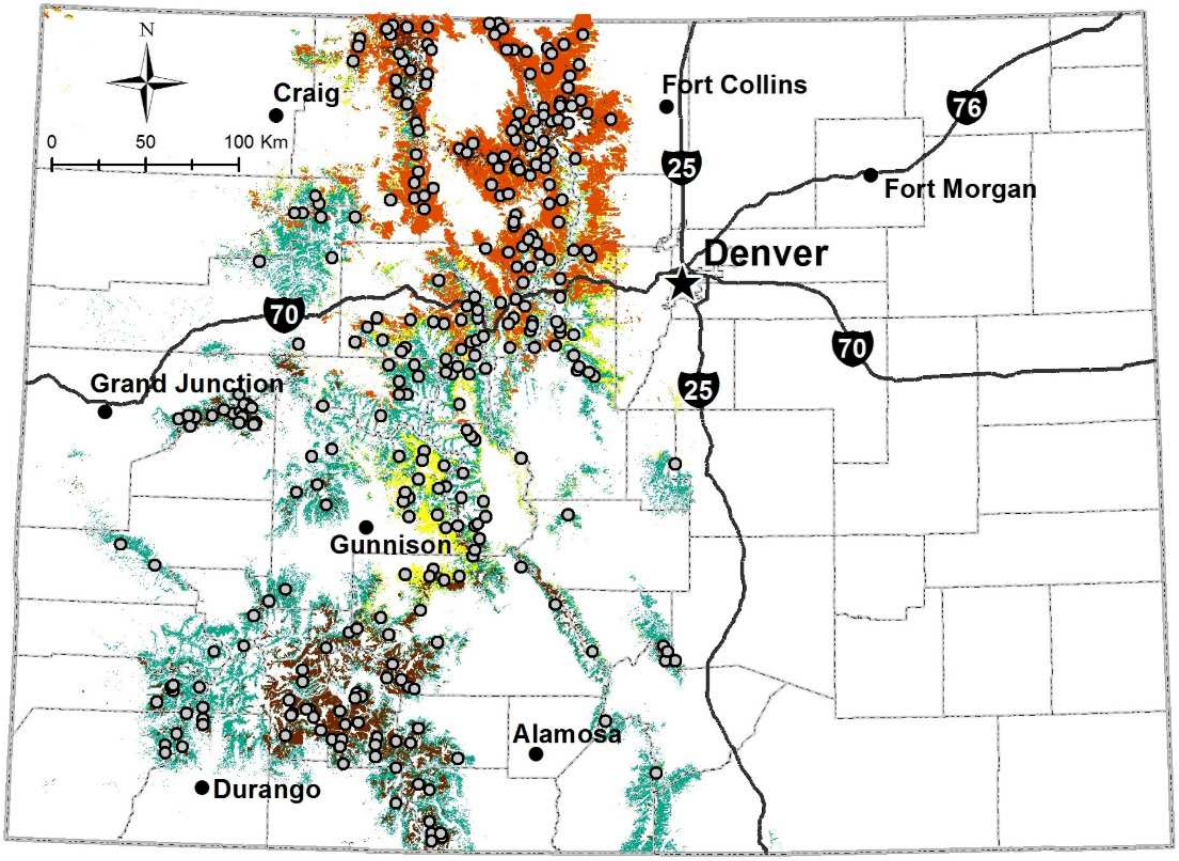

Figure 2.1: Randomly selected sampling sites (gray circles) where passive infrared game cameras were deployed in spruce-fir (green) and lodgepole pine (yellow) forests in Colorado, USA, 2013–2014. Brown and orange are the approximate extents of spruce beetle and mountain pine beetle impacts in spruce-fir and lodgepole pine forests, respectively, as of 2014. Reprinted from “Mammalian responses to changed forest conditions resulting from bark beetle outbreaks in the southern Rocky Mountains," by Ivan et al. [2]

2.5.2 Sampling Design

The primary goal of Ivan et al. [2] was to assess mammalian responses to bark beetle outbreaks, thus sites were randomly selected to facilitate inference on the beetle outbreak covariates. Beetle outbreak covariates included the number of years since the initial outbreak (YSO) and the severity of the outbreak measured by mean overstory mortality (severity). The sample of $n = 300$, 1 km^2 sites was evenly split across the two dominant forest types, spruce-fir and lodgepole pine. Additional environmental covariates were collected at each site, and a description of these is included in Appendix A.4.

Passive infrared camera traps (Reconyx PC800, Holmen, Wisconsin, USA) were deployed near the center of each site. Cameras were approximately 0.5 m above the ground and pointed toward a lure tree 4–5 m away [177]. The setup was designed to maximize detections of both large and small-bodied mammals in the local community while minimizing attraction of individuals from outside the sampling region of the site. The sampling regions were likely not closed to immigration/emigration; thus, we interpret elevated detections at a site as more individuals using, as opposed to occupying, that site [178]. For additional details regarding the sampling design and study area see Ivan et al. [2].

2.5.3 Model Fitting

We fit both the Royle-Nichols and probit occupancy models to the camera trap data binned into 20 two-day occasions because simulations showed this was the number of replications needed to identify a quadratic effect of occasion on individual detection probability. Not all cameras were operational for the entire 40 day sampling period, and thus the number of occasions varied from 7-20. We discarded four sites at which the camera was operational for less than one occasion. We also discarded another 12 sites that had been infested by bark beetles for more than 10 years. Ivan et al. [2] truncated the bark beetle infestation covariate at 10 years because estimates of response curves beyond 10 years would be unreliable with so few sites. The final sample size was $n = 284$ sites. We built distribution models for the 13 species for which Ivan et al. [2] performed a single

species analysis; several rare species were excluded from analysis due to insufficient detections. We note, however, that these rare species parameters may be identifiable in the joint model as has been the case in previous studies [179, 173, 150, 180, 181, 182]. Our final dataset then included 3692 unique encounter histories at $n = 284$ sites, stacked across $K = 13$ species.

Ivan et al. [2] used a sequential procedure similar to that described in Lebreton et al. [183] to select the covariates in the occupancy and detection processes for each species. We adopted their detection model and used the same covariates but a different set of basis functions for YSO. Ivan et al. [2] treated YSO as a grouping variable and considered probability of use response curves that allowed for cubic associations and delayed responses to bark beetle infestation. Multiple response curves were model averaged to produce predictive YSO response curves for each species. We used orthogonal polynomial basis functions for the YSO variable in the species intensity models. The basis functions included a linear (YSO1) and quadratic (YSO2) effect. Appendix A.4 provides a full description of the intensity and detection models. All continuous covariates were scaled to have mean 0 and variance 1.

We fit all models using MCMC. To improve mixing and predictive ability, we regularized the coefficients $\boldsymbol{\beta}$ and $\boldsymbol{\alpha}$ with informative priors: $\boldsymbol{\beta} \sim \mathcal{N}(\mathbf{0}, \boldsymbol{I})$ and $\boldsymbol{\alpha} \sim \mathcal{N}(\mathbf{0}, \boldsymbol{I})$ [162]. We specified a vague prior of $\boldsymbol{\Sigma}^{-1} \sim \text{Wishart}(15, (15\boldsymbol{I})^{-1})$ for the species variance-covariance matrix [184]. For the Royle-Nichols model, we used Gibbs sampling based on conjugate priors for parameters $\boldsymbol{\Sigma}_{spp}$, $\boldsymbol{\eta}$, and $\boldsymbol{\beta}$ and Metropolis-Hastings updates for $\boldsymbol{N}$, $\boldsymbol{\lambda}$, and $\boldsymbol{\alpha}$. Derivations of the conjugate full-conditional distributions are provided in Appendix B.2 with details about the Metropolis-Hastings updates. We tuned the Metropolis-Hastings updates so that acceptance rates varied between 20-40% for $\boldsymbol{\alpha}$, $\boldsymbol{N}$, and $\boldsymbol{\lambda}$. Using data augmentation [84, 81, 82, 83], all the parameters of the probit model can be sampled with Gibbs updates.

We set $\tau^2 = 2.25$ in both equations (2.9) and (2.13). This choice was supported by the asymptotic equivalence between Poisson and logistic regression. In a generalized occupancy model, the latent probability of occupancy is specified as $\text{logit}(\psi_i) \sim \mathcal{N}(\boldsymbol{x}_i'\boldsymbol{\beta}, \tau^2)$. Hanson et al. [185] investigated the relationship between the prior on $\boldsymbol{\beta}$ and induced prior on the latent probability of

success ψ_i in logistic regression; their work showed that specifying an uninformative normal prior on $\boldsymbol{\beta}$ (i.e., setting τ^2 large) induces a U-shaped prior for ψ_i with most of the density concentrated near 0 and 1. Broms et al. [157] recommended setting $\tau^2 = 2.25$ in occupancy models, which results in a relatively flat prior for ψ. For rare species, λ_i in equations (2.9) and (2.13) is analogous to ψ_i, and specifying a variance of $\tau^2 = 2.25$ is minimally informative.

Baddeley [186] motivated the asymptotic equivalence of Poisson and logistic regression in a spatial context where counts of points from a non-homogeneous Poisson process are recorded in a lattice; they showed that, as the grid cells of the lattice become infinitesimally small, the inference yielded from Poisson and logistic regression are equivalent. This result can be applied more generally to any dataset where there is a high proportion of zero counts. We demonstrate the asymptotic equivalence between Poisson and logistic regression in the Royle-Nichols model in Appendix A.3.

We ran the MCMC algorithm for $L = 50000$ iterations, and discarded the first 12500 iterations as burn-in. We fit an SDM, unrestricted JSDM, and restricted JSDM of both the Royle-Nichols and probit occupancy models. The *Results* section presents inference for regression coefficients for all six model fits.

2.5.4 Results

Ivan et al. [2] fit SDMs to infer changes in mammalian use of stands impacted by the bark beetle epidemic. The impact of bark beetle damage was measured by years since initial infestation (YSO) and severity of outbreak quantified by mean overstory mortality (DeafConif). The posterior distributions of the regression coefficients varied between the probit SDM and unrestricted JSDM, although the magnitude of difference differed by species (Figure 2.2). The posterior variances of the SDM regression coefficients were smaller than the unrestricted JSDM but also closer to zero. Posterior variances and means of the restricted probit JSDM regression coefficients quite similar to those from unrestricted JSDM. The only noticeable difference between the unrestricted and

restricted regression coefficients was that the restricted coefficients had slightly smaller posterior variances on average.

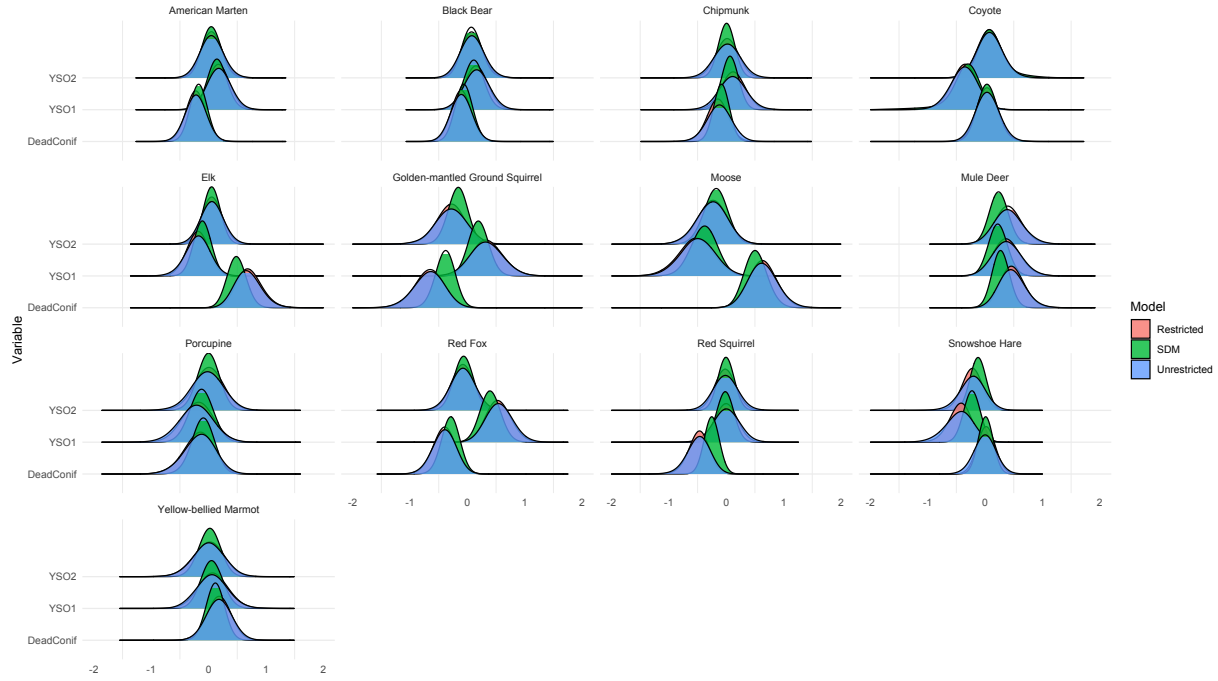

Figure 2.2: Marginal posterior distributions of infestation regression parameters. Posterior distributions shown are from the probit SDM, unrestricted JSDM, and restricted JSDM. DeadConif is the overstory mortality percentage, a proxy for severity of bark beetle infestation. YSO1 is the linear effect of the number of years since a site was infested with bark beetles. YSO2 is the quadratic effect. Figure created in R 4.1.2 [3].

As with the probit modeling results, posterior distributions of the regression coefficients in the Royle-Nichols SDM were more concentrated near zero than those of the JSDM (Figure 2.3). Also, posterior distributions of the restricted JSDM regression coefficients were slightly tighter and centered closer to zero.

We calculated the unrestricted and restricted posterior correlation matrices for both the probit and Royle-Nichols models. Pairwise differences between each entry of the posterior mean of the four correlation matrices were bounded between $(-0.2, 0.2)$, so only the correlation matrix of the unrestricted Royle-Nichols model is shown (Figure 2.4). The posterior distributions of the pairwise correlations all overlapped zero except for the pairwise correlations between coyotes and golden-

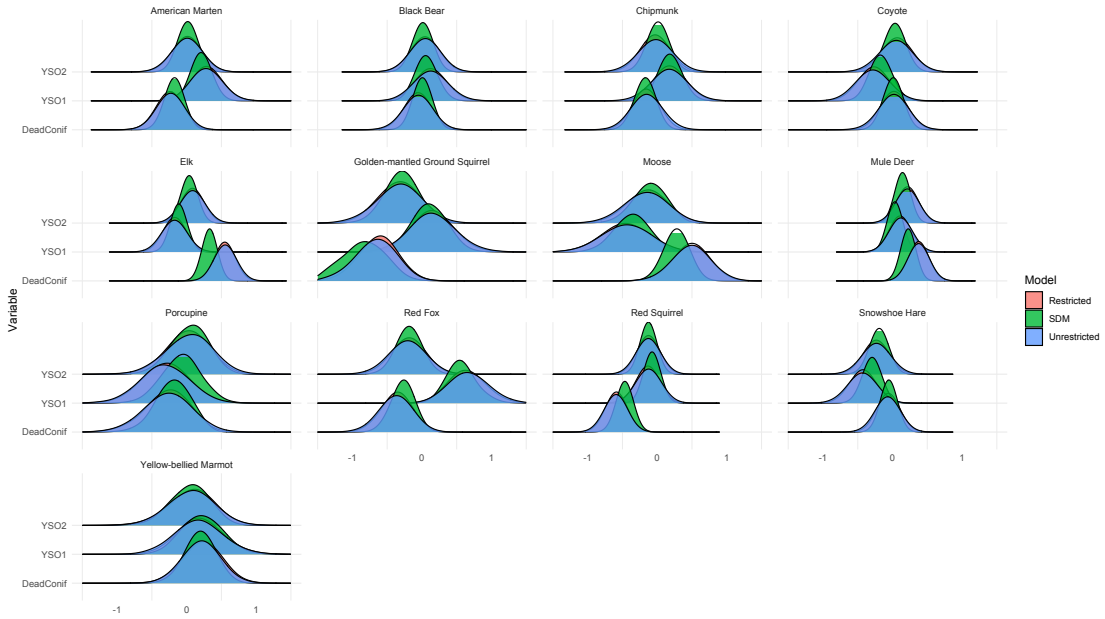

Figure 2.3: Marginal posterior distributions of infestation regression parameters. Posterior distributions shown are from the Royle-Nichols SDM, unrestricted JSDM, and restricted JSDM. DeadConif is the overstory mortality percentage, a proxy for severity of bark beetle infestation. YSO1 is the linear effect of the number of years since a site was infested with bark beetles. YSO2 is the quadratic effect. Figure created in R 4.1.2 [3].

mantled ground squirrels, coyotes and red squirrels, and golden-mantled ground squirrels and red squirrels. In the restricted probit JSDM, the correlations between coyotes and snowshoe hares, and snowshoe hares and red squirrels also did not overlap zero.

We calculated the posterior R^2 of confounding for each covariate in each species specific model as described in (2.20). All posterior R^2 were below 0.05 for both the Royle-Nichols and probit models giving no indication of community confounding for all covariates considered.

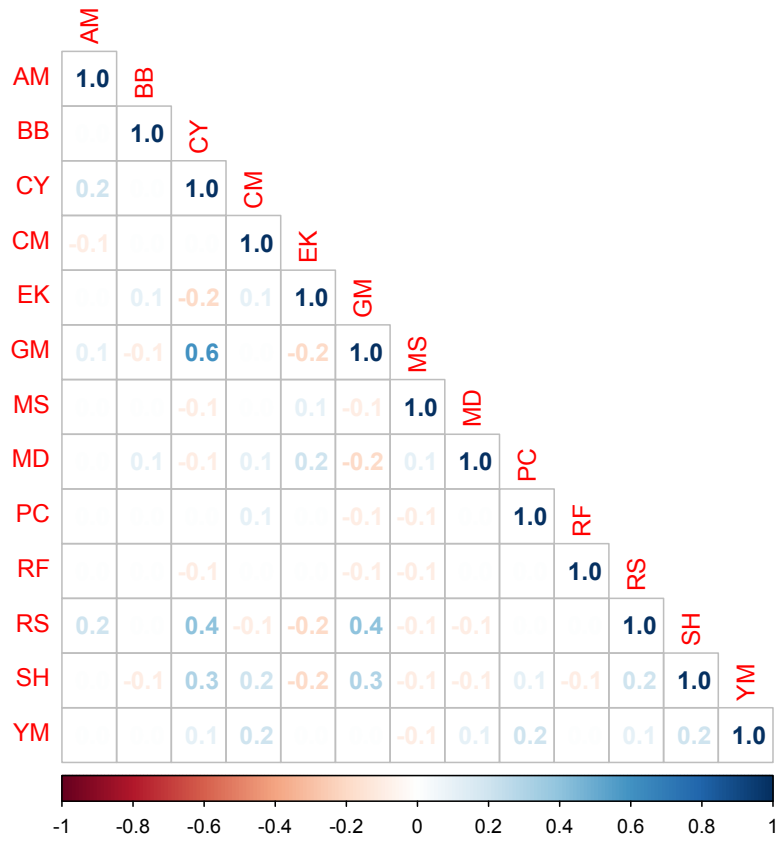

Figure 2.4: Posterior mean of species correlation matrix. Estimates are from the Royle-Nichols unrestricted joint species distribution model. AM = American Marten, BB = Black Bear, CY = Coyote, CM = Chipmunk spp., Ek = Elk, GM = Golden-mantled Ground Squirrel, MS = Moose, MD = Mule Deer, PC = Porcupine, RF = Red Fox, RS = Red Squirrel, SH = Snowshoe Hare, YM = Yellow-bellied Marmot. Figure created in R 4.1.2 [3].

2.6 Discussion

We found that confounding between the fixed and random species effects can reduce sampling efficiency in MCMC algorithms and that orthogonalizing the fixed and random species effects can alleviate this problem when fitting some joint species distribution models. In the simulation study, we discovered that, even when the data were not confounded, orthogonalizing the fixed and random species effects still conferred a computational benefit for the normal and probit model. This was also true for our case study where the mean effective sample size of the conditional habitat effects $\boldsymbol{\beta}$ in the probit model was 32% larger when fit with the restricted parameterization. The effective sample size of $\boldsymbol{\eta}$ in the probit model was 3% greater for the restricted parameterization.

The case study indicated that inference on species-environment associations in occupancy models can change based on whether the distribution model accounts for community structure. Orthogonalizing the fixed and random species effects in the probit and Royle-Nichols model slightly reduced but did not nullify the differences as in the case for normal data. The similarity between the restricted and unrestricted JSDM coupled with the lack of evidence for community confounding suggests additional mechanisms lead inference in SDMs and JSDMs to differ, a finding consistent with Caradima et al. [187]. Overall, there was still large agreement in posterior inference produced by the SDM and JSDMs for both occupancy models. In additional simulation studies on the probit and Rolye-Nichols occopancy models, we found that community confounding can lead to more large differences between the SDM and unrestricted JSDM and that the restricted JSDM again mitigates but rarely nullifies these differences.

We were also interested in whether the Royle-Nichols model could identify additional associations compared with the probit model. The Royle-Nichols model measures associations conditional on an intensity process rather than an occupancy, and intensity is likely a function of additional factors beyond those influencing occupancy [93, 94, 95]. For the camera trap data, the opposite was true, in that the probit model identified more environmental-species and species-species associations. One possible explanation for this is that the probit model is more parsimonious which sharpens posterior distributions.

A related method to restricted regression, which orthogonalizes the fixed and random effects, is principal components regression, which performs an orthogonalization procedure solely among the fixed effects. To motivate their similarities, consider a simpler case where the latent intensities, $\boldsymbol{\lambda}$, of the K species in our community were known. We could construct K regression models for predicting each species intensity as follows:

$$\boldsymbol{\lambda}_k = \boldsymbol{X}_k\boldsymbol{\beta}_k + \boldsymbol{\Lambda}_{-k}\boldsymbol{\eta}_k + \boldsymbol{\epsilon}, \tag{2.21}$$

where $\boldsymbol{\Lambda}_{-k} = (\boldsymbol{\lambda}_1, \ldots, \boldsymbol{\lambda}_{k-1}, \boldsymbol{\lambda}_{k+1}, \ldots, \boldsymbol{\lambda}_K)$ is a matrix of the $K-1$ other species intensities. If $\boldsymbol{X}_k$ and $\boldsymbol{\Lambda}_{-k}$ were highly collinear, principal component regression might be applied. Principal components regression is so named because it decomposes the variation explained by $\boldsymbol{X}_k$ and $\boldsymbol{\Lambda}_{-k}$ into $p = p_1 + p_2$ principal components, $\boldsymbol{\Gamma}_k = (\boldsymbol{\gamma}_1, \ldots, \boldsymbol{\gamma}_p)_k$, where p_1 and p_2 are the number of columns of $\boldsymbol{X}_k$ and $\boldsymbol{\Lambda}_{-k}$ respectively. The p principal components retain all the information explained by $\boldsymbol{X}_k$ and $\boldsymbol{\Lambda}_{-k}$ but are orthogonal. The regression model

$$\boldsymbol{\lambda}_k = \boldsymbol{W}_k\boldsymbol{\theta} + \boldsymbol{\epsilon}, \tag{2.22}$$

$$\boldsymbol{W}_k = (\boldsymbol{X}_k, \boldsymbol{\Lambda}_{-k})\,\boldsymbol{\Gamma}_k, \tag{2.23}$$

often improves sampling efficiency and can recover the posterior means and variances of $\boldsymbol{\beta}_k$ and $\boldsymbol{\eta}_k$ in equation (2.21). However, inference on $\boldsymbol{\beta}_k$ and $\boldsymbol{\eta}_k$ is often adjusted by truncating off the last $p - r$, for $r < p$, eigenvectors of $\boldsymbol{\Gamma}_k$ and employing the new design matrix

$$\boldsymbol{W}_k^\star = (\boldsymbol{X}_k, \boldsymbol{\Lambda}_{-k})\,\boldsymbol{\Gamma}_k^\star, \tag{2.24}$$

$$\boldsymbol{\Gamma}_k^\star = (\boldsymbol{\gamma}_1, \ldots, \boldsymbol{\gamma}_r)\,. \tag{2.25}$$

By retaining only the first r principal components, the smallest sources of variation are ignored in the estimation of $\boldsymbol{\beta}_k$ and $\boldsymbol{\eta}_k$. Jeffers [188] implemented this approach truncating off the last 7 of 13 principal components to adjust the estimates of regression coefficients relating various tree characteristics to maximum compressive strength. Other studies have selected a subset of principal components based on their strength of association with the response variable [189, 190, 191, 192]. In some cases, the coefficient estimates from these reduced rank approaches appeared more tenable than those from the full rank specifications based on known physical relationships between the predictors and response. Thus, like restricted regression, principal components regression can used for solely computation purposes or to adjust inference.

Recently, concerns regarding the coverage properties of the fixed effects estimator under restricted regression have been expressed [128, 129]. For example, Zimmerman and Ver Hoef [129] showed that applying any restricted regression method to a SGLMM leads to frequentest coverage of the fixed effects that is lower than the corresponding non-spatial model. Similarly, Khan and Calder [128] found that when fitting a restricted version of the SGLMM with an intrinsic conditional autoregressive prior, credible intervals of the fixed effects from the restricted model were generally nested inside those yielded by the non-spatial model. Given these results, both Zimmerman and Ver Hoef [129] and Khan and Calder [128] recommended reverting to inference from the non-spatial model, rather than that of the restricted SGLMM, when inference from the unrestricted SGLMM appears untenable.

We did not observe the same pattern in our restricted JSDM but found the length of credible intervals of the restricted regression coefficients to generally be between that of the SDM and unrestricted JSDM. Nonetheless, if higher coverage is desired, one can always extract the conditional coefficients from the restricted JSDM while still benefiting from the increased stability that results from orthogonalizing the fixed and random effets. When deciding between inference from the restricted and unrestricted JSDM, one should also consider the random species effects $\boldsymbol{\eta}$. Because the random effect $\boldsymbol{\eta}$ is rarely of interest in spatial applications, there has been little investigation on

the inferential impacts of restricted regression on $\boldsymbol{\eta}$. Such investigation, however, may be helpful in determining the appropriateness of restricted regression for JSDMs.

There are several conceptual facets to consider regarding the applications of restricted regression in joint species distribution modeling. Frequently, JSDMs are described as accounting for residual correlations between species that cannot be explained by the environmental covariates [17, 187, 89]. We have shown, however, that in some JSDMs, the random species effect can explain variation that is collinear with environmental covariates. Only in the restricted JSDM, does the random species effect explain variation that is residual to the environmental covariates attributing all contested sources of variation to the fixed effect. Yet, given that species environmental requirement can fluctuate based on their symbiotic relationships, one might argue that interplay between the environmental effects and interspecies dependence is ecology warranted. Therefore, any method that removes the conditional nature of these effects like restricted regression is inappropriate.

JSDMs have been described as correcting our knowledge of species-environment relationship by accounting for interspecies dependence [17]. Poggiato et al. [17] argued that JSDMs help us better quantify uncertainty regarding species-environment relationships, but they cannot explain discrepancies in a species theoretical and realized niche. We agree that phenomenological JSDMs should not be used to disentangle the marginal effects of environment and interspecies dependence on species distributions and would recommend the development of mechanistic models to investigate interspecies-environment associations.

Experimental methods and modeling techniques for alleviating confounding have been proposed in ecology. Hefley et al. [72] showed that replicate populations can help disentangle confounded fixed and random effects. In the context of joint species distribution modeling, replication involves analyzing several communities simultaneously, which is often infeasible. Hefley et al. [72] also recommended explicit population models rather than phenomenological regression-based models for analysis of temporally confounded count data. Similarly, Fieberg et al. [71] advocated for mechanistic models guided by causal diagrams for analyzing temporally confounded animal

movement data. An avenue of future research for joint species distribution modeling is to compare inference from phenomenological regression-based models, such as the one proposed here, with that of models that explicitly include ecological mechanisms such as competitive exclusion, mutualism, and predation. Because community and temporal confounding have the same mathematical framework, mechanistic models are a promising solution for confounded multispecies data.

In summary, we specified a JSDM that accounts for interspecies dependence at the intensity level, and examined how inference from the joint model differed from the joint probit model. We performed a simulation study on three JSDMs to examine the computational difficulties associated with community confounding and investigated whether orthogonalizing the fixed and random species effect could alleviate these difficulties. Further, we considered how inference in both occupancy models differed depending on the assumed community structure. Lastly, we discussed how joint species distribution modeling is distinct from spatial and time series applications in that the random effect is almost always of inferential interest, and hence, adjustments to the regression coefficients, $\boldsymbol{\beta}$, and random effects, $\boldsymbol{\eta}$, should both be considered. Our main conclusion is that, even for researchers who desire inference solely on the conditional relationship between the fixed species-environment and random species effects, fitting the JSDM with a restricted parameterization can give computational benefits.

Chapter 3

Melding Wildlife Surveys to Improve Conservation Inference

3.1 Introduction

Integrated models that allow for the unified analysis of multiple datasets have been described as integrated analysis [31], integrated distribution models [102], shared parameter models [32], joint models [33], Markov combination [103], Bayesian melding [104], data assimilation [34], data reconciliation [105], and data fusion [35] and have applications in econometrics, biostatistics, conservation biology, atmospheric sciences, and oceanography. The joint likelihood of integrated models conditions multiple datasets on link parameters in a way that can often improve predictive performance and parameter precision [38].

Markov combination [103] facilitates joint inference on a link parameter expressed in several submodels but is not applicable when the prior marginal distributions of the link parameter differ across submodels. Goudie et al. [123] introduced Markov melding for combining related submodels that have differing marginal distributions for the link parameter. In this setting, the joint model is constructed through marginal replacement, where the prior marginal distributions for the link parameter across submodels are replaced with a common pooled prior marginal distribution. Markov melding facilitates joint inference on a link parameter in one submodel that can be expressed as non-invertible functions of other submodel parameters. For example, suppose we have submodels for learning about adult and juvenile survival, but we are interested in learning about aggregate survival, which is a weighted average of the two. Markov melding uses marginal replacement to form a melded posterior distribution for the link parameter that accounts for its implied prior and likelihood in each submodel. Recently, Manderson and Goudie [64] proposed chained Markov

melding, an extension that facilitates joint inference for a sequence of submodels connected by multiple link parameters.

The earliest applications of integrated modeling frameworks in the context of wildlife management arose in fisheries science [106], but wide adoption of the framework in the broader fields of conservation biology and ecology began in the early 2000s [31, 193]. In particular, integrated population models (IPMs), which are an application of integrated models, have been used to understand population dynamics for species of conservation concern [38, 193]. Despite the success of IPMs, few other integrated modeling approaches have been proposed in conservation biology. One persistent challenge is the lack of spatial and temporal conformity across datasets. Additional methodological challenges include differences in the quantity or observational uncertainty of the data sources, and sampling bias in one or more datasets [102, 194, 36]. Such challenges are encountered when developing integrated models for species of conservation concern (SCC) because of their elusiveness, restricted range, or small population size [195].

We developed an integrated model that facilitates joint inference of aerial and ground surveys of LEPC, an SCC that has experienced range and population declines since the 1980s [56, 57, 59]. Joint modeling of these data is challenging because LEPC are simultaneously monitored by several entities who operate independently in different regions. As a result, the surveys vary in their spatial and temporal resolutions, sample size, and observational uncertainties. Additionally for some surveys, LEPC were preferentially sampled in regions presumed to have high abundances which may bias inference [196].

We facilitated shared inference of multiple LEPC surveys by chained Markov melding [64] density estimates derived from submodels describing the observation processes of the aerial and ground surveys into a joint response model. Melding refines the submodel density estimates to those that agree with the spatio-temporal patterns observed in both surveys. By joining the submodels through derived quantities, we addressed the differences in the spatial and temporal scales of the surveys. Accommodating these differences in scales with a traditional integrated model is difficult because density is a non-invertible function of submodel parameters. Our modeling ap-

proach attenuated the impacts of potential sampling biases and accounted for the distinct sources of observational error so that all data sources can be assimilated to improve predictive performance. Lastly, the Markov melding approach improved computation by enabling submodel specific data augmentation techniques and avoiding high-dimensional parameter updates by fitting the integrated model in stages.

The paper is organized as follows. In Section 3.2, we provide a brief history of LEPC conservation and discuss current needs for informing management. Section 3.3 details the sampling protocols of the aerial (3.3.1) and ground (3.3.2) surveys. Section 3.4 describes submodels accounting for the observation process of each survey and a joint response model for linking inference across surveys. In Section 3.5, we describe the Markov melding techniques used to facilitate posterior inference for our integrated model. Section 3.6 includes the results our simulation study and LEPC abundance analysis. Section 3.7 concludes with a discussion of our findings.

3.2 Lesser prairie-chicken Conservation

The LEPC is a member of the family Phasianidae and is indigenous to the southern Great Plains of the United States. Like other species in its family, the LEPC has experienced range and population declines since the 1980s primarily due to habitat loss, degradation, and fragmentation [56, 57, 59], but curtailment of natural fires, overgrazing, and climate change have also contributed [58].

We studied spatio-temporal patterns in LEPC abundance across the state of Kansas because an estimated 70% of the total LEPC population resides in the state [60]. Our modeling approach, however, can accommodate data sources from the other states in the LEPC range. In Kansas, LEPC inhabit Sand Sagebrush Prairie (SSPR), Mixed Grass Prairie (MGPR), Shortgrass Prairie/Conservation Reserve Program Mosaic (SGPR) ecoregions, which cover the southwest, southeast, and northern regions of western Kansas respectively.

Recently, the United States Fish and Wildlife Service listed the LEPC for federal protections under the Endangered Species Act [55]. The Northern Distinct Population Segment, which encom-

passes the SSPR, MGPR, and SGPR ecoregions, is categorized as threatened. Improved estimation of spatio-temporal population change, especially range-wide, would help inform conservation practices for the species [60].

Population monitoring of LEPC relies on spring counts of individuals on leks [61]. A lek is an aggregation of males defending a small territory and communally calling and performing displays to attract and mate with females [58]. Leks are generally located in sparse vegetation on hilltops and ridgelines and commonly include more than 10 individuals which makes detection by audio and visual cues of the otherwise cryptic individuals easier [58].

Historically, LEPC populations have been monitored using counts of individuals at leks from ground surveys conducted by state wildlife agencies. Lack of spatial randomness in the ground surveys, however, makes inferring species-habitat associations difficult and density estimates imprecise and potentially biased [196]. Since 2012, several entities have collectively supported annual range-wide aerial surveys of LEPCs. The aerial surveys follow a spatially random sampling design and have thereby improved range-wide density estimates [61, 197]. Two drawbacks of the aerial surveys is that they encounter fewer individuals per unit of area searched and have higher operating costs. These limitations have led managers to consider integrated models that could leverage ground survey data and reduce reliance on aerial surveys.

Over the last two decades, there have been numerous studies related to LEPC conservation but few have assimilated multiple data sources due to the methodological challenges described by Zipkin et al. [36]. Ross et al. [63] developed an IPM for assimilating count, survival, and fecundity data that suggested observed declines in LEPC abundance following droughts [198] were driven by higher juvenile and chick mortality. The findings of Ross et al. [63] prompted managers to consider habitat improvements that focus on increasing and maintaining grasslands that can buffer the population against the harmful effects of severe drought. By melding available data sources, we improve spatio-temporal density estimates and facilitate prediction at unsampled regions to identify vulnerable populations and prioritize landscapes for conservation action. Our

approach can also quantify the inferential cost and reduced predictive performance associated with less frequent aerial surveys. In what follows, we describe the aerial and ground survey protocols.

3.3 Survey Protocols

3.3.1 Aerial

The Kansas estimated occupied range (EOR) for LEPC was partitioned into $n^A = 299$, $15 \times 15 = 225$ km^2, survey blocks [61]. A spatially random subset of blocks were selected for sampling, and the subset selected differed by year (Figure 3.1). No blocks were surveyed in 2019. Two

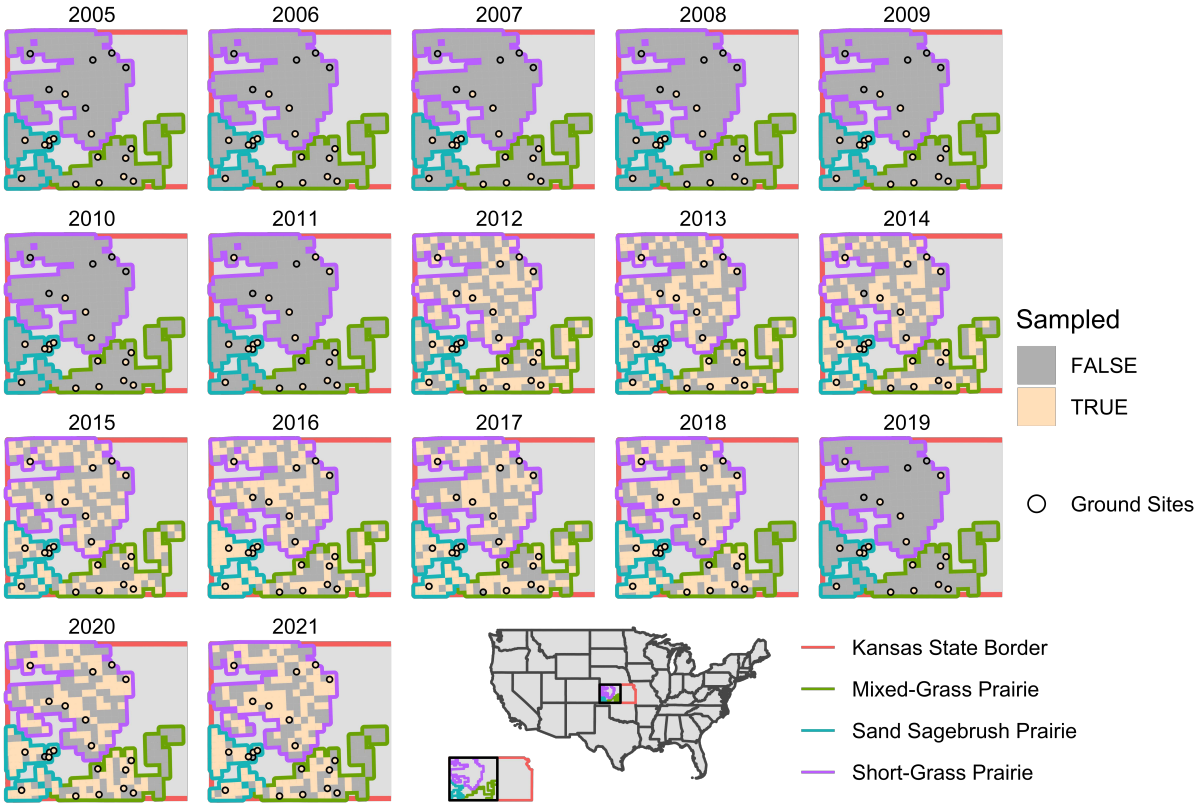

Figure 3.1: Map of Kansas lesser prairie-chicken aerial survey blocks and Kansas Department of Wildlife and Parks ground monitoring sites. Golden fill indicates the block/site was sampled during that year. The region encompassed by all three ecoregions in the map is Kansas estimated occupied range.

north-south oriented, 15-km transects were surveyed by helicopter in blocks selected for sampling. Selected transects were surveyed once during the LEPC breeding season (March 15-May 15) and

within 0.5 hours prior to and 2 hours after sunrise to maximize detection of individuals present at leks. The helicopter was operated by one pilot and three observers. As the pilot flew at a speed of 60 km per hour and altitude of 25 meters above ground, observers attempted to visually locate prairie-chicken. When one or more prairie-chicken were located, the pilot navigated to the location and recorded the geographic coordinate and number of individuals observed. For an in-depth description of the aerial survey protocol and design, see Nasman et al. [197] and Van Pelt et al. [60].

3.3.2 Ground

Kansas Department of Wildlife and Parks (KDWP) preferentially located 21 ground survey routes for monitoring LEPC in representative, high quality LEPC habitat across Kansas EOR. Each route was approximately 16 km long and the ground survey attempted to census all leks within 1.6 kilometers of the road for a region of approximately 51.2 km^2. Routes were surveyed (March 20-April 20) and within 0.5 hours prior to and 1.5 hours after sunrise.

All routes were surveyed at least twice per year in two parts. First, the listening portion of the route was conducted; leks were audibly detected and their locations approximated, but not confirmed. On the same morning, the surveyor navigated to each lek detected, prompted the individuals to take flight (flushed), and recorded the count of individuals and location. Surveyors also revisited sites at which leks were previously recorded because LEPC are known to return to historical lek sites [58]. The ground survey is a census of the leks in the survey area but it is not a census of the population because some individuals may not be present at their lek at the time it was flushed.

3.4 Methods

In northwestern Kansas, the LEPC EOR overlaps with the range of its sister species the greater prairie-chicken (*Tympanuchus cupido*; hereafter GEPC). Species verification was sometimes infeasible for the aerial and ground surveys and observations of GEPC are included in both datasets.

We proposed distance sampling (Section 3.4.1) and N-mixture (Section 3.4.2) submodels that analyzed counts of prairie-chicken (LEPC and GEPC). We then derived the block-level densities of LEPC in northwestern Kansas by multiplying the combined LEPC and GEPC density estimates by known LEPC proportions (Section 3.4.3). The spatio-temporal submodel assimilates the LEPC density estimates derived from the other two submodels in a joint response that induced the integrated model. The integrated model accounted for the uncertainty in both datasets, the underlying ecological processes, and the parameters.

3.4.1 Aerial Distance Sampling Submodel

We developed a distance sampling model to describe the observational uncertainty associated with aerial surveys of prairie-chickens. We let v_{itl} represent the number of observers who detected group $l = 1, \ldots, L_{it}^A$ in sampling region $i = 1, \ldots, n^A$ during year $t = 1, \ldots, T^A$. Assuming all observers had equal skill in detecting prairie-chicken groups and observers detected the groups independently, a model for v_{itl} is

$$v_{itl} \sim \text{Binomial}(B_{itl}, \rho_{itl}), \tag{3.1}$$

where B_{itl} is the total number of observers for which group l was visible and ρ_{itl} is the observer detection probability for group l, assumed to be identical for all observers. The visibility of group l to each observer depended on their distance from the transect, d_{itl}, and side of the transect, ϵ_{itl} ($\epsilon_{itl} = 1$ indicates group on left side). Groups more than 7 meters left of the transect were visible to both the front and rear left-hand side observers; groups within 7 meters of the transect were only visible to the front left-hand side observer; and groups more than 7 meters right of the transects were only visible to the right-hand observer. Hence, $B_{itl} = 2$ for $\epsilon_{itl} = 1$ and $d_{itl} > 7$, but $B_{itl} = 1$ otherwise. Detected prairie-chicken groups were announced only after they were out of view for all observers to ensure independent detections.

We modeled the detection probability of group l, ρ_{itl}, as a function of the group's distance from the transect at detection, d_{itl}, count of individuals at detection, N_{itl}^A, and ecoregion, such that

$\text{logit}(\boldsymbol{\rho}) = \left(\boldsymbol{X}_\rho, \boldsymbol{N}^A, \boldsymbol{d}\right)\boldsymbol{\beta}_\rho$, where $\boldsymbol{X}_\rho$ is a binary matrix with unique intercepts for each ecoregion, and $(\cdot)$ denotes a column-wise bind of the listed matrices. The regression model provides additional flexibility for estimating the detectability of prairie-chicken groups, and the entries of $\boldsymbol{\beta}_\rho$ are identifiable under the double observer design [199]. We treat detections of the two left-hand observers as fully independent but alternative approaches that allow for dependence in detectability as a result of unmeasured covariates and animal movement have been proposed [200, 201]. Under our modeling framework, we assume that heterogeneity in prairie-chicken group detectability is well characterized by distance from the transect and size of the group. We also assumed groups are stationary, but note that there were a small number of transiting individuals.

Some groups for which $v_{itl} = 0$ were not in the dataset because they went undetected. To account for these missed individuals, we employed a parameter expanded data augmentation (PX-DA) approach [134]. Specifically, we augmented the dataset with many undetected groups and let $z_{itl} \in \{0, 1\}$ indicate whether group l belonged to the sample population of groups in region i. If a group was detected (i.e., $v_{itl} > 0$), then it must be part of the sample population in region i (i.e., $z_{itl} = 1$).

For undetected groups, z_{itl}, N^A_{itl}, d_{itl}, and ϵ_{itl} were all unknown and hence estimated. To denote the observed and unobserved components of partially latent parameters, we use the superscripts o and u, respectively. Heuristically, we conceptualize the model as proposing groups of prairie-chicken that the aerial survey may have missed; we proposed a group of prairie-chicken with count $N^{A,u}_{itl}$, distance from the transect d^u_{itl}, and on side ϵ^u_{itl} of the transect, and then used the observations from our detected groups (i.e., $\boldsymbol{N}^{A,o}$, $\boldsymbol{d}^o$, $\boldsymbol{\epsilon}^o$) to determine if group l could have been part of our sample population (i.e., $z^u_{itl} = 1$) but went undetected (i.e., $v_{itl} = 0$). We chose the prior distributions for d_{itl} and ϵ_{itl} to induce a uniform distribution of groups within the survey region. See Appendix B.1.1 for a full description of prior distributions. Royle et al. [134] referred to the total number of both observed and unobserved groups as the super-population, and the size of the super-population, M, must be specified *a priori*. Appendix B.2 discusses recommendations for choosing M. We calculate the total number of groups in the sample population of region i during

year t as the derived quantity $L_{it}^A = \sum_{l=1}^{M} z_{itl}$. Note that in this data augmentation framework L_{it}^A includes the detected groups as well as groups that may have existed in the survey region but went undetected.

The aerial survey was conducted during the breeding season to maximize detection of leks, but smaller, non-lekking groups as well as individual prairie-chicken were also detected. We accounted for the occurrence of lek and non-lek observations in the observed prairie-chicken counts using a zero-truncated Poisson (ZTP) mixture model

$$N_{itl}^A \sim \begin{cases} \text{ZTP}(\lambda_{it}), & \text{for } \omega_{itl} = 1 \\ \text{ZTP}(\lambda_0), & \text{for } \omega_{itl} = 0 \end{cases}, \tag{3.2}$$

$$\omega_{itl} \sim \text{Bernoulli}(p_\omega), \tag{3.3}$$

where ω_{itl} is the indicator of whether group l is a lek, λ_{it} is the mean number of individuals per lek in region i during year t, and λ_0 is the homogeneous mean number of individuals for non-lek observations. Both distributions in the Poisson mixture, equation (3.2), are zero-truncated because if a group exists, it must have ≥ 1 individuals.

We treated ω_{itl} as a latent variable because it was often infeasible to determine the lek status of a prairie-chicken group from the air. For monitoring purposes, KDWP defines a lek as 3 or more individuals on a display site [202]. In our case, the latent lek indicators ω_{itl} accommodated the bimodality of the count data and carried fewer assumptions regarding the composition of a lek.

Mean lek size varies temporally and with environmental factors [6, 57]. We specified a heterogeneous mean lek size across sites i and years t, λ_{it}, which we modeled with covariates (i.e., $\log(\boldsymbol{\lambda}) = \boldsymbol{X}_\lambda \boldsymbol{\beta}_\lambda$). The design matrix $\boldsymbol{X}_\lambda$ includes unique intercepts for each ecoregion and additional continuous covariates. The covariates capture heterogeniety in mean lek size related to landcover, habitat patch size, anthropogenic disturbance, and climatic stochasticity. See Appendix B.3 for a description of all covariates, and how they were collected.

We specified a binomial model to account for variability in the number of prairie-chicken groups such that

$$L_{it}^{A} \sim \text{Binomial}(M, \psi_{it}), \tag{3.4}$$

where ψ_{it} is the probability that a group belonged to the sample population of region i during year t. The parameter ψ_{it} controls the number of prairie-chicken groups within a region, with greater ψ_{it} implying more groups. Heterogeneity in prairie-chicken use of habitat within the EOR has also been documented [203], motivating the logit model, $\text{logit}(\boldsymbol{\psi}) = \boldsymbol{X}_{\psi}\boldsymbol{\beta}_{\psi}$. We chose the same suite of covariates for explaining heterogeneity in the number of groups as those used for explaining lek size (i.e., $\boldsymbol{X}_{\psi} = \boldsymbol{X}_{\lambda}$).

We specified diffuse exchangeable Gaussian priors for the regression coefficients $\boldsymbol{\beta}_{\rho}$, $\boldsymbol{\beta}_{\lambda}$, and $\boldsymbol{\beta}_{\psi}$. We used a vague $\text{Uniform}(0, 1)$ prior for the proportion of prairie-chicken groups that are leks, p_{ω}, and an informative $\text{Gamma}(1.78, 0.675)$ prior for the mean number of individuals for non-lek observations λ_0. A full description of the priors is provided in Appendix B.1.1.

3.4.2 N-mixture Submodel

We developed a submodel for describing observational uncertainty in KDWP prairie-chicken ground surveys. We let F_{itlj} denote the ground count of male prairie-chicken on occasion j at lek site l in sampling region i during year t. To account for variability in the counts induced by imperfect male lek attendance, we adopted a N-mixture model [204],

$$F_{itlj} \sim \text{Binomial}(N_{itl}^{G}, p) \text{ for } j = 1, \ldots, J_{itl}, \tag{3.5}$$

where p represents the homogeneous probability that a male belonging to lek site l was present at the lek when it is surveyed. We assumed a Poisson model for the latent lek abundances, $N_{itl}^{G} \sim \text{Poisson}(\exp(\boldsymbol{w}_{it}'\boldsymbol{\eta}))$, where $\boldsymbol{w}_{it}$ is the same set of covariates used in the aerial model but with unique measurements because the aerial and ground sample regions differed. Note that

zero abundances, $N_{itl} = 0$, were possible because surveyors revisited historical lek sites that may not have been visited by any individuals in year t. It follows that $\exp(\boldsymbol{w}_{it}'\boldsymbol{\eta})$ is the expected number of individuals per lek site rather than the expected number of individuals per active lek, and the regression coefficient $\boldsymbol{\eta}$ dictates the relationship between the expected number of individuals at a lek site and the covariates associated with that lek site. We specified a diffuse exchangeable Gaussian prior for $\boldsymbol{\eta}$ and a vague Uniform$(0, 1)$ prior for the male lek attendance probability p (see Appendix B.1.2 for more details of the prior specification).

3.4.3 Integrated Model

We induced an integrated model for the aerial and ground surveys by specifying a spatio-temporal submodel that couples the survey specific density estimates in a joint response. While density is not a parameter in either the aerial distance sampling submodel (ADSM) or N-mixture submodel, each submodel includes density as a derived quantity. For the ADSM, samples of block-level LEPC density in the aerial lattice are obtained by

$$y_{it}^A = f(\boldsymbol{N}_{it}^{A,o}, \boldsymbol{z}_{it}^o, \boldsymbol{N}_{it}^{A,u}, \boldsymbol{z}_{it}^u) = \sum_{l=1}^{M} N_{itl}^A z_{itl} \kappa_i / S^A, \tag{3.6}$$

where S^A is the prespecified area of the sampling region (Appendix B.2) and κ_i is the proportion of LEPC in sampling region i [5]. Proportions vary from 0.001-1 for blocks in the SGPR but equal 1 for all blocks in the MGPR and SSPR. Likewise, for the N-mixture submodel,

$$y_{it}^G = g(\boldsymbol{N}_{it}^G) = \sum_{l=1}^{L_{it}^G} 2 N_{itl}^G \kappa_i / S_i^G, \tag{3.7}$$

where S_i^G is area of survey route i, L_{it}^G is the number of lek sites at site i in year t, and the 2 assumes equal sex ratios in the LEPC population [205]. Equation (3.7) also assumes no females were present at the time the lek site was flushed which is a common assumption but could lead to inflated estimates of y_{it}^G. Both y_{it}^A and y_{it}^G are unobserved because they are functions of, at least partially, unobserved submodel parameters.

Given the annual density estimates for the $n^A = 299$ aerial blocks arranged in a lattice as well as the $n^G = 21$ ground survey routes (Figure 3.1), we proposed a joint response model for annual density at the $n^A + n^G = 320$ sampling regions. Omitting the superscripts A and G, we let y_{it} represent the density of LEPC in sampling region i during year t. Because some sampling regions can have a LEPC density of exactly zero, we considered the following tobit model [131]:

$$y_{it} = \begin{cases} \zeta_{it}, & \text{for } \zeta_{it} > 0 \\ 0, & \text{for } \zeta_{it} \leq 0 \end{cases}, \tag{3.8}$$

$$\boldsymbol{\zeta}_t \sim \mathcal{N}(\boldsymbol{\xi}_t, \sigma_d^2 \boldsymbol{R}_d(\phi)). \tag{3.9}$$

Tobit models are often used in the context of censoring where the true state of interest, $\boldsymbol{\zeta}_t$, is only observable in a certain range. Our density data were not censored explicitly, but the tobit model accounted for the mixture of discrete and continuous components in the response and promoted conjugacy of the latent states ζ_{it} and ξ_{it}. Both ζ_{it} and ξ_{it} may be viewed as the latent density of LEPC in a region with negative values indicating the relative probability that the density is zero. To account for spatial structure, we assumed an exponentially decaying correlation matrix $\boldsymbol{R}_d(\phi)$, where the entry in the ith row and jth column is defined as $r_d(i, j, \phi) = \exp(-d_{ij}/\phi)$, d_{ij} is the Euclidean distance between sampling regions i and j in meters, and ϕ is the spatial range parameter.

We accounted for temporal dependence by specifying autoregressive random effects in (9)

$$\boldsymbol{\xi}_t \sim \mathcal{N}((\boldsymbol{\xi}_{t-1}, \boldsymbol{W}_{t-1})\,\boldsymbol{\alpha}, \boldsymbol{\Sigma}_\tau), \tag{3.10}$$

where $\boldsymbol{W}_{t-1}$ is a matrix of covariates measured across all sampling regions in year $t-1$, and we modeled the initial state as $\boldsymbol{\xi}_0 = \boldsymbol{X}_0\boldsymbol{\gamma}$. Many environmental factors known to be associated with LEPC density were constant over the $T = 17$ years considered in our analysis, and so the set of covariates used in $\boldsymbol{W}_t$ is reduced from those in $\boldsymbol{X}_0$ (see Appendix B.3). In addition to the

landcover and climatic covariates used in the ADSM and N-mixture submodel, we also included a binary covariate that indicated whether a survey block or ground site was north of Interstate 70. LEPC to GEPC ratios decrease sharply north of Interstate 70 [5], and the binary covariate was helpful for explaining spatial heterogeneity in LEPC density that was difficult to characterize with the other covariates. We considered a block diagonal structure for $\boldsymbol{\Sigma}_\tau$ with distinct covariance matrices $\sigma_\tau^{2,A}\boldsymbol{R}_\tau^A$ and $\sigma_\tau^{2,G}\boldsymbol{R}_\tau^G$ for the aerial and ground survey regions, respectively. We let $\boldsymbol{R}_\tau^A = (\text{diag}(\boldsymbol{A}\mathbf{1}) - \rho\boldsymbol{A})^{-1}$, where $\boldsymbol{A}$ is the adjacency matrix from the aerial survey lattice, which has entries $a(i,j) = 1$ if blocks i and j are neighboring and $a(i,j) = 0$ otherwise, and $\text{diag}(\boldsymbol{A}\mathbf{1})$ denotes the diagonal matrix of the row sums of $\boldsymbol{A}$. We specified $\rho \to 1$ to induce an intrinsic conditional autoregressive covariance matrix that allows for dependence among regions organized in a lattice [206]. For the ground sites, we designated a simple diagonal structure $\boldsymbol{R}_\tau^G = \boldsymbol{I}$. We used diffuse exchangeable Gaussian priors for the regression coefficients $\boldsymbol{\gamma}$ and $\boldsymbol{\alpha}$, a discrete uniform prior for ϕ, and vague inverse-gamma priors for the variance parameters σ_d^2, $\sigma_\tau^{2,A}$, and $\sigma_\tau^{2,G}$.

The joint posterior distribution associated with our full integrated model is

$$[\boldsymbol{\beta}_\lambda, \boldsymbol{\beta}_\rho, \boldsymbol{\beta}_\psi, \boldsymbol{\gamma}, \boldsymbol{\alpha}, \boldsymbol{\eta}, \boldsymbol{\zeta}, \boldsymbol{\xi}, \boldsymbol{\omega}, p_\omega, p, \sigma_\tau^{2,A}, \sigma_\tau^{2,G}, \sigma_d^2, \phi, \boldsymbol{N}^{A,u}, \boldsymbol{N}^G, \boldsymbol{z}^u, \boldsymbol{d}^u, \boldsymbol{\epsilon}^u | \boldsymbol{N}^{A,o}, \boldsymbol{z}^o, \boldsymbol{d}^o, \boldsymbol{\epsilon}^o, \boldsymbol{v}, \boldsymbol{F}] \tag{3.11}$$

$$\propto \prod_{t=1}^{T^G}\prod_{i=1}^{n^A}\prod_{l=1}^{M}\left([v_{itl}|N_{itl}^A, z_{itl}, d_{itl}, \epsilon_{itl}, \boldsymbol{\beta}_\rho][N_{itl}^A|\boldsymbol{\beta}_\lambda, \lambda_0, \omega_{itl}][\omega_{itl}|p_\omega][z_{itl}|\boldsymbol{\beta}_\psi]\right)[\boldsymbol{\beta}_\lambda][\boldsymbol{\beta}_\rho][\boldsymbol{\beta}_\psi][\boldsymbol{d}^u][\boldsymbol{\epsilon}^u][\lambda_0][p_\omega] \tag{3.12}$$

$$\times \prod_{t=1}^{T^G}\prod_{i=1}^{n^G}\left(\prod_{l=1}^{L_{it}^G}\Big(\prod_{j=1}^{J_{itl}}[F_{itlj}|N_{itl}^G, p]\Big)[N_{itl}^G|\boldsymbol{\eta}]\right)[\boldsymbol{\eta}][p] \tag{3.13}$$

$$\times \prod_{t=1}^{T^G}\left([\boldsymbol{N}_t^G, \boldsymbol{N}_t^A, \boldsymbol{z}_t|\boldsymbol{\xi}_t, \sigma_d^2, \phi][\boldsymbol{\xi}_t|\boldsymbol{\xi}_{t-1}, \boldsymbol{\alpha}, \sigma_\tau^{2,A}, \sigma_\tau^{2,G}]\right)[\boldsymbol{\gamma}][\boldsymbol{\alpha}][\sigma_d^2][\sigma_\tau^{2,A}][\sigma_\tau^{2,G}][\phi], \tag{3.14}$$

where we use the bracket notation to denote probability distributions [96]. The joint distributions of the ADSM, N-mixture submodel, and spatio-temporal tobit submodel (STTM) are given by equations (3.12), (3.13), and (3.14), respectively. The three submodels induced the integrated model through the link parameters $y_{it}^A = f(\boldsymbol{N}_{it}^{A,o}, \boldsymbol{z}_{it}^o, \boldsymbol{N}_{it}^{A,u}, \boldsymbol{z}_{it}^u)$ and $y_{it}^G = g(\boldsymbol{N}_{it}^G)$. A directed acyclic graph of our integrated model is shown in Figure 3.2, and a full model statement with priors is provided in Appendix B.1.3.

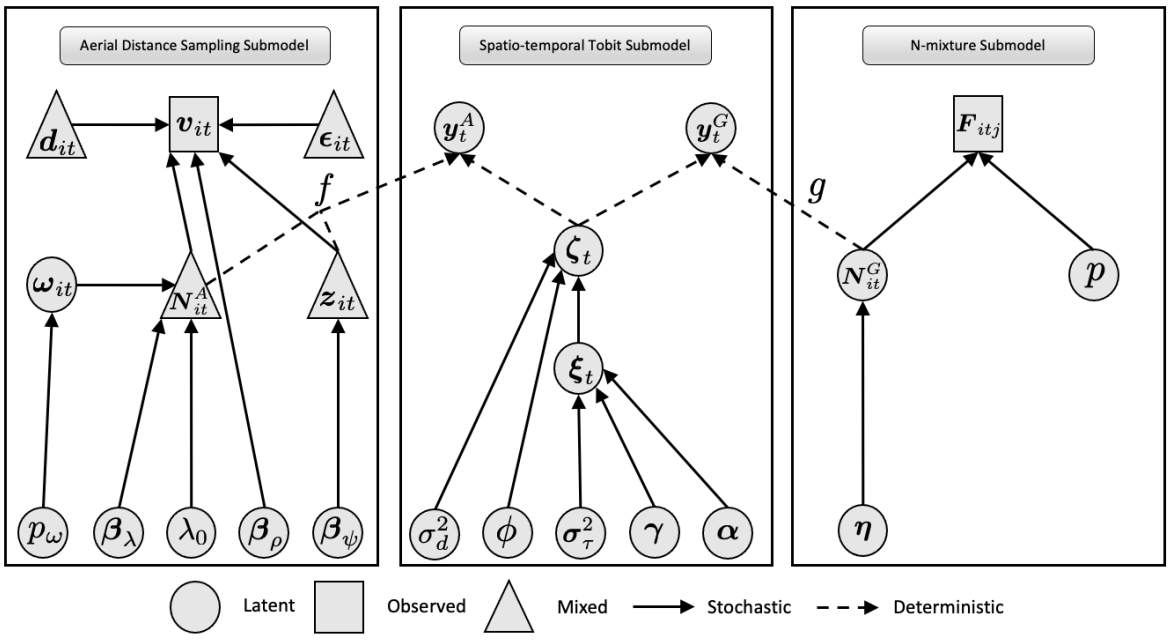

Figure 3.2: Directed acyclic graph of integrated model. Note that $\boldsymbol{\sigma}_\tau^2 = (\sigma_\tau^{2,A}, \sigma_\tau^{2,G})'$.

3.5 Posterior Inference

The crux of fitting our integrated model was that the link parameters $\boldsymbol{y}^A$ and $\boldsymbol{y}^G$ are non-invertible functions of the submodel parameters $\boldsymbol{z}$, $\boldsymbol{N}^A$, and $\boldsymbol{N}^G$. We adopted a chained Markov melding approach [64] that facilitated joint inference for $\boldsymbol{y}^A$ and $\boldsymbol{y}^G$ accounting for the data, prior information, and assumptions in all three submodels. We derive the joint melded distribution for $\boldsymbol{y} = (\boldsymbol{y}^{A\prime}, \boldsymbol{y}^{G\prime})'$ as follows [64]:

$$[\boldsymbol{y}, \cdot]_{\text{meld}} = [\boldsymbol{y}]_{\text{pool}} [\cdot|\boldsymbol{y}]_{\text{ADSM}} [\cdot|\boldsymbol{y}]_{\text{STTM}} [\cdot|\boldsymbol{y}]_{\text{N-mix}}, \tag{3.15}$$

$$= [\boldsymbol{y}]_{\text{pool}} \frac{[\cdot, \boldsymbol{y}^A]_{\text{ADSM}}}{[\boldsymbol{y}^A]_{\text{ADSM}}} \frac{[\cdot, \boldsymbol{y}]_{\text{STTM}}}{[\boldsymbol{y}]_{\text{STTM}}} \frac{[\cdot, \boldsymbol{y}^G]_{\text{N-mix}}}{[\boldsymbol{y}^G]_{\text{N-mix}}}, \tag{3.16}$$

where "$\cdot$" is a placeholder for all parameters other than $\boldsymbol{y}$ in the joint and conditional distributions, $[\boldsymbol{y}]_{\text{pool}}$ is the pooled prior marginal distribution, and $[\cdot, \boldsymbol{y}]_{\mathcal{M}}$ and $[\boldsymbol{y}]_{\mathcal{M}}$ denote the joint and prior marginal distribution of $\boldsymbol{y}$ in submodel $\mathcal{M}$, respectively. In the first equality, equation (3.15), we perform marginal replacement to establish a common prior marginal distribution for $\boldsymbol{y}$ across all submodels [123]. Equation (3.15) is the minimally modified joint distribution with marginal

$[\boldsymbol{y}]_{\text{pool}}$. Note that neither of the conditional distributions $[\cdot|\boldsymbol{y}]_{\text{ADSM}}$ or $[\cdot|\boldsymbol{y}]_{\text{N-mix}}$ in equation (3.15) have an analytical closed form because both f and g are non-invertible in equations (3.6) and (3.7), respectively. We therefore rewrite the joint melded distribution as a product of the submodel joint distributions over the prior marginals for posterior inference, equation (3.16).

Another difficulty in posterior inference is that all three submodel marginal distributions in equation (3.16) are analytically intractable. Goudie et al. [123] recommended approximating the submodel marginal distributions with kernel density estimators, but this approach can lead to numerical instabilities in implementation [207]. We obviated approximating the submodel marginal distributions by constructing $[\boldsymbol{y}]_{\text{pool}}$ using chained product of experts (PoE) pooling [64],

$$[\boldsymbol{y}]_{\text{pool}} = \frac{1}{K}[\boldsymbol{y}^A]_{\text{ADSM}}[\boldsymbol{y}]_{\text{STTM}}[\boldsymbol{y}^G]_{\text{N-mix}}, \text{ for } K = \int [\boldsymbol{y}^A]_{\text{ADSM}}[\boldsymbol{y}]_{\text{STTM}}[\boldsymbol{y}^G]_{\text{N-mix}} d\boldsymbol{y}. \tag{3.17}$$

Under PoE pooling, the melded posterior for $\boldsymbol{y}$ is proportional to a product of the submodel joint distributions, which simplifies implementation. One caution regarding PoE is that the pooled prior is often unintuitive and may not be a good summary of the submodel marginal distributions [123]. We simulated draws from $[\boldsymbol{y}^A]_{\text{ADSM}}$, $[\boldsymbol{y}]_{\text{STTM}}$, and $[\boldsymbol{y}^G]_{\text{N-mix}}$ using standard (forward) Monte Carlo methods and found that the implied prior marginals were vague because the specified priors for submodel parameters $\boldsymbol{\beta}_\lambda$, $\boldsymbol{\alpha}$, $\boldsymbol{\eta}$, etc., were also vague. Because of the limited impact of prior information and pooling function on posterior inference for $\boldsymbol{y}$, we used PoE pooling for computational convenience, but see [123] for a suite of other pooling options.

Targeting $[\boldsymbol{y}, \cdot]_{\text{meld}}$ with a standard MCMC algorithm would involve computationally infeasible block updates for $\boldsymbol{N}^A$, $\boldsymbol{N}^G$, and $\boldsymbol{z}$ because $\boldsymbol{y}^A = f(\boldsymbol{N}^A, \boldsymbol{z})$ and $\boldsymbol{y}^G = g(\boldsymbol{N}^G)$. We avoided high-dimensional parameter updates by targeting the melded posterior with a multistage MCMC algorithm. We sampled from $[\boldsymbol{y}^A, \cdot]_{\text{ADSM}}$ and $[\boldsymbol{y}^G, \cdot]_{\text{N-mix}}$ using two independent Metropolis-Hastings-within-Gibbs algorithms. We promoted conjugacy of the linear predictor, $\boldsymbol{\beta}_\psi$, using Pólya-Gamma data augmentation [91], which can improve sampling efficiency in ecological binary regression models [92]. Appendix B.2 includes additional implementation details for the first-stage sampler.

In the second-stage, density samples from the first-stage were used as the proposals in the STTM, equation (3.14). For MCMC iteration k in the second-stage, we drew a sub-sample denoted by $\boldsymbol{y}^{X,(\star)}$, $X \in \{A, G\}$ from the first-stage samples of submodel $\mathcal{M}$, $\mathcal{M} \in \{\text{ADSM}, \text{N-mix}\}$, randomly with replacement, and the Metropolis-Hastings ratio was

$$\frac{[\boldsymbol{y}^{X,(\star)}, \cdot]_{\text{STTM}}[\boldsymbol{y}^{X,(\star)}, \cdot]_{\mathcal{M}}[\boldsymbol{y}^{X,(k-1)}, \cdot]_{\mathcal{M}}}{[\boldsymbol{y}^{X,(k-1)}, \cdot]_{\text{STTM}}[\boldsymbol{y}^{X,(k-1)}, \cdot]_{\mathcal{M}}[\boldsymbol{y}^{X,(\star)}, \cdot]_{\mathcal{M}}} = \frac{[\boldsymbol{y}^{X,(\star)}, \cdot]_{\text{STTM}}}{[\boldsymbol{y}^{X,(k-1)}, \cdot]_{\text{STTM}}},$$

where $\boldsymbol{y}^{X,(k-1)}$ is the current value of $\boldsymbol{y}^X$ in the chain. The refined samples from the second-stage constitute draws from $[\boldsymbol{y}^X, \cdot]_{\text{meld}}$. A heuristic for the multistage MCMC algorithm is that it further refines $[\boldsymbol{y}^X, \cdot]_{\mathcal{M}}$ by selecting samples that conform with the spatio-temporal trends observed in both datasets. To improve mixing, we updated the elements of $\boldsymbol{y}^X$ one at a time. See Appendix B.2 for a complete description of the second-stage sampler and implementation details.

3.6 Results

3.6.1 Simulation Study

We assessed the impacts of Markov melding on predictive performance and inference for a simplified version of our integrated model. Using the STTM (Section 3.4.3), we simulated a network of densities at which we generated distance sampling or N-mixture survey data. We rounded the densities simulated from the STTM to the nearest whole number and let that represent the number individuals available for detection at each site. For the aerial sites, we then located simulated individuals uniformly within the survey area. We fit the simulated aerial survey data using a simplified single observer distance sampling model with half-normal detection function (see Appendix B.1.4). Distances and the parameters of the detection function were specified such that on average, the observer detected half of the individuals in the survey region. At the ground sites, we set the simulated number of individuals equal to N_{it}^G and drew counts for $J = 4$ occasions using a simplified N-mixture model (Appendix B.1.5) with $p = 0.5$.

We simulated datasets under three different sample size ratios, and also considered datasets simulated with and without preferential sampling. The sample ratios varied from 5 to 20 times more aerial sites than ground sites, with the number of ground sites fixed at $n^G = 10$. For each sample size ratio, we generated 400 datasets. Each dataset in the STTM consisted of 300 locations. For half of the datasets, we randomly drew a sub-sample of locations for the aerial and ground sites. For the other half, we drew a random sub-sample of aerial sites, but selected the 10 ground sites from the set of 300 that had the highest expected mean density given by $\boldsymbol{\zeta}_0 = \boldsymbol{X}_0\boldsymbol{\gamma}$ (Model B.1.3). The motivation behind our preferential sampling mechanism is that the ground sites in the LEPC case study were opportunistically located based on habitat characteristics known to be associated with higher LEPC density (e.g., large grassland patches and low anthropogenic disturbance).

We obtained posterior inference for all $2 \times 3 \times 200 = 1200$ datasets using the Markov melding techniques described in Section 5 of the manuscript (*Posterior Inference*) with PoE pooling. The first-stage MCMC algorithm fit the simplified N-mixture and aerial distance sampling submodels in parallel for $10,000$ iterations. The second stage fit the STTM for $20,000$ iterations. For each model fit, we calculated the mean empirical coverage rate, mean absolute error of the posterior mean, and posterior standard deviation of aerial sites densities (Figure 3.3). The results did not differ by sample size ratio or sampling regime. In each case, inference from the integrated model at the aerial sites maintained the same empirical coverage rate of the ADSM but reduced uncertainty and bias. Metrics for the ground sites, not shown, were similar to the aerial sites. The coverage rates for ground sites mimicked those obtained from the N-mixture model in the first-stage but the refined second-stage estimates from the STTM had lower uncertainty and bias.

3.6.2 Sensitivity Analysis

We performed a sensitivity analysis to assess the inferential cost of conducting aerial surveys less frequently. We considered four different scenarios of missing aerial survey data, but assumed that ground data were available for all ground sites across the 17 years. For each scenario, we simulated 35 datasets from the STTM (Section 3.4.3) using the design and covariance matrices

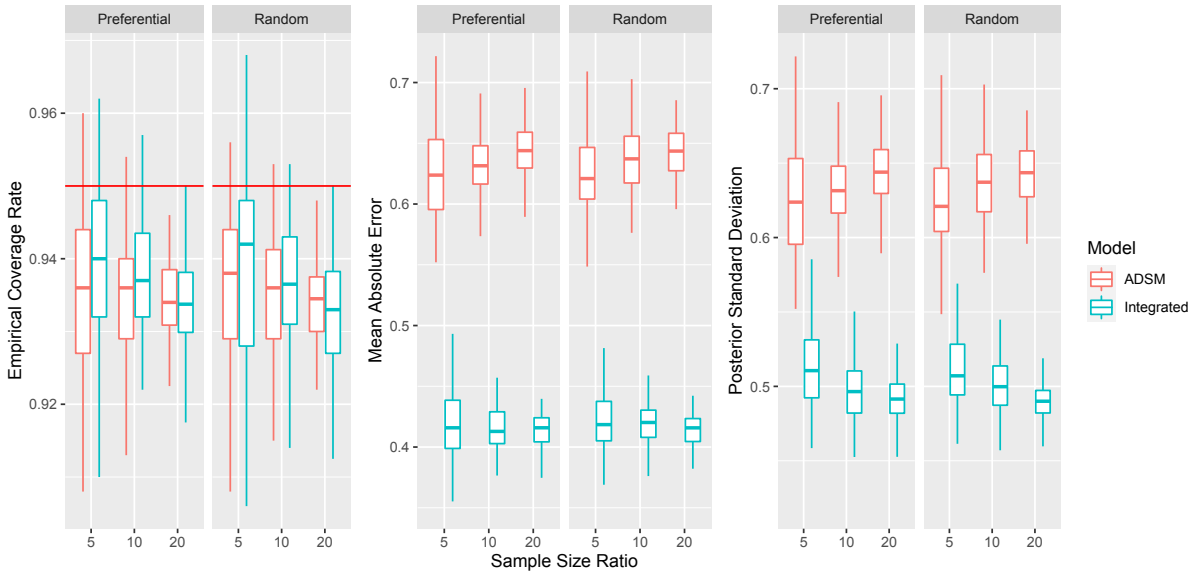

Figure 3.3: Performance metrics for ADSM and full integrated model. Boxplots show empirical coverage rates, posterior mean absolute errors, and posterior standard deviations for aerial site densities. The red line is the targeted nominal coverage rate of 95%.

from the LEPC case study. All parameters in the STTM were set to the posterior mean calculated from the fitting the integrated model to the LEPC data. We simulated data for the aerial and ground surveys and fit the integrated model using the same submodels and approach as described in Section 3.6.1. Figure 3.4 provides the root mean squared error (RMSE) for site level densities and annual abundances for each scenario.

All scenarios with missing aerial survey data resulted in substantially higher site level RMSEs than Scenario 1 where aerial surveys were conducted every year. Site level RMSEs were similar for all scenarios for years in which an aerial survey was conducted but much higher in years with no aerial survey because of increased uncertainty. For annual abundance estimation across the EOR, predictive performance was similar across the scenarios with the caveat that Scenarios 2-4 occasionally yielded poor predictive performance. As aerial survey effort decreased, the chances of poor predictive performance increased.

Overall, site level density estimates were more sensitive to reduced survey effort than range-wide abundance estimates. Reduced aerial survey effort may be adequate for monitoring range-wide populations but could struggle to document fluctuations in the LEPC that are spatially het-

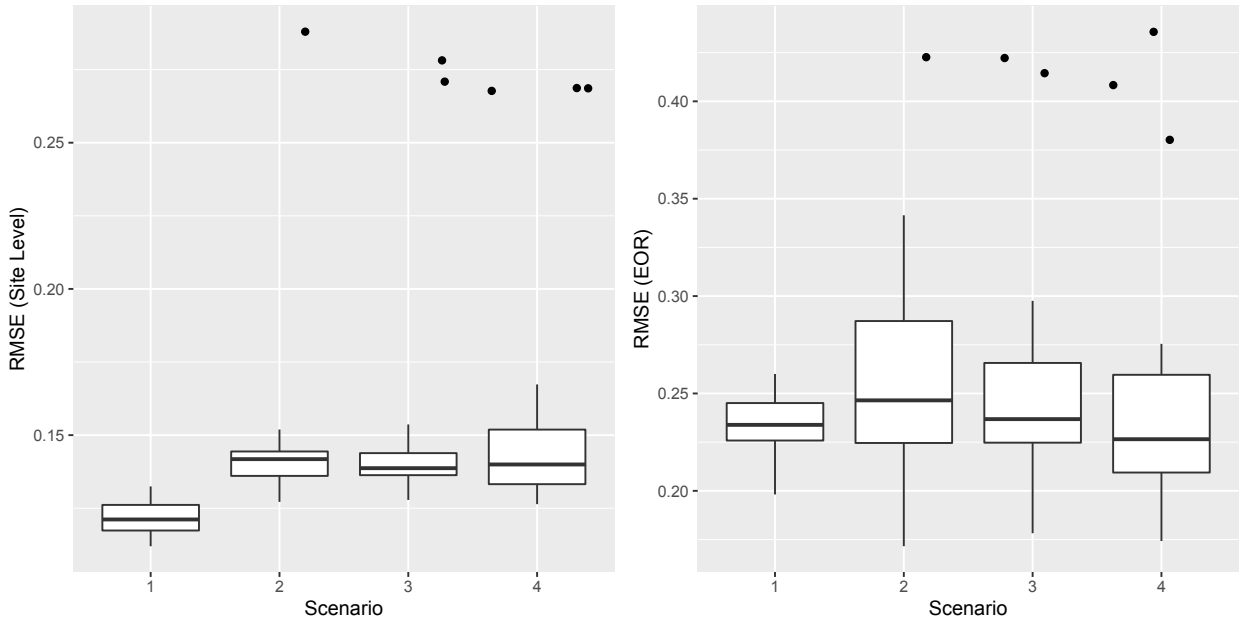

Figure 3.4: Impact on predictive performance of integrated model for differing scenarios of missing aerial survey data. In Scenarios 1-4, aerial survey data is available every year, twice every three years, once every two years, and once every three years, respectively. The left panel is the RMSE of site-level densities. The right panel is the RMSE of annual abundance predictions divided by the population size. Dots above boxplots represent outliers as defined as values which exceed 1.5 times the interquartile range over the 75th percentile. Dots positioned randomly within groups on x-axis to decrease overlap.

erogeneous. From a conservation perspective, spatially coarse abundance predictions can be problematic as they have the potential to overlook the contribution of vulnerable subpopulations.

While range-wide predictive performance was similar across all scenarios, Scenarios 2-4 occasionally performed very poorly. LEPC populations follow a boom-or-bust life history strategy [198], which results in large inter-annual variation in abundance that makes prediction difficult. In 2013, a bust was observed that reduced the estimated Kansas LEPC population size by 14%. Without aerial survey data, it would have been difficult to quantify the magnitude of the bust. Thus, reduced aerial effort sampling regimes risk misestimating LEPC boom and busts.

3.6.3 Case Study

The melded density estimates for the Kansas EOR from the integrated model are similar to the density estimates of the ADSM but have reduced uncertainty and are shifted slightly for some years (Figure 3.5). Shifts in the melded posterior tend to mirror trends estimated from the ground

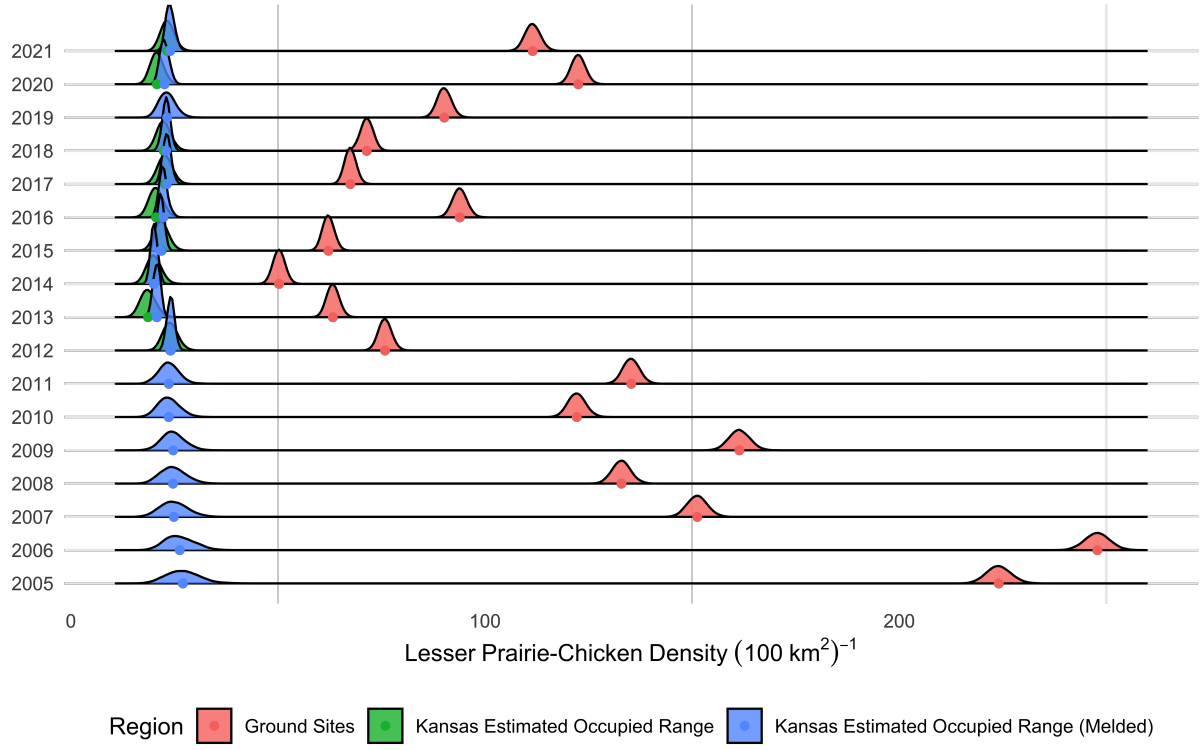

Figure 3.5: Posterior distributions of annual density for lesser prairie-chicken across Kansas estimated occupied range and ground sites from 2005-2021. Red are the posterior annual densities measured across the 21 ground sites estimated from the N-mixture submodel. Green are the posterior annual densities for Kansas estimated occupied range inferred from the aerial distance sampling submodel. Blue are the refined posteriors for Kansas estimated occupied range derived from melding the aerial distance sampling and N-mixture submodel densities into the spatial temporal tobit model. Posterior means of each distribution are shown as dots.

surveys. For example, from 2015-2016 there was an estimated decline in LEPC densities according to the aerial survey data, but densities increased across the ground sites. The melded posterior for 2016 incorporates trends from the ground survey and shifts the posterior right. The largest fluctuation in LEPC density was in 2013 following the extreme drought conditions of 2011 and 2012 [57]. Both the raw aerial and melded density estimates show a decline, but the fluctuation in the melded estimates is more nuanced. In general, the melded densities estimate have a smoother temporal trajectory compared to the raw aerial estimates. In Appendix B.4, we compare the estimates of our ADSM with those of Nasman et al. [197]. We provide posterior inference for covariate effects in the STTM in Appendix B.5.

The integrated model facilitates inference for LEPC density at unsampled regions via the joint melded distribution so that annual density estimates across Kansas EOR during years which no aerial survey was conducted (2005-2011 and 2019) can still be inferred. The Kansas EOR density estimates from 2005-2011 exhibit greater uncertainty but have long right tails to reflect higher densities observed at the ground survey regions. A map of estimated LEPC across Kansas EOR is given in Figure 3.6. The southwest region of the SGPR consistently boasted the highest densities followed by the western portion of the MGPR. The SSPR had the lowest densities and show a decreasing pattern over time. Mean estimates were higher in the northern region of the SGPR from 2005-2011 but have large uncertainty because of no aerial or ground surveys during that period (Figure 3.1).

3.7 Discussion

We demonstrated a flexible approach for joint inference from multiple surveys. The need to incorporate mixed surveys into a unified statistical analysis is a common challenge in ecology. Integrated distribution models leverage presence only, detection/nondetection, and count data to infer species latent point patterns [102, 194]. Liu et al. [208] developed models for inferring animal trajectories from GPS and "Dead-Reckoning" tags. Their model is an adaptation of Bayesian melding models that were originally proposed in atmospheric sciences for linking observations from monitoring stations and the outputs of deterministic climate models to a common Gaussian process [104, 209].

Markov melding handles the observational process and spatial support of each data source in separate submodels which can accommodate more complex distributional assumptions. Furthermore, Markov melding facilitates joint inference on quantities that are multivariate non-invertible functions of submodel parameters. This quality is especially appealing in ecology where many popular models provide inference on the parameter of interest through derived quantities. Markov melding may also reduce computation time when submodels handling the observational uncertainty of each dataset are fit in parallel.

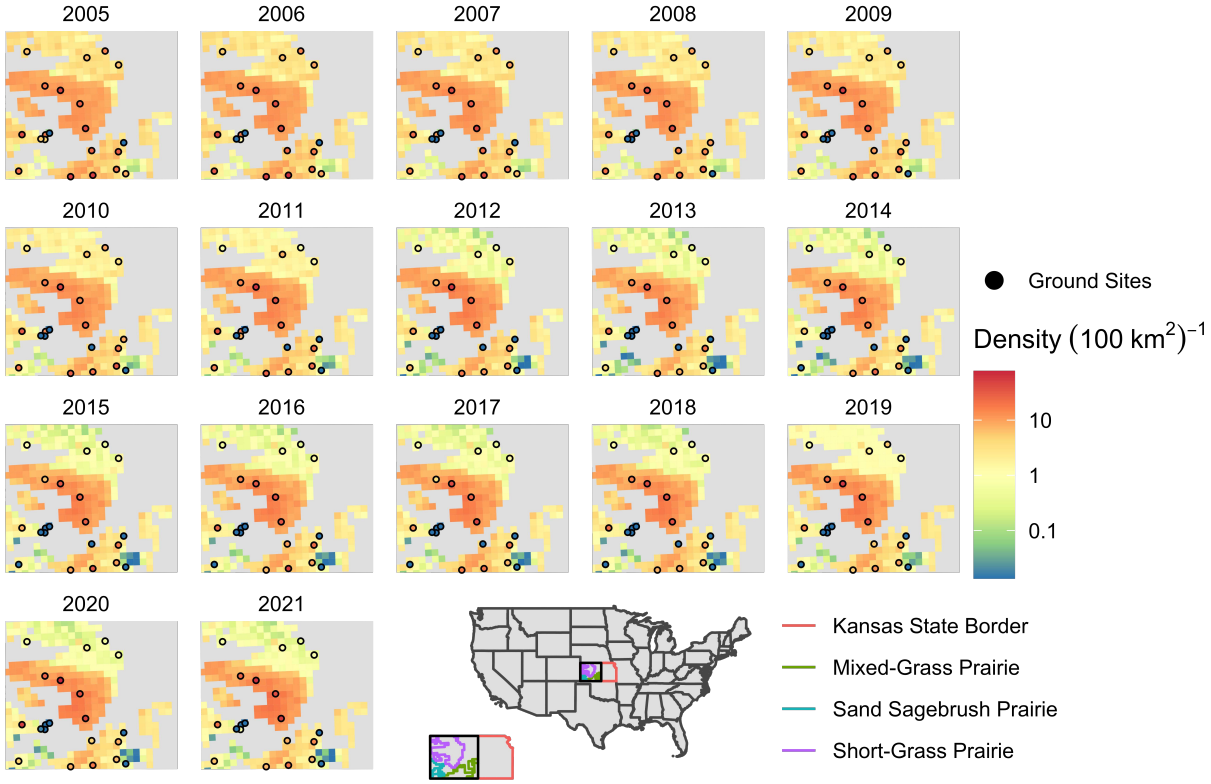

Figure 3.6: Map of estimated lesser prairie-chicken densities across Kansas estimated occupied range and ground sites from 2005-2021. Ecoregions are delineated by outline color in the inset maps. Posterior mean densities are shown for each survey block and the 21 ground sites (circles). All densities estimates are from the melded model.

The integrated model allowed us to reduce uncertainty in annual density estimates by refining the initial density posterior distributions from the submodels to concur with spatio-temporal trends observed across both datasets. Through the melded joint distribution, the integrated model also provided inference for density at unsampled regions that account for the contributions of both datasets. Inferring annual density estimates from the ground sites alone would be inaccurate because of preferential sampling [196]. The historical density estimates of the integrated model, however, accounted for the uncertainty in both datasets and leveraged trends in temporal dependence and covariate associations learned from the aerial survey data. The historical density estimates, which provide insights about longer scale trends in LEPC density, are important for assessing recovery of the species [60].

We developed a modeling approach for integrating inference from aerial and ground surveys of LEPC in Kansas, but our approach can be generalized to accommodate other surveys. Most immediately, our approach can accommodate the ground surveys from the other states in the LEPC range. Ground surveys are distinct by state, but each survey produces estimates of density in a particular region and our approach can accommodate differences in observational error. Furthermore, we could extend our current model to account for population dynamics by including an additional submodel that characterizes changes in site-level counts due to annual variability in survival, fecundity, and immigration. The extended IPM could produce spatio-temporal predictions that explicitly account for the contributions of recruitment and survival which could help understand the driver of population change and inform conservation practices for the species [60].

Accounting for observational error is often a necessity when developing models for SCC [53]. By taking a Markov melding approach, we showed how surveys with unique observational uncertainties and scales can be incorporated into a joint response. Furthermore, we facilitated computation by fitting the model in stages which obviated high-dimensional parameter updates and induced conjugacy for several parameters in the submodels. Another computational advantage of Markov melding is that it enabled model specific data augmentation strategies such as PX-DA in the ADSM and tobit regression in the STTM. Our scalable approach for joint Bayesian inference serves as a

foundation for developing future integrated models for mixed surveys of wildlife abundance in other studies.

Chapter 4

Data Assimilation with Melded Integrated Population Models

Documenting the decline of a species is challenging because many species experienced the most precipitous declines prior to human monitoring. Population trajectories inferred from recently collected data often show stability or even improvement [13], but can overlook long-term declines that preceded data collection [14]. Declines may also be spatially heterogeneous, and spatially restricted monitoring programs can wrongly conclude population stability while a regional population heads to extirpation [15]. Ideally, data for informing species conservation would be range-wide, collected over a long time period following standardized design-based sampling protocols that include randomization and consistent sampling methods with only minimal observational uncertainty. Rarely are such data available from one source [210]. Integrated models have been proposed for drawing from the strengths of many datasets to provide inference in scenarios where the individual datasets are insufficient.

One popular adaptation of integrated models in conservation biology is integrated population models (IPMs). IPMs were first proposed in the 1980s [106], but wide adoption of IPMs in the broader fields of conservation biology and ecology began in the early 2000s [31, 193]. Schaub et al. [38] describe IPMs as integrated models that link changes in population abundance and vital rates in a common model to account for the likelihoods of all existing datasets. These datasets often include capture-recapture data, birth rates, movement, and population counts to learn about survival, recruitment, immigration and emigration, and abundance, respectively. By assimilating all data sources into one model, IPMs have been shown to promote parameter identifiability and precision [114, 120] and provide inference on demographic causes of population change [38].

In ornithology, IPMs have informed conservation practices for numerous species of conservation concern [117, 211, 212, 213, 214, 215]. These IPMs adopted a state-space framework in

which observed indices of abundance are linked to vital rates in a Leslie matrix model [116],

$$\begin{bmatrix} N_1 \\ \vdots \\ N_A \end{bmatrix}_{t+1} = \begin{bmatrix} \rho_1 & \cdots & \cdots & \cdots & \rho_A \\ \phi_1 & 0 & \cdots & \cdots & 0 \\ 0 & \phi_2 & 0 & \cdots & 0 \\ \vdots & \vdots & \vdots & \vdots & \vdots \\ 0 & \cdots & 0 & \phi_{A-1} & \phi_A \end{bmatrix}_t \begin{bmatrix} N_1 \\ \vdots \\ N_A \end{bmatrix}_t, \tag{4.1}$$

where $\boldsymbol{N}_t = (N_{1t}, \ldots, N_{At})'$ is a vector of female abundance in age classes $a \in \{1, \ldots, A\}$ at time t and ρ_{at} and ϕ_{at} are the age-specific productivity and survival in year t, respectively. All quantities in the Leslie matrix are generally unknown but informed by a variety of datasets. For example, Schaub et al. [211] used the number of fledglings produced from surveyed broods, number of occupied territories, survival data, and age-at-death data to inform latent quantities.

In some cases, data sources might not be available for learning about the desired quantities directly but are derived as submodel outputs. For example, Schaub et al. [124] specified a Bayesian state-space IPM to understand local population dynamics in Eurasian wrynecks (*Jynx torquilla*). Because count data were not directly available for wrynecks, Schaub et al. [124] fit a Bayesian dynamic occupancy model [216] to infer annual trends in wryneck occupancy, which they treated as an index of abundance. The annual number of occupied sites along with its posterior standard deviation were treated as fixed parameters in a log-normal distribution and used as a population index and a measure of the observational error, respectively. King et al. [117] fit a generalized linear model (GLM) to derive annual log abundances of northern lapwings (*Vanellus vanellus*). King et al. [117] used the Monte Carlo estimate of the mean log abundance and variance from the GLM as fixed parameters in a log-normal distribution to approximate the observational error of the population counts in a Bayesian state-space IPM. While these approximate approaches for including the observational error of the count data into an IPM may not impact inference, a more cohesive approach would derive the joint distribution of all quantities that explicitly accounts for the uncertainty in each data source.

We present a Markov melding approach to integrated population modeling that allows quantities associated with population dynamics to be derived from complex non-invertible functions of submodel parameters [123]. Manderson and Goudie [64] were the first to propose Markov melding in the context of IPMs with an extension called chained Markov melding. Chained Markov melding reconciles differences in the marginal distributions for parameters linking a sequence of submodels to construct a unified joint distribution. The joint distribution provides inference for latent quantities of interest and accounts for the data, assumptions, and priors across all submodels. Manderson and Goudie [64] facilitated efficient posterior sampling with a parallel multistage MCMC algorithm.

We demonstrate the chained Markov melding approach to integrated population modeling in a case study of LEPC abundance. The LEPC is a federally protected species [55]. Understanding drivers of LEPC demography is key to informing conservation [58]. Integrated population modeling of LEPC data is challenging because data informing population abundance come from multiple surveys with different designs. Data documenting annual fluctuations in LEPC recruitment are not directly available but rather inferred from several datasets and additional prior information [63, 217] on LEPC productivity.

Aerial and ground surveys have complementary strengths and weaknesses [60, 61]. Aerial surveys follow a spatially random sampling design that provides inference on range-wide LEPC abundance [61, 5]. Two shortcomings of aerial surveys are that they have only been conducted since 2012 and observe relatively few LEPC in low density regions. Ground surveys have a long history and observe more individuals per unit of area than the aerial surveys. Inferring range-wide abundance from the ground surveys is questionable because individuals counted may not be from the local population [218] and the ground sites were preferentially located in regions known to have high LEPC densities [196].

Over the past two decades, there have been numerous studies informing LEPC conservation, but few have assimilated multiple data sources. Persistent challenges to data assimilation for LEPC include differing sample designs across surveys and uneven observational uncertainties or sampling

biases across datasets [36]. Ross et al. [63] developed an IPM for assimilating count, survival, and productivity data from Kansas that suggested observed declines in LEPC abundance following droughts [198] were driven by increased juvenile mortality. The findings of Ross et al. [63] prompted managers to consider habitat improvements that focus on increasing and maintaining grasslands that can buffer the population against the harmful effects of severe drought [219]. Van Ee et al. [220] proposed an integrated model for melding inference from aerial and ground surveys to improve predictive performance in Kansas.

We propose an IPM for melding inference from range-wide LEPC ground, aerial, and demographic surveys spanning five states. To our knowledge, this is the first IPM developed for the entire distribution of a federally protected species. By taking a flexible Markov melding approach to posterior inference, we assimilate a diverse assemblage of datasets collected over the last two decades into one cohesive framework. Equipped with this wealth of data, we provide annual estimates of population vital rates and identify life history strategies for four ecoregions. We derive the contribution of each data source to posterior inference and account for varying effort across surveys and years. In a simulation study, we quantify decreases in predictive performance associated with reduced aerial survey effort to inform future monitoring of LEPC.

In Section 4.1, we provide background for LEPC conservation. Section 4.2 includes a description of the data used to fit our IPM. In Section 4.3, we specify models for analyzing each data source independently and then a population model for inducing joint inference on submodel derived quantities. We describe the chained Markov melding approach used to facilitate posterior inference for our IPM in Section 4.4. Section 4.5 is a summary of the results; and Section 4.6 is a concluding discussion of our findings.

4.1 Lesser Prairie-Chicken Conservation

The LEPC is a member of the family Phasianidae and endemic to the southwestern Great Plains. The LEPC has experienced occupied range and population declines since the 1980s primarily due to habitat loss and fragmentation but habitat degradation from curtailment of natural

fires, overgrazing, oil and gas, transmission, and wind energy development, and climate change are also drivers of the decline [58, 1, 4, 56]. LEPC inhabit four ecoregions [60]. The Shinnery Oak Prairie Ecoregion (SOPR) exists in northwestern Texas and eastern New Mexico; the Sand Sagebrush Prairie Ecoregion (SSPR) covers portions of southeastern Colorado, southwestern Kansas, and the northwestern Oklahoma panhandle; the Mixed-Grass Prairie Ecoregion (MGPR) spans southern Kansas, western Oklahoma, and the northeastern Texas panhandle; and the Short-Grass Prairie/Conservation Reserve Program Mosaic Ecoregion (SGPR) is in northwestern Kansas with a small section in eastern Colorado (Figure 4.1).

In 2023, the United States Fish and Wildlife Service (USFWS) listed the LEPC for federal protections as two population segments under the 1973 Endangered Species Act [55]. The northern population segment, which encompasses the SSPR, MGPR, and SGPR ecoregions, is classified as threatened, and the southern population segment in the SOPR is endangered. Life-history strategies and drivers of population decline vary by ecoregion [221, 222, 223], and populations may be locally adapted for the ecoregions they inhabit [20]. Modeling frameworks to inform LEPC conservation must account for spatial heterogeneity in vital rates so that conservation practices can be curtailed to each ecoregion [60].

LEPC population monitoring is coordinated across several federal and state conservation agencies. Colorado Parks and Wildlife (CPW), Kansas Department of Wildlife and Parks (KDWP), Oklahoma Department of Wildlife Conservation (ODWC), Texas Parks and Wildlife Department (TPWD), and New Mexico Department of Game and Fish (NMDGF) have monitored LEPC populations with ground surveys as early as the 1940s. Ground surveys were used as an index of abundance but did not provide inference on range-wide abundance because of sampling biases [218]. Lack of spatial randomness in the state ground surveys also made inferring species-habitat associations difficult. Since 2012, the Western Association of Fish and Wildlife Agencies (WAFWA), USFWS, CPW, KDWP, ODWC, TPWD, and NMDGF have collectively supported annual range-wide aerial survey of LEPC conducted by Western EcoSystems Technology, Inc. (WEST). While the aerial surveys have provided inference on range-wide abundance [61, 5], their cost has led re-

searchers to consider integrated models that could leverage multiple datasets and reduce reliance on annual aerial surveys.

Several universities and non-profit organizations have conducted demographic studies of LEPC [224, 225, 4, 222, 223, 226, 1, 227, 221, 228, 229]. Researchers tagged individuals to estimate spatial-temporal variability in survival and productivity. Researchers visited nesting females to collect data on nest success, clutch size, and hatchability. The ensuing broods were also monitored to document chick survival.

4.2 Data Sources

We compiled data from studies across the LEPC occupied range. Most data compiled were collected in the last decade, but some data sources were collected as early as 2001. We acquired annual range-wide counts of LEPC from state and federal wildlife agencies. Demographic data related to LEPC survival and productivity were provided by universities in Colorado, Kansas, Oklahoma, New Mexico, and Texas. A map of the aerial, ground, and demographic survey regions is shown in Figure 4.1. The map shows the total area surveyed from 2001 to 2022, but note that a reduced number of sites were surveyed annually. An animation of the annual survey effort is available in the supplementary files.

4.2.1 Ground Surveys

Historically, LEPC populations were monitored using lek counts from ground surveys conducted by the five state wildlife agencies in which the LEPC occurs. In some states, ground surveys began as early as the 1940s, but standardized protocols were not established in most states until the early 2000s. Population monitoring of LEPC relies on spring counts of individuals on leks [61]. A lek is an aggregation of males defending a small territory and communally calling and performing displays to attract and mate with females [58]. Leks are generally located in sparse vegetation on hilltops and ridgelines and can include more than 10 individuals, which makes detection by audio and visual cues of the otherwise cryptic individuals easier [58, 230].

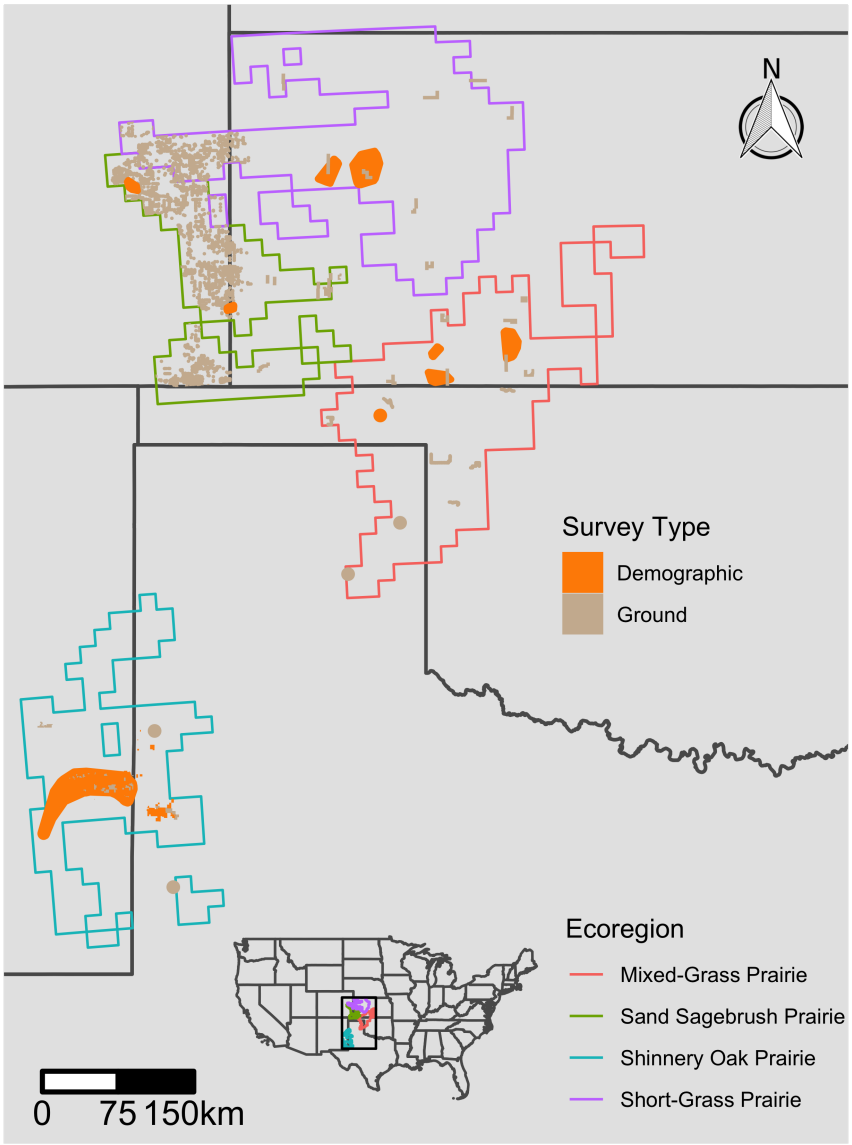

Figure 4.1: Lesser prairie-chicken demographic and ground survey regions over aerial survey blocks grouped by ecoregion. Demographic data acquired from Unger [4] were collected in Beaver County, Oklahoma (orange circle, exact location not shown for data privacy purposes). Texas Parks & Wildlife Department ground survey regions in Hemphill, Gray, Bailey, and Gaines counties (gray circles) are also not shown. Ground survey site in Cochran/Yoakum county represented by gray polygon between gray dots in Texas Shinnery Oak Prairie.

Ground surveys were completed from 30 minutes before sunrise to 2 hours after when LEPC leks are most active during March 15 to May 15. The spatial coverage of ground surveys varied by state, but in each state, surveyors attempted to census leks within a prespecified region. Most land in the LEPC range is privately owned, and state wildlife agencies opportunistically collected data along public roads and in regions where they were granted access. KDWP surveyed 21 routes (6 SSPR, 8 SGPR, and 7 MGPR) annually. Each route was approximately 16-km long, and ground surveyors attempted to census all leks within 1.6 km of the road for a region of approximately 51.2 km^2. Likewise, ODWC annually surveyed five 51.2 km^2 MGPR regions. TPWD monitored five LEPC survey regions (2 MGPR, 3 SOPR) varying from 37.2 to 272.3 km^2. NMDGF surveyed 31 sites in the SOPR for a total area of 141 km^2. CPW surveyors visited unique sites each year, and the total area covered varied annually. We used ground surveys from each state starting in 2005, and Table 4.1 provides the total area surveyed in each ecoregion annually.

Table 4.1: State agency lesser prairie-chicken ground survey effort (km^2) split by year and ecoregion. SOPR = Shinnery Oak Prairie Ecoregion, SSPR = Sand Sagebrush Prairie Ecoregion, MGPR = Mixed-Grass Prairie Ecoregion, and SGPR = Short Grass Prairie/Conservation Reserve Program Mosaic Ecoregion.

Year	2005	2006	2007	2008	2009	2010	2011	2012	2013	2014	2015	2016	2017	2018	2019	2020	2021	2022	**Total**
SOPR	251	212	208	254	250	250	254	251	283	291	335	397	401	360	360	360	360	426	5505
SSPR	289	289	289	289	289	289	289	289	289	1808	1245	1488	637	739	1158	1270	1856	1319	13951
MGPR	893	893	893	893	893	893	836	893	893	893	893	893	841	841	893	893	893	893	15906
SGPR	104	155	155	155	155	155	310	434	434	372	434	434	434	434	258	434	434	434	5720
Total	1470	1481	1544	1591	1587	1587	1689	1866	1898	3363	2907	3171	2313	2374	2669	2957	3543	3071	52068

Surveyors recorded the number of individuals on leks passively with binoculars or by navigating to the lek and prompting the individuals to take flight (flush). Because the number of individuals attending a lek varies, surveyors attempted to record multiple counts per lek with replicate counts spaced at least one day apart. Most leks were counted twice, but many leks only received one count. Ground surveys are considered a census of the leks in the survey area, but not a census of the population because some individuals may not be present at their lek at the time it was flushed and some individuals may not attend any leks. The lek counts do not represent the local or regional

abundance of LEPC but provide an estimate of relative change for estimating trends in population growth rates [231, 63, 217].

4.2.2 Aerial Surveys

The aerial survey was designed to obtain unbiased estimates of LEPC abundance across the entire range. Surveyors partitioned the LEPC estimated occupied range into 225 km^2 (15×15-km) survey blocks [61]. A spatially balanced subset of blocks was selected for sampling in each ecoregion [232], and the subsets selected differed by year. The LEPC estimated occupied range used for extrapolating range-wide abundance also varied. Due to lack of funding, no blocks were surveyed in 2019. Table 4.2 gives the annual area surveyed in each ecoregion.

In survey blocks selected for sampling, a helicopter crew flew two north-south 15-km transects at a speed of 60 km per hour and altitude of 25 m above ground. Transects were flown once each year. Observers scanned the ground for groups of LEPC (where a group is defined as 1 or more individuals). When a group was spotted, the crew navigated to the location the group was first spotted and recorded the location and number of individuals observed. Like the ground surveys, aerial surveys were conducted during the LEPC breeding season (March 15 - May 15) and from 30 minutes before sunrise to 2 hours after to maximize detection of individuals present at leks. For an in-depth description of the aerial survey protocol and design, see Nasman et al. [5] and McRoberts et al. [233].

Table 4.2: Western EcoSystems Technology, Inc. lesser prairie-chicken aerial survey effort (km^2) split by year and ecoregion. Area surveyed is based on a strip width of $600 \times 2 = 1200$ m (Appendix C.1). SOPR = Shinnery Oak Prairie Ecoregion, SSPR = Sand Sagebrush Prairie Ecoregion, MGPR = Mixed-Grass Prairie Ecoregion, and SGPR = Short Grass Prairie/Conservation Reserve Program Mosaic Ecoregion.

Year	2012	2013	2014	2015	2016	2017	2018	2019	2020	2021	2022	**Total**
SOPR	3132	3204	3204	3204	3204	3708	3852	0	3888	3852	3780	35028
SSPR	1368	2700	2700	2700	2700	2592	2556	0	2484	2484	2520	24804
MGPR	3240	3600	3564	3636	3564	3924	4212	0	4428	4644	4320	39132
SGPR	3708	3384	3384	3384	3384	3420	3456	0	3564	3492	3780	34956
Total	11448	12888	12852	12924	12852	13644	14076	0	14364	14472	14400	133920

4.2.3 Survival

We compiled survival data for 653 individuals from several studies conducted between 2008-2019 across all five states and four ecoregions. The captured individuals were banded with either a very-high-frequency (VHF) necklace style radio-transmitter or 22-g, rump-mounted satellite transmitter (platform transmitter terminal [PTT], Microwave Telemetry, Columbia, MD, USA) and their sex, age, and other morphological data were recorded. Biologists approximated the locations of individuals banded with VHF transmitted via triangulation and recorded the spatial locations logged for individuals banded with PTTs. Biologists attempted to verify the survival status of individuals at least once each month. Because of emigration out of the study region and failed transmitters, some banded individuals were censored before a mortality event was observed. Detailed descriptions of the capture methods, monitoring protocols, and study areas for all survival data are available from the sources cited in Table 4.3.

Table 4.3: Study areas, time periods, and sample sizes for LEPC survival studies. The last column indicates the total number of individuals monitored in each study.

Sources	States	Ecoregions	Years	Males	Females	Total
Grisham and Boal [221]	TX	SOPR	2008-2011	45	57	102
Harryman et al. [228]	TX	SOPR	2015-2017	19	6	25
Kunkel [226]	NM	SOPR	2016-2017	38	17	55
Lawrence et al. [1]	NM	SOPR	2013-2015	114	64	178
Robinson et al. and Parker et al. [229, 227]	KS, CO	SSPR, MGPR, SGPR	2013-2019	24	269	293
Total				240	413	653

4.2.4 Productivity

We compiled productivity data for 457 females from several studies conducted between 2001-2018. Movement patterns of tagged females were examined to determine nest initiation. At the nest, biologists recorded the number of eggs and floated 3-4 eggs to estimate nest incubation and predict hatch date. In some cases, incubation date was also inferred from the movements patterns of the female. Biologists returned to the nest at the predicted hatch date or if location data indicated a female had departed the nest. A nest was recorded successful ($\geq$1 egg hatched) if biologists

found pipped egg shells in the nest or egg shells with intact membranes. Because females may attempt multiple nesting events per year and several females were monitored across multiple years, there were more nesting attempts than females. The number of eggs hatched was only recorded for successful nests and was also not available for all studies. The number of females, nesting attempts, clutch counts, and hatch events recorded in each study are summarized in Table 4.4.

We acquired data for estimating brood survival from Lautenbach [234]. In 2013 and 2014, Lautenbach [234] monitored the broods of 45 successfully hatched nests across the SSPR, MGPR, and SGPR of Kansas and Colorado. For each brood, the number of chicks hatched was recorded. Biologists visited broods at least weekly until 60 days post hatch. On each visit, biologists flushed the brood and recorded the number of chicks observed.

Table 4.4: Study areas, time periods, and sample sizes for LEPC productivity studies. The last column indicates the total number of females monitored in each study. Lawrence et al. [1] did not analyze productivity data from the 45 females captured in New Mexico in 2013-2015 but describes the study area, capture, and monitoring methods. Clutch and hatch give the number of observations from each study used for estimation not the number of eggs laid and hatched, respectively.

Sources	States	Ecoregions	Years	Females	Nest	Clutch	Hatch
Grisham et al. [224]	NM	SOPR	2001-2010	152	205	134	0
Grisham et al. [225]	TX	SOPR	2008-2011	30	42	36	16
Unger [4]	OK	MGPR	2013-2016	21	33	23	6
Lautenbach et al. [222]	KS, CO	SSPR, MGPR, SGPR	2013-2016	187	253	248	78
Kunkel [226]	NM	SOPR	2016-2017	9	12	0	0
Lawrence et al. [1]	NM	SOPR	2013-2015	45	60	44	22
Parker et al. [227]	KS	MGPR	2017-2018	13	27	28	10
		Total		457	632	513	132

4.3 Methods

We developed an IPM for linking submodel derived quantities in a common model for LEPC population dynamics. We specified submodels for describing the observational uncertainty of each dataset and derived the joint distribution of the parameters implied by the submodel assumptions, data, and prior information with chained Markov melding. By taking a Markov melding approach,

we could adopt submodels previously proposed for analyzing the LEPC datasets while still facilitating joint inference. We proposed a population model using the Leslie matrix, equation (4.1), concept to explain underlying demographic variation in the LEPC population and link inferential quantities of interest from count and demographic submodels. Some parameters in the Leslie matrix are complex derived quantities of multiple submodels, and we show how to facilitate posterior inference in this context.

In northwestern Kansas and eastern Colorado, the LEPC EOR overlaps with the range of the greater prairie-chicken (*Tympanuchus cupido*; hereafter GRPC). Species verification was infeasible for the aerial and ground surveys and observations of GRPC were included in both datasets. We proposed distance sampling (Section 4.3.1) and N-mixture (Section 4.3.2) submodels that analyzed counts of prairie-chicken (LEPC and GRPC). We then derived the block-level abundances of LEPC in northwestern Kansas and eastern Colorado by multiplying the combined LEPC and GRPC abundances estimates by known LEPC proportions (Section 4.3.5).

4.3.1 Aerial Distance Sampling Submodel

We developed a distance sampling model for inferring abundance from aerial surveys with imperfect detection of prairie-chicken groups. The distance sampling model has previously been described in Van Ee et al. [220]. The helicopter crew included three observers and a pilot. The pilot sat in the front-right seat and their detections of prairie-chicken groups were not used for model fitting. The rear-right observer cannot see directly forward and scanned the ground 7 m right and beyond of the flight transect. Likewise, the rear-left observer scanned 7 m left and beyond of the transect. The front-left observer scanned the ground within 7 m of the transect and 7 m left and beyond of the transect. Detected prairie-chicken groups were announced only after they were out of view for all observers to ensure independent detections.

We let v_{itl} denote the number of observers who detected group $l = 1, \ldots, L_{it}^A$ in block $i = 1, \ldots, n^A$ during year $t = 1, \ldots, T^A$. Assuming all observers had equal skill in detecting prairie-chicken groups and that groups were detected independently, we modeled the number of detections

for group l as

$$v_{itl} \sim \text{Binomial}(O_{itl}, \zeta_{itl}) \tag{4.2}$$

where $O_{itl} \in \{1, 2\}$ was the number of observers for which group l was visible and ζ_{itl} was the observer detection probability for group l, which we assumed to be equal for all observers. Groups located 7 m left and beyond of the transect were visible to both left-hand side observers and $O_{itl} = 2$, but for all other groups $O_{itl} = 1$. We specified that the detectability of prairie-chicken groups varied based on their ecoregion, distance from the transect, d_{itl}, and size, N_{itl}. Our logistic regression model was $\text{logit}(\boldsymbol{\zeta}) = \left(\boldsymbol{X}_\zeta, \boldsymbol{N}^A, \boldsymbol{d}\right)\boldsymbol{\beta}_\zeta$, where $\boldsymbol{X}_\zeta$ is a binary matrix with unique intercepts for each ecoregion, and $(\cdot)$ denotes a column-wise bind of the listed matrices.

The entries of $\boldsymbol{\beta}_\zeta$ are not uniquely identifiable under a traditional single observer design but provide additional flexibility for estimating the detection function in a double observer framework. We treat detections of the two left-hand observers as fully independent but alternative approaches that allow for dependence in detectability as a result of unmeasured covariates and animal movement have been proposed [200, 201]. Under our modeling framework, we assumed that heterogeneity in prairie-chicken group detectability was well characterized by distance from the transect and size of the group. We also assumed groups were stationary, but note that there were a small number of transiting individuals.

We adopted a parameter expanded data augmentation approach [134] to account for undetected prairie-chicken groups in the aerial survey region. We assumed a super population of $M > L_{it}^A$ groups existed in the survey region of each block, and let $z_{itl} \in \{0, 1\}$ indicate whether group l was available for detection. For all detected individuals (i.e., $v_{itl} = 1$), we knew $z_{itl} = 1$, but for undetected individuals z_{itl} was unknown and had to be estimated. Royle et al. [134] referred to the groups for which $z_{itl} = 1$ as the sample population and recommended the sum of the sample group counts as an estimate of abundance for the survey region. Note that the estimated abundances are insensitive to the super population size as long as M is specified to be large. Considerations for selecting M are discussed in Appendix C.1.

For undetected groups, N_{itl}^{A} and d_{itl} were unknown and hence estimated. The side the group was located on, denoted by ϵ_{itl}, was also unknown and estimated. We use the superscripts o and u to denote the observed and unobserved components of partially latent parameters, respectively. Heuristically, we conceptualized the model as proposing groups of prairie-chicken that the aerial survey may have missed; we proposed a group of prairie-chicken with count $N_{itl}^{A,u}$, distance from the transect d_{itl}^{u}, and on side ϵ_{itl}^{u} of the transect, and then used the observations from our detected groups (i.e., $\boldsymbol{N}^{A,o}$, $\boldsymbol{d}^{o}$, $\boldsymbol{\epsilon}^{o}$) to determine if group l could have been part of our sample population (i.e., $z_{itl}^{u} = 1$) but went undetected (i.e., $v_{itl} = 0$). We chose the prior distributions for d_{itl} and ϵ_{itl} to induce a uniform distribution of groups within the survey region. See Appendix C.2 for a full description of all prior distributions and model specifications.

We assumed the distribution of the sample population indicators differed by block and year by letting

$$z_{itl} \sim \text{Bernoulli}(\psi_{it}), \text{ for } l = 1, \ldots, M, \tag{4.3}$$

where ψ_{it} is the probability that a group belonged to the sample population of block i during year t. The parameter ψ_{it} controls the number of prairie-chicken groups within the sampling region, with greater ψ_{it} implying more groups. Heterogeneity in prairie-chicken occupancy within the EOR has been documented [203], motivating the logit model, $\text{logit}(\boldsymbol{\psi}) = \boldsymbol{X}_{\psi}\boldsymbol{\beta}_{\psi}$. The design matrix $\boldsymbol{X}_{\psi}$ includes unique intercepts for the four ecoregions and an additional six continuous covariates. The covariates capture heterogeneity in the number of groups related to landcover, habitat patch size, anthropogenic disturbance, grassland restoration, and drought. See Appendix B.3 for a description of all covariates, and how they were collected.

The aerial survey was conducted during the breeding season to maximize detection of leks, but smaller, non-lekking groups as well as individual prairie-chicken were also detected. We accommodated the lek and non-lek observations in the observed prairie-chicken counts using a

zero-truncated Poisson (ZTP) mixture model

$$N_{itl}^{A} \sim \begin{cases} \text{ZTP}(\lambda_{it}), & \text{for } \omega_{itl} = 1 \\ \text{ZTP}(\lambda_{0}), & \text{for } \omega_{itl} = 0 \end{cases}, \tag{4.4}$$

$$\omega_{itl} \sim \text{Bernoulli}(p_{\omega}), \tag{4.5}$$

where $\lambda_{it}/(1 - e^{-\lambda_{it}})$ is the mean number of individuals per lek in region i during year t, $\lambda_0/(1 - e^{-\lambda_0})$ is the homogeneous mean number of individuals for non-lek observations, and ω_{itl} is the indicator of whether group l is a lek. Both distributions in the Poisson mixture, equation (4.4), are zero-truncated because if a group exists, it must have ≥ 1 individuals.

Mean lek size varies temporally and with environmental factors (6, 57). We specified a heterogeneous mean lek size across sites i and years t, λ_{it}, which we modeled with covariates (i.e., $\log(\boldsymbol{\lambda}) = \boldsymbol{X}_{\lambda}\boldsymbol{\beta}_{\lambda}$). We used the same suite of covariates for explaining heterogeneity in lek size as those used for explaining variability in the number of groups (i.e., $\boldsymbol{X}_{\lambda} = \boldsymbol{X}_{\psi}$). We treated ω_{itl} as a latent variable because it was often infeasible to determine the lek status of a LEPC group from the air. For monitoring purposes, KDWP defines a lek as 3 or more individuals on a display site [202]. In our case, the latent lek indicators ω_{itl} accommodated the bimodality of the count data and carried fewer assumptions regarding the composition of a lek.

4.3.2 N-mixture Submodel

We developed a submodel for describing observational uncertainty in prairie-chicken ground surveys. We let $G_{\iota tlj}$ denote the ground count of prairie-chickens on occasion j at lek site l in sampling region ι during year t. To account for variability in the counts induced by imperfect lek attendance, we adopted an N-mixture model [204],

$$G_{\iota tlj} \sim \text{Binomial}(N_{\iota tl}^{G}, p_e) \text{ for } j = 1, \ldots, J_{\iota tl}, \tag{4.6}$$

where p_e represents the homogeneous probability that an individual belonging to lek site l in ecoregion e was present at the lek when it is surveyed. We assumed a Poisson model for the latent lek abundances $N^G_{\iota tl} \sim \text{Poisson}(\boldsymbol{w}'_{\iota t}\boldsymbol{\eta})$, where $\boldsymbol{w}_{\iota t}$ is a vector of the covariates used in Section 4.3.1. Note that zero abundances, $N_{\iota tl} = 0$, were possible because surveyors revisited historical lek sites that may not have been visited by any individuals in year t. It follows then that $\boldsymbol{w}'_{\iota t}\boldsymbol{\eta}$ is the expected number of individuals per lek site rather than the number of expected individuals per active lek.

4.3.3 Survival Submodel

We developed a staggered entry, known-fate model [235] to infer trends in adult LEPC survival. Let $s_{lemt} \in \{0, 1\}$ represent the state (one for alive, zero for dead) of individual l from ecoregion e in month m of year t. We adopted a binary regression model for the observed fates,

$$s_{letm} \sim \text{Bernoulli}(\phi^A_{letm}), \tag{4.7}$$

where ϕ^A_{letm} is the adult monthly survival. Under 5% of individuals had partial encounter histories where a live individual was censored but reentered the study in a later month. Following previous studies of LEPC survival [1, 221, 228, 226], we fit our known-fate model to the censored individuals using the methods of Cooch and White [236] and White and Burnham [237], which ignore fates missing as a result of censoring.

LEPC have similar survival for all individuals past sexual maturity [219], and we let ϕ^A denote the survival for all adult individuals. Individuals entered the study in different months. We modeled heterogeneity in individual monthly survival probabilities as

$$\text{logit}(\phi^A_{letm}) = \mu^{\phi^A}_{el} + \beta^{\phi^A}_1 \text{SEX}_l + \beta^{\phi^A}_2 \text{BREED}_m + \beta^{\phi^A}_3 (\text{SEX}_l \times \text{BREED}_m) + \beta^{\phi^A}_4 \text{PDSI}_{etm}, \tag{4.8}$$

where $\mu^{\phi^A}_{el}$ is the mean survival for individual l in ecoregion e, SEX_l indicates the sex of individual l, BREED_m is the indicator of whether or not the observation fell in the breeding season, defined as March-June [6], and PDSI_{etm} is the Palmer Drought Severity Index for ecoregion e during month m of year t.

We modeled the $\mu_{el}^{\phi^A}$ hierarchically based on the individual's ecoregion, $\mu_{el}^{\phi^A} \sim \mathcal{N}(\mu_e^{\phi^A}, \sigma_{\phi^A}^2)$. The hierarchical formulation allows individual monthly survival to deviate from the mean response but shrinks the survival probability of individuals with few observations toward the overall ecoregion mean $\mu_e^{\phi^A}$. We assumed $\sigma_{\phi^A}^2$ and $\boldsymbol{\beta}^{\phi^A}$ were the same for all ecoregions and specified a vague inverse-gamma prior for the variance parameter and diffuse normal priors for the regression coefficients. Based on previous studies of LEPC survival [238, 239], we specified informative normal priors for the μ^{ϕ^A}. We set the prior means equal to the means reported by Hagen et al. [238] and Lyons et al. [239] but set the prior variance equal to double the variance reported. The 95% prior credible intervals for monthly survival were $(0.79, 0.96)$, $(0.89, 0.97)$, and $(0.88, 0.98)$ for females in the SOPR, SSPR, and MGPR, respectively. No prior information was available for the SGPR ecoregion, and we set a less informative 95% prior credible interval for female monthly survival of $(0.75, 0.99)$. Exact prior specifications are given in Appendix C.2.

4.3.4 Productivity Submodels

We proposed a known-fate model for describing variability in LEPC nesting survival. Let $F_{letd} \in \{0, 1\}$ be the indicator on the fate (one for alive, zero for failed) of a nest initiated by female l in ecoregion e on day $d = 1, 2, \ldots, D_i$ of year t. As described in Section 4.2.4, not all nests are visited daily and F_{letd} can be unknown for a sequence of days. We assumed that $F_{let1} = 1$ and $F_{litD_{let}}$ is known. We modeled the fate histories of nests with the binary autoregressive process

$$F_{letd} \sim \begin{cases} \text{Bernoulli}(\phi_{letm}^N) & , F_{let,d-1} = 1 \\ 0 & , F_{let,d-1} = 0 \end{cases}, \tag{4.9}$$

where ϕ_{letm}^N is the daily nesting survival. We modeled heterogeneity in female daily nesting survival as

$$\text{logit}(\phi_{letm}^N) = \mu_{el}^{\phi^N} + \beta_1^{\phi^N} \text{AGE}_l + \beta_2^{\phi^N} \text{PDSI}_{etm}, \tag{4.10}$$

where AGE_l is the indicator on the age class of female l (after-second-year or second-year).

We modeled the $\mu_{el}^{\phi^N}$ hierarchically based on the females ecoregions, $\mu_{el}^{\phi^N} \sim \mathcal{N}(\mu_e^{\phi^N}, \sigma_{\phi^N}^2)$. We specified a vague inverse-gamma prior for the variance parameter $\sigma_{\phi^N}^2$ and diffuse normal priors for the regression coefficients $\boldsymbol{\beta}^{\phi^N}$. Informed by preliminary work on LEPC daily nesting survival [240, 241, 242, 243], we set 95% prior credible intervals for daily nesting survival of second-year females at $(0.958, 0.996)$, $(0.931, 0.993)$, $(0.931, 0.996)$, and $(0.955, 0.994)$ in the SOPR, SSPR, MGPR, and SGPR ecoregions, respectively. For each ecoregion, the prior mean equaled the rate reported in the previous study, but we set the prior variance at double the uncertainty previously reported.

We let C_{letm} denote the clutch size of a nest of female l in ecoregion e during month m of year t. We accounted for spatial and temporal heterogeneity in clutch sizes with the Poisson regression model

$$C_{letm} \sim \text{Poisson}(\delta_{letm}), \tag{4.11}$$

$$\log(\delta_{letm}) = \mu_e^{\delta} + \beta_1^{\delta}\text{AGE}_l + \beta_2^{\delta}\text{PDSI}_{etm}, \tag{4.12}$$

where μ_e^{δ} is the log transformed mean clutch size for ecoregion e. There were only 7 observations of clutch sizes in the SSPR, and to reduce uncertainty, we specified the common distribution $\mu_e^{\delta} \sim \mathcal{N}(\mu^{\delta}, \sigma_{\delta}^2)$ for ecoregion means. We used a diffuse normal prior for μ^{δ} and regression coefficients $\boldsymbol{\beta}^{\delta}$ and a vague inverse-gamma prior for the variance parameter σ_{δ}^2.

We let H_{letm} be the number of eggs hatched from a nest of female l in ecoregion e during year t. To account for spatial and temporal heterogeneity in hatchability, we specified a Binomial regression model

$$H_{letm} \sim \text{Binomial}(C_{letm}, \pi_{letm}), \tag{4.13}$$

$$\text{logit}(\pi_{letm}) = \mu_e^{\pi} + \beta_1^{\pi}\text{AGE}_l + \beta_2^{\pi}\text{PDSI}_{etm}, \tag{4.14}$$

where μ_e^π is the logit transformed mean hatch probability for nests in ecoregion e. As with clutch sizes, we had few observations in the SSPR, and we let $\mu_e^\pi \sim \mathcal{N}(\mu^\pi, \sigma_\pi^2)$ to reduce uncertainty. We used diffuse normal priors for the μ^π and regression coefficients $\boldsymbol{\beta}^\pi$ and a vague inverse-gamma prior for the variance parameter σ_π^2.

We adopted the model of Lyons et al. [244] for estimating brood survival from repeated counts of unmarked chicks. Let $y_{ld} \in \{0, 1, 2, \dots\}$ be the number of living chicks counted in a brood of female l on day $d \in \{1, 2, \dots, 60\}$. Note that the number and times of counts differed for each brood. We assumed the number of chicks alive at hatch is known for each brood and denoted it by B_{i0}. Further, we assumed that females do not adopt chicks from other broods. Following Lyons et al. [244], we proposed the brood survival model

$$y_{ld} \sim \text{Binomial}(B_{ld}, q), \tag{4.15}$$

$$B_{l,d+1} \sim \text{Binomial}(B_{ld}, \phi_d^B), \tag{4.16}$$

where B_{ld} is the number of chicks alive in the brood of female l on day d, ϕ_d^B is the daily survival for all broods on day d, and q is the probability of detecting a chick assumed to be equal across all occasions and broods. Following Pitman et al. [241], we assumed different daily survival for the early and late brood rearing periods defined as hatch to 14 days post-hatch and 15–60 days post-hatch, respectively. We set a uniform prior for chick detection probability q. We set an informative Beta$(290.40, 15.28)$ prior for daily survival in the early period and informative Beta$(437.23, 9.84)$ for the late period. We set the prior means equal to the rates reported by Pitman et al. [241] and set the prior variances at double the variances reported. The informative priors implied 95% prior credible intervals for daily survival of (0.92, 0.97) and (0.96, 0.99) for the early and late brood rearing period, respectively.

4.3.5 Population Model

We specified a population model following the structure of the Leslie matrix, equation (4.1), to link quantities from the count and demographic submodels and learn about annual patterns

in LEPC abundance, survival, and productivity. We derived the estimated annual abundance of LEPCs in each ecoregion as

$$N_{et}^{A} = \sum_{i \in e(i)} \sum_{l=1}^{M} N_{itl}^{A} z_{itl} \kappa_i, \tag{4.17}$$

where $\sum_{i \in e(i)}$ is the sum over all blocks in ecoregion e and κ_i is the proportion of LEPC of all prairie-chicken in block i [5]. Proportions vary from 0.001-1 for blocks in the SGPR but equal 1 for all blocks in the SOPR, SSPR, and MGPR. Likewise, for the ground surveys, we derived an index of ecoregional annual abundance as

$$N_{et}^{G} = \sum_{\iota \in e(\iota)} \sum_{l=1}^{L_{\iota t}^{G}} N_{\iota tl}^{G} \kappa_{\iota}, \tag{4.18}$$

where $\sum_{l=1}^{L_{\iota t}^{G}}$ is the sum over all $L_{\iota t}^{G}$ lek sites in sample region ι during year t and $\sum_{\iota \in e(\iota)}$ is the sum over all ground sampling regions that belong to ecoregion e. We refer to the derived abundances from the ground surveys as an index of abundance because sites were preferentially located. Following Ross et al. [63] and Fritts et al. [217], we assumed the ground surveys were indicative of demographic patterns in the broader population and could be used to infer trends in LEPC survival and productivity. We inferred range-wide abundances from the aerial abundances alone.

We derived the annual ecoregion survival for each sex as

$$\phi_{ket}^{A} = \prod_{m=1}^{12} \phi_{ketm}^{A}, \tag{4.19}$$

where ϕ_{ketm}^{A} is the mean monthly survival for an individual of sex k. We defined productivity as the expected number of individuals produced per female surviving to their first breeding season. Productivity is a function of female nesting and renesting propensity, nest survival, clutch size, hatchability, brood survival, and juvenile survival. Following Hagen et al. [6] and Cummings et al.

[245], we derived the productivities

$$\rho_{aet} = \left(\xi_e^1 + \left(1 - (\phi_{aet}^N)^{24}\right)\xi_e^2\right)(\phi_{aet}^N)^{24}\delta_{aet}\pi_{aet}(\phi_1^B)^{14}(\phi_2^B)^{16}\phi_e^J, \tag{4.20}$$

where ρ_{aet} is the mean productivity of females in age class a in ecoregion e during year t; ξ_e^1 and ξ_e^2 are ecoregion specific nesting and renesting propensities; ϕ_1^B and ϕ_2^B are the daily chick survival for the early and late brood rearing period; and ϕ_e^J is the ecoregion specific juvenile survival defined as the probability a juvenile survives from 30 days post hatch to sexual maturity. To calculate the mean nesting success rate, we raised daily nesting survival to the mean number of exposure days (i.e., termination minus incubation date) for successful nests [246]. We calculated the mean annual daily nesting survival ϕ_{aet}^N, clutch size δ_{aet}, and hatchability π_{aet} using equations (4.10), (4.12), and (4.14), respectively, but replaced the monthly PDSI value with the breeding season average for that year.

We did not have data to facilitate posterior inference for quantities ξ_e^1, ξ_e^2, and ϕ_e^J, but prior information was available. We specified informative Beta priors for ξ_e^1 and ξ_e^2 based on previous studies [225, 240, 241, 242, 247]. As before, we matched the prior means to those reported by previous studies but increased prior uncertainty by doubling the prior variance. The 95% prior credible intervals for nesting propensity were $(0.53, 0.86)$, $(0.86, 0.97)$, $(0.37, 0.86)$, and $(0.70, 1.00)$ in the SOPR, SSPR, MGPR, and SGPR, respectively. The 95% prior credible intervals for renesting propensity were $(0.00, 0.21)$, $(0.21, 0.43)$, $(0.00, 0.66)$, and $(0.01, 0.27)$. Priors for ϕ_e^J were informed by Cummings et al. [245], and the 95% prior credible intervals were $(0.68, 1.00)$, $(0.33, 0.83)$, $(0.54, 0.87)$, and $(0.30, 0.77)$.

We completed our population model by allowing for demographic stochasticity. We adopted a Poisson-Binomial IPM to describe changes in abundance because of interannual variation in

survival and productivity [38],

$$N^X_{et} = N^X_{\female et,ASY} + N^X_{\male et,ASY} + N^X_{\female et,SY} + N^X_{\male et,SY}, \tag{4.21}$$

$$N^X_{\male e,t+1,ASY} \sim \text{Binomial}\left(N^X_{\male et,ASY} + N^X_{\male et,SY}, \phi^A_{\male et}\right), \tag{4.22}$$

$$N^X_{\female e,t+1,ASY} \sim \text{Binomial}\left(N^X_{\female et,ASY} + N^X_{\female et,SY}, \phi^A_{\female et}\right), \tag{4.23}$$

$$N^X_{e,t+1,SY} \sim \text{Poisson}\left(N^X_{\female et,SY}\rho_{et,SY} + N^X_{\female et,ASY}\rho_{et,ASY}\right), \tag{4.24}$$

where $X \in \{A, G\}$ indicates which survey the abundance is derived from, and SY and ASY are abbreviations for the age classes second-year and after-second-year, respectively. We assumed equal sex ratios at birth (i.e., $N^X_{\male et,SY} = N^X_{\female et,SY} = N^X_{et,SY}/2$). The population model connects all posterior quantities of interest into one cohesive IPM. Figure 4.2 gives a directed acyclic graph of the full IPM.

Ross et al. [63] proposed a Poisson-Binomial IPM for understanding changes in relative LEPC female abundance. Their IPM linked survival and productivity data with ground surveys in Kansas. Ross et al. [63] split productivity into fecundity and chick survival. Fecundity was defined as number of hatched chicks produced per female and accounts for the contributions of nesting initiation, nesting survival, clutch size, and hatchability in our productivity submodel. Chick survival was the number of hatched chicks that survived to the next breeding season and accounts for brood and juvenile survival. Ross et al. [63] also assumed equal survival and productivity across age classes and ecoregions in Kansas, whereas we allowed for unique vital rates in each ecoregion and productivity to differ by age class.

Abadi et al. [120] demonstrated the Poisson-Binomial population model, equations (4.21)-(4.24), can be extended to account for the demographic contributions of immigration and emigration. Genetic evidence suggests that movement between ecoregions is limited [20], and we assumed the effect of immigration and emigration on population demography was negligible. One violation of this assumption was the 2016-2019 translocation project that moved a total 411 individuals from the SGPR to the SSPR [62]. Because the number of translocated birds in each age

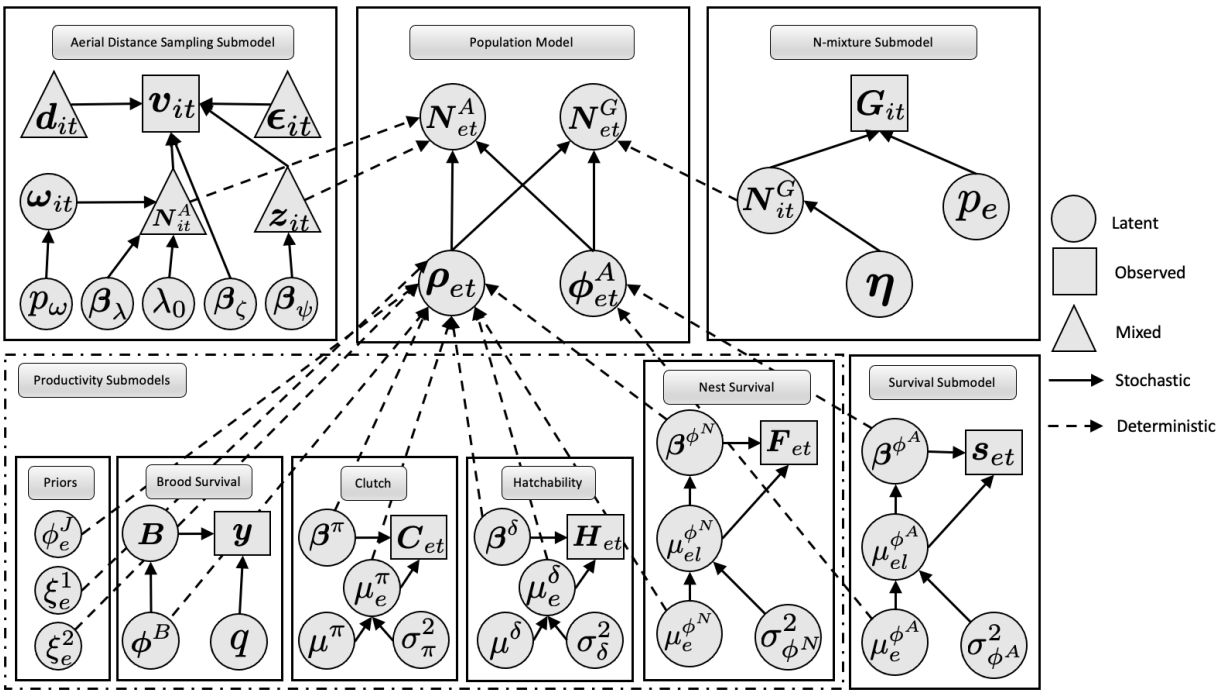

Figure 4.2: Directed acyclic graph of integrated population model for LEPC. All quantities in the population model, $\boldsymbol{N}^A_{et}$, $\boldsymbol{N}^G_{et}$, $\boldsymbol{\rho}_{et}$, and $\boldsymbol{\phi}_{et}$, are non-invertible deterministic functions of submodel parameters.

and sex class is known, we adjusted the SGPR and SSPR annual abundances accordingly without including a stochastic element for immigration and emigration.

We derived annual population growth rates for each ecoregion as $r_{et} = N^A_{e,t+1}/N^A_{et}$. We used the abundances inferred from the aerial survey for deriving growth rates because they provided an unbiased estimate of the true ecoregional abundance unlike the ground abundances that were preferentially sampled. Following Ross et al. [63], we also calculated the posterior temporal correlation between $\boldsymbol{r}_e$ and the vital rates $\boldsymbol{\phi}^A_{\female e}$, $\boldsymbol{\phi}^A_{\male e}$, $\boldsymbol{\rho}_{e,SY}$, and $\boldsymbol{\rho}_{e,ASY}$. The posterior correlations between annual vital rates and growth rates helped quantify the relative drivers of population change in each ecoregion [248, 249].

4.4 Posterior Inference

Abundances derived in equations (4.17) and (4.18) were not corrected for survey effort and can bias posterior inference for annual survival and productivity. For example, if survey effort is greater for year t than $t+1$ in ecoregion e, the posterior expectations of ϕ^A_{ket} and ρ_{aet} will be biased low.

We standardized abundances in equations (4.21)-(4.24) by multiplying the ecoregional densities in year $t+1$ by the area surveyed in year t. The derived abundances represent the expected size of the population in year $t+1$ assuming survey effort had been constant.

One could consider multiplying all annual densities by a common area, but such an approach would bias posterior variances and muddle the contributions of the aerial and ground data on posterior inference for survival and productivity. The posterior variances of the parameters in the Poisson-Binomial IPM, equations (4.21)-(4.24), are inversely related to the size of the population index N_{et}^{X}. Intuitively, monitoring a larger population provides greater insights into dynamics, and see Appendix C.3 for a statistical derivation. By multiplying the annual density estimates by survey effort, we properly adjusted the uncertainty of the posterior distributions.

Manderson and Goudie [64] introduced chained Markov melding for reconciling differences in prior information expressed in a sequence of submodels linked by common quantities. The approach facilitates inference when the linking quantities are expressed as deterministic non-invertible functions of submodel parameters. In such scenarios, capturing the prior and posterior correlation among parameters is not possible with standard Bayesian methodology. We extended the framework of Manderson and Goudie [64] by proposing an IPM composed of two chains of submodels that intersect in a common population model.

We let $\boldsymbol{\phi}$ and $\boldsymbol{\rho}$ be the vectors of annual survival and productivity across all sex and age classes, respectively. We derived the joint melded distribution for $\boldsymbol{\theta} = (\boldsymbol{N}^{A\prime}, \boldsymbol{N}^{G\prime}, \boldsymbol{\phi}', \boldsymbol{\rho}')'$ as follows [64]:

$$
\begin{aligned}
[\boldsymbol{\theta}, \cdot]_{\text{meld}} &= [\boldsymbol{\theta}]_{\text{pool}}[\cdot|\boldsymbol{\theta}]_{\text{ADSM}}[\cdot|\boldsymbol{\theta}]_{\text{pop}}[\cdot|\boldsymbol{\theta}]_{\text{N-mix}}[\cdot|\boldsymbol{\theta}]_{\text{surv}}[\cdot|\boldsymbol{\theta}]_{\text{prod}}, && (4.25)\\
&= [\boldsymbol{\theta}]_{\text{pool}}[\cdot|\boldsymbol{N}^{A}]_{\text{ADSM}}[\cdot|\boldsymbol{\theta}]_{\text{pop}}[\cdot|\boldsymbol{N}^{G}]_{\text{N-mix}}[\cdot|\boldsymbol{\phi}]_{\text{surv}}[\cdot|\boldsymbol{\rho}]_{\text{prod}}, && (4.26)\\
&= [\boldsymbol{\theta}]_{\text{pool}}\frac{[\cdot, \boldsymbol{N}^{A}]_{\text{ADSM}}}{[\boldsymbol{N}^{A}]_{\text{ADSM}}}\frac{[\cdot, \boldsymbol{\theta}]_{\text{pop}}}{[\boldsymbol{\theta}]_{\text{pop}}}\frac{[\cdot, \boldsymbol{N}^{G}]_{\text{N-mix}}}{[\boldsymbol{N}^{G}]_{\text{N-mix}}}\frac{[\cdot, \boldsymbol{\phi}]_{\text{surv}}}{[\boldsymbol{\phi}]_{\text{surv}}}\frac{[\cdot, \boldsymbol{\rho}]_{\text{prod}}}{[\boldsymbol{\rho}]_{\text{prod}}}, && (4.27)
\end{aligned}
$$

where $[\boldsymbol{\theta}]_{\text{pool}}$ is the pooled prior marginal distribution, and $[\cdot, \boldsymbol{\theta}]_{\mathcal{M}}$ and $[\boldsymbol{\theta}]_{\mathcal{M}}$ denote the joint and prior marginal distribution of $\boldsymbol{\theta}$ in submodel $\mathcal{M}$, respectively. We abbreviate the aerial distance sampling, N-mixture, population, survival, and productivity submodels as ADSM, N-mix, pop,

surv, and prod, respectively. We use the "$\cdot$" notation to denote data and all parameters other than $\boldsymbol{\theta}$ in the conditional distribution $[\cdot|\boldsymbol{\theta}]_{\mathcal{M}}$.

In the first equality, equation (4.25), we performed marginal replacement to establish a common prior marginal distribution for $\boldsymbol{\theta}$ across all submodels [123]. Goudie et al. [123] proved that marginal replacement minimizes the Kullback–Leibler divergence between the melded distribution and original joint distribution under the constraint that the updated joint distribution admits $[\boldsymbol{\theta}]_{\text{pool}}$ as a marginal. Therefore, we can view equation (4.25) as the minimally modified joint distribution with marginal $[\boldsymbol{\theta}]_{\text{pool}}$. Equation (4.25) also assumed conditional independence among all datasets given the link parameters $[\boldsymbol{\theta}]$. This assumption was violated in practice as the same females tagged for survival analysis were also monitored for productivity data. In addition, birds tagged for survival analysis were often captured at ground survey sites where lek counts were recorded. Abadi et al. [120] showed that assuming conditional independence among the count, survival, and productivity datasets when individuals occur in multiple datasets generally has negligible impacts on posterior inference.

Moving from equation (4.25) to (4.26), we removed independent variables from the submodel conditional distributions. In equation (4.26), the conditional distributions $[\cdot|\boldsymbol{N}^A]_{\text{ADSM}}$, $[\cdot|\boldsymbol{N}^G]_{\text{N-mix}}$, $[\cdot|\boldsymbol{\phi}]_{\text{surv}}$, and $[\cdot|\boldsymbol{\rho}]_{\text{prod}}$ are unknown because the linking quantities are non-invertible functions of submodel parameters. Therefore, in equation (4.27), we expressed the joint melded distribution as a product of the submodel joint distributions over the marginal distributions for posterior inference. The joint melded posterior, equation (4.27), is highly flexible and allows us to incorporate prior dependence among the quantities expressed in $\boldsymbol{\theta}$ while still accounting for prior information included at smaller time scales in the other submodels. For example, we could specify prior density dependence by putting a joint prior on $\boldsymbol{N}$, $\boldsymbol{\phi}$, and $\boldsymbol{\rho}$ that has non-zero covariance. For our purposes, we assumed independent priors in the population model (i.e., $[\boldsymbol{\theta}]_{\text{pop}} = [\boldsymbol{N}]_{\text{pop}}[\boldsymbol{\phi}]_{\text{pop}}[\boldsymbol{\rho}]_{\text{pop}}$).

Manderson and Goudie [64] propose several methods for forming the pooled prior marginal distributions. Following Van Ee et al. [220], we used chained product of experts (PoE) for the

ecoregional abundances.

$$[\boldsymbol{N}]_{\text{pool}} = \frac{1}{K}[\boldsymbol{N}^A]_{\text{ADSM}}[\boldsymbol{N}]_{\text{pop}}[\boldsymbol{N}^G]_{\text{N-mix}},\ K = \sum_{\boldsymbol{N}}[\boldsymbol{N}^A]_{\text{ADSM}}[\boldsymbol{N}]_{\text{pop}}[\boldsymbol{N}^G]_{\text{N-mix}}. \tag{4.28}$$

Under PoE pooling, the pooled prior marginal distribution for $\boldsymbol{N}$ cancels with its submodel marginal distributions. All submodel marginal distributions for $\boldsymbol{N}$ are analytically intractable and need to be estimated for implementation. Goudie et al. [123] recommended approximating the submodel marginal distributions with kernel density estimators, but this approach can lead to numerical instabilities in implementation [207]. By using chained product of experts (PoE), we obviate approximating the submodel marginal distributions.

The submodel marginal distributions $[\boldsymbol{\phi}]_{\text{surv}}$ and $[\boldsymbol{\rho}]_{\text{prod}}$ are also non-tractable because of the complex transformations in equations (4.19) and (4.20). We chose $[\boldsymbol{\rho}]_{\text{pool}} = [\boldsymbol{\phi}]_{\text{surv}}[\boldsymbol{\rho}]_{\text{prod}}$ and under PoE pooling for $\boldsymbol{N}$, the joint melded posterior, equation (4.25), can be written

$$[\boldsymbol{\theta}, \cdot]_{\text{meld}} \propto [\cdot, \boldsymbol{N}^A]_{\text{ADSM}}[\cdot, \boldsymbol{N}^G]_{\text{N-mix}}[\boldsymbol{N}^A, \boldsymbol{N}^G|\boldsymbol{\phi}, \boldsymbol{\rho}]_{\text{pop}}[\cdot, \boldsymbol{\phi}]_{\text{surv}}[\cdot, \boldsymbol{\rho}]_{\text{prod}}. \tag{4.29}$$

The choice of pooled prior $[\boldsymbol{\rho}]_{\text{pool}} = [\boldsymbol{\phi}]_{\text{surv}}[\boldsymbol{\rho}]_{\text{prod}}$ in equation (4.29) is referred to as dictatorial pooling and assumes prior information from one submodel is authoritative [123]. Dictatorial pooling is appealing for $\boldsymbol{\rho}$ in the LEPC case study because prior information is available for quantities influencing productivity (e.g., nesting survival, nesting propensity, juvenile survival, etc.) but not productivity itself. We let the hierarchical prior in the productivity submodels dominate the contribution of prior information in the joint distribution. In situations where prior information is also available for productivity directly or when the productivity and survival priors are dependent, see Manderson and Goudie [64] for alternative pooling functions.

We proposed a parallel multistage MCMC algorithm for drawing samples of $\boldsymbol{\theta}$ from the joint melded distribution, equation (4.29). In the first stage, we fit the aerial distance sampling, N-mixture, survival, and productivity submodels in parallel using standard Metropolis-Hastings within Gibbs algorithm. We promoted conjugacy of the regression coefficients $\boldsymbol{\beta}_{\psi}$, $\boldsymbol{\beta}^{\phi^A}$, $\boldsymbol{\beta}^{\phi^N}$, and $\boldsymbol{\beta}^{\phi^\pi}$

using Pólya-Gamma data augmentation [91]. First stage samples of annual ecoregion productivities were generated using equation (4.20) with a random value of ξ_e^1, ξ_e^2, and ϕ_e^J drawn from their prior distributions each iteration of the MCMC algorithm. The productivity submodel can also be parallelized by fitting brood, nesting, clutch, and hatch data independently. For the LEPC case study, we used a unified productivity MCMC algorithm for fitting the nesting survival, clutch, and hatch submodels. We used a separate MCMC algorithm for brood survival because the algorithm required many more iterations to converge (Table 4.5).

In the second-stage, we used samples of $\boldsymbol{\theta}$ derived from the first-stage as the proposals in the population model, equations (4.21)-(4.24). For MCMC iteration k in the second-stage, we drew a sub-sample denoted by $\boldsymbol{\theta}^{(\star)}$ from the first-stage samples randomly with replacement, and the Metropolis-Hastings ratio was

$$\frac{[\boldsymbol{N}^{A(\star)}, \boldsymbol{N}^{G(\star)} | \boldsymbol{\phi}^{(\star)}, \boldsymbol{\rho}^{(\star)}]_{\text{pop}}}{[\boldsymbol{N}^{A(k-1)}, \boldsymbol{N}^{G(k-1)} | \boldsymbol{\phi}^{(k-1)}, \boldsymbol{\rho}^{(k-1)}]_{\text{pop}}}, \tag{4.30}$$

where $\boldsymbol{\theta}^{(k-1)}$ is the current value of $\boldsymbol{\theta}$ in the Markov chain. Because we draw $\boldsymbol{\theta}$ from the first-stage samples, the proposal distribution for $\boldsymbol{\theta}$ cancels with the submodel joint distributions in equation (4.29). The refined samples from the second-stage constitute draws from $[\boldsymbol{\theta}, \cdot]_{\text{meld}}$. The dimension of $\boldsymbol{\theta}$ is large. We improved parameter mixing and MCMC convergence by updating the elements of the subvectors $\boldsymbol{N}^A$, $\boldsymbol{N}^G$, $\boldsymbol{\phi}$, and $\boldsymbol{\rho}$ one at a time. We provide a complete description of our multistage MCMC algorithm in Appendix C.1.

We discarded a portion of samples from each MCMC algorithm as burn-in and thinned the remaining sample for proposals of $\boldsymbol{\theta}$ in the population model (Table 4.5). The potential scale reduction factor for all parameters from the first stage was less than 1.1 indicating convergence [250]. We coded our multistage MCMC algorithms in both `R` and `C++` using the `R` package `Rcpp`. Fitting the aerial distance sampling submodel constituted a computational bottleneck, and we coded its MCMC algorithm in `C++` to decrease runtime [148]. We assessed the effect of the ground surveys on posterior inference for survival and productivity by fitting our IPM to the aerial counts

alone. Section 4.5 shows posterior inference for vital rates and abundance when we fit the IPM to subsets of the available data sources.

Table 4.5: Markov chain Monte Carlo details for fitting submodels to lesser prairie-chicken data sources. Retention is the percentage of samples kept of the total sample size after burn-in. ADSM=aerial distance sampling submodel.

Model	Language	Run Time (hrs)	Iterations	Burn-in	Retention	Posterior Sample
ADSM (4.3.1)	C++	4.3	$70,000$	$20,000$	40%	$20,000$
N-mixture (4.3.2)	R	1.4	$200,000$	$100,000$	20%	$20,000$
Survival (4.3.3)	R	1.2	$11,000$	$1,000$	100%	$10,000$
Nest, Clutch, Hatch (4.3.4)	R	1.9	$11,000$	$1,000$	100%	$10,000$
Brood Survival (4.3.4)	C++	0.2	$1,000,000$	$100,000$	1%	$10,000$
Population (4.3.5)	C++	6.5	$100,000,000$	$500,000$	0.01%	$10,000$

4.5 Results

On average, male annual survival was 15% greater than female survival when fitting the IPM to all available data sources (Figure 4.3). Survival was similar for the MGPR and SGPR but 13% and 15% greater for males and females in the SOPR, respectively. Survival in the SSPR was 3% greater for males and females than in the MGPR and SGPR. The posterior variance of all distributions decreased in the second stage when conditioned on the aerial surveys, and posterior means were similar. Assimilating the ground surveys increased female survival by 2%, but decreased male survival by 8% on average across ecoregions.

After-second-year females had 20% greater productivity than second-year females on average (Figure 4.4). Productivity was again similar across the SSPR, MGPR, and SGPR, but lower in the SOPR (-19% and -21% for after-second-year and second-year females, respectively). The marginal posterior distributions for productivity estimated from the demographic data alone have large uncertainty. The productivity posterior distributions are functions of the quantities ξ_e^1, ξ_e^2, and ϕ_e^J which were only informed by prior information (Section 4.3.5). Refining the posterior distributions by filtering for the samples of productivity that conformed with the aerial surveys substantially reduced uncertainty and increased posterior means by 12% for both age classes. Con-

ditioning productivity on the ground surveys further reduced uncertainty and increased posterior means by another 4%.

Female and male survivorship were strongly correlated with annual growth rates in the SOPR and SSPR, respectively, when we fit the IPM to both the aerial and ground surveys (Table 4.6). These associations vanished when fitting the model to the aerial counts alone. Annual growth rates in the MGPR and SGPR were not correlated with female survival. There was a negative association between growth rates and male suvival in the SGPR when we fit the IPM to both the aerial and ground surveys.

Across all model fits to both the full and reduced datasets, there was strong evidence for the contributions of after-second-year and second-year female productivity on annual growth rates. Posterior correlations for productivity and growth rates increased when we fit the IPM to both the aerial and ground surveys. Annual growth rates in the SOPR were most strongly correlated with productivity, but for all ecoregions, the posterior probability that the correlation was greater than 0 was 1.

Table 4.6: Temporal posterior correlations for annual growth and vital rates. Posterior correlations are split by the group of datasets used to estimate the quantity. Posterior means of Pearson correlation coefficients (95% credible intervals) shown.

Data Sources	Ground, Aerial, Demographic	Aerial & Demographic	Ground, Aerial, Demographic	Aerial & Demographic
Ecoregion	Male Survival		Female Survival	
SOPR	0.25 (-0.07, 0.55)	-0.13 (-0.55, 0.32)	0.43 (0.06, 0.72)	-0.11 (-0.46, 0.27)
SSPR	0.56 (0.31, 0.77)	0.13 (-0.34, 0.56)	0.09 (-0.24, 0.40)	0.05 (-0.41, 0.48)
MGPR	0.16 (-0.2, 0.48)	-0.02 (-0.48, 0.44)	-0.06 (-0.48, 0.38)	-0.07 (-0.49, 0.36)
SGPR	-0.26 (-0.48, 0.00)	0.02 (-0.44, 0.47)	0.12 (-0.21, 0.43)	-0.01 (-0.41, 0.40)
Ecoregion	After-Second-Year Female Productivity		Second-Year Female Productivity	
SOPR	0.93 (0.87, 0.97)	0.81 (0.61, 0.93)	0.89 (0.80, 0.95)	0.79 (0.59, 0.92)
SSPR	0.82 (0.65, 0.93)	0.53 (0.11, 0.83)	0.72 (0.51, 0.87)	0.52 (0.11, 0.82)
MGPR	0.74 (0.48, 0.91)	0.58 (0.20, 0.84)	0.84 (0.69, 0.94)	0.68 (0.36, 0.89)
SGPR	0.70 (0.28, 0.92)	0.51 (0.09, 0.81)	0.90 (0.80, 0.96)	0.60 (0.22, 0.85)

Figure 4.5 shows the annual ecoregion abundance for the aerial survey period (2012-2022). On average, abundance was greatest in the SGPR and lowest in the SSPR. Integrating the demography data decreased uncertainty and also highlighted interannual variability in abundance. Integrating

the ground surveys further reduced uncertainty. All ecoregions show a decrease in annual abundance in 2012-2014 followed by a period of growth from 2015-2017.

In Appendix C.1, we provide the annual ecoregion abundances posteriors from 2005-2011 and compare our posteriors from 2012-2022 with the estimates of Nasman et al. [5]. All ecoregion abundances show a sharp decline from 2005-2011. The abundances estimates from our IPM fit to all available datasets were similar to those of Nasman et al. [5] but had less uncertainty. In Appendix C.5, we provide posterior means and 95% credible intervals for annual abundance, survival, and productivity in each ecoregion.

4.5.1 Simulation Study

We assessed the impacts of assimilating more data sources on predictive performance and posterior inference for a simplified version of our melded IPM over a period of $T = 20$ years. Using the submodels described in Sections 4.3.3 and 4.3.4, we simulated survival and productivity data. All parameters were set to their posterior means obtained from fitting the submodels to the LEPC datasets. We calculated annual survival using equation (4.19) and the simulated monthly survival. We calculated annual productivity using equation (4.20) with η_e^1, η_e^2, and ϕ_e^J fixed at their prior means. We then set the initial abundance of LEPC in each ecoregion at the posterior mean abundance of LEPC in 2011 inferred from our IPM, and simulated annual abundance in each ecoregion for $T = 20$ years using the Poisson-Binomial population model, equations (4.21)-(4.21), and simulated vital rates.

Following Van Ee et al. [220], we simulated data for simplified distance sampling and N-mixture submodels as a representation of the aerial and ground surveys. Full model specifications are available in Appendix B.1. We set the maximum number of individuals available for detection for each survey equal to the simulated range-wide density multiplied by the mean ecoregion survey effort for each method (Tables 4.1 and 4.2). The detection parameters in the survey submodels were specified so that posterior standard deviations for annual LEPC densities approximated those from

the real data analysis. We fit the simplified IPM to the simulated datasets with the same methods described in Section 4.4. Table 4.7 provides the model fitting details for each submodel.

Table 4.7: Markov chain Monte Carlo details for fitting submodels to simulated lesser prairie-chicken datasets. Retention is the percentage of samples kept of the total sample size after burn-in.

Model	Language	Iterations	Burn-in	Retention	Posterior Sample
Distance Sampling (Appendix B.1.4)	R	$2,000$	0	100%	$2,000$
N-mixture (Appendix B.1.5)	R	$30,000$	0	7%	$2,000$
Survival (4.3.3)	R	$1,000$	100	100%	900
Nest, Clutch, Hatch (4.3.4)	R	$2,000$	100	100%	$1,900$
Brood Survival (4.3.4)	C++	$20,000$	$10,000$	19%	$1,900$
Population (4.3.5)	R	$500,000$	0	2%	$10,000$

In our simulation study, we accessed predictive performance and posterior inference when the survival and productivity submodels were misspecified. We simulated all datasets as previously described with the exception that we added extra temporal variability to annual vital rates. We performed 70 simulations and in half of the simulations, we simulated extra temporal variability in LEPC vital rates.

Coverage rates and posterior mean absolute error (MAE) were similar for annual survival regardless of which datasets were used for posterior inference (Figure 4.6). The IPM slightly decreased posterior standard deviations and including ground surveys in the IPM further reduced uncertainty. Reduction in the uncertainty of annual survival from including additional data sources did not depend on whether the demographic submodels were misspecified or not. Overall, model misspecifation increased MAE and decreased coverage.

Coverage rates for productivity were high. Recall productivity is a function of the quantities ξ_e^1, ξ_e^2, and ϕ_e^J which are only informed by prior sources of information. As a result, uncertainty for annual productivity is large, yielding large coverage rates. Both MAE and posterior standard deviation decreased in the IPM and further reductions were achieved when ground surveys used. As with survival, model misspecifation increased MAE.

Coverage rates were similar for abundance, but including demography and ground data reduced posterior standard deviations and MAE. Metrics were similar regardless of whether the data were simulated with model misspecifation or not.

We also assessed the predictive performance of our IPM for reduced aerial survey effort. We simulated datasets as described above but fit the IPM without the density samples derived from the distance sampling model in selected years. We considered four scenarios: aerial surveys conducted every year, every 2 out of 3 years, every other year, and once every 3 years. For each scenario, we performed 30 simulations.

Predictive performance for survival, ϕ, was unaffected by the temporal frequency of aerial survey effort or whether an aerial survey was conducted that year. Including the ground surveys in the IPM decreased root mean squared error (RMSE) by 5% on average. Predictive performance for productivity, ρ, decreased as aerial survey effort decreased, but there was little difference in RMSE for years with an aerial survey versus without. On average, RMSE was 15% lower for productivity when we included the ground surveys in the IPM. Predictive performance for abundance N decreased with reduced aerial survey effort and was lower in years without an aerial survey. Including ground surveys in the IPM decreased RMSE for abundance by 8% on average.

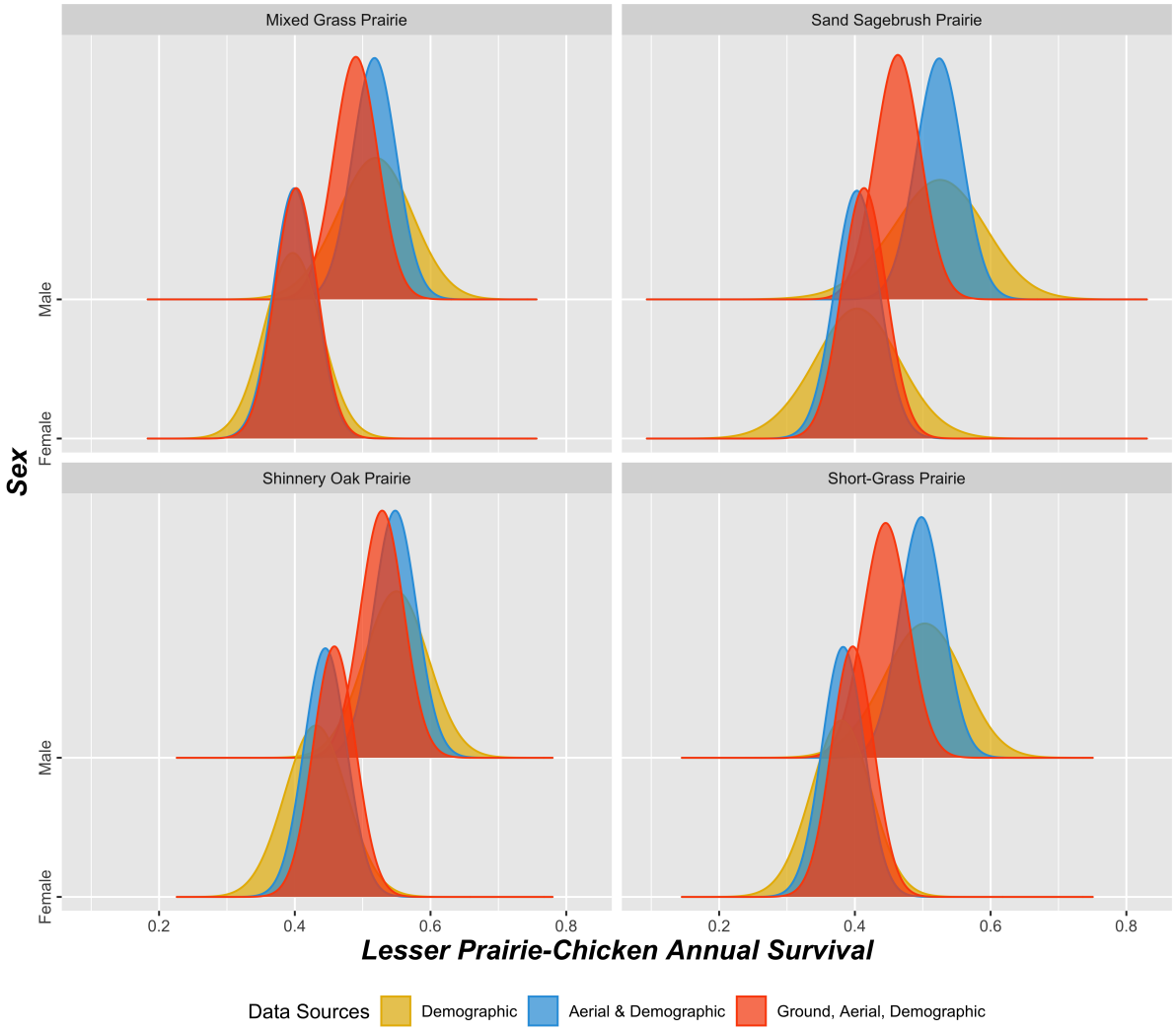

Figure 4.3: Posterior distributions of mean ecoregional survival split by sex. Color indicates which data sources were used to facilitate posterior inference. The yellow posterior distribution is estimated in the first stage of the multistage MCMC algorithm with the survival submodel (Section 4.3.3), and blue and red are the refined posterior distributions from the second stage estimated with the IPM (Section 4.3.5). All three posterior distributions account for prior information specified in Section 4.3.3.

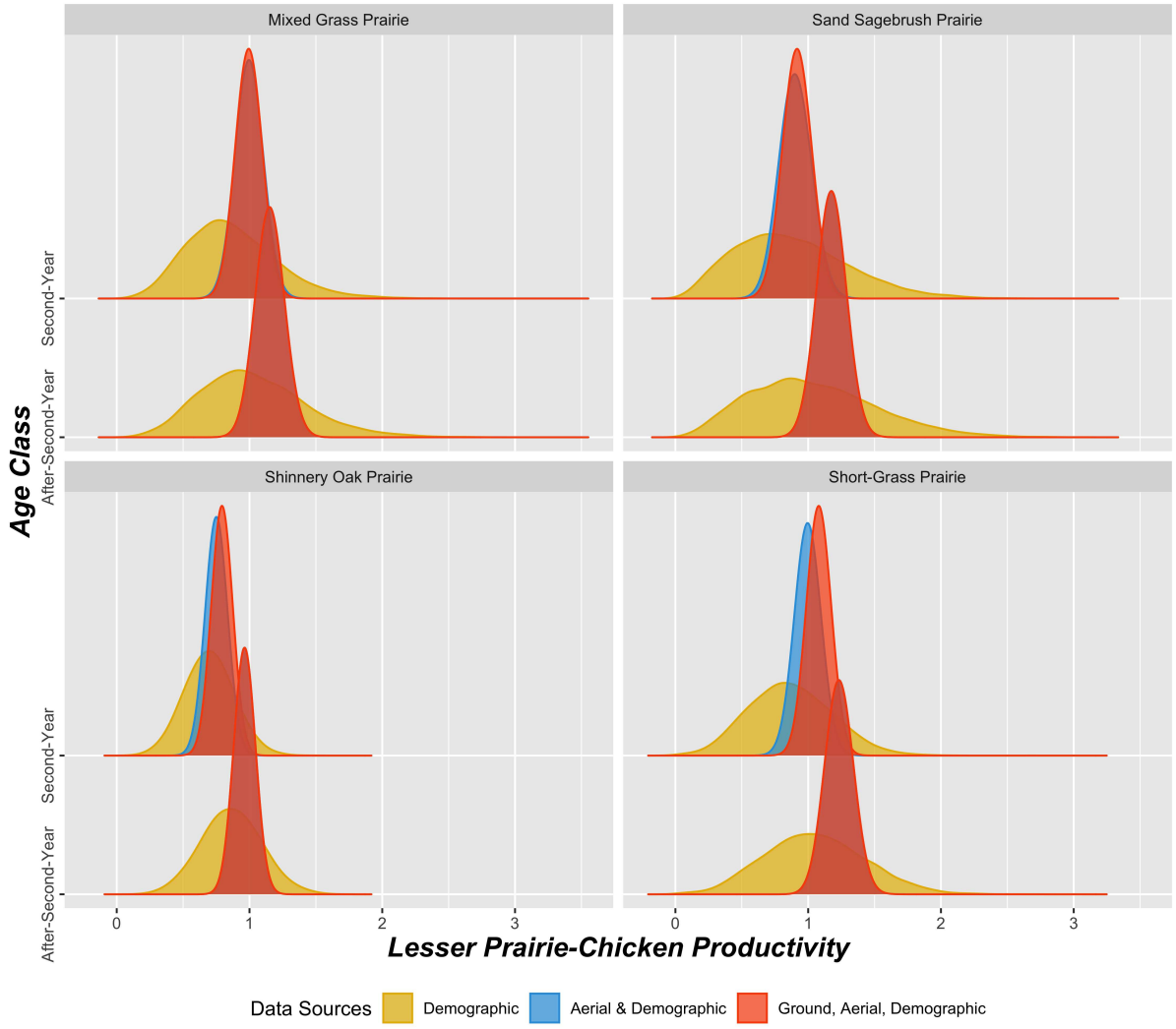

Figure 4.4: Posterior distributions of mean ecoregion productivity split by age class. We define productivity as the expected number of off-spring produced per female that reach sexual maturity. Color indicates which data sources were used to facilitate posterior inference. The yellow posterior distribution is estimated in the first stage of the multistage MCMC algorithm with the productivity submodels (Section 4.3.4), and blue and red are the refined posterior distributions from the second stage estimated with the IPM (Section 4.3.5). All three posterior distributions account for prior information specified in Section 4.3.4.

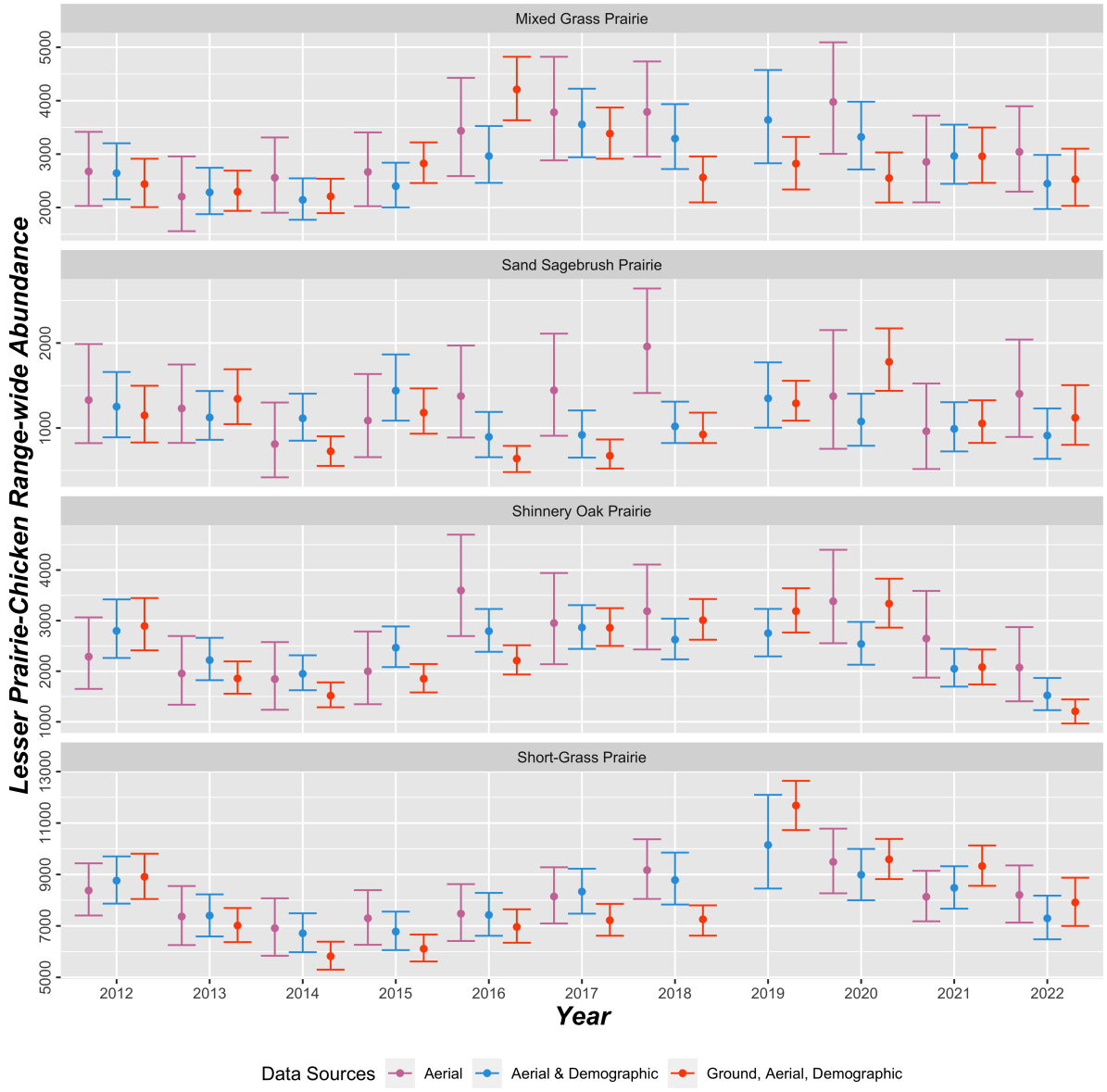

Figure 4.5: Posterior means and 95% credible intervals of annual ecoregional abundances. Color indicates which data sources were used for posterior inference. The purple credible intervals indicate the abundance estimates from the first stage of the MCMC algorithm which fits the aerial surveys to the aerial distance sampling submodel (Section 4.3.1). Blue and red denote the refined credible intervals from the second stage that condition on the demographic surveys and demographic and ground survey survey, respectively. The red and blue credible intervals account for the birds translocated from the SGPR to the SSPR during the 2016-2019 translocation project (Section 4.3.5). The purple credible intervals do not.

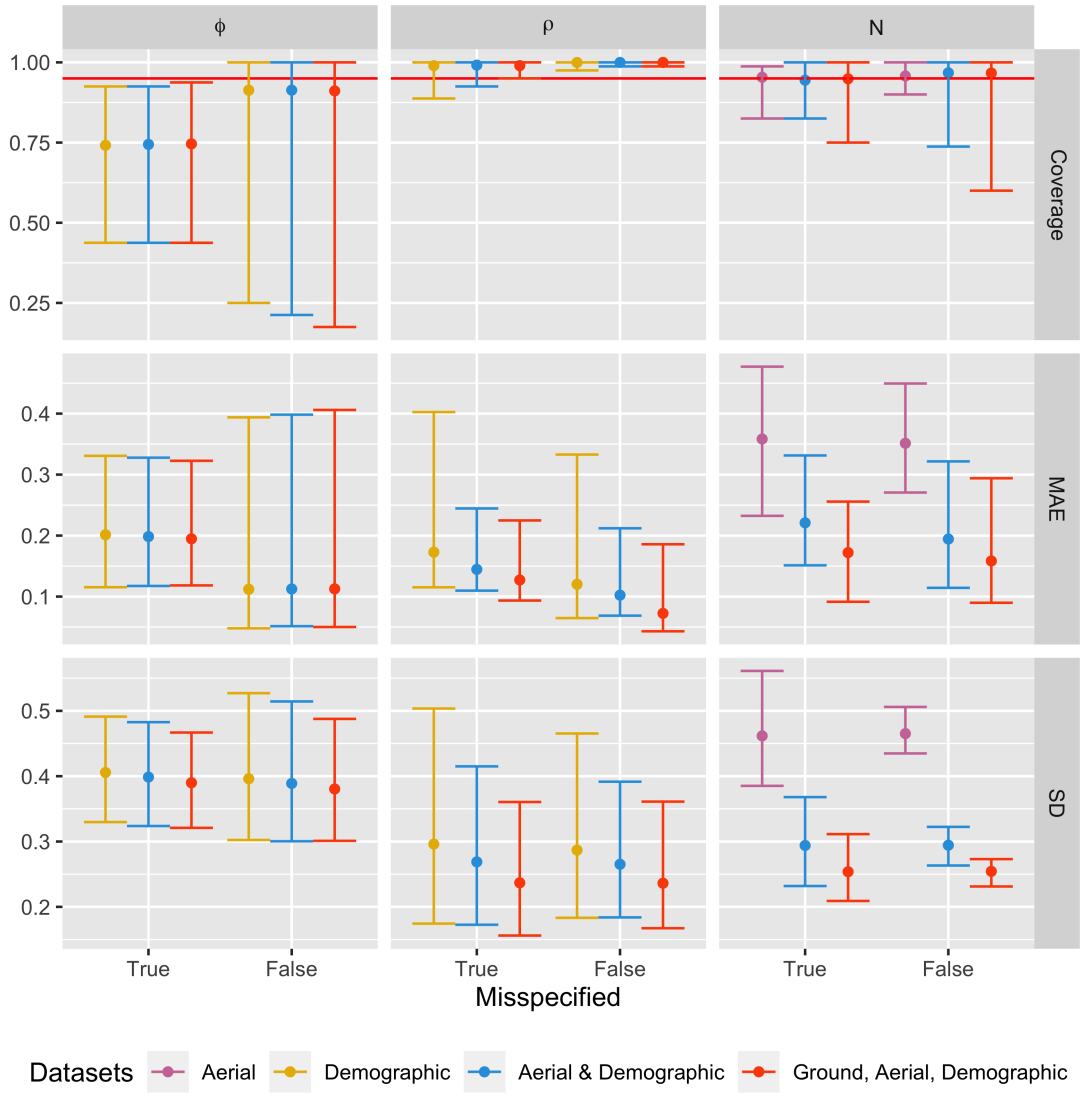

Figure 4.6: Means, minima, and maxima of empirical coverage (Coverage), posterior mean absolute error (MAE), and posterior standard deviation (SD) for abundance and vital rates. Color indicates which datasets were used for posterior inference. Yellow and purple indicate the performance metrics from the first stage of the MCMC algorithm using either the simulated demographic or aerial data alone, respectively. Blue and red denote the metrics from the second stage that condition on either the simulated aerial data alone or aerial and ground data, respectively. The horizontal red line indicates the targeted nominal coverage rate of 95%.

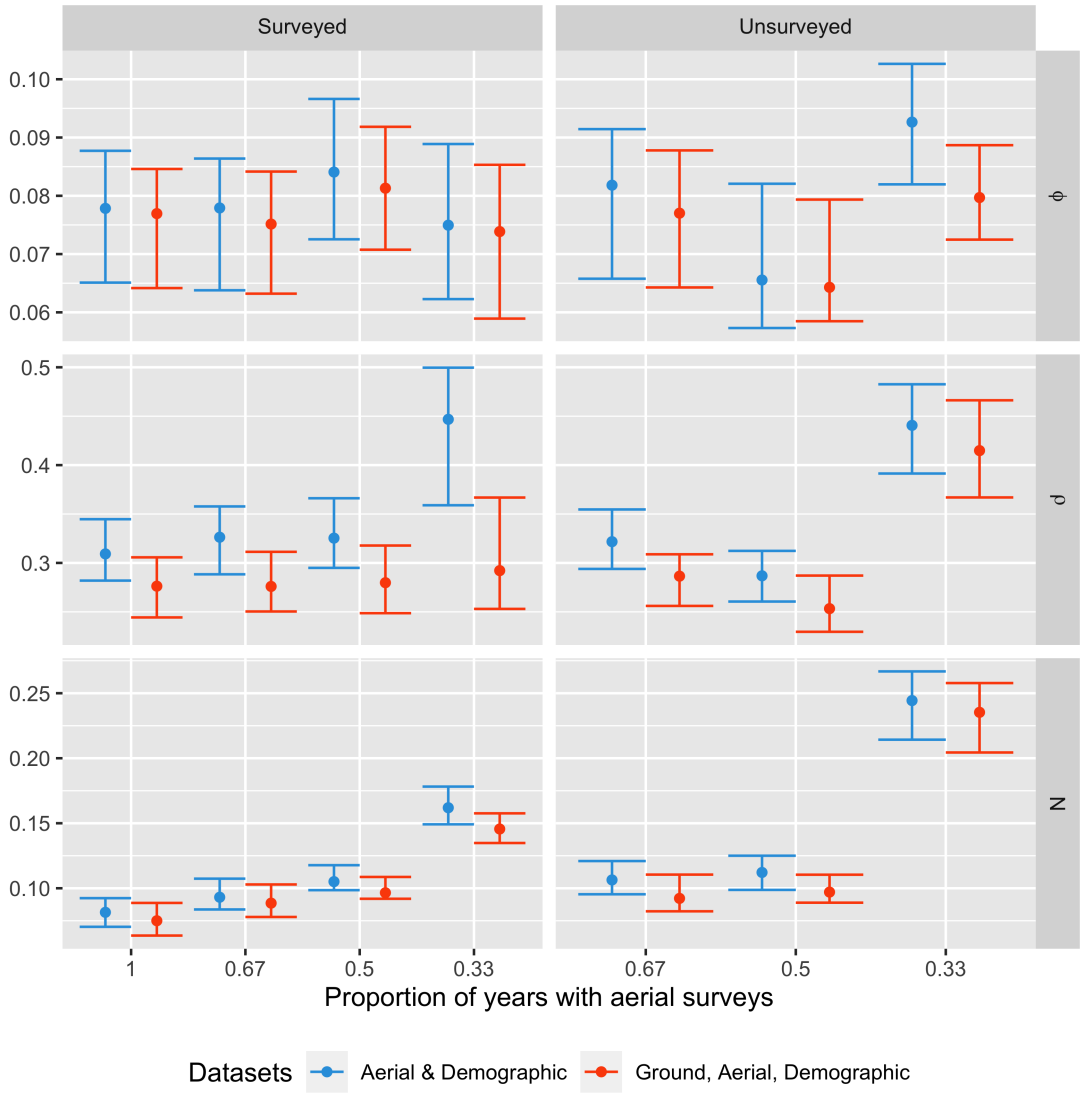

Figure 4.7: Medians and interquartile ranges of root mean squared errors (RMSE) for LEPC abundance and vital rates. Color indicates which datasets were used for posterior inference. Blue corresponds to the predictive performance of the IPM when using aerial and demographic data. Red is the predictive performance of the IPM when using aerial, ground, and demographic data. The x-axis indicates the temporal frequency of aerial survey effort. The left panels correspond to predictive performance in years during which an aerial survey was conducted and the right panel is predictive performance in years without an aerial survey.

4.6 Discussion

We demonstrated a flexible approach for facilitating posterior inference from an IPM composed from a chain of submodels. By linking the aerial and ground surveys to a common population model, we reduced bias and uncertainty for vital rates and abundance relative to submodels which analyzed the data sources independently. In the simulation study, we found our IPM was robust to model misspecification. We discovered that assimilating the ground surveys into the IPM was especially helpful for predicting abundance when aerial surveys were conducted less frequently and that abundance could still be reliably inferred in years during which no aerial survey was conducted. IPMs have been lauded for their ability to promote parameter identifiablility and provide novel insights into population dynamics [124]. Assimilating both aerial and ground surveys into our IPM allowed us to identify drivers of population growth that would have been overlooked had we fit the IPM to the aerial surveys alone.

We accounted for the effect of varying effort across years and surveys on posterior inference by weighting trend estimates by the area surveyed. Zipkin and Saunders [36] highlighted that addressing uneven quantities and information contents in multiple data sources is a persistent challenge for integrated modeling. Van Ee et al. [220] developed a spatio-temporal model for facilitating joint inference from aerial and ground surveys of LEPC in Kansas. Van Ee et al. [220] also took a chained Markov melding approach so that the observational uncertainty of each survey could be propagated into a spatio-temporal model for LEPC densities. In the model of Van Ee et al. [220], the contribution of each survey to posterior inference was controlled by the number of sites sampled.

In our IPM, the contribution of aerial and ground surveys was not governed by the number of sites, but rather, the number of individuals encountered (see Appendix C.3). The intuition for this result is that sampling regions without LEPC provide no information about trends in demography. The contribution of the ground surveys to posterior inference may seem large given the aerial survey searches nearly 10 times more area annually. While aerial surveys cover a wide region, many of the areas surveyed have low densities, resulting in relatively few birds encountered. Ground

surveys are primarily restricted to densely populated areas, where a relatively large number of birds were counted per unit of area searched. As a result, the number of birds encountered by each method is comparable, and this gives the data sources similar power to shape posterior inference for population vital rates.

We assumed that the preferentially sampled ground surveys were representative of trends in the broader LEPC population by linking them to vital rates. Linking multiple datasets directly to the parameter of interest generally improves posterior inference relative to more indirect approaches that facilitate joint inference through covariate effects or covariance structure [210]. In the context of integrated distribution models, Pacifici et al. [210] showed that predictive performance can decrease when assimilating a data source of poor quality: large uncertainty or systematic bias. The mean posterior correlation between annual ecoregion abundance estimates from the aerial distance sampling and N-mixture submodel was 0.38 indicating synchrony between estimated trends. We conclude, as have previous analyses [63, 217], that LEPC ground surveys are suitable for estimating vital rates.

Our results corroborate previous findings by Ross et al. [63] and Hagen et al. [6] that LEPC growth rates are more sensitive to productivity than survival. Demography differed by ecoregion. In the MGPR and SGPR, growth rates were predominately driven by the productivity of second-year females. Growth rates in the SSPR and SOPR showed the strongest associations with the productivity of after-second-year females and weaker associations with survival. Because of greater survival, more females reach their second and third breeding season in the SOPR and SSPR elevating the importance of after-second-year over second-year female productivity in driving growth rates [251]. We only observed positive correlations between growth rates and survival in the SOPR and SSPR. The mean annual densities (birds/100 km^2) of LEPC over the last decade were 8, 4, 10, and 29 in the SOPR, SSPR, MGPR, and SOPR, respectively. The elevated importance of survival in the SSPR and SOPR is likely a function of lower population densities that limit breeding opportunity and thereby productivity but potentially increase survival.

A lack of association between annual growth rates and female survivorship in the MGPR and SGPR was also identified by Ross et al. [63]. One explanation is that LEPC females may have increased survivorship in low growth years due to a boom-or-bust fecundity life history strategy. We found a negative association between survivorship and productivity in all ecoregions, with the highest female survival observed during the extreme, rangewide drought of 2011-2013 [57]. Nesting and brood rearing subjects females to avian and mammalian predators [238, 221], and differences in male and female survivorship were completely explained by elevated female mortality during the breeding season in our survival submodel (Appendix C.6). Females are also more likely to engage in long distance movements than males, and long distance movements were most common during the breeding season, which could also contribute to lower female survival [252]. In the SOPR, Grisham et al. [221] observed that females did not incubate eggs during drought conditions, which increased female survival in drought years. This reproductive strategy may be unique to the SOPR and could explain greater female survival in the ecoregion [221, 251]. More broadly, elevated female survival during drought could be a function of early nest failure and abandonment that reduces females vulnerability to predators, hyperthermia, and dehydration [221, 253].

Because LEPC only live a few years, Hagen et al. [6] and Ross et al. [63] hypothesized that populations can exhibit large interannual swings driven by variability in productivity. Using the aerial survey data alone, the annual ecoregion abundance estimates were relatively flat from 2012-2022 and year-to-year fluctuations were masked by large uncertainty. Including the ground surveys, posterior distributions for annual abundances sharpened across all ecoregions and periods of growth and decline were more easily identified. Ground surveys also influenced posterior inference for annual productivity with the largest influences in the SOPR and SSPR. On average, aerial surveys detected 40.9 and 22.7 individuals annually in the SOPR and SSPR, respectively, and the lack of detections heightens the influence of the ground surveys on posterior inference for vital rates in these ecoregions.

We assessed the predictive performance of our IPM for reduced aerial survey effort. RMSE for survival was similar across all scenarios of aerial survey effort likely because interannual variability

in LEPC survival is small. RMSE for productivity and abundance was sensitive to the degree of aerial survey effort, and predictive performance decreased precipitously when the amount of effort was reduced to one aerial survey every three years. While including the ground surveys in the IPM did decrease RMSE for abundance and productivity, overall, it did not appreciably attenuate the increase in RMSE induced by reducing aerial survey effort to once every third year. We conclude that current ground surveys are a valuable supplement to the aerial surveys but insufficient for estimating LEPC abundance on their own.

The number of endangered and vulnerable species continues to grow globally [7, 8], and multi-group monitoring efforts are often necessary for understanding the drivers of species decline [254]. Joint analysis of all the available datasets generally improves prediction and provides novel insights into population dynamics [38, 255, 256, 220], but specifying computationally feasible models that assimilate datasets with mismatching spatial or temporal scales, unique observational uncertainties, and sampling biases is difficult [36].

We developed an IPM for inferring spatial heterogeneity in population dynamics of a federally endangered across its entire range. By taking a Markov melding approach, we were able to mimic modeling frameworks previously proposed for analyzing the individual datasets while still deriving a joint posterior distribution that accounted for the contributions of all datasets and prior information. Because the approach fits the submodels in parallel, we reduced computation time, relative to an IPM that is fit to all datasets simultaneously. Our approach allowed us to model population trends informed by two distinct surveys, and by capitalizing on the strengths of each survey, we improved parameter precision for vital rates and provided inference for range-wide abundance over a longer time period. The ability to induce joint inference for a collection of related submodels is a powerful tool, and we have shown how the Markov melding approach can both simplify and streamline model development.

Chapter 5

Conclusion

I developed computationally efficient integrated models for drawing inference from multi-source ecological data. A common theme across all analyses was the need for ecological inference that could not be inferred from a single source. In Chapter 2, I assessed the impact of the bark beetle epidemic on mammals in the Rocky Mountains. By modeling the multispecies data jointly, I was able to estimate the impact of bark beetle infestation conditional on co-occurrence patterns in the mammalian community. In Chapter 3, I sought to improve historical inference for LEPC abundance and provide a future framework for predicting LEPC abundance. By assimilating data from preferential surveys of LEPC, I reduced the uncertainty associated with abundance of LEPC in unsampled regions. I extended the previous model to included additional demography surveys of the species in Chapter 4. I linked quantities from the demographic and abundance submodels in a common mechanistic model to understand drivers of LEPC abundance.

Each analysis presented implementation challenges. Confounding in the joint distribution model resulted in poor parameter mixing and algorithm instability. I described a restricted regression approach for orthogonalizing the fixed and random effects to stabilize model fitting. In Chapter 3 and 4, I specified joint models for LEPC abundance that could not be fit with standard Bayesian methodology. I implemented Markov melding and demonstrated its flexibility for drawing inference from a chain of submodels. By taking a Markov melding approach, I was able to induce joint inference across several datasets whilst preserving the original submodels that were aided by a variety of data augmentation schemes. The Markov melding approach may be practically useful to practitioners. Developing a cohesive integrated model for all data sources is daunting, but submodels suited for the individual datasets are easier to specify. Markov melding forms the joint distribution implied by the submodels and bypasses specification of one unified model.

5.1 Future Directions

Many integrated modeling frameworks lack formal model selection criterion [36, 115]. In the Markov melding framework, one approach would be to maximize the model selection criterion for each submodel. A challenge with this approach is propagating the model selection uncertainty into the melded joint distribution. Consider the general Markov melding framework presented in Section 1.2.3 with datatsets $\boldsymbol{Y} = (Y_1, \ldots, Y_M)$ and linking parameter θ, and suppose multiple variants of each submodel are under consideration. Let $\mathcal{M}_l$ denote the lth variant, $l \in \{1, \ldots, m_l\}$, of submodel m. Consider a Bayesian model averaging approaching to incorporating model selection uncertainty into the joint melded distribution.

Following Hooten and Hefley [42], the model averaged posterior distribution of θ in submodel m is given by

$$[\theta|Y_m] = \sum_{l=1}^{L_m} [\theta|Y_m, \mathcal{M}_{ml}] P(\mathcal{M}_{ml}|Y_m), \tag{5.1}$$

where $P(\mathcal{M}_l|Y_m)$ is the posterior probability of model variant $\mathcal{M}_{ml}$ given the dataset Y_m. Using Bayes rule, we can reexpress the model probability as

$$P(\mathcal{M}_l|Y_m) = \frac{[Y_m|\mathcal{M}_{ml}]P(\mathcal{M}_{ml})}{\sum_{l=1}^{L_m}[Y_m|\mathcal{M}_{ml}]P(\mathcal{M}_{ml})}, \tag{5.2}$$

where $P(\mathcal{M}_{ml})$ is the prior probability for variant l of submodel m and $[Y_m|\mathcal{M}_{ml}]$ is the marginal distribution Y_m given variant $\mathcal{M}_{ml}$. The marginal distribution $[Y_m|\mathcal{M}_{ml}]$ is sometimes called the "evidence," and variants that give a higher density to the observed data are more likely to have generated the data.

Calculating $[Y_m|\mathcal{M}_{ml}]$ requires marginalizing over the link parameter

$$[Y_m|\mathcal{M}_{ml}] = \int [Y_m, \theta|\mathcal{M}_{ml}] d\theta. \tag{5.3}$$

The integral in equation (5.3) is generally intractable, and a variety of methods have been proposed for approximating the marginal distribution $[Y_m|\mathcal{M}_{ml}]$ [257, 258]. For simplicity, assume $[Y_m|\mathcal{M}_{ml}]$ is known. The melded model averaged joint distribution can be expressed

$$[\theta, \boldsymbol{Y}]_{\text{meld}} = [\theta]_{\text{pool}} \prod_{m=1}^{M} \frac{[\theta, Y_m]_m}{[\theta]_m} \tag{5.4}$$

$$= [\theta]_{\text{pool}} \prod_{m=1}^{M} \sum_{l=1}^{L_n} \frac{[\theta, Y_m|\mathcal{M}_{ml}]P(\mathcal{M}_{ml})}{[\theta|\mathcal{M}_{ml}]}, \tag{5.5}$$

but a method for obtaining posterior samples of θ is this context is unclear. A future avenue could be investigating efficient algorithms for propagating model selection uncertainty into the joint melded distribution for θ and $\boldsymbol{Y}$.

Bibliography

[1] Andrew J Lawrence, Scott A Carleton, William R Gould, and Clay T Nichols. Lesser prairie-chicken survival in varying densities of energy development. *The Journal of Wildlife Management*, 85(6):1256–1266, 2021.

[2] Jacob Ivan, Amy Seglund, Richard Truex, and Eric Newkirk. Mammalian responses to changed forest conditions resulting from bark beetle outbreaks in the southern Rocky Mountains. *Ecosphere*, 9, 08 2018.

[3] R Core Team. *R: A Language and Environment for Statistical Computing*. R Foundation for Statistical Computing, Vienna, Austria, 2021.

[4] Ashley Marie Unger. *Playing Chicken: At the Intersection of Anthropogenic Development and Lesser Prairie-Chickens*. PhD thesis, Oklahoma State University, 2017.

[5] Kristen Nasman, Troy Rintz, Guy DiDonato, and Faith Kulzer. Range-wide population size of the lesser prairie-chicken: 2012 to 2022. Technical report, Western EcoSystems Technology, Incorporated, 2022.

[6] Christian A Hagen, Brett K Sandercock, James C Pitman, Robert J Robel, and Roger D Applegate. Spatial variation in lesser prairie-chicken demography: A sensitivity analysis of population dynamics and management alternatives. *The Journal of Wildlife Management*, 73(8):1325–1332, 2009.

[7] Will Steffen, Paul J Crutzen, and John R McNeill. The Anthropocene: Are humans now overwhelming the great forces of nature. *Ambio-Journal of Human Environment Research and Management*, 36(8):614–621, 2007.

[8] Will Steffen, Wendy Broadgate, Lisa Deutsch, Owen Gaffney, and Cornelia Ludwig. The trajectory of the Anthropocene: The great acceleration. *The Anthropocene Review*, 2(1):81–98, 2015.

[9] Gerardo Ceballos, Paul R Ehrlich, Anthony D Barnosky, Andrés García, Robert M Pringle, and Todd M Palmer. Accelerated modern human–induced species losses: Entering the sixth mass extinction. *Science Advances*, 1(5):e1400253, 2015.

[10] Gretchen C Daily and Pamela A Matson. Ecosystem services: From theory to implementation. *Proceedings of the National Academy of Sciences*, 105(28):9455–9456, 2008.

[11] J Emmett Duffy. Why biodiversity is important to the functioning of real-world ecosystems. *Frontiers in Ecology and the Environment*, 7(8):437–444, 2009.

[12] Paul R Ehrlich and Robert M Pringle. Where does biodiversity go from here? A grim business-as-usual forecast and a hopeful portfolio of partial solutions. *Proceedings of the National Academy of Sciences*, 105(1):11579–11586, 2008.

[13] Brian Leung, Anna L Hargreaves, Dan A Greenberg, Brian McGill, Maria Dornelas, and Robin Freeman. Clustered versus catastrophic global vertebrate declines. *Nature*, 588(7837):267–271, 2020.

[14] Michel Loreau, Bradley J Cardinale, Forest Isbell, Tim Newbold, Mary I O'Connor, and Claire de Mazancourt. Do not downplay biodiversity loss. *Nature*, 601(7894):E27–E28, 2022.

[15] Michael Gilpin. *Metapopulation Dynamics: Empirical and Theoretical Investigations*. Academic Press, 2012.

[16] Pieter J Den Boer. Spreading of risk and stabilization of animal numbers. *Acta Biotheoretica*, 18(1-4):165–194, 1968.

[17] Giovanni Poggiato, Tamara Münkemüller, Daria Bystrova, Julyan Arbel, James S Clark, and Wilfried Thuiller. On the interpretations of joint modeling in community ecology. *Trends in Ecology and Evolution*, 36(5):391–401, 2021.

[18] Jason M Tylianakis, Raphael K Didham, Jordi Bascompte, and David A Wardle. Global change and species interactions in terrestrial ecosystems. *Ecology Letters*, 11(12):1351–1363, 2008.

[19] Andrew Gonzalez, Bradley J Cardinale, Ginger RH Allington, Jarrett Byrnes, K Arthur Endsley, Daniel G Brown, David U Hooper, Forest Isbell, Mary I O'Connor, and Michel Loreau. Estimating local biodiversity change: A critique of papers claiming no net loss of local diversity. *Ecology*, 97(8):1949–1960, 2016.

[20] Sara J Oyler-McCance, Randall W DeYoung, Jennifer A Fike, Christian A Hagen, Jeff A Johnson, Lena C Larsson, and Michael A Patten. Rangewide genetic analysis of lesser prairie-chicken reveals population structure, range expansion, and possible introgression. *Conservation Genetics*, 17:643–660, 2016.

[21] David Warton, F. Guillaume Blanchet, Robert O'Hara, Otso Ovaskainen, Sara Taskinen, Steven Walker, and Francis Hui. So many variables: Joint modeling in community ecology. *Trends in Ecology and Evolution*, 30:766–779, 10 2015.

[22] Laura J Pollock, Reid Tingley, William K Morris, Nick Golding, Robert B O'Hara, Kirsten M Parris, Peter A Vesk, and Michael A McCarthy. Understanding co-occurrence by modelling species simultaneously with a Joint Species Distribution Model (JSDM). *Methods in Ecology and Evolution*, 5(5):397–406, 2014.

[23] William F Morris and Daniel Doak. *Quantitative Conservation Biology: Theory and Practice of Population Viability Analysis*. Sinauer, Sunderland, Massachusetts, USA, 2002.

[24] David C Coleman. *Big Ecology: The Emergence of Ecosystem Science*. University of California Press, 2010.

[25] Gary M Olson, Ann Zimmerman, Nathan Bos, and William A Wulf. *The Evolution of Collaboration in Ecology: Lessons from the US Long-Term Ecological Research Program*. MIT Press, 2008.

[26] Blake M Allan, Dale G Nimmo, Daniel Ierodiaconou, Jeremy VanDerWal, Lian Pin Koh, and Euan G Ritchie. Futurecasting ecological research: the rise of technoecology. *Ecosphere*, 9(5):e02163, 2018.

[27] PJ Stephenson. Technological advances in biodiversity monitoring: applicability, opportunities and challenges. *Current Opinion in Environmental Sustainability*, 45:36–41, 2020.

[28] Dilek Fraisl, Gerid Hager, Baptiste Bedessem, Margaret Gold, Pen-Yuan Hsing, Finn Danielsen, Colleen B Hitchcock, Joseph M Hulbert, Jaume Piera, Helen Spiers, Martin Thiel, and Mordechai Haklay. Citizen science in environmental and ecological sciences. *Nature Reviews Methods Primers*, 2(1):64, 2022.

[29] Timothy H Tear, J Michael Scott, Patricia H Hayward, and Brad Griffith. Recovery plans and the Endangered Species Act: Are criticisms supported by data? *Conservation Biology*, 9(1):182–195, 1995.

[30] John Fieberg and Stephen P Ellner. Stochastic matrix models for conservation and management: a comparative review of methods. *Ecology Letters*, 4(3):244–266, 2001.

[31] Mark N Maunder and André E Punt. A review of integrated analysis in fisheries stock assessment. *Fisheries Research*, 142:61–74, 2013.

[32] Dimitris Rizopoulos, Geert Verbeke, and Geert Molenberghs. Shared parameter models under random effects misspecification. *Biometrika*, 95(1):63–74, 2008.

[33] Michael S Wulfsohn and Anastasios A Tsiatis. A joint model for survival and longitudinal data measured with error. *Biometrics*, 53(1):330–339, 1997.

[34] Michael Ghil and Paola Malanotte-Rizzoli. Data assimilation in meteorology and oceanography. In *Advances in Geophysics*, volume 33, pages 141–266. Elsevier, 1991.

[35] Benjamin Kedem, Victor De Oliveira, and Michael Sverchkov. *Statistical Data Fusion*. World Scientific, 2017.

[36] Elise F Zipkin, Erin R Zylstra, Alexander D Wright, Sarah P Saunders, Andrew O Finley, Michael C Dietze, Malcolm S Itter, and Morgan W Tingley. Addressing data integration challenges to link ecological processes across scales. *Frontiers in Ecology and the Environment*, 19(1):30–38, 2021.

[37] Heather E Johnson, L Scott Mills, John D Wehausen, and Thomas R Stephenson. Combining ground count, telemetry, and mark–resight data to infer population dynamics in an endangered species. *Journal of Applied Ecology*, 47(5):1083–1093, 2010.

[38] Michael Schaub and Fitsum Abadi. Integrated population models: A novel analysis framework for deeper insights into population dynamics. *Journal of Ornithology*, 152(1):227–237, 2011.

[39] Axel Finke, Ruth King, Alexandros Beskos, and Petros Dellaportas. Efficient sequential Monte Carlo algorithms for integrated population models. *Journal of Agricultural, Biological and Environmental Statistics*, 24:204–224, 2019.

[40] Ken Newman, Ruth King, Víctor Elvira, Perry de Valpine, Rachel S McCrea, and Byron JT Morgan. State-space models for ecological time-series data: Practical model-fitting. *Methods in Ecology and Evolution*, 14(1):26–42, 2023.

[41] L Mark Berliner. Hierarchical Bayesian time series models. In *Maximum Entropy and Bayesian Methods*, pages 15–22. Springer, 1996.

[42] Mevin B Hooten and Trevor J Hefley. *Bringing Bayesian Models to Life*. CRC Press, 2019.

[43] James S Clark. *Models for Ecological Data: An Introduction*. Princeton University Press, 2007.

[44] Michael A McCarthy. *Bayesian Methods for Ecology*. Cambridge University Press, 2007.

[45] J Andrew Royle and Robert M Dorazio. *Hierarchical Modeling and Inference in Ecology: The Analysis of Data from Populations, Metapopulations and Communities*. Elsevier, 2008.

[46] Ruth King, Byron Morgan, Olivier Gimenez, and Steve Brooks. *Bayesian Analysis for Population Ecology*. CRC Press, 2009.

[47] William A Link and Richard J Barker. *Bayesian Inference: With Ecological Applications*. Academic Press, 2009.

[48] Marc Kéry and Michael Schaub. *Bayesian Population Analysis Using WinBUGS: A Hierarchical Perspective*. Academic Press, 2011.

[49] Eric Parent and Etienne Rivot. *Introduction to Hierarchical Bayesian Modeling for Ecological Data*. CRC Press, 2012.

[50] N Thompson Hobbs and Mevin B Hooten. *Bayesian Models*. Princeton University Press, 2015.

[51] Andrew Gelman, John B Carlin, Hal S Stern, and Donald B Rubin. *Bayesian Data Analysis*. Chapman and Hall/CRC, 1995.

[52] Robert M Dorazio. Bayesian data analysis in population ecology: motivations, methods, and benefits. *Population Ecology*, 58(1):31–44, 2016.

[53] Rui F Fernandes, Daniel Scherrer, and Antoine Guisan. Effects of simulated observation errors on the performance of species distribution models. *Diversity and Distributions*, 25(3):400–413, 2019.

[54] Barbara Bentz, Craig Allen, Matthew Ayres, Ed Berg, Allan Carroll, E. Hansen, Hicke J, Joyce L, Jesse Logan, McMahon J, William Macfarlane, Steve Munson, Jose Negron, Timothy Paine, James Powell, Kenneth Raffa, Jacques Regniere, Reid M, William Romme, and Wood D. Bark beetle outbreaks in western North America: Causes and consequences. USDA Forest Service, Salt Lake, City, Utah, USA. Technical report, 01 2009.

[55] U.S. Fish and Wildlife Service. Endangered and threatened wildlife and plants; lesser prairie-chicken; final rule. 2023.

[56] Christian A Hagen, Brent E Jamison, Kenneth M Giesen, and Terry Z Riley. Guidelines for managing lesser prairie-chicken populations and their habitats. *Wildlife Society Bulletin*, 32(1):69–82, 2004.

[57] Christian A Hagen, Edward O Garton, Grant Beauprez, Brett S Cooper, Kent A Fricke, and Brad Simpson. Lesser prairie-chicken population forecasts and extinction risks: An evaluation 5 years post–catastrophic drought. *Wildlife Society Bulletin*, 41(4):624–638, 2017.

[58] David A Haukos and Clint Boal. *Ecology and Conservation of Lesser Prairie-Chickens*. CRC Press, 2016.

[59] U.S. Fish and Wildlife Service. Species Status Assessment for the Lesser Prairie-Chicken (*Tympanuchus pallidicinctus*), version 2.2. 110 pp. 2021.

[60] William E Van Pelt, Sean Kyle, Jim Pitman, David Klute, Grant Beauprez, Doug Schoeling, Allan Janus, and J Haufler. The lesser prairie-chicken range-wide conservation plan. *Western Association of Fish and Wildlife Agencies, Cheyenne, Wyoming, USA*, 367, 2013.

[61] Lyman McDonald, Grant Beauprez, Grant Gardner, Jim Griswold, Christian Hagen, Fawn Hornsby, David Klute, Sean Kyle, James Pitman, Troy Rintz, Doug Schoeling, and Bill Van Pelt. Range-wide population size of the lesser prairie-chicken: 2012 and 2013. *Wildlife Society Bulletin*, 38(3):536–546, 2014.

[62] Liam A Berigan, Carly SH Aulicky, Elisabeth C Teige, Daniel S Sullins, David A Haukos, Kent A Fricke, Jonathan H Reitz, Liza G Rossi, Kraig A Schultz, and Andrew M Ricketts. Availability of lesser prairie-chicken nesting habitat impairs restoration success. *Wildlife Society Bulletin*, 46(5):e1379, 2022.

[63] Beth E Ross, David A Haukos, Christian A Hagen, and James Pitman. Combining multiple sources of data to inform conservation of lesser prairie-chicken populations. *The Auk: Ornithological Advances*, 135(2):228–239, 2018.

[64] Andrew A Manderson and Robert JB Goudie. Combining chains of Bayesian models with Markov melding. *Bayesian Analysis*, 1(1):1–34, 2022.

[65] Christopher K Wikle and Mevin B Hooten. A general science-based framework for dynamical spatio-temporal models. *Test*, 19(3):417–451, 2010.

[66] Noel Cressie and Christopher K Wikle. *Statistics for Spatio-Temporal Data*. John Wiley & Sons, 2015.

[67] Christopher K Wikle, Andrew Zammit-Mangion, and Noel Cressie. *Spatio-Temporal Statistics with R*. Chapman and Hall/CRC, 2019.

[68] Henry R Scharf, Xinyi Lu, Perry J Williams, and Mevin B Hooten. Constructing flexible, identifiable and interpretable statistical models for binary data. *International Statistical Review*, 90(2):328–345, 2022.

[69] Ray Hilborn and Marc Mangel. *The Ecological Detective*. Princeton University Press, 2013.

[70] Trevor J Hefley, Mevin B Hooten, Ephraim M Hanks, Robin E Russell, and Daniel P Walsh. The Bayesian group lasso for confounded spatial data. *Journal of Agricultural, Biological and Environmental Statistics*, 22(1):42–59, 2017.

[71] John Fieberg, Mark Ditmer, and Robert Freckleton. Understanding the causes and consequences of animal movement: A cautionary note on fitting and interpreting regression models with time-dependent covariates. *Methods in Ecology and Evolution*, 3(6):983–991, 2012.

[72] Trevor J Hefley, Mevin B Hooten, John M Drake, Robin E Russell, and Daniel P Walsh. When can the cause of a population decline be determined? *Ecology Letters*, 19(11):1353–1362, 2016.

[73] Arka Daw, Anuj Karpatne, William Watkins, Jordan Read, and Vipin Kumar. Physics-guided neural networks (PGNN): An application in lake temperature modeling. *arXiv preprint arXiv:1710.11431*, 2017.

[74] Mevin B Hooten and Christopher K Wikle. A hierarchical Bayesian non-linear spatio-temporal model for the spread of invasive species with application to the Eurasian Collared-Dove. *Environmental and Ecological Statistics*, 15(1):59–70, 2008.

[75] Perry J Williams, Mevin B Hooten, Jamie N Womble, George G Esslinger, Michael R Bower, and Trevor J Hefley. An integrated data model to estimate spatiotemporal occupancy, abundance, and colonization dynamics. *Ecology*, 98(2):328–336, 2017.

[76] Xinyi Lu, Perry J Williams, Mevin B Hooten, James A Powell, Jamie N Womble, and Michael R Bower. Nonlinear reaction–diffusion process models improve inference for population dynamics. *Environmetrics*, 31(3):e2604, 2020.

[77] Wilson J Wright, Peter N Neitlich, Alyssa E Shiel, and Mevin B Hooten. Mechanistic spatial models for heavy metal pollution. *Environmetrics*, 33(8):e2760, 2022.

[78] J.A. Royle and J.D. Nichols. Estimating abundance from repeated presence-absence data or point counts. *Ecology*, 84:777–790, 2003.

[79] Jennifer A. Hoeting, Molly Leecaster, and David Bowden. An improved model for spatially correlated binary responses. *Journal of Agricultural, Biological, and Environmental Statistics*, 5(1):102–114, 2000.

[80] Darryl I MacKenzie, James D Nichols, Gideon B Lachman, Sam Droege, J Andrew Royle, and Catherine A Langtimm. Estimating site occupancy rates when detection probabilities are less than one. *Ecology*, 83(8):2248–2255, 2002.

[81] Mevin B Hooten, David R Larsen, and Christopher K Wikle. Predicting the spatial distribution of ground flora on large domains using a hierarchical Bayesian model. *Landscape Ecology*, 18(5):487–502, 2003.

[82] Robert M Dorazio and Daniel Taylor Rodriguez. A Gibbs sampler for Bayesian analysis of site-occupancy data. *Methods in Ecology and Evolution*, 3(6):1093–1098, 2012.

[83] Devin S Johnson, Paul B Conn, Mevin B Hooten, Justina C Ray, and Bruce A Pond. Spatial occupancy models for large data sets. *Ecology*, 94(4):801–808, 2013.

[84] James H Albert and Siddhartha Chib. Bayesian analysis of binary and polychotomous response data. *Journal of the American Statistical Association*, 88(422):669–679, 1993.

[85] Richard A Stanton Jr, Frank R Thompson III, and Dylan C Kesler. Site occupancy of brown-headed nuthatches varies with habitat restoration and range-limit context. *The Journal of Wildlife Management*, 79(6):917–926, 2015.

[86] Mathias W. Tobler, Alfonso Zúñiga Hartley, Samia E. Carrillo-Percastegui, and George V. N. Powell. Spatiotemporal hierarchical modelling of species richness and occupancy using camera trap data. *Journal of Applied Ecology*, 52(2):413–421, 2015.

[87] Christopher T. Rota, Marco A. R. Ferreira, Roland W. Kays, Tavis D. Forrester, Elizabeth L. Kalies, William J. McShea, Arielle W. Parsons, and Joshua J. Millspaugh. A multispecies occupancy model for two or more interacting species. *Methods in Ecology and Evolution*, 7(10):1164–1173, 2016.

[88] Christopher T Rota, Christopher K Wikle, Roland W Kays, Tavis D Forrester, William J McShea, Arielle W Parsons, and Joshua J Millspaugh. A two-species occupancy model accommodating simultaneous spatial and interspecific dependence. *Ecology*, 97(1):48–53, 2016.

[89] Mathias W. Tobler, Marc Kéry, Francis K. C. Hui, Gurutzeta Guillera-Arroita, Peter Knaus, and Thomas Sattler. Joint species distribution models with species correlations and imperfect detection. *Ecology*, 100(8):e02754, 2019.

[90] Rahel Sollmann, Mitchell Joseph Eaton, William A Link, Paul Mulondo, Samuel Ayebare, Sarah Prinsloo, Andrew J Plumptre, and Devin S Johnson. A Bayesian Dirichlet process

community occupancy model to estimate community structure and species similarity. *Ecological Applications*, 31(2):e02249, 2021.

[91] Nicholas G Polson, James G Scott, and Jesse Windle. Bayesian inference for logistic models using Pólya–Gamma latent variables. *Journal of the American Statistical Association*, 108(504):1339–1349, 2013.

[92] Allan E Clark and Res Altwegg. Efficient Bayesian analysis of occupancy models with logit link functions. *Ecology and Evolution*, 9(2):756–768, 2019.

[93] John L. Orrock, John F. Pagels, William J. McShea, and Elizabeth K. Harper. Predicting presence and abundance of a small mammal species: The effect of scale and resolution. *Ecological Applications*, 10(5):1356–1366, 2000.

[94] Ana M Cingolani, Marcelo Cabido, Diego E Gurvich, Daniel Renison, and Sandra Díaz. Filtering processes in the assembly of plant communities: Are species presence and abundance driven by the same traits? *Journal of Vegetation Science*, 18(6):911–920, 2007.

[95] Reilly R. Dibner, Daniel F. Doak, and Melanie Murphy. Discrepancies in occupancy and abundance approaches to identifying and protecting habitat for an at-risk species. *Ecology and Evolution*, 7(15):5692–5702, 2017.

[96] Alan E Gelfand and Adrian FM Smith. Sampling-based approaches to calculating marginal densities. *Journal of the American Statistical Association*, 85(410):398–409, 1990.

[97] Alexander Topchy, Anil K Jain, and William Punch. A mixture model for clustering ensembles. In *Proceedings of the 2004 SIAM International Conference on Data Mining*, pages 379–390. SIAM, 2004.

[98] Dan Guo, Wengang Zhou, Meng Wang, and Houqiang Li. Sign language recognition based on adaptive HMMs with data augmentation. In *2016 IEEE International Conference on Image Processing (ICIP)*, pages 2876–2880. IEEE, 2016.

[99] Bo Zong, Qi Song, Martin Renqiang Min, Wei Cheng, Cristian Lumezanu, Daeki Cho, and Haifeng Chen. Deep autoencoding Gaussian mixture model for unsupervised anomaly detection. In *International Conference on Learning Representations*, 2018.

[100] Radford M Neal. Markov chain sampling methods for Dirichlet process mixture models. *Journal of Computational and Graphical Statistics*, 9(2):249–265, 2000.

[101] Yee Teh, Michael Jordan, Matthew Beal, and David Blei. Sharing clusters among related groups: Hierarchical Dirichlet processes. *Advances in Neural Information Processing Systems*, 17, 2004.

[102] Nick JB Isaac, Marta A Jarzyna, Petr Keil, Lea I Dambly, Philipp H Boersch-Supan, Ella Browning, Stephen N Freeman, Nick Golding, Gurutzeta Guillera-Arroita, Peter A Henrys, Susan Jarvis, Josè Lahoz-Monfort, Jorn Pagel, Oliver L Pescott, Reto Schmucki, Emily G Simmonds, and Robert B O'Hara. Data integration for large-scale models of species distributions. *Trends in Ecology & Evolution*, 35(1):56–67, 2020.

[103] A Philip Dawid and Steffen L Lauritzen. Hyper Markov laws in the statistical analysis of decomposable graphical models. *The Annals of Statistics*, 21(3):1272–1317, 1993.

[104] Montserrat Fuentes and Adrian E Raftery. Model evaluation and spatial interpolation by Bayesian combination of observations with outputs from numerical models. *Biometrics*, 61(1):36–45, 2005.

[105] Ephraim M Hanks, Mevin B Hooten, and Fred A Baker. Reconciling multiple data sources to improve accuracy of large-scale prediction of forest disease incidence. *Ecological Applications*, 21(4):1173–1188, 2011.

[106] David Fournier and Chris P Archibald. A general theory for analyzing catch at age data. *Canadian Journal of Fisheries and Aquatic Sciences*, 39(8):1195–1207, 1982.

[107] H Ronald Pulliam. On the relationship between niche and distribution. *Ecology Letters*, 3(4):349–361, 2000.

[108] Antoine Guisan and Wilfried Thuiller. Predicting species distribution: offering more than simple habitat models. *Ecology Letters*, 8(9):993–1009, 2005.

[109] Thomas Harvey Johnston. The relation of climate to the spread of prickly pear. *Transactions of the Royal Society of South Australia*, 48:269–295, 1924.

[110] MP Austin. Role of regression analysis in plant ecology. In *Proceedings of the Ecological Society of Australia*, volume 6, pages 63–75, 1971.

[111] Jarno Vanhatalo, Marcelo Hartmann, and Lari Veneranta. Additive multivariate Gaussian processes for joint species distribution modeling with heterogeneous data. *Bayesian Analysis*, 15:415–447, 2020.

[112] David J Harris. Generating realistic assemblages with a joint species distribution model. *Methods in Ecology and Evolution*, 6(4):465–473, 2015.

[113] David P Wilkinson, Nick Golding, Gurutzeta Guillera-Arroita, Reid Tingley, and Michael A McCarthy. Defining and evaluating predictions of joint species distribution models. *Methods in Ecology and Evolution*, 12(3):394–404, 2021.

[114] Panagiotis Besbeas, Stephen Freeman, Byron Morgan, and EA Catchpole. Integrating mark–recapture–recovery and census data to estimate animal abundance and demographic parameters. *Biometrics*, 58(3):540–547, 2002.

[115] Michael Schaub and Marc Kery. *Integrated Population Models: Theory and Ecological Applications with R and JAGS*. Academic Press, 2021.

[116] Hal Caswell. A general formula for the sensitivity of population growth rate to changes in life history parameters. *Theoretical Population Biology*, 14(2):215–230, 1978.

[117] Ruth King, Stephen P Brooks, Chiara Mazzetta, Stephen N Freeman, and Byron JT Morgan. Identifying and diagnosing population declines: A Bayesian assessment of lapwings in the

UK. *Journal of the Royal Statistical Society: Series C (Applied Statistics)*, 57(5):609–632, 2008.

[118] Douglas J Tempel, MZ Peery, and Ralph J Gutierrez. Using integrated population models to improve conservation monitoring: California spotted owls as a case study. *Ecological Modelling*, 289:86–95, 2014.

[119] Trivellore Raghunathan, Kaushik Ghosh, Allison Rosen, Paul Imbriano, Susan Stewart, Irina Bondarenko, Kassandra Messer, Patricia Berglund, James Shaffer, and David Cutler. Combining information from multiple data sources to assess population health. *Journal of Survey Statistics and Methodology*, 9(3):598–625, 2021.

[120] Fitsum Abadi, Olivier Gimenez, Bruno Ullrich, Raphaël Arlettaz, and Michael Schaub. Estimation of immigration rate using integrated population models. *Journal of Applied Ecology*, 47(2):393–400, 2010.

[121] Matthieu Paquet, Jonas Knape, Debora Arlt, Pär Forslund, Tomas Pärt, Øystein Flagstad, Carl G. Jones, Malcolm A. C. Nicoll, Ken Norris, Josephine M. Pemberton, Håkan Sand, Linn Svensson, Vikash Tatayah, Petter Wabakken, Camilla Wikenros, Mikael Åkesson, and Matthew Low. Integrated population models poorly estimate the demographic contribution of immigration. *Methods in Ecology and Evolution*, 12(10):1899–1910, 2021.

[122] Sofia M Massa and Steffen L Lauritzen. Combining statistical models. *Algebraic Methods in Statistics and Probability II*, 516:239–259, 2010.

[123] Robert JB Goudie, Anne M Presanis, David Lunn, Daniela De Angelis, and Lorenz Wernisch. Joining and splitting models with Markov melding. *Bayesian Analysis*, 14(1):81, 2019.

[124] Michael Schaub, Thomas S Reichlin, Fitsum Abadi, Marc Kéry, Lukas Jenni, and Raphaël Arlettaz. The demographic drivers of local population dynamics in two rare migratory birds. *Oecologia*, 168:97–108, 2012.

[125] Brian J. Reich, James S. Hodges, and Vesna Zadnik. Effects of residual smoothing on the posterior of the fixed effects in disease-mapping models. *Biometrics*, 62(4):1197–1206, 2006.

[126] James S. Hodges and Brian J. Reich. Adding spatially-correlated errors can mess up the fixed effect you love. *The American Statistician*, 64(4):325–334, 2010.

[127] Christopher Paciorek. The importance of scale for spatial-confounding bias and precision of spatial regression estimators. *Statistical Science: A Review Journal of the Institute of Mathematical Statistics*, 25:107–125, 02 2010.

[128] Kori Khan and Catherine A Calder. Restricted spatial regression methods: Implications for inference. *Journal of the American Statistical Association*, pages 1–13, 2020.

[129] Dale L Zimmerman and Jay M Ver Hoef. On deconfounding spatial confounding in linear models. *The American Statistician*, pages 1–9, 2021.

[130] Ephraim M. Hanks, Erin M. Schliep, Mevin B. Hooten, and Jennifer A. Hoeting. Restricted spatial regression in practice: geostatistical models, confounding, and robustness under model misspecification. *Environmetrics*, 26(4):243–254, 2015.

[131] Takeshi Amemiya. Tobit models. *Advanced Econometrics*, pages 360–411, 1985.

[132] Benjamin M Bolker, Mollie E Brooks, Connie J Clark, Shane W Geange, John R Poulsen, M Henry H Stevens, and Jada-Simone S White. Generalized linear mixed models: A practical guide for ecology and evolution. *Trends in Ecology & Evolution*, 24(3):127–135, 2009.

[133] Hayato Iijima. A review of wildlife abundance estimation models: comparison of models for correct application. *Mammal Study*, 45(3):177–188, 2020.

[134] J Andrew Royle, K Ullas Karanth, Arjun M Gopalaswamy, and N Samba Kumar. Bayesian inference in camera trapping studies for a class of spatial capture–recapture models. *Ecology*, 90(11):3233–3244, 2009.

[135] Peter W Glynn and Philip Heidelberger. Experiments with initial transient deletion for parallel, replicated steady-state simulations. *Management Science*, 38(3):400–418, 1992.

[136] Russell Bradford and Alun Thomas. Markov chain Monte Carlo methods for family trees using a parallel processor. *Statistics and Computing*, 6(1):67–75, 1996.

[137] Jeffrey S Rosenthal. Parallel computing and Monte Carlo algorithms. *Far East Journal of Theoretical Statistics*, 4(2):207–236, 2000.

[138] Arthur P Dempster, Nan M Laird, and Donald B Rubin. Maximum likelihood from incomplete data via the EM algorithm. *Journal of the Royal Statistical Society: Series B (Methodological)*, 39(1):1–22, 1977.

[139] Håvard Rue, Sara Martino, and Nicolas Chopin. Approximate Bayesian inference for latent Gaussian models by using integrated nested Laplace approximations. *Journal of the Royal Statistical Society: Series B (Statistical Methodology)*, 71(2):319–392, 2009.

[140] Simo Särkkä. *Bayesian Filtering and Smoothing*. Cambridge University Press, 2013.

[141] David Lunn, Jessica Barrett, Michael Sweeting, and Simon Thompson. Fully Bayesian hierarchical modelling in two stages, with application to meta-analysis. *Journal of the Royal Statistical Society: Series C (Applied Statistics)*, 62(4):551–572, 2013.

[142] Nicolas Chopin, Pierre E Jacob, and Omiros Papaspiliopoulos. SMC^2: An efficient algorithm for sequential analysis of state space models. *Journal of the Royal Statistical Society: Series B (Statistical Methodology)*, 75(3):397–426, 2013.

[143] Mevin B Hooten, Frances E Buderman, Brian M Brost, Ephraim M Hanks, and Jacob S Ivan. Hierarchical animal movement models for population-level inference. *Environmetrics*, 27(6):322–333, 2016.

[144] Brian D Gerber, Mevin B Hooten, Christopher P Peck, Mindy B Rice, James H Gammonley, Anthony D Apa, and Amy J Davis. Accounting for location uncertainty in azimuthal telemetry data improves ecological inference. *Movement Ecology*, 6(1):1–14, 2018.

[145] Mevin B Hooten, Devin S Johnson, and Brian M Brost. Making recursive Bayesian inference accessible. *The American Statistician*, 75(2):185–194, 2021.

[146] Ian Taylor, Andee Kaplan, and Brenda Betancourt. Fast Bayesian record linkage for streaming data contexts. *arXiv*, 2023.

[147] Hanna M McCaslin, Abigail B Feuka, and Mevin B Hooten. Hierarchical computing for hierarchical models in ecology. *Methods in Ecology and Evolution*, 12(2):245–254, 2021.

[148] Dirk Eddelbuettel and Romain François. Rcpp: Seamless R and C++ integration. *Journal of Statistical Software*, 40:1–18, 2011.

[149] Res Altwegg and James D Nichols. Occupancy models for citizen-science data. *Methods in Ecology and Evolution*, 10(1):8–21, 2019.

[150] Francis Hui, David Warton, Scott Foster, and Piers Dunstan. To mix or not to mix: Comparing the predictive performance of mixture models vs. separate species distribution models. *Ecology*, 94:1913–9, 09 2013.

[151] César Augusto Estevo, Mariana Baldy Nagy-Reis, and James D Nichols. When habitat matters: Habitat preferences can modulate co-occurrence patterns of similar sympatric species. *PloS One*, 12(7):e0179489, 2017.

[152] David Steen, Christopher McClure, Jean Brock, D. Rudolph, Josh Pierce, James Lee, W. Humphries, Beau Gregory, William Sutton, Lora Smith, Danna Baxley, Dirk Stevenson, and Craig Guyer. Snake co-occurrence patterns are best explained by habitat and hypothesized effects of interspecific interactions. *Journal of Animal Ecology*, 83(1):286–295, 2014.

[153] Mary Susanne Wisz, Julien Pottier, W Daniel Kissling, Loïc Pellissier, Jonathan Lenoir, Christian F Damgaard, Carsten F Dormann, Mads C Forchhammer, John-Arvid Grytnes, Antoine Guisan, Risto K Heikkinen, Toke T Hoye, Ingolf Kuhn, Miska Lauto, Luigi Maiorano, Marie-Charlotte Nilsson, Signe Normand, Eric Ockinger, Niels M Schmidt, Mette Termansen, Allan Timmermann, David A Wardle, Peter Aastrup, and Jens-Christian Svenning. The role of biotic interactions in shaping distributions and realised assemblages of species: Implications for species distribution modelling. *Biological Reviews*, 88(1):15–30, 2013.

[154] David P Wilkinson, Nick Golding, Gurutzeta Guillera-Arroita, Reid Tingley, and Michael A McCarthy. A comparison of joint species distribution models for presence–absence data. *Methods in Ecology and Evolution*, 10(2):198–211, 2019.

[155] Robert M Dorazio and J Andrew Royle. Estimating size and composition of biological communities by modeling the occurrence of species. *Journal of the American Statistical Association*, 100(470):389–398, 2005.

[156] Robert M Dorazio, J Andrew Royle, Bo Söderström, and Anders Glimskär. Estimating species richness and accumulation by modeling species occurrence and detectability. *Ecology*, 87(4):842–854, 2006.

[157] Kristin M. Broms, Mevin B. Hooten, and Ryan M. Fitzpatrick. Model selection and assessment for multi-species occupancy models. *Ecology*, 97(7):1759–1770, 2016.

[158] David H Maphisa, Hanneline Smit-Robinson, and Res Altwegg. Dynamic multi-species occupancy models reveal individualistic habitat preferences in a high-altitude grassland bird community. *PeerJ*, 7:e6276, 2019.

[159] Jordi Bascompte. Mutualistic networks. *Frontiers in Ecology and the Environment*, 7(8):429–436, 2009.

[160] Nicole M Van Dam. How plants cope with biotic interactions. *Plant Biology*, 11(1):1–5, 2009.

[161] Kristin M Broms, Devin S Johnson, Res Altwegg, and Loveday L Conquest. Spatial occupancy models applied to atlas data show Southern Ground Hornbills strongly depend on protected areas. *Ecological Applications*, 24(2):363–374, 2014.

[162] Mevin B. Hooten and Nathaniel. T. Hobbs. A guide to Bayesian model selection for ecologists. *Ecological Monographs*, 85(1):3–28, 2015.

[163] John Hughes and Murali Haran. Dimension reduction and alleviation of confounding for spatial generalized linear mixed models. *Journal of the Royal Statistical Society: Series B (Statistical Methodology)*, 75(1):139–159, 2013.

[164] Jonathan R Bradley, Scott H Holan, and Christopher K Wikle. Multivariate spatio-temporal models for high-dimensional areal data with application to longitudinal employer-household dynamics. *Annals of Applied Statistics*, 9(4):1761–1791, 2015.

[165] Daisuke Murakami and Daniel A Griffith. Random effects specifications in eigenvector spatial filtering: A simulation study. *Journal of Geographical Systems*, 17(4):311–331, 2015.

[166] Hauke Thaden and Thomas Kneib. Structural equation models for dealing with spatial confounding. *The American Statistician*, 72(3):239–252, 2018.

[167] Marcos Oliveira Prates, Renato Martins Assunção, and Erica Castilho Rodrigues. Alleviating spatial confounding for areal data problems by displacing the geographical centroids. *Bayesian Analysis*, 14(2):623–647, 2019.

[168] Francesca Dominici, Aidan McDermott, and Trevor J. Hastie. Improved semiparametric time series models of air pollution and mortality. *Journal of the American Statistical Association*, 99(468):938–948, 2004.

[169] E. Andrés Houseman, Brent A. Coull, and James P. Shine. A nonstationary negative binomial time series with time-dependent covariates: Enterococcus counts in Boston Harbor. *Journal of the American Statistical Association*, 101(476):1365–1376, 2006.

[170] Robert R Corbeil and Shayle R Searle. Restricted maximum likelihood (REML) estimation of variance components in the mixed model. *Technometrics*, 18(1):31–38, 1976.

[171] Andrew J. Tyre, Brigitte Tenhumberg, Scott A. Field, Darren Niejalke, Kirsten Parris, and Hugh P. Possingham. Improving precision and reducing bias in biological surveys: Estimating false-negative error rates. *Ecological Applications*, 13(6):1790–1801, 2003.

[172] James S Clark, David Bell, Chengjin Chu, Benoit Courbaud, Michael Dietze, Michelle Hersh, Janneke HilleRisLambers, Inés Ibášez, Shannon LaDeau, Sean McMahon, Jessica Metcalf, Jacqueline Mohan, Emily Moran, Luke Pangle, Scott Pearson, Carl Salk, Zehao Shen, Denis Valle, and Peter Wyckoff. High-dimensional coexistence based on individual variation: a synthesis of evidence. *Ecological Monographs*, 80(4):569–608, 2010.

[173] Otso Ovaskainen and Janne Soininen. Making more out of sparse data: hierarchical modeling of species communities. *Ecology*, 92(2):289–295, 2011.

[174] Henry Scheffe. *The Analysis of Variance*, volume 72. John Wiley & Sons, 1959.

[175] James S Hodges and Murray K Clayton. Random effects old and new. *Statistical Science*, 2011.

[176] Joshua Chi-Chun Chan and Ivan Jeliazkov. MCMC estimation of restricted covariance matrices. *Journal of Computational and Graphical Statistics*, 18(2):457–480, 2009.

[177] Kevin A. Blecha. *Risk-reward tradeoffs in the foraging strategy of cougar (Puma concolor): prey distribution, anthropogenic development, and patch selection*. PhD thesis, Colorado State University, Fort Collins, Colorado, USA, 2015.

[178] Darryl I MacKenzie, James D Nichols, J. Andrew Royle, Kenneth H Pollock, Larissa L Bailey, and James E Hines. *Occupancy Estimation and Modeling: Inferring Patterns and Dynamics of Species Occurrence*. Academic Press, 11 2006.

[179] Antoine Guisan, Stuart Weiss, and Andrew Weiss. GLM versus CCA spatial modeling of plant species distribution. *Plant Ecology*, 143:107–122, 07 1999.

[180] Bénédicte Madon, David I. Warton, and Miguel B. Araújo. Community-level vs species-specific approaches to model selection. *Ecography*, 36(12):1291–1298, 2013.

[181] Otso Ovaskainen, Nerea Abrego, Panu Halme, and David Dunson. Using latent variable models to identify large networks of species-to-species associations at different spatial scales. *Methods in Ecology and Evolution*, 7:549–555, 11 2015.

[182] Gleb Tikhonov, Nerea Abrego, David Dunson, and Otso Ovaskainen. Using joint species distribution models for evaluating how species-to-species associations depend on the environmental context. *Methods in Ecology and Evolution*, 8:443–452, 04 2017.

[183] Jean-Dominique Lebreton, Kenneth P. Burnham, Jean Clobert, and David R. Anderson. Modeling survival and testing biological hypotheses using marked animals: A unified approach with case studies. *Ecological Monographs*, 62(1):67–118, 1992.

[184] Yeojin Chung, Andrew Gelman, Sophia Rabe-Hesketh, Jingchen Liu, and Vincent Dorie. Weakly informative prior for point estimation of covariance matrices in hierarchical models. *Journal of Educational and Behavioral Statistics*, 40(2):136–157, 2015.

[185] Timothy E Hanson, Adam J Branscum, and Wesley O Johnson. Informative g-priors for logistic regression. *Bayesian Analysis*, 9(3):597–612, 2014.

[186] A. Baddeley, M. Berman, N.I. Fisher, Andrew Hardegen, R.K. Milne, D. Schuhmacher, R. Shah, and R. Turner. Spatial logistic regression and change-of-support in poisson point processes. *Electronic Journal of Statistics*, 4:1151–1201, 01 2010.

[187] Bogdan Caradima, Nele Schuwirth, and Peter Reichert. From individual to joint species distribution models: A comparison of model complexity and predictive performance. *Journal of Biogeography*, 46(10):2260–2274, 2019.

[188] John NR Jeffers. Two case studies in the application of principal component analysis. *Journal of the Royal Statistical Society: Series C (Applied Statistics)*, 16(3):225–236, 1967.

[189] Carter R Hill, Thomas B Fomby, and Stan R Johnson. Component selection norms for principal components regression. *Communications in Statistics-Theory and Methods*, 6(4):309–334, 1977.

[190] Ernest C Kung and Taher A Sharif. Regression forecasting of the onset of the indian summer monsoon with antecedent upper air conditions. *Journal of Applied Meteorology and Climatology*, 19(4):370–380, 1980.

[191] Gary Smith and Frank Campbell. A critique of some ridge regression methods. *Journal of the American Statistical Association*, 75(369):74–81, 1980.

[192] Ian T Jolliffe. A note on the use of principal components in regression. *Journal of the Royal Statistical Society: Series C (Applied Statistics)*, 31(3):300–303, 1982.

[193] Elise F Zipkin and Sarah P Saunders. Synthesizing multiple data types for biological conservation using integrated population models. *Biological Conservation*, 217:240–250, 2018.

[194] Emily G Simmonds, Susan G Jarvis, Peter A Henrys, Nick JB Isaac, and Robert B O'Hara. Is more data always better? A simulation study of benefits and limitations of integrated distribution models. *Ecography*, 43(10):1413–1422, 2020.

[195] Ângela Lomba, Loïc Pellissier, Christophe Randin, Joana Vicente, Francisco Moreira, Joao Honrado, and Antoine Guisan. Overcoming the rare species modelling paradox: A novel hierarchical framework applied to an Iberian endemic plant. *Biological Conservation*, 143(11):2647–2657, 2010.

[196] Peter J Diggle, Raquel Menezes, and Ting-li Su. Geostatistical inference under preferential sampling. *Journal of the Royal Statistical Society: Series C (Applied Statistics)*, 59(2):191–232, 2010.

[197] Kristen Nasman, Troy Rintz, Rebecca Clark, Grant Gardner, and Lyman McDonald. Range-wide population size of the lesser prairie-chicken: 2012 to 2021. Technical report, Western EcoSystems Technology, Incorporated, 2021.

[198] Beth E Ross, David Haukos, Christian Hagen, and James Pitman. The relative contribution of climate to changes in lesser prairie-chicken abundance. *Ecosphere*, 7(6):e01323, 2016.

[199] David Borchers, Jeffrey Laake, C Southwell, and Charles Paxton. Accommodating unmodeled heterogeneity in double-observer distance sampling surveys. *Biometrics*, 62(2):372–378, 2006.

[200] Stephen T Buckland, Jeffrey L Laake, and David L Borchers. Double-observer line transect methods: Levels of independence. *Biometrics*, 66(1):169–177, 2010.

[201] David L Borchers, Peter Nightingale, Ben C Stevenson, and Rachel M Fewster. A latent capture history model for digital aerial surveys. *Biometrics*, 78(1):274–285, 2022.

[202] Robin Jennison, Jim Pitman, Joe Kramer, and Mike Mitchener. Prairie-chicken lek survey-2011. Technical report, Kansas Department of Wildlife and Parks, 2011.

[203] Christian A Hagen, David C Pavlacky Jr, Kristen Adachi, Fawn E Hornsby, Troy J Rintz, and Lyman L McDonald. Multiscale occupancy modeling provides insights into range-wide conservation needs of lesser prairie-chicken (*Tympanuchus pallidicinctus*). *The Condor: Ornithological Applications*, 118(3):597–612, 2016.

[204] J Andrew Royle. N-mixture models for estimating population size from spatially replicated counts. *Biometrics*, 60(1):108–115, 2004.

[205] Howard Campbell. A population study of lesser prairie-chickens in New Mexico. *The Journal of Wildlife Management*, 36(3):689–699, 1972.

[206] Jay M Ver Hoef, Erin E Peterson, Mevin B Hooten, Ephraim M Hanks, and Marie-Josèe Fortin. Spatial autoregressive models for statistical inference from ecological data. *Ecological Monographs*, 88(1):36–59, 2018.

[207] Andrew A Manderson and Robert JB Goudie. A numerically stable algorithm for integrating Bayesian models using Markov melding. *Statistics and Computing*, 32(2):1–13, 2022.

[208] Yang Liu, James V Zidek, Andrew W Trites, and Brian C Battaile. Bayesian data fusion approaches to predicting spatial tracks: Application to marine mammals. *The Annals of Applied Statistics*, 10(3):1517–1546, 2016.

[209] Nancy J McMillan, David M Holland, Michele Morara, and Jingyu Feng. Combining numerical model output and particulate data using Bayesian space–time modeling. *Environmetrics*, 21(1):48–65, 2010.

[210] Krishna Pacifici, Brian J Reich, David AW Miller, Beth Gardner, Glenn Stauffer, Susheela Singh, Alexa McKerrow, and Jaime A Collazo. Integrating multiple data sources in species distribution modeling: a framework for data fusion. *Ecology*, 98(3):840–850, 2017.

[211] Michael Schaub, Adrian Aebischer, Olivier Gimenez, Silvia Berger, and Raphaël Arlettaz. Massive immigration balances high anthropogenic mortality in a stable eagle owl population: Lessons for conservation. *Biological Conservation*, 143(8):1911–1918, 2010.

[212] Amy J Davis, Mevin B Hooten, Michael L Phillips, and Paul F Doherty Jr. An integrated modeling approach to estimating Gunnison sage-grouse population dynamics: Combining index and demographic data. *Ecology and Evolution*, 4(22):4247–4257, 2014.

[213] Andrew C Olsen, John P Severson, Jeremy D Maestas, David E Naugle, Joseph T Smith, Jason D Tack, Kate H Yates, and Christian A Hagen. Reversing tree expansion in sagebrush steppe yields population-level benefit for imperiled grouse. *Ecosphere*, 12(6):e03551, 2021.

[214] Brian Millsap, Guthrie Zimmerman, William Kendall, Joseph Barnes, Melissa Braham, Bryan Bedrosian, Douglas Bell, Peter Bloom, Ross Crandall, Robert Domenech, Daniel Driscoll, Adam Duerr, Rick Gerhardt, Samantha Gibbs, Alan Harmata, Kenneth Jacobson, Todd Katzner, Robert Knight, J. Lockhart, and James Watson. Age-specific survival rates, causes of death, and allowable take of golden eagles in the western United States. *Ecological Applications*, 32(3):e2544, 2022.

[215] Mitch D Weegman, Ray T Alisauskas, Dana K Kellett, Qing Zhao, Scott Wilson, and Tomáš Telenskỳ. Local population collapse of Ross's and lesser snow geese driven by failing recruitment and diminished philopatry. *Oikos*, 2022(5):e09184, 2022.

[216] Andrew J Royle and Marc Kéry. A Bayesian state-space formulation of dynamic occupancy models. *Ecology*, 88(7):1813–1823, 2007.

[217] Sarah Rebecah Fritts, Blake A Grisham, Robert D Cox, Clint W Boal, David A Haukos, Patricia McDaniel, Christian A Hagen, and Daniel U Greene. Interactive effects of severe drought and grazing on the life history cycle of a bioindicator species. *Ecology and Evolution*, 8(18):9550–9562, 2018.

[218] Roger D Applegate. Use and misuse of prairie chicken lek surveys. *Wildlife Society Bulletin*, pages 457–459, 2000.

[219] Daniel S Sullins, John D Kraft, David A Haukos, Samantha G Robinson, Jonathan H Reitz, Reid T Plumb, Joseph M Lautenbach, Jonathan D Lautenbach, Brett K Sandercock, and Christian A Hagen. Demographic consequences of conservation reserve program grasslands for lesser prairie-chickens. *The Journal of Wildlife Management*, 82(8):1617–1632, 2018.

[220] Justin Van Ee, Christian Hagen, David Pavlacky, Kent Fricke, Matthew Koslovsky, and Mevin Hooten. Melding wildlife surveys to improve conservation inference. *Biometrics*, 2023.

[221] Blake A Grisham and Clint W Boal. Causes of mortality and temporal patterns in breeding season survival of lesser prairie-chickens in shinnery oak prairies. *Wildlife Society Bulletin*, 39(3):536–542, 2015.

[222] Joseph M Lautenbach, David A Haukos, Daniel S Sullins, Christian A Hagen, Jonathan D Lautenbach, James C Pitman, Reid T Plumb, Samantha G Robinson, and John D Kraft. Factors influencing nesting ecology of lesser prairie-chickens. *The Journal of Wildlife Management*, 83(1):205–215, 2019.

[223] Jonathan D Lautenbach, David A Haukos, Joseph M Lautenbach, and Christian A Hagen. Ecological disturbance through patch-burn grazing influences lesser prairie-chicken space use. *The Journal of Wildlife Management*, 85(8):1699–1710, 2021.

[224] Blake A Grisham, Clint W Boal, David A Haukos, Dawn M Davis, Kathy K Boydston, Charles Dixon, and Willard R Heck. The predicted influence of climate change on lesser prairie-chicken reproductive parameters. *PLoS One*, 8(7):e68225, 2013.

[225] Blake A Grisham, Philip K Borsdorf, Clint W Boal, and Kathy K Boydston. Nesting ecology and nest survival of lesser prairie-chickens on the Southern High Plains of Texas. *The Journal of Wildlife Management*, 78(5):857–866, 2014.

[226] Alex Kunkel. *Breeding Season Survival of Lesser Prairie-Chickens (Tympanuchus Pallidicinctus) and Fire Ecology in the Shinnery Oak Prairie of Eastern New Mexico*. PhD thesis, New Mexico State University, 2020.

[227] Nicholas J Parker, Daniel S Sullins, David A Haukos, Kent A Fricke, Christian A Hagen, and Adam A Ahlers. Demographic effects of a megafire on a declining prairie grouse in the mixed-grass prairie. *Ecology and Evolution*, 12(12):e9544, 2022.

[228] Samuel WH Harryman, Blake A Grisham, Clint W Boal, Samantha S Kahl, Russell L Martin, and Christian A Hagen. Multiscale habitat selection of lesser prairie-chickens in a

row-crop and conservation reserve program land matrix. *Journal of Fish and Wildlife Management*, 10(1):126–136, 2019.

[229] Samantha G Robinson, David A Haukos, Reid T Plumb, Joseph M Lautenbach, Daniel S Sullins, John D Kraft, Jonathan D Lautenbach, Christian A Hagen, and James C Pitman. Nonbreeding home-range size and survival of lesser prairie-chickens. *The Journal of Wildlife Management*, 82(2):413–423, 2018.

[230] Matthew J Butler, Warren B Ballard, R Douglas Holt, and Heather A Whitlaw. Sound intensity of booming in lesser prairie-chickens. *The Journal of Wildlife Management*, 74(5):1160–1162, 2010.

[231] David K Dahlgren, Michael R Guttery, Terry A Messmer, Danny Caudill, Robert Dwayne Elmore, Renee Chi, and David N Koons. Evaluating vital rate contributions to Greater Sage-Grouse population dynamics to inform conservation. *Ecosphere*, 7(3):e01249, 2016.

[232] Don L Stevens Jr. and Anthony R Olsen. Spatially balanced sampling of natural resources. *Journal of the American Statistical Association*, 99(465):262–278, 2004.

[233] Jon T McRoberts, Matthew J Butler, Warren B Ballard, Heather A Whitlaw, David A Haukos, and Mark C Wallace. Detectability of lesser prairie-chicken leks: A comparison of surveys from aircraft. *The Journal of Wildlife Management*, 75(4):771–778, 2011.

[234] Joseph Mark Lautenbach. *Lesser prairie-chicken reproductive success, habitat selection, and response to trees*. PhD thesis, Kansas State University, 2015.

[235] Kenneth H Pollock, Scott R Winterstein, Christine M Bunck, and Paul D Curtis. Survival analysis in telemetry studies: The staggered entry design. *The Journal of Wildlife Management*, 53(1):7–15, 1989.

[236] Evan G. Cooch and Gary C. White. *Program MARK, "A gentle introduction"*. 2008.

[237] Gary C White and Kenneth P Burnham. Program MARK: survival estimation from populations of marked animals. *Bird Study*, 46(sup1):S120–S139, 1999.

[238] Christian A Hagen, James C Pitman, Brett K Sandercock, Robert J Robel, and Roger D Applegate. Age-specific survival and probable causes of mortality in female lesser prairie-chickens. *The Journal of Wildlife Management*, 71(2):518–525, 2007.

[239] Eddie K Lyons, Bret A Collier, Nova J Silvy, Roel R Lopez, Benjamin E Toole, Ryan S Jones, and Stephen J DeMaso. Breeding and non-breeding survival of lesser prairie-chickens *Tympanuchus pallidicinctus* in Texas, USA. *Wildlife Biology*, 15(1):89–96, 2009.

[240] Tamara L Fields, Gary C White, Wendell C Gilgert, and Randy D Rodgers. Nest and brood survival of lesser prairie-chickens in west central Kansas. *The Journal of Wildlife Management*, 70(4):931–938, 2006.

[241] James C Pitman, Christian A Hagen, Brent E Jamison, Robert J Robel, Thomas M Loughin, and Roger D Applegate. Nesting ecology of Lesser Prairie-Chickens in sand sagebrush prairie of Southwestern Kansas. *The Wilson Journal of Ornithology*, 118(1):23–35, 2006.

[242] Dawn M Davis. Nesting ecology and reproductive success of Lesser Prairie-Chickens in shinnery oak-dominated rangelands. *The Wilson Journal of Ornithology*, 121(2):322–327, 2009.

[243] Ryan Sterling Jones. *Seasonal survival, reproduction, and use of wildfire areas by lesser prairie chickens in the northeastern Texas Panhandle*. PhD thesis, Texas A & M University, 2010.

[244] Timothy P Lyons, Kirk W Stodola, and Thomas J Benson. Estimating the survival of unmarked young from repeated counts. *Wildlife Biology*, 2020(1):1–9, 2020.

[245] Jonathan W Cummings, Sarah J Converse, Clinton T Moore, David R Smith, Clay T Nichols, Nathan L Allan, and Chris M O'Meilia. A projection of lesser prairie chicken (*Tym-*

panuchus pallidicinctus) populations range-wide. Technical report, US Geological Survey, 2017.

[246] Stephen J Dinsmore, Gary C White, and Fritz L Knopf. Advanced techniques for modeling avian nest survival. *Ecology*, 83(12):3476–3488, 2002.

[247] Eddie K Lyons, Ryan S Jones, John P Leonard, Benjamin E Toole, Robert A McCleery, Roel R Lopez, Markus J Peterson, Stephen J DeMaso, and Nova J Silvy. Regional variation in nesting success of lesser prairie-chickens. *Studies in Avian Biology*, 39:223–231, 2011.

[248] Michael Schaub, Hans Jakober, and Wolfgang Stauber. Strong contribution of immigration to local population regulation: Evidence from a migratory passerine. *Ecology*, 94(8):1828–1838, 2013.

[249] Mitch D Weegman, Stuart Bearhop, Anthony D Fox, Geoff M Hilton, Alyn J Walsh, Jennifer L McDonald, and David J Hodgson. Integrated population modelling reveals a perceived source to be a cryptic sink. *Journal of Animal Ecology*, 85(2):467–475, 2016.

[250] Andrew Gelman and Donald B Rubin. Inference from iterative simulation using multiple sequences. *Statistical Science*, 7(4):457–472, 1992.

[251] Michael A Patten, Donald H Wolfe, Steve K Sherrod, and Eyal Shochat. Effects of microhabitat and microclimate selection on adult survivorship of the lesser prairie-chicken. *The Journal of Wildlife Management*, 69(3):1270–1278, 2005.

[252] Julia E Earl, Samuel D Fuhlendorf, David Haukos, Ashley M Tanner, Dwayne Elmore, and Scott A Carleton. Characteristics of lesser prairie-chicken (*Tympanuchus pallidicinctus*) long-distance movements across their distribution. *Ecosphere*, 7(8):e01441, 2016.

[253] Blake A Grisham, Alixandra J Godar, Clint W Boal, and David A Haukos. Interactive effects between nest microclimate and nest vegetation structure confirm microclimate thresholds for Lesser Prairie-Chicken nest survival. *The Condor: Ornithological Applications*, 118(4):728–746, 2016.

[254] David AW Miller, Krishna Pacifici, Jamie S Sanderlin, and Brian J Reich. The recent past and promising future for data integration methods to estimate species' distributions. *Methods in Ecology and Evolution*, 10(1):22–37, 2019.

[255] Robert J Fletcher, Robert A McCleery, Daniel U Greene, and Courtney A Tye. Integrated models that unite local and regional data reveal larger-scale environmental relationships and improve predictions of species distributions. *Landscape Ecology*, 31:1369–1382, 2016.

[256] J.B. Grace, T.M. Anderson, E.W. Seabloom, and et al. Integrative modelling reveals mechanisms linking productivity and plant species richness. *Nature*, 529:390–393, 2016.

[257] Bradley P Carlin and Thomas A Louis. *Bayesian Methods for Data Analysis*. CRC Press, 2008.

[258] Alan E Gelfand and Dipak K Dey. Bayesian model choice: Asymptotics and exact calculations. *Journal of the Royal Statistical Society: Series B (Methodological)*, 56(3):501–514, 1994.

Appendix A

Supplemental Material for Chapter 2

A.1 Joint Occupancy Models

A.1.1 Royle-Nichols

$$y_{ijk} \sim \text{Bernoulli}(\rho_{ijk}),\ \rho_{ijk} = 1 - (1 - r_{jk})^{N_{ik}},\ \text{logit}(r_{jk}) = g(j, \boldsymbol{\alpha}_k),$$

$$N_{ik} \sim \text{Pois}(\lambda_{ik}),$$

$$\log(\boldsymbol{\lambda}) = \mathcal{N}(\boldsymbol{X}\boldsymbol{\beta} + \boldsymbol{\eta}, \tau^2 \boldsymbol{I}),$$

$$\boldsymbol{\eta} \sim \mathcal{N}(\boldsymbol{0}, \boldsymbol{\Sigma}_{spp} \otimes \boldsymbol{I}_n),$$

$$\boldsymbol{\alpha} \sim \mathcal{N}(\boldsymbol{\mu}_{\boldsymbol{\alpha}}, \boldsymbol{\Sigma}_{\boldsymbol{\alpha}}),$$

$$\boldsymbol{\beta} \sim \mathcal{N}(\boldsymbol{\mu}_{\boldsymbol{\beta}}, \boldsymbol{\Sigma}_{\boldsymbol{\beta}}),$$

$$\boldsymbol{\Sigma}_{spp}^{-1} \sim \text{Wishart}(\boldsymbol{S}/\nu, \nu).$$

A.1.2 Probit

$$y_{ijk} \sim \begin{cases} \text{Bernoulli}(p_{ijk}), & z_{ik} = 1 \\ 0, & z_{ik} = 0 \end{cases},$$

$$\Phi(\boldsymbol{p}) = \boldsymbol{W}\boldsymbol{\alpha},$$

$$z_{ik} \sim \text{Bernoulli}(\psi_{ik}),$$

$$\Phi(\boldsymbol{\psi}) = \mathcal{N}(\boldsymbol{X}\boldsymbol{\beta} + \boldsymbol{\eta}, \boldsymbol{I}),$$

$$\boldsymbol{\eta} \sim \mathcal{N}(\boldsymbol{0}, \boldsymbol{\Sigma}_{spp} \otimes \boldsymbol{I}_n),$$

$$\boldsymbol{\alpha} \sim \mathcal{N}(\boldsymbol{\mu}_{\boldsymbol{\alpha}}, \boldsymbol{\Sigma}_{\boldsymbol{\alpha}}),$$

$$\boldsymbol{\beta} \sim \mathcal{N}(\boldsymbol{\mu}_{\boldsymbol{\beta}}, \boldsymbol{\Sigma}_{\boldsymbol{\beta}}),$$

$$\boldsymbol{\Sigma}_{spp}^{-1} \sim \text{Wishart}(\boldsymbol{S}/\nu, \nu).$$

A.2 MCMC Implementation

For the sites at which we never detected species k, we sample N_{ik} using a Poisson Gibbs update.

$$
\begin{aligned}
\left[N_{ik}|\cdot\right] &\propto \left(\prod_{j=1}^{J_i}[y_{ijk}|N_{ik},\boldsymbol{\alpha}_k]\right)[N_i|\lambda_{ik}],\\
&\propto \left(\prod_{j=1}^{J_i}\{1-(1-r_{ij})^{N_{ik}}\}^{y_{ijk}}\{(1-r_{ij})^{N_{ik}}\}^{1-y_{ijk}}\right)\frac{\left(\lambda_{ik}\right)^{N_{ik}}}{N_{ik}!},
\end{aligned}
$$

For $\boldsymbol{y}_{ik}=\mathbf{0}$, we have,

$$
\begin{aligned}
&\propto \left(\prod_{j=1}^{J_i}(1-r_{ij})\right)^{N_{ik}}\frac{\left(\lambda_{ik}\right)^{N_{ik}}}{N_{ik}!},\\
&\propto \frac{\left(\prod_{j=1}^{J_i}(1-r_{ij})\lambda_{ik})\right)^{N_i}}{N_{ik}!},\\
&\propto \frac{\exp\left(\prod_{j=1}^{J_i}(1-r_{ij})\lambda_{ik}\right)\left(\prod_{j=1}^{J_i}(1-r_{ij})\lambda_{ik})\right)^{N_i}}{N_{ik}!},\\
&= \text{Pois}\left(\prod_{j=1}^{J_i}(1-r_{ij})\lambda_{ik}\right).
\end{aligned}
$$

For any other sequence of detections, the full-conditional distribution for N_{ik} is not tractable, and we use Metropolis-Hastings based on the following MH ratio:

$$
\text{MH}=\frac{\left(\prod_{j=1}^{J_i}[y_{ijk}|N_{ik}^{(\star)},\boldsymbol{\alpha}_k^{(l-1)}]\right)[N_{ik}^{(\star)}|\lambda_{ik}^{(l-1)}][N_{ik}^{(\star)}|N_{ik}^{(l-1)}]}{\left(\prod_{j=1}^{J_i}[y_{ijk}|N_{ik}^{(l-1)},\boldsymbol{\alpha}_k^{(l-1)}]\right)[N_{ik}^{((l-1)}|\lambda_{ik}^{(l-1)}][N_{ik}^{(l-1)}|N_{ik}^{(\star)}]},
$$

where the distribution $[N_{ik}^{(\star)}|N_{ik}^{(l-1)}]$ is the proposal; we used a zero truncated Poisson to ensure that $N_{ik}>0$ at sites for which there was at least one detection.

The full-conditional distribution for λ is also irregular, and we update the λ_{ik} using Metropolis-Hastings with a normal random walk proposal. The MH ratio is as follows:

$$
\text{MH}=\frac{[N_{ik}^{(l-1)}|\lambda_{ik}^{(\star)}][\lambda_{ik}^{(\star)}|\boldsymbol{\beta}_k^{(l-1)},\eta_{ik}^{(l-1)}]}{[N_{ik}^{(l-1)}|\lambda_{ik}^{(l-1)}][\lambda_{ik}^{(l-1)}|\boldsymbol{\beta}_k^{(l-1)},\eta_{ik}^{(l-1)}]},
$$

$$\left[\log \lambda_{ik} | \boldsymbol{\beta}_k, \eta_{ik}^{(l-1)}\right] = \mathcal{N}(\boldsymbol{x}'_{ik}\boldsymbol{\beta}_k^{(l-1)} + \eta_{ik}^{(l-1)}, \tau^2).$$

The priors for $\boldsymbol{\beta}$, $\boldsymbol{\eta}$, and $\boldsymbol{\Sigma}_{spp}$ are conjugate, and the full-conditional distributions are tractable. Below are the derivations.

$$
\begin{aligned}
&[\boldsymbol{\beta}|\cdot] \propto [\boldsymbol{\lambda}|\boldsymbol{\beta}, \boldsymbol{\eta}, \boldsymbol{\Sigma}_{spp}][\boldsymbol{\beta}], \\
&\propto \exp\left(-\frac{1}{2}(\log(\boldsymbol{\lambda}) - (\boldsymbol{X}\boldsymbol{\beta} + \boldsymbol{\eta}))'(\tau^2\boldsymbol{I})^{-1}(\log(\boldsymbol{\lambda}) - (\boldsymbol{X}\boldsymbol{\beta} + \boldsymbol{\eta}))\right) \\
&\times \exp\left(-\frac{1}{2}(\boldsymbol{\beta} - \boldsymbol{\mu}_{\boldsymbol{\beta}})'\boldsymbol{\Sigma}_{\boldsymbol{\beta}}^{-1}(\boldsymbol{\beta} - \boldsymbol{\mu}_{\boldsymbol{\beta}})\right), \\
&\propto \exp\left(-\frac{1}{2}(-2\boldsymbol{\beta}'((\tau^2\boldsymbol{I})^{-1}(\log(\boldsymbol{\lambda}) - \boldsymbol{\eta}) + {\boldsymbol{\Sigma}_{\boldsymbol{\beta}}}^{-1}\boldsymbol{\mu}_{\boldsymbol{\beta}}) + \boldsymbol{\beta}'(\boldsymbol{X}'(\tau^2\boldsymbol{I})^{-1}\boldsymbol{X} + {\boldsymbol{\Sigma}_{\boldsymbol{\beta}}}^{-1})\boldsymbol{\beta})\right), \\
&\implies [\boldsymbol{\beta}|\cdot] = \mathcal{N}(\boldsymbol{A}^{-1}\boldsymbol{b}, \boldsymbol{A}^{-1}),
\end{aligned}
$$

where,

$$\boldsymbol{A}^{-1} = \tau^{-2}\boldsymbol{X}'\boldsymbol{X} + {\boldsymbol{\Sigma}_{\boldsymbol{\beta}}}^{-1},$$

$$\boldsymbol{b} = \tau^{-2}\boldsymbol{X}'(\log(\boldsymbol{\lambda}) - \boldsymbol{\eta}) + {\boldsymbol{\Sigma}_{\boldsymbol{\beta}}}^{-1}\boldsymbol{\mu}_{\boldsymbol{\beta}}.$$

$$
\begin{aligned}
&[\boldsymbol{\eta}|\cdot] \propto [\boldsymbol{\lambda}|\boldsymbol{\beta}, \boldsymbol{\eta}, \boldsymbol{\Sigma}_{spp}][\boldsymbol{\eta}], \\
&\propto \exp\left(-\frac{1}{2}(\log(\boldsymbol{\lambda}) - (\boldsymbol{X}\boldsymbol{\beta} + \boldsymbol{\eta}))'((\tau^2\boldsymbol{I})^{-1}(\log(\boldsymbol{\lambda}) - (\boldsymbol{X}\boldsymbol{\beta} + \boldsymbol{\eta}))\right) \\
&\times \exp\left(-\frac{1}{2}(\boldsymbol{\eta}(\boldsymbol{\Sigma}_{spp} \otimes \boldsymbol{I}_n)^{-1}\boldsymbol{\eta})\right), \\
&\propto \exp\left(-\frac{1}{2}(-2\boldsymbol{\eta}'((\tau^2\boldsymbol{I})^{-1}(\log(\boldsymbol{\lambda}) - \boldsymbol{X}\boldsymbol{\beta}) + \boldsymbol{\eta}'((\tau^2\boldsymbol{I})^{-1} + (\boldsymbol{\Sigma}_{spp} \otimes \boldsymbol{I}_n)^{-1})\boldsymbol{\eta})\right), \\
&\implies [\boldsymbol{\eta}|\cdot] = \mathcal{N}(\boldsymbol{A}^{-1}\boldsymbol{b}, \boldsymbol{A}^{-1}),
\end{aligned}
$$

where,

$\boldsymbol{A}^{-1} = \tau^{-2}\boldsymbol{I} + (\boldsymbol{\Sigma}_{spp} \otimes \boldsymbol{I}_n)^{-1}$,

$\boldsymbol{b} = \tau^{-2}(\log(\boldsymbol{\lambda}) - \boldsymbol{X}\boldsymbol{\beta})$.

Denote $\boldsymbol{\Delta} = \left(\boldsymbol{\eta}_1 \ldots, \boldsymbol{\eta}_K\right)_{n \times K}$.

$$
\begin{aligned}
&[\boldsymbol{\Sigma}_{spp}|\cdot] \propto [\boldsymbol{\eta}|\boldsymbol{\Sigma}_{spp}][\boldsymbol{\Sigma}_{spp}], \\
&\propto |\boldsymbol{\Sigma}_{spp} \otimes \boldsymbol{I}_n|^{-\frac{1}{2}} \exp\left(-\frac{1}{2}(\boldsymbol{\eta}'(\boldsymbol{\Sigma}_{spp} \otimes \boldsymbol{I}_n)^{-1}\boldsymbol{\eta})\right) \\
&\times |\boldsymbol{\Sigma}_{spp}|^{-(\nu+K+1)/2} \exp\left(-\frac{1}{2}\text{tr}(\boldsymbol{S}\boldsymbol{\Sigma}_{spp}^{-1})\right), \\
&\propto |\boldsymbol{\Sigma}_{spp}|^{-\frac{n}{2}} |\boldsymbol{I}_n|^{-\frac{K}{2}} \exp\left(-\frac{1}{2}(\boldsymbol{\eta}'(\boldsymbol{\Sigma}_{spp}^{-1} \otimes \boldsymbol{I}_n)\boldsymbol{\eta})\right) \\
&\times |\boldsymbol{\Sigma}_{spp}|^{-(\nu+K+1)/2} \exp\left(-\frac{1}{2}\text{tr}(\boldsymbol{S}\boldsymbol{\Sigma}_{spp}^{-1})\right), && \text{Props. of } \otimes, \\
&\propto |\boldsymbol{\Sigma}_{spp}|^{-(\nu+n+K+1)/2} \exp\left(-\frac{1}{2}\boldsymbol{\Delta}'\boldsymbol{\Delta}\boldsymbol{\Sigma}_{spp}^{-1}\right) \exp\left(-\frac{1}{2}\text{tr}(\boldsymbol{S}\boldsymbol{\Sigma}_{spp}^{-1})\right), && \text{Prop. of vec} \\
&\propto |\boldsymbol{\Sigma}_{spp}|^{-(\nu+n+K+1)/2} \exp\left(-\frac{1}{2}\text{tr}(\boldsymbol{\Delta}'\boldsymbol{\Delta}\boldsymbol{\Sigma}_{spp}^{-1})\right) \exp\left(-\frac{1}{2}\text{tr}(\boldsymbol{S}\boldsymbol{\Sigma}_{spp}^{-1})\right), && \text{Prop. of trace} \\
&\propto |\boldsymbol{\Sigma}_{spp}|^{-(\nu+n+K+1)/2} \exp\left(-\frac{1}{2}\text{tr}([\boldsymbol{\Delta}'\boldsymbol{\Delta} + \boldsymbol{S}]\boldsymbol{\Sigma}_{spp}^{-1})\right), \\
&\implies [\boldsymbol{\Sigma}_{spp}|\cdot] = \text{Inv-Wishart}(\nu + n, \boldsymbol{\Delta}'\boldsymbol{\Delta} + \boldsymbol{S}).
\end{aligned}
$$

A.3 Asymptotic Equivalence of Poisson and Logistic Regression

Consider the models,

$$\begin{aligned} &y_i \sim \text{Bernoulli}(\rho_i),\ \rho_i = 1-(1-r)^{z_i}, \\ &z_i \sim \text{Bernoulli}(\psi_i),\ \text{logit}(\psi_i) = \boldsymbol{x}_i'\boldsymbol{\beta}, \\ &\text{where } z_i = \mathcal{I}(N_i > 0), \end{aligned} \tag{Model A}$$

$$\begin{aligned} &y_i \sim \text{Bernoulli}(\rho_i),\ \rho_i = 1-(1-r)^{N_i}, \\ &N_i \sim \text{Pois}(\lambda_i),\ \log(\lambda_i) = \boldsymbol{x}_i'\boldsymbol{\beta}. \end{aligned} \tag{Model B}$$

$$\begin{aligned} \ell_A(\boldsymbol{\beta}|\boldsymbol{Y}) &= \sum_{i=1}^{n}\left(y_i \log\left(\frac{\rho_i}{1-\rho_i}\right) + \log(1-\rho_i) + z_i \log\left(\frac{\psi_i}{1-\psi_i}\right) + \log(1-\psi_i)\right) \\ &= \sum_{z_i=1}\left(y_i \log\left(\frac{r}{1-r}\right) + \log(1-r) + \log\left(\frac{\psi_i}{1-\psi_i}\right) + \log(1-\psi_i)\right) + \\ &\sum_{z_i=0}\log(1-\psi_i). \end{aligned}$$

We denote $n_0 = n - \sum_{i=1}^{n} z_i$ and let $n_0 \longrightarrow \infty$. Then

$$\ell_A(\boldsymbol{\beta}|\boldsymbol{Y}) \approx \sum_{z_i=0}\log(1-\psi_i) \approx -\sum_{z_i=0}\psi_i,$$

Name	Discription
Aspen	Percent of canopy cover that is Aspen
Bare	Percent bare ground of all material < 0.25 m in height
Canopy	Percent canopy cover (all species pooled)
DeadDown	Percent of ground cover due to dead and down trees
ELEV	Elevation of site (meters)
Habitat	Binary indicator of whether site was lodgepole pine or spruce-fir dominated
ShrubHt	Shrub height (meters)
TWIP	Topographic wetness index plus an index of soil moisture based on slope, basin characteristics, and solar radiation
TPI	Topographic position index of concavity or convexity to indicate position along a slope from valley to ridge top
UCCover	Percent of shrub cover due to coniferous species
UDCover	Percent of shrub cover due to deciduous species
WILD	Binary indicator of whether site was located in a federally designated wilderness or not

where the approximation follows from the Taylor series expansion of $\log(1-x)$ when x is small. Next, observe

$$\begin{aligned}\ell_B(\boldsymbol{\beta}|\boldsymbol{Y}) &= \sum_{i=1}^{n}\left(y_i \log\left(\frac{\rho_i}{1-\rho_i}\right) + \log(1-\rho_i) + N_i\log(\lambda_i) - \lambda_i\right) \\ &= \sum_{N_i>0}\left(y_i \log\left(\frac{\rho_i}{1-\rho_i}\right) + \log(1-\rho_i) + N_i\log(\lambda_i) - \lambda_i\right) + \\ &\sum_{N_i=0} -\lambda_i\end{aligned}$$

Again, let $n_0 \longrightarrow \infty$. Then

$$\ell_B(\boldsymbol{\beta}|\boldsymbol{Y}) \approx -\sum_{N_i=0}\lambda_i \approx -\sum_{z_i=0}\psi_i,$$

for ψ_i small. Hence, the likelihoods are approximately equal for $n_0 \longrightarrow \infty$, and inference on $\boldsymbol{\beta}$ will be similar for models A and B.

A.4 Habitat Covariates

For details on how habitat covariates were collected, see Ivan et al. (2018).

Species	Intensity	Detection
American Marten	Bare, WILD	QUAD
Black Bear	TWIP, ELEV, WILD	LIN
Chipmunk	Canopy, TWIP, TPI	LIN
Coyote	ShrubHt, Bare, TWIP, TPI	CONT
Elk	UCCover, Bare, TWIP, TPI	QUAD
Golden-mantled Ground Squirrel	Aspen, Bare	LIN
Moose	Aspen, ShrubHt, TWIP, ELEV	QUAD
Mule Deer	UDCover, DeadDown, Bare	CONT
Porcupine	Habitat, Bare, WILD	LIN
Red Fox	Aspen, DeadDown, TPI, WILD	LIN
Red Squirrel	Habitat, Bare, WILD	LIN
Snowshoe Hare	Habitat, Aspen, Bare	CONT
Yellow-bellied Marmot	WILD	CONT

A.5 Species Design Matrices

In addition to the covariates shown in the table, each design matrix in the intensity model also included a species specific intercept as well as the bark beetle covariates (severity, YSO1, and YSO2). We specified the following for our detection model:

$$\text{logit}(r_j) = \begin{cases} \alpha_0 & \text{, CONT} \\ \alpha_0 + \alpha_1 j & \text{, LIN} \\ \alpha_0 + \alpha_1 j + \alpha_2 j^2 & \text{, QUAD} \end{cases} .$$

We centered the occasions to have mean 0 in the linear model and used orthogonal polynomial basis functions for the quadratic model.

Appendix B

Supplemental Material for Chapter 3

B.1 Model Statements

B.1.1 Aerial Distance Sampling Submodel

$$v_{itl} \sim \text{Binomial}(B_{itl}, \rho_{itl}),$$

$$B_{itl} = \begin{cases} 2, & \text{for } d_{itl} > 7,\ \epsilon_{itl} = 1, \text{ and } z_{itl} = 1 \\ 1, & \text{for } d_{itl} > 7,\ \epsilon_{itl} = 0, \text{ and } z_{itl} = 1 \\ 1, & \text{for } d_{itl} \leq 7 \text{ and } z_{itl} = 1 \\ 0, & \text{for } z_{itl} = 0 \end{cases},$$

$$\text{logit}(\boldsymbol{\rho}) = \left(\boldsymbol{X}_{\rho}, \boldsymbol{N}^{A}, \boldsymbol{d}\right) \boldsymbol{\beta}_{\rho}, \boldsymbol{\beta}_{\rho} \sim \mathcal{N}(\mathbf{0}, 2.25\boldsymbol{I}),$$

$$N^{A}_{itl} \sim \begin{cases} \text{ZTP}(\lambda_{it}), & \text{for } \omega_{itl} = 1 \\ \text{ZTP}(\lambda_{0}), & \text{for } \omega_{itl} = 0 \end{cases},$$

$$\omega_{itl} \sim \text{Bernoulli}(p_{\omega}),$$

$$d_{itl} \sim \text{Unif}(0, \nu_{d}),$$

$$z_{itl} \sim \text{Bernoulli}(\psi_{it}),$$

$$\epsilon_{itl} \sim \text{Bernoulli}(0.5),$$

$$\text{logit}(\boldsymbol{\psi}) = \boldsymbol{X}_{\psi}\boldsymbol{\beta}_{\psi}, \boldsymbol{\beta}_{\psi} \sim \mathcal{N}(\mathbf{0}, 2.25\boldsymbol{I}),$$

$$\log(\boldsymbol{\lambda}) = \boldsymbol{X}_{\lambda}\boldsymbol{\beta}_{\lambda}, \boldsymbol{\beta}_{\lambda} \sim \mathcal{N}(\mathbf{0}, 10\boldsymbol{I}),$$

$$\lambda_{0} \sim \text{Gamma}(1.78, 0.675),$$

$$p_{\omega} \sim \text{Uniform}(0, 1).$$

We set an informative prior for λ_0 so that the mean size of a non-lek group observations was 1.2 and resulted in a prior probability of approximately 0.95 that a non-lek observation contains fewer than 4 individuals. The variance of λ_0 implied the prior probability of a non-lek observation having less than 10 individuals was nearly 1.

B.1.2 N-mixture Submodel

$$
\begin{aligned}
&F_{itlj} \sim \text{Binomial}(N^G_{itl}, p) \text{ for } j = 1, \ldots, J_{itl},\\
&N^G_{itl} \sim \text{Poisson}(\exp(\boldsymbol{w}'_{it}\boldsymbol{\eta})) \text{ for } l = 1, \ldots, L^G_{it},\\
&\boldsymbol{\eta} \sim \mathcal{N}(\mathbf{0}, 10\boldsymbol{I}),\\
&p \sim \text{Uniform}(0, 1).
\end{aligned}
$$

B.1.3 Spatio-temporal Tobit Submodel

$$y_{it} = \begin{cases} \zeta_{it}, & \text{for } \zeta_{it} > 0 \\ 0, & \text{for } \zeta_{it} \leq 0 \end{cases},$$

$$\boldsymbol{\zeta}_t \sim \mathcal{N}(\boldsymbol{\xi}_t, \sigma_d^2 \boldsymbol{R}_d(\phi)),$$

$$\boldsymbol{\xi}_t \sim \mathcal{N}((\boldsymbol{\xi}_{t-1}, \boldsymbol{W}_{t-1})\,\boldsymbol{\alpha}, \text{Block-Diagonal}(\sigma_\tau^{2,A}\boldsymbol{R}_\tau^A, \sigma_\tau^{2,G}\boldsymbol{R}_\tau^G)),$$

$$\boldsymbol{\xi}_0 = \boldsymbol{X}_0\boldsymbol{\gamma},$$

$$\boldsymbol{\gamma} \sim \mathcal{N}(\mathbf{0}, 100\boldsymbol{I}),$$

$$\boldsymbol{\alpha} \sim \mathcal{N}(\mathbf{0}, 100\boldsymbol{I}),$$

$$\sigma_d^2 \sim \mathcal{IG}(0.01, 100),$$

$$\sigma_\tau^{2,A} \sim \mathcal{IG}(0.01, 100),$$

$$\sigma_\tau^{2,G} \sim \mathcal{IG}(0.01, 100),$$

$$\phi \sim \text{Discrete-Uniform}(1, 1001, 2001, \ldots, 99001).$$

B.1.4 Simulation Study ADSM

$$v_{itl} \sim \begin{cases} \text{Bernoulli}(\exp(-d^2/\sigma^2)), & z_{itl} = 1 \\ 0, & z_{itl} = 0 \end{cases},$$

$$z_{itl} \sim \text{Bernoulli}(\psi_{it}),$$

$$\psi_{it} \sim \text{Unif}(0, 1),$$

$$d_{itl} \sim \text{Unif}(0, 1),$$

$$\sigma_{itl} \sim \text{Unif}(0, 10).$$

B.1.5 Simulation Study N-mixture Submodel

$$
\begin{aligned}
F_{itj} &\sim \text{Binomial}(N_{it}^G, p) \text{ for } j = 1, \ldots, 4, \\
N_{it}^G &\sim \text{Poisson}(\mu_{it}), \\
\mu_{it} &\sim \text{Gamma}(0.01, 0.01), \\
p &\sim \text{Uniform}(0, 1).
\end{aligned}
$$

B.2 Implementation

We set $\nu_d = 600$ which results in an approximate survey region of $S = 2{\times}2{\times}15{\times}0.6 = 36\,\text{km}^2$ per survey block. We augmented our dataset to allow for $M = 20$ groups per survey region. Both ν_d and M were adequately large to accommodate uncertainty in the maximum detection distance and true number of LEPC groups in the sample population of each survey region [134]. Both ν_d and M can be set larger with no inferential impact on density but will increase computational burden because of the expanded parameter space.

The first-stage algorithm targeted samples from the joint distribution of the ADSM and N-mixture submodel with two independent Metropolis-Hastings-within-Gibbs algorithms. The full-conditional distributions of the parameters $\boldsymbol{\beta}_\lambda, \boldsymbol{\beta}_\rho, \boldsymbol{N}^{A,u}, \boldsymbol{d}^u, \boldsymbol{\epsilon}^u$, and $\boldsymbol{N}^G$ were non-tractable, thus we used a Metropolis-Hastings algorithm. To improve mixing, we updated the elements of each vector-valued parameter individually. We used normal random walk proposals for $\boldsymbol{\beta}_\lambda$, $\boldsymbol{\beta}_\rho$, and $\boldsymbol{\eta}$, and tuned the proposals such that acceptance rates varied between 20-40%. Proposals for $\boldsymbol{N}^{A,u}, \boldsymbol{z}^u, \boldsymbol{d}^u, \boldsymbol{\epsilon}^u$, and $\boldsymbol{N}^G$ were generated from their prior distributions. The full-conditional distributions of $\boldsymbol{\omega}$, p_ω, $\boldsymbol{z}^u$, and p were tractable, and we sampled directly from them using Gibbs updates. We obtained samples of $\boldsymbol{\beta}_\psi$ using Pólya-Gamma data augmentation [91]. We also considered Pólya-Gamma and Albert-Chib [84] data augmentation strategies for the linear predictor $\boldsymbol{\beta}_\rho$ but found neither improved sampling efficiency.

The second-stage MCMC algorithm melded the submodel density samples y_{it}^A and y_{it}^G into the joint response spatial-temporal tobit model (STTM). Keeping notation general, we suppress the superscripts A and G, and let $\mathcal{M}$ denote a generic submodel (in our case either the ADSM or N-mixture submodel). To meld the density samples, we drew a sub-sample of y_{it} from $[y_{it}^{(\star)}, \cdot]_{\mathcal{M}}$, denoted by $y_{it}^{(\star)}$, from the first-stage randomly with replacement, and the Metropolis-Hastings ratio was

$$\frac{[y_{it}^{(\star)}|\cdot]_{\text{STTM}}}{[y_{it}^{(k-1)}|\cdot]_{\text{STTM}}}, \tag{B.1}$$

where $[y_{it}^{(\star)}|\cdot]_{\text{STTM}}$ is the conditional distribution of $y_{it}^{(\star)}$ given the current value of all other parameters in the STTM. Letting $\theta^{(k)}$ denote the value of parameter θ at iteration k, we have that for $y_{it}^{(\star)} = 0$,

$$[y_{it}^{(\star)}|\cdot]_{\text{STTM}} = \mathcal{P}(\zeta_{it} \leq 0|\boldsymbol{\zeta}_{-it}^{(k-1)}, \boldsymbol{\xi}_t^{(k-1)}, {\sigma_d}^{2,(k-1)}, \phi^{(k-1)}) = \Phi(0|\tilde{\mu}^{(k-1)}, \tilde{\sigma}^{2,(k-1)}), \tag{B.2}$$

and if $y_{it}^{(\star)} > 0$, then

$$[y_{it}^{(\star)}|\cdot]_{\text{STTM}} = \mathcal{N}(\tilde{\mu}^{(k-1)}, \tilde{\sigma}^{2,(k-1)}), \tag{B.3}$$

where Φ is the cumulative distribution function of the standard normal distribution and

$$\tilde{\mu}^{(k-1)} = \xi_{it}^{(k-1)} + \boldsymbol{r}_{d,i-i}(\phi^{(k-1)}) \left(\boldsymbol{R}_{d,-i-i}(\phi^{(k-1)})\right)^{-1} \left(\boldsymbol{\zeta}_{-it}^{(k-1)} - \boldsymbol{\xi}_{-it}^{(k-1)}\right), \tag{B.4}$$

$$\tilde{\sigma}^{2,(k-1)} = \sigma_d^{2,(k-1)} \left(r_{d,ii}(\phi^{(k-1)}) - \boldsymbol{r}_{d,i-i}(\phi^{(k-1)}) \left(\boldsymbol{R}_{d,-i-i}(\phi^{(k-1)})\right)^{-1} \boldsymbol{r}_{d,-ii}(\phi^{(k-1)})\right). \tag{B.5}$$

The acceptance rates of our Metropolis-Hastings algorithms for y_{it}^A and y_{it}^G were 11% and 45%, respectively.

For $y_{it} > 0$, ζ_{it} is known and $\zeta_{it} = y_{it}$, but for $y_{it} = 0$, ζ_{it} is latent and must be sampled from its full-conditional distribution. We sampled the vector of latent quantities $\boldsymbol{\zeta}_t^u$ with a Gibbs update

because its full-conditional distribution is multivariate normal truncated at 0. The full-conditional distributions of $\boldsymbol{\xi}_t$, $\boldsymbol{\gamma}$, and $\boldsymbol{\alpha}$ are multivariate normal and were sampled from using Gibbs updates. We also used Gibbs updates for the variance parameters $\sigma^{2,A}_\tau$, $\sigma^{2,G}_\tau$, and σ^2_d which have inverse-gamma full-conditional distributions. A Metropolis-Hastings algorithm was employed for updating ϕ. We precalculated the exponentially decaying distance correlation matrices, $\boldsymbol{R}(\phi)$, associated with each support value of ϕ to improve computation.

We coded our multistage MCMC algorithm in `Rcpp` to decrease runtime [148]. The first-stage sampler which targets the posteriors of the ADSM and N-mixture submodel were run in parallel for $100,000$ iterations. We discarded the $10,000$ iterations as burn-in and drew randomly with replacement from the remaining sample for proposals of $\boldsymbol{y}^A$ and $\boldsymbol{y}^G$ in the STTM. The second-stage sampler was run for $80,000$ iterations after of burn-in of $20,000$. Total run times for the first and second stages were 129 and 111 minutes, respectively (2.5 Ghz 28-core Intel Xeon W processor). The potential scale reduction factor for all parameters from the first and second stage was less than 1.1 indicating convergence [250].

B.3 Covariates

We selected a parsimonious suite of covariates previously shown to be associated with lesser prairie-chicken demography, occupancy, and abundance that quantified differences in landcover, habitat patch size, anthropogenic disturbance, grassland restoration and drought. Table B.1 provides a description of each covariate and indicates its source. All covariates were measured at the 15×15-km survey block resolution except for Palmer Drought Severity Index (PDSI), which was extracted from National Oceanic and Atmospheric Administration climate divisions. All continuous covariates except for PDSI were standardized to have mean 0 and variance 1. To derive covariate values for the ground sites, we calculated a weighted average of the survey block covariate values based on the percentage of area the ground survey region included each block. Only PDSI was temporally indexed. All other covariates were static and measured in 2012.

Table B.1: Covariates available at following links:
WEST (field-collected data from WEST aerial surveys),
NLCD (https://www.mrlc.gov/data/references/national-land-cover-database-2011-nlcd2011),
NRCS (https://www.nrcs.usda.gov/wps/portal/nrcs/site/national/home/),
NOAA (https://www.ncei.noaa.gov/access/monitoring/historical-palmers/maps).

Name	Description	Source
Ecoregion	Ecoregion identifier (1 = SOPR, 2 = SSPR, 3 = MGPR, 4 = SGPR)	WEST
Development	Percentage of area (%) with anthropogenic development.	NLCD
CRP	Percentage of area (%) enrolled in the Conservation Reserve Program.	N/A
Grassland patch size	Average size (km^2) of grassland landcover patches.	NLCD
Shrubland	Percentage of area (%) dominated by shrubs, including trees <5 m tall.	NLCD
Woodland	Percentage of area (%) with tree canopy cover >1%.	NRCS
PDSI	Palmer Drought Severity Index averaged over March, April, and May.	NOAA

B.4 Comparison of ADSM Inference with WEST Annual Reports

Western EcoSystems Technology, Inc. (WEST) uses the aerial survey data to infer annual fluctuations in ecoregion wide LEPC densities. We compared the unrefined density estimates from our ADSM with the density estimates reported by Nasman et al. [197]. Figure B.1 shows the SGPR ecoregion annual density estimates along with their associated uncertainties. Note that the estimates of Nasman et al. [197] are calculated for the full SSPR, MGPR, and SGPR ecoregions, which span Kansas, Colorado, Oklahoma, and Texas, whereas our density estimates are clipped to Kansas. Therefore, only the density estimates for the SGPR are directly comparable across models because the ecoregion is only in Kansas. Neither set of estimates shown were adjusted for the occurrence of greater prairie-chicken in the northern region of the SGPR.

In general, mean annual density estimates for the SGPR were similar across the two models, but the ADSM resulted in smoother temporal process and had less uncertainty than the distance sampling model of Nasman et al. [197]. We included covariates in our ADSM that quantified heterogeneity in landscapes and climatic factors such as drought to facilitate learning about shared patterns in LEPC density across Kansas EOR. Consequently, SGPR annual density estimates from the ASDM are informed by trends observed across all ecoregions. This may explain the reduced un-

certainty of the ADSM estimates compared with those inferred from the distance sampling model of Nasman et al. [197], which treated ecoregions independently.

The largest discrepancy in annual density estimates between the ADSM and Nasman et al. [197] was for the SGPR ecoregion in 2016. Nasman et al. [197] estimated a decline whereas our ADSM estimated an annual density similar to 2015. Our ADSM included PDSI as a covariate which was estimated to have a positive association with LEPC density (i.e., higher densities following wetter years). PDSI was above average for 2016 (i.e., a relatively wet year), which could explain the higher density estimates that resulted from our ADSM in 2016.

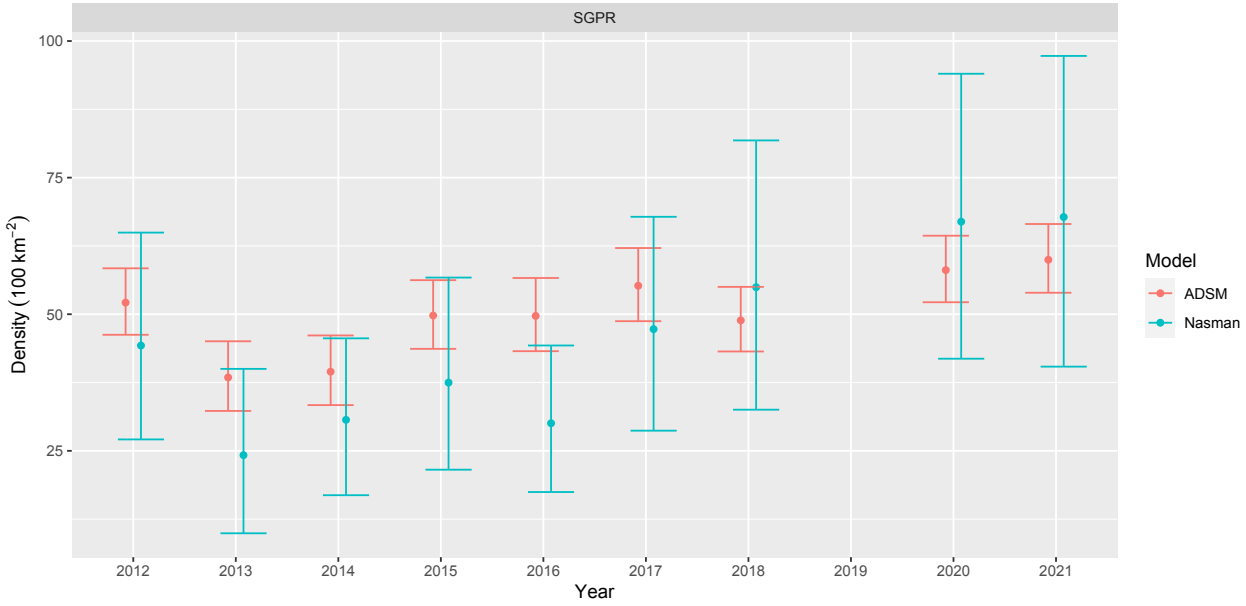

Figure B.1: SGPR ecoregion annual density estimates of LEPC from 2012-2021. Posterior means and 90% credible intervals of annual density estimated with the ADSM shown in red. Mean estimates and 90% confidence intervals of annual density from Nasman et al. (2021) are in turquoise. Note that density estimates from both models include observations of greater prairie-chicken in the northern region of the SGPR

B.5 Inference For Covariate Associations

Posterior mean LEPC densities were highest in the SGPR ecoregion and lowest in the SSPR (Table B.2). The MGPR ecoregion had interemediate LEPC densities. LEPC densities were lower

in regions with a higher percentage of anthropogenic disturbance and tree canopy cover. LEPC density was positively associated with the percentage of area enrolled in the Conservation Reserve Program (CRP), percentage of area dominated by shrubs, and average size of grassland landcover patches. Density in the SGPR decreased sharply north of Interstate 70.

Table B.2: Posterior means and credible interval for regression coefficients $\boldsymbol{\gamma}$ and $\boldsymbol{\alpha}$.

Covariate	Parameter	Posterior Mean	Credible Interval (90%)
SSPR	γ_0	0.029	(-0.147, 0.197)
MGPR	γ_1	0.286	(0.165, 0.418)
SGPR	γ_2	0.602	(0.488, 0.718)
Development	γ_3	-0.103	(-0.133, -0.073)
CRP	γ_4	0.069	(0.046, 0.094)
Grassland patch size	γ_5	0.273	(0.206, 0.341)
Shrubland	γ_6	0.191	(0.126, 0.257)
Woodland	γ_7	-0.084	(-0.133, -0.041)
I-70	γ_8	-0.383	(-0.462, -0.309)
PDSI	α_1	0.001	(-0.004, 0.005)

Appendix C

Supplemental Material for Chapter 4

C.1 Implementation

We set $\nu_d = 600$, which resulted in an approximate survey region of $S = 2 \times 2 \times 15 \times 0.6 = 36$ km^2 per survey block. We augmented our dataset to allow for $M = 20$ groups per survey region. Both ν_d and M were adequately large to accommodate uncertainty in the maximum detection distance and true number of lesser prairie-chicken groups in the sample population of each survey region [134]. Both ν_d and M can be set larger with no inferential effect on density but will increase computational burden because of the expanded parameter space.

The first-stage algorithm targeted samples from the joint distribution of the aerial distance sampling, N-mixture, survival and productivity submodels with standard independent Metropolis-within-Gibbs samplers. The full-conditional distributions of the parameters $\boldsymbol{\beta}_\lambda$, $\boldsymbol{\beta}_\zeta$, $\boldsymbol{\eta}$, $\boldsymbol{\beta}^\delta$, μ^δ, $\boldsymbol{B}$, $\boldsymbol{N}^{A,u}$, $\boldsymbol{d}^u$, $\boldsymbol{\epsilon}^u$, and $\boldsymbol{N}^G$ were non-tractable. We used a Metropolis-Hastings algorithm to obtain posterior samples of each quantity. To improve mixing, we updated the elements of each vector-valued parameter individually. We used normal random walk proposals for $\boldsymbol{\beta}_\lambda$, $\boldsymbol{\beta}_\rho$, $\boldsymbol{\beta}^\delta$, and $\boldsymbol{\eta}$, and tuned the proposals such that acceptance rates varied between 20-40%. Proposals for $\boldsymbol{N}^{A,u}, \boldsymbol{z}^u, \boldsymbol{d}^u, \boldsymbol{\epsilon}^u$, and $\boldsymbol{N}^G$ were generated from their prior distributions. The full-conditional distributions of $\boldsymbol{\omega}$, p_ω, $\boldsymbol{z}^u$, ϕ_1^B, ϕ_2^B, μ^δ, μ^π, μ_e^π, $\mu_e^{\phi^N}$, $\mu_{el}^{\phi^N}$, $\mu_e^{\phi^A}$, $\mu_{el}^{\phi^A}$, σ_π^2, σ_δ^2, $\sigma_{\phi^N}^2$, $\sigma_{\phi^A}^2$, q, and p_e were tractable, and we sampled directly from them using Gibbs updates. We obtained samples of $\boldsymbol{\beta}_\psi$, $\boldsymbol{\beta}^\delta$, $\boldsymbol{\beta}^{\phi^N}$, and $\boldsymbol{\beta}_{\phi^A}$ using Pólya-Gamma data augmentation [91]. We also considered Pólya-Gamma and Probit [84] data augmentation strategies for the linear predictor $\boldsymbol{\beta}_\zeta$ but found neither improved sampling efficiency.

In the second-stage of the MCMC algorithm, we drew sub-samples of N_{et}^A, N_{et}^G, ϕ_{ket}^A and ρ_{aet} for proposal in the population model. We introduce the notation $N_{et}^X(S)$ to denote the abundance of individuals inhabiting a region of size S in ecoregion e during year t for survey method $X \in \{A, G\}$. To update the aerial and ground abundances, for MCMC iteration l, we drew a sub-

sample of the annual ecoregional abundance ${N^X_{e,t+1}}^{(\star)}(\mathcal{S}^X_{e,t+1})$ randomly with replacement from the first-stage, where $\mathcal{S}^X_{e,t+1}$ is the total area of ecoregion e during year $t+1$ for method X. For aerial surveys, $\mathcal{S}^A_{e,t+1}$ equals the total area covered by all blocks in the sampling frame of ecoregion e during year $t+1$ and represents the total area of the ecoregion. For ground surveys, $\mathcal{S}^G_{e,t+1}$ equals the total area covered by all ground sampling regions in ecoregion e during year $t+1$ which is much less than the total area of the ecoregion. We then calculated the estimated density ${Y^X_{e,t+1}}^{(\star)} = {N^X_{e,t+1}}^{(\star)}(\mathcal{S}^X_{e,t+1})/\mathcal{S}^X_{e,t+1}$. Finally, we calculated the approximate number of birds encountered by multiplying the annual ecoregional density estimate by the survey effort for method X, ${N^X_{e,t+1}}^{(\star)}(S^X_{e,t+1}) = {Y^X_{e,t+1}}^{(\star)} S^X_{e,t+1}$, where $S^X_{e,t+1}$ is the area surveyed (Tables 4.1 and 4.2). We then drew

$${N^X_{e,t+1,SY}}^{(\star)}(S^X_{e,t+1}) \sim \text{Poisson}({N^X_{♀et,ASY}}^{(l-1)}(S^X_{e,t+1})\rho_{et,ASY}{}^{(l-1)} + {N^X_{♀et,SY}}^{(l-1)}(S^X_{e,t+1})\rho_{et,SY}{}^{(l-1)}), \quad \text{(C.1)}$$

$${N^X_{♀e,t+1,ASY}}^{(\star)}(S^X_{e,t+1}) \sim \text{Binomial}({N^X_{♀et,ASY}}^{(l-1)}(S^X_{e,t+1}), {\phi^A_{♀et}}^{(l-1)}), \quad \text{(C.2)}$$

and calculated

$${N^X_{♂e,t+1,ASY}}^{(\star)}(S^X_{e,t+1}) = {N^X_{e,t+1}}^{(\star)}(S^X_{e,t+1}) - {N^X_{♀e,t+1,ASY}}^{(\star)}(S^X_{e,t+1}) - {N^X_{e,t+1,SY}}^{(\star)}(S^X_{e,t+1}). \quad \text{(C.3)}$$

The Metropolis-Hastings ratio was

$$\frac{[{N^X_{e,t+2,SY}}^{(l-1)}(S^X_{e,t+1})|{N^X_{♀e,t+1,ASY}}^{(\star)}(S^X_{e,t+1}), {N^X_{♀e,t+1,SY}}^{(\star)}(S^X_{e,t+1}), \rho_{e,t+1,ASY}{}^{(l-1)}, \rho_{e,t+1,SY}{}^{(l-1)}]}{[{N^X_{e,t+2,SY}}^{(l-1)}(S^X_{e,t+1})|{N^X_{♀e,t+1,ASY}}^{(l-1)}(S^X_{e,t+1}), {N^X_{♀e,t+1,SY}}^{(l-1)}(S^X_{e,t+1}), \rho_{e,t+1,ASY}{}^{(l-1)}, \rho_{e,t+1,SY}{}^{(l-1)}]} \times \quad \text{(C.4)}$$

$$\frac{[{N^X_{♀e,t+2,ASY}}^{(l-1)}(S^X_{e,t+1})|{N^X_{♀e,t+1,ASY}}^{(\star)}(S^X_{e,t+1}), {N^X_{♀e,t+1,SY}}^{(\star)}(S^X_{e,t+1}), {\phi^A_{♀e,t+1}}^{(l-1)}]}{[{N^X_{♀e,t+2,ASY}}^{(l-1)}(S^X_{e,t+1})|{N^X_{♀e,t+1,ASY}}^{(l-1)}(S^X_{e,t+1}), {N^X_{♀e,t+1,SY}}^{(l-1)}(S^X_{e,t+1}), {\phi^A_{♀e,t+1}}^{(l-1)}]} \times \quad \text{(C.5)}$$

$$\frac{[{N^X_{♂e,t+2,ASY}}^{(l-1)}(S^X_{e,t+1})|{N^X_{♂e,t+1,ASY}}^{(\star)}(S^X_{e,t+1}), {N^X_{♂e,t+1,SY}}^{(\star)}(S^X_{e,t+1}), {\phi^A_{♂e,t+1}}^{(l-1)}]}{[{N^X_{♂e,t+2,ASY}}^{(l-1)}(S^X_{e,t+1})|{N^X_{♂e,t+1,ASY}}^{(l-1)}(S^X_{e,t+1}), {N^X_{♂e,t+1,SY}}^{(l-1)}(S^X_{e,t+1}), {\phi^A_{♂e,t+1}}^{(l-1)}]} \times \quad \text{(C.6)}$$

$$\frac{[{N^X_{♂e,t+1,ASY}}^{(\star)}(S^X_{e,t+1})|{N^X_{♂et,ASY}}^{(l-1)}(S^X_{e,t+1}), {N^X_{♂et,SY}}^{(l-1)}(S^X_{e,t+1}), {\phi^A_{♂et}}^{(l-1)}]}{[{N^X_{♂e,t+1,ASY}}^{(l-1)}(S^X_{e,t+1})|{N^X_{♂et,ASY}}^{(l-1)}(S^X_{e,t+1}), {N^X_{♂et,SY}}^{(l-1)}(S^X_{e,t+1}), {\phi^A_{♂et}}^{(l-1)}]}, \quad \text{(C.7)}$$

where equation (C.4) is a Poisson probability mass function and equations (C.5)-(C.7) are Binomial probability mass functions. For adult survival, we drew a sub-sample, ${\phi^A_{ket}}^{(\star)}$, from the first-stage

randomly with replacement, and the Metropolis-Hastings ratio was

$$\prod_{X\in A,G}\left(\frac{[N^{X}_{ke,t+1,ASY}{}^{(l-1)}(S^{X}_{et})|N^{X}_{ket,ASY}{}^{(l-1)}(S^{X}_{et}),N^{X}_{ket,SY}{}^{(l-1)}(S^{X}_{et}),\phi^{A}_{ket}{}^{(\star)}]}{[N^{X}_{ke,t+1,ASY}{}^{(l-1)}(S^{X}_{et})|N^{X}_{ket,ASY}{}^{(l-1)}(S^{X}_{et}),N^{X}_{ket,SY}{}^{(l-1)}(S^{X}_{et}),\phi^{A}_{ket}{}^{(l-1)}]}\right). \tag{C.8}$$

Likewise, for productivity, we drew a sub-sample, $\rho_{aet}{}^{(\star)}$, from the first-stage randomly with replacement, and the Metropolis-Hastings ratio was

$$\prod_{X\in A,G}\left(\frac{[N^{X}_{e,t+1,SY}{}^{(l-1)}(S^{X}_{et})|N^{X}_{\varphi,et,ASY}{}^{(l-1)}(S^{X}_{et}),N^{X}_{\varphi,et,SY}{}^{(l-1)}(S^{X}_{et}),\rho_{-aet}{}^{(l-1)},\rho_{aet}{}^{(\star)}]}{[N^{X}_{e,t+1,SY}{}^{(l-1)}(S^{X}_{et})|N^{X}_{\varphi,et,ASY}{}^{(l-1)}(S^{X}_{et}),N^{X}_{\varphi,et,SY}{}^{(l-1)}(S^{X}_{et}),\rho_{-aet}{}^{(l-1)},\rho_{aet}{}^{(l-1)}]}\right). \tag{C.9}$$

C.2 Model Statements

C.2.1 Aerial Distance Sampling Submodel

$$v_{itl} \sim \text{Binomial}(B_{itl}, \zeta_{itl}), \tag{C.10}$$

$$O_{itl} = \begin{cases} 2, & \text{for } d_{itl} > 7,\ \epsilon_{itl} = 1, \text{ and } z_{itl} = 1 \\ 1, & \text{for } d_{itl} > 7,\ \epsilon_{itl} = 0, \text{ and } z_{itl} = 1 \\ 1, & \text{for } d_{itl} \leq 7 \text{ and } z_{itl} = 1 \\ 0, & \text{for } z_{itl} = 0 \end{cases}, \tag{C.11}$$

$$\text{logit}(\boldsymbol{\zeta}) = \left(\boldsymbol{X}_{\zeta}, \boldsymbol{N}^{A}, \boldsymbol{d}\right) \boldsymbol{\beta}_{\zeta},\ \boldsymbol{\beta}_{\zeta} \sim \mathcal{N}(\mathbf{0}, 2.25\boldsymbol{I}), \tag{C.12}$$

$$N_{itl}^{A} \sim \begin{cases} \text{ZTP}(\lambda_{it}), & \text{for } \omega_{itl} = 1 \\ \text{ZTP}(\lambda_{0}), & \text{for } \omega_{itl} = 0 \end{cases}, \tag{C.13}$$

$$\omega_{itl} \sim \text{Bernoulli}(p_{\omega}), \tag{C.14}$$

$$d_{itl} \sim \text{Unif}(0, \nu_{d}), \tag{C.15}$$

$$z_{itl} \sim \text{Bernoulli}(\psi_{it}), \tag{C.16}$$

$$\epsilon_{itl} \sim \text{Bernoulli}(0.5), \tag{C.17}$$

$$\text{logit}(\boldsymbol{\psi}) = \boldsymbol{X}_{\psi}\boldsymbol{\beta}_{\psi}, \boldsymbol{\beta}_{\psi} \sim \mathcal{N}(\mathbf{0}, 2.25\boldsymbol{I}), \tag{C.18}$$

$$\log(\boldsymbol{\lambda}) = \boldsymbol{X}_{\lambda}\boldsymbol{\beta}_{\lambda}, \boldsymbol{\beta}_{\lambda} \sim \mathcal{N}(\mathbf{0}, 10\boldsymbol{I}), \tag{C.19}$$

$$\lambda_{0} \sim \text{Gamma}(1.78, 0.675), \tag{C.20}$$

$$p_{\omega} \sim \text{Uniform}(0, 1). \tag{C.21}$$

We set the informative prior for λ_0 so that the mean size of a non-lek group observations was 1.2 and resulted in a prior probability of approximately 0.95 that a non-lek observation contained

fewer than 4 individuals. The variance of λ_0 implied the prior probability of a non-lek observation having less than 10 individuals was nearly 1.

C.2.2 N-mixture Submodel

$$G_{i'tlj} \sim \text{Binomial}(N^G_{i'tl}, p_e) \text{ for } j = 1, \ldots, J_{i'tl}, \tag{C.22}$$

$$N^G_{i'tl} \sim \text{Poisson}(\exp(\boldsymbol{w}'_{i't}\boldsymbol{\eta})) \text{ for } l = 1, \ldots, L^G_{i't}, \tag{C.23}$$

$$\boldsymbol{\eta} \sim \mathcal{N}(\mathbf{0}, 10\boldsymbol{I}), \tag{C.24}$$

$$p_e \sim \text{Uniform}(0, 1). \tag{C.25}$$

C.2.3 Survival Submodel

$$s_{letm} \sim \text{Bernoulli}(\phi^A_{letm}), \tag{C.26}$$

$$\text{logit}(\phi^A_{letm}) = \mu^{\phi^A}_{el} + \beta^{\phi^A}_1 \text{SEX}_l + \beta^{\phi^A}_2 \text{BREED}_m + \beta^{\phi^A}_3 (\text{SEX}_l \times \text{BREED}_m) + \beta^{\phi^A}_4 \text{PDSI}_{etm}, \tag{C.27}$$

$$\mu^{\phi^A}_{el} \sim \mathcal{N}(\mu_e, \sigma^2_{\phi^A}), \tag{C.28}$$

$$\mu^{\phi^A}_{SOPR} \sim \mathcal{N}(2.27, 2 \times 0.48^2), \tag{C.29}$$

$$\mu^{\phi^A}_{SSPR} \sim \mathcal{N}(2.70, 2 \times 0.33^2), \tag{C.30}$$

$$\mu^{\phi^A}_{MGPR} \sim \mathcal{N}(2.90, 2 \times 0.45^2), \tag{C.31}$$

$$\mu^{\phi^A}_{SGPR} \sim \mathcal{N}(3.80, 2 \times 0.86^2), \tag{C.32}$$

$$\boldsymbol{\beta}^{\phi^A} \sim \mathcal{N}(\mathbf{0}, 100^2\boldsymbol{I}), \tag{C.33}$$

$$\sigma^2_{\phi^A} \sim \mathcal{IG}(0.001, 1000). \tag{C.34}$$

C.2.4 Nesting Survival Submodel

$$F_{letd} \sim \begin{cases} \text{Bernoulli}(\phi^N_{letm}) & , F_{let,d-1} = 1 \\ 0 & , F_{let,d-1} = 0 \end{cases}, \tag{C.35}$$

$$\text{logit}(\phi^N_{letm}) = \mu^{\phi^N}_{el} + \beta^{\phi^N}_1 \text{AGE}_l + \beta^{\phi^N}_2 \text{PDSI}_{etm}, \tag{C.36}$$

$$\mu^{\phi^N}_{el} \sim \mathcal{N}(\mu_e, \sigma^2_{\phi^N}), \tag{C.37}$$

$$\mu^{\phi^N}_{SOPR} \sim \mathcal{N}(4.29, 2 \times 0.61^2), \tag{C.38}$$

$$\mu^{\phi^N}_{SSPR} \sim \mathcal{N}(3.81, 2 \times 0.61^2), \tag{C.39}$$

$$\mu^{\phi^N}_{MGPR} \sim \mathcal{N}(4.13, 2 \times 0.61^2), \tag{C.40}$$

$$\mu^{\phi^N}_{SGPR} \sim \mathcal{N}(4.08, 2 \times 0.75^2), \tag{C.41}$$

$$\boldsymbol{\beta}^{\phi^N} \sim \mathcal{N}(\mathbf{0}, 100^2 \boldsymbol{I}), \tag{C.42}$$

$$\sigma^2_{\phi^N} \sim \mathcal{IG}(0.001, 1000). \tag{C.43}$$

C.2.5 Brood Survival Submodel

$$y_{ld} \sim \text{Binomial}(B_{ld}, q), \tag{C.44}$$

$$B_{l,d+1} \sim \text{Binomial}(B_{ld}, \phi^B_d), \tag{C.45}$$

$$\phi^B_d = \phi^B_1 \sim \text{Beta}(290.40, 15.28), \text{ for } d \leq 14, \tag{C.46}$$

$$\phi^B_d = \phi^B_2 \sim \text{Beta}(437.23, 9.84), \text{ for } d > 14. \tag{C.47}$$

C.2.6 Clutch Submodel

$$C_{letm} \sim \text{Poisson}(\delta_{letm}), \tag{C.48}$$

$$\log(\delta_{letm}) = \mu_e^{\delta} + \beta_1^{\delta}\text{AGE}_l + \beta_2^{\delta}\text{PDSI}_{etm}, \tag{C.49}$$

$$\boldsymbol{\beta}^{\delta} \sim \mathcal{N}(\mathbf{0}, 100^2\boldsymbol{I}), \tag{C.50}$$

$$\mu_e^{\delta} \sim \mathcal{N}(\mu^{\delta}, \sigma_{\delta}^2), \tag{C.51}$$

$$\mu^{\delta} \sim \mathcal{N}(0, 100^2), \tag{C.52}$$

$$\sigma_{\delta}^2 \sim \mathcal{IG}(0.001, 1000). \tag{C.53}$$

C.2.7 Hatch Submodel

$$H_{letm} \sim \text{Binomial}(C_{letm}, \pi_{letm}), \tag{C.54}$$

$$\text{logit}(\pi_{letm}) = \mu_e^{\pi} + \beta_1^{\pi}\text{AGE}_l + \beta_2^{\pi}\text{PDSI}_{etm}, \tag{C.55}$$

$$\boldsymbol{\beta}^{\pi} \sim \mathcal{N}(\mathbf{0}, 100^2\boldsymbol{I}), \tag{C.56}$$

$$\mu_e^{\pi} \sim \mathcal{N}(\mu^{\pi}, \sigma_{\pi}^2), \tag{C.57}$$

$$\mu^{\pi} \sim \mathcal{N}(0, 100^2), \tag{C.58}$$

$$\sigma_{\pi}^2 \sim \mathcal{IG}(0.001, 1000). \tag{C.59}$$

C.2.8 Juvenile Survival Priors

$$\phi^J_{SOPR} \sim \text{Beta}(10.35, 1.15), \tag{C.60}$$

$$\phi^J_{SSPR} \sim \text{Beta}(8.22, 5.71), \tag{C.61}$$

$$\phi^J_{MGPR} \sim \text{Beta}(19.44, 7.56), \tag{C.62}$$

$$\phi^J_{SGPR} \sim \text{Beta}(10.22, 8.03). \tag{C.63}$$

C.2.9 Nesting and Re-nesting Propensity Priors

$$\xi^1_{SOPR} \sim \text{Beta}(19.59, 8.00), \qquad \xi^2_{SOPR} \sim \text{Beta}(1.35, 17.99), \tag{C.64}$$

$$\xi^1_{SSPR} \sim \text{Beta}(83.72, 7.28), \qquad \xi^2_{SSPR} \sim \text{Beta}(20.41, 45.43), \tag{C.65}$$

$$\xi^1_{MGPR} \sim \text{Beta}(8.44, 4.95), \qquad \xi^2_{MGPR} \sim \text{Beta}(0.36, 2.20), \tag{C.66}$$

$$\xi^1_{SGPR} \sim \text{Beta}(2.95, 0.09), \qquad \xi^2_{SGPR} \sim \text{Beta}(1.39, 13.36). \tag{C.67}$$

C.2.10 Population Model

$$N_{et} = N_{♀et,ASY} + N_{♂et,ASY} + N_{♀et,SY} + N_{♂et,SY}, \tag{C.68}$$

$$N_{♂e,t+1,ASY} \sim \text{Binomial}\left(N_{♂et,ASY} + N_{♂et,SY}, \phi^A_{♂et}\right), \tag{C.69}$$

$$N_{♀e,t+1,ASY} \sim \text{Binomial}\left(N_{♀et,ASY} + N_{♀et,SY}, \phi^A_{♀et}\right), \tag{C.70}$$

$$N_{e,t+1,SY} \sim \text{Poisson}\left(N_{♀et,SY}\rho_{et,SY} + N_{♀et,ASY}\rho_{et,ASY}\right), \tag{C.71}$$

$$N_{♂e,t+1,SY} = N_{♀e,t+1,SY} = N_{e,t+1,SY}/2. \tag{C.72}$$

C.3 Varying Survey Effort on Posterior Inference for Vital Rates

The conditional expectation of survival is unaffected by the area surveyed, but the conditional variance is proportional to the area surveyed. We show the derivation for male survivorship noting the derivation for female survivorship is analogous. As in Section C.1, we let $Y_{♂\,et,ASY}$ and $Y_{♂\,et,SY}$ be the densities of after-second-year (ASY) and second-year (SY) males in ecoregion e during year t and S_{et} denote the area surveyed. We estimate the approximate number of ASY and SY males encountered as $N_{♂\,et,ASY} = Y_{♂\,et,ASY}S_{et}$ and $N_{♂\,et,SY} = Y_{♂\,et,SY}S_{et}$. Assuming a flat improper prior for male adult survival, $[\phi^A_{♂\,et}] \propto 1$, the conditional expectation for $\phi^A_{♂\,et}$ from equation (C.69) is

$$\mathbb{E}[\phi^A_{♂\,et}|Y_{♂\,et,ASY}, Y_{♂\,et,SY}, S_{et}] \tag{C.73}$$

$$= \frac{N_{♂\,e,t+1,ASY}(S_{et})}{N_{♂\,et,ASY}(S_{et}) + N_{♂\,et,SY}(S_{et})} = \frac{Y_{♂\,e,t+1,ASY}}{Y_{♂\,et,ASY} + Y_{♂\,et,SY}} = \tilde{\phi^A}_{♂\,et}, \tag{C.74}$$

which is independent of S_{et}. The conditional variance, however, is

$$\text{Var}[\phi^A_{♂\,et}|Y_{♂\,et,ASY}, Y_{♂\,et,SY}, S_{et}] \tag{C.75}$$

$$= \frac{\tilde{\phi^A}_{♂\,et}\left(1 - \tilde{\phi^A}_{♂\,et}\right)}{N_{♂\,et,ASY}(S_{et}) + N_{♂\,et,SY}(S_{et})} = \frac{\tilde{\phi^A}_{♂\,et}\left(1 - \tilde{\phi^A}_{♂\,et}\right)}{S_{et}(Y_{♂\,et,ASY} + Y_{♂\,et,SY})}. \tag{C.76}$$

The same is true for $\rho_{et,SY}$ and $\rho_{et,ASY}$ in equation (C.71). Without loss of generality, we derive the conditional expectation and variance for $\rho_{et,SY}$ assuming an improper flat prior and $\rho_{et,ASY}$ known. The conditional expectation of $\rho_{et,SY}$ from equation (C.71) is

$$\mathbb{E}[\rho_{et,SY}|Y_{♀et,ASY}, Y_{♀et,SY}, \rho_{et,ASY}, S_{et}] = \tag{C.77}$$

$$\frac{N_{e,t+1,SY}(S_{et}) - N_{♀et,ASY}(S_{et})\rho_{et,ASY}}{N_{♀et,SY}(S_{et})} = \frac{Y_{e,t+1,SY} - Y_{♀et,ASY}\rho_{et,ASY}}{Y_{♀et,SY}} = \tilde{\rho}_{et,SY}. \tag{C.78}$$

The conditional variance is

$$\text{Var}[\rho_{et,SY}|Y_{♀et,ASY}, Y_{♀et,SY}, \rho_{et,ASY}, S_{et}] = \tag{C.79}$$

$$\frac{N_{♀et,SY}(S_{et})\tilde{\rho}_{et,SY} + N_{♀et,ASY}(S_{et})\rho_{et,ASY}}{\left(N_{♀et,SY}(S_{et})\right)^2} = \frac{Y_{♀et,SY}\tilde{\rho}_{et,SY} + Y_{♀et,ASY}\rho_{et,ASY}}{S_{et}\left(Y_{♀et,SY}\right)^2}. \tag{C.80}$$

It follows that posterior inference for vital rates both depends on the trend in annual density, $Y_{e,t+1}/Y_{et}$, as well as the number of individuals used to estimate that trend, $N_{et}(S_{et})$.

C.4 Comparison of Integrated Population Model Posterior Inference with WEST Aerial Survey Annual Reports

Western EcoSystems Technology, Inc. (WEST) uses the aerial surveys to infer annual fluctuations in ecoregion wide lesser prairie-chicken abundance. We compared abundance estimates from our integrated population model with those reported by [5]. Figure C.1 shows the ecoregion annual abundance estimates along with their associated uncertainties. In general, mean annual abundance estimates were similar across the two models, but the integrated population model had less uncertainty and provided inference for range-wide abundance in years during which no aerial surveys were conducted (2005-2011 and 2019).

The reduced uncertainty of the integrated population model abundance estimates highlights lesser prairie-chicken booms and busts. For example, from 2015-2016, the MGPR experienced a boom where the population grew by $> 30\%$ according to the points estimates from both models. The confidence intervals for annual abundance estimated by [5] largely overlap, but in the integrated population model, the credible intervals are separated and the boom is identified. Likewise, in 2013, the SGPR experienced a bust that reduced the population by more than 20%. In the model of [5], the magnitude of the bust is qualified by large uncertainty in annual abundance estimates, but the integrated population model provides more certainty that a large decline occurred.

We observed the largest discrepancies in abundance estimates between the models in the SOPR. The two starkest differences were in 2015 and 2022, which were the years estimated to have the

lowest abundance according to the model of [5]. Aerial detections for these years were low with a total of 10 birds detected across 7 groups in 2015 and 9 birds across 7 groups in 2022. The lower bounds of the WEST estimates in these years are below the number of birds counted by the ground surveys in the SOPR, which only surveyed 1% of the ecoregion.

Limited aerial detections also made abundance estimation in the SSPR difficult. Only three birds were detected in the SSPR in 2020, and the low sample size prevented [5] from calculating the uncertainty of the point estimate. The integrated population model leverages the demographic and ground surveys to infer a probable range-wide abundance when aerial detections were limited.

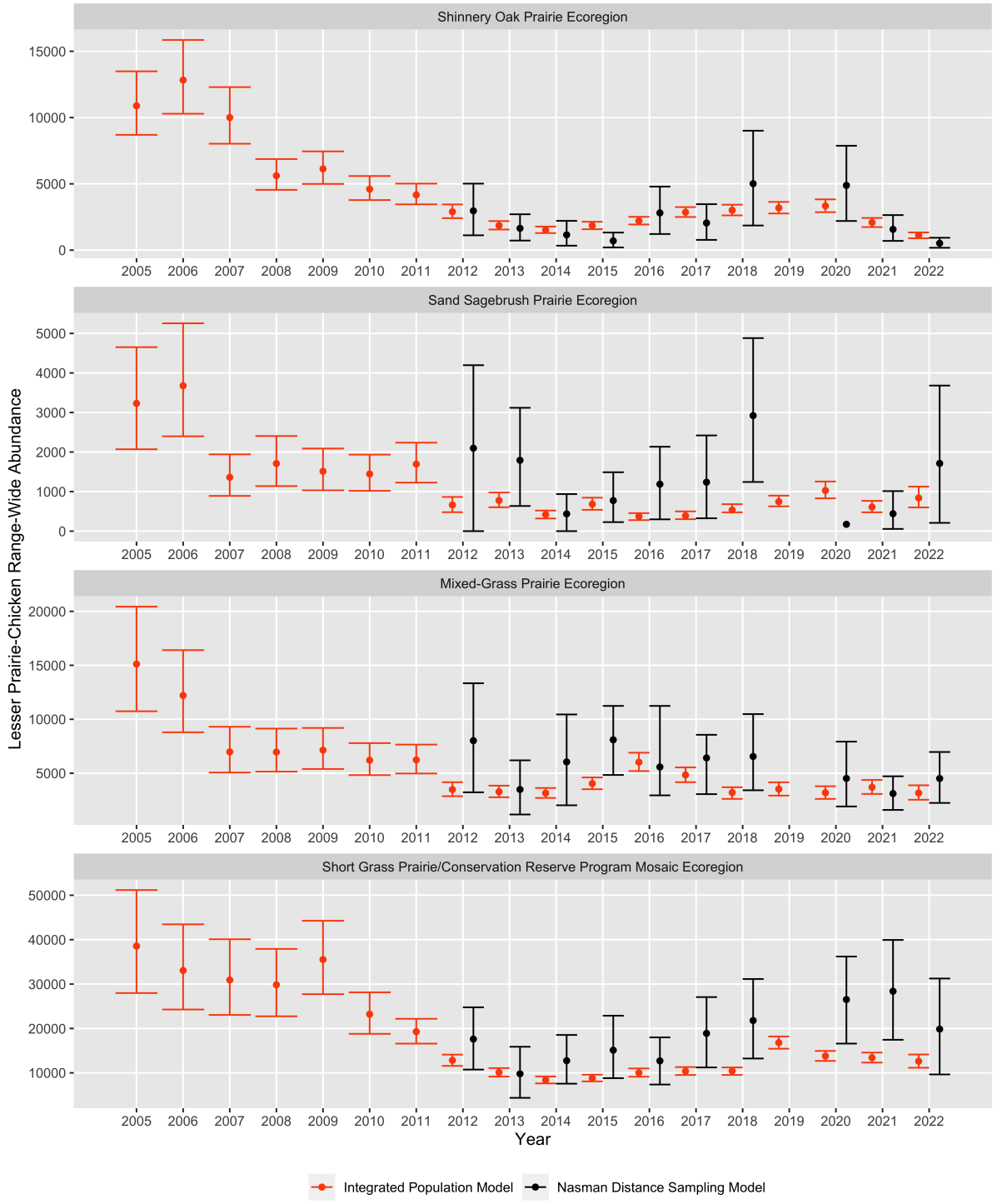

Figure C.1: Lesser prairie-chicken ecoregion annual abundance estimates from 2005-2022. Posterior means and 90% credible intervals from integrated population model fit to the ground, aerial, and demography data in red. Mean estimates and 90% confidence intervals from [5] are in black.

C.5 Annual Abundance and Vital Rates

Table C.1: Posterior means (95% credible intervals) for lesser prairie-chicken range-wide abundance split by ecoregion and year. Posterior means derived from integrated population model fit to aerial, ground and demographic surveys. SOPR = Shinnery Oak prairie Ecoregion, SSPR = Sand sagebrush Prairie Ecoregion, MGPR = Mixed-Grass Prairie Ecoregion, and SGPR = Short Grass Prairie/Conservation Reserve Program Mosaic Ecoregion.

Year	SOPR	SSPR	MGPR	SGPR	Total
2005	10888 (8696, 13486)	3230 (2070, 4652)	15114 (10744, 20434)	38551 (27973, 51170)	67783 (55734, 81404)
2006	12827 (10287, 15852)	3677 (2398, 5255)	12207 (8795, 16408)	33057 (24269, 43451)	61768 (51670, 73069)
2007	10004 (8026, 12295)	1360 (891, 1941)	6978 (5064, 9304)	30914 (23046, 40085)	49256 (40724, 58960)
2008	5615 (4549, 6869)	1710 (1139, 2405)	6963 (5147, 9135)	29825 (22744, 37912)	44113 (36545, 52446)
2009	6131 (4994, 7449)	1513 (1032, 2089)	7141 (5392, 9197)	35513 (27723, 44252)	50298 (42118, 59363)
2010	4601 (3778, 5590)	1445 (1019, 1934)	6204 (4825, 7791)	23204 (18790, 28137)	35454 (30659, 40661)
2011	4168 (3454, 5016)	1694 (1227, 2237)	6234 (4975, 7655)	19284 (16592, 22172)	31381 (28228, 34733)
2012	2893 (2412, 3446)	663 (479, 864)	3490 (2872, 4168)	12823 (11578, 14113)	19868 (18389, 21434)
2013	1857 (1555, 2194)	776 (604, 976)	3283 (2772, 3850)	10093 (9168, 11074)	16008 (14882, 17179)
2014	1516 (1287, 1779)	419 (320, 521)	3159 (2711, 3633)	8377 (7626, 9191)	13471 (12550, 14431)
2015	1852 (1581, 2142)	682 (538, 846)	4044 (3518, 4607)	8796 (8085, 9591)	15373 (14404, 16397)
2016	2210 (1935, 2514)	369 (278, 456)	6024 (5200, 6900)	10018 (9132, 11004)	18622 (17357, 19962)
2017	2859 (2500, 3247)	389 (302, 499)	4843 (4168, 5540)	10387 (9525, 11307)	18477 (17290, 19704)
2018	3009 (2622, 3427)	533 (475, 681)	3208 (2624, 3702)	10443 (9530, 11224)	17193 (16120, 18213)
2019	3187 (2766, 3640)	745 (627, 898)	3533 (2927, 4159)	16813 (15436, 18191)	24278 (22690, 25860)
2020	3335 (2861, 3830)	1026 (830, 1254)	3194 (2621, 3795)	13796 (12694, 14940)	21352 (20004, 22740)
2021	2081 (1739, 2428)	608 (476, 765)	3704 (3081, 4380)	13422 (12317, 14575)	19816 (18484, 21183)
2022	1119 (896, 1337)	838 (600, 1125)	3165 (2543, 3882)	12611 (11153, 14141)	17733 (16096, 19443)

Table C.2: Posterior means (95% credible intervals) for female lesser prairie-chicken annual survival split by ecoregion and year. Posterior means derived from integrated population model fit to aerial, ground and demographic surveys. SOPR = Shinnery Oak Prairie Ecoregion, SSPR = Sand Sagebrush Prairie Ecoregion, MGPR = Mixed-Grass Prairie Ecoregion, and SGPR = Short Grass Prairie/Conservation Reserve Program Mosaic Ecoregion.

Year	SOPR	SSPR	MGPR	SGPR	Mean
2005	0.49 (0.40, 0.58)	0.39 (0.27, 0.51)	0.38 (0.31, 0.45)	0.39 (0.32, 0.45)	0.41 (0.37, 0.45)
2006	0.50 (0.44, 0.54)	0.40 (0.28, 0.52)	0.40 (0.34, 0.45)	0.39 (0.32, 0.45)	0.42 (0.38, 0.46)
2007	0.42 (0.36, 0.49)	0.31 (0.23, 0.41)	0.40 (0.34, 0.46)	0.39 (0.32, 0.45)	0.38 (0.35, 0.42)
2008	0.43 (0.36, 0.50)	0.40 (0.29, 0.52)	0.38 (0.31, 0.46)	0.38 (0.31, 0.44)	0.40 (0.36, 0.44)
2009	0.48 (0.41, 0.55)	0.41 (0.30, 0.52)	0.39 (0.33, 0.45)	0.36 (0.29, 0.43)	0.41 (0.37, 0.45)
2010	0.44 (0.37, 0.51)	0.41 (0.29, 0.52)	0.39 (0.33, 0.45)	0.32 (0.23, 0.41)	0.39 (0.35, 0.43)
2011	0.44 (0.37, 0.51)	0.41 (0.30, 0.53)	0.40 (0.34, 0.46)	0.36 (0.28, 0.43)	0.40 (0.36, 0.44)
2012	0.47 (0.37, 0.56)	0.34 (0.24, 0.44)	0.41 (0.34, 0.49)	0.38 (0.32, 0.44)	0.40 (0.36, 0.44)
2013	0.46 (0.37, 0.55)	0.47 (0.34, 0.60)	0.44 (0.37, 0.51)	0.43 (0.35, 0.50)	0.45 (0.40, 0.50)
2014	0.49 (0.41, 0.58)	0.40 (0.29, 0.51)	0.42 (0.37, 0.49)	0.42 (0.35, 0.49)	0.44 (0.40, 0.48)
2015	0.46 (0.39, 0.53)	0.42 (0.30, 0.53)	0.42 (0.36, 0.48)	0.41 (0.34, 0.47)	0.43 (0.39, 0.47)
2016	0.50 (0.41, 0.59)	0.45 (0.34, 0.55)	0.37 (0.29, 0.45)	0.40 (0.33, 0.46)	0.43 (0.38, 0.47)
2017	0.49 (0.42, 0.54)	0.35 (0.22, 0.47)	0.37 (0.29, 0.44)	0.39 (0.32, 0.45)	0.40 (0.35, 0.44)
2018	0.48 (0.41, 0.53)	0.34 (0.22, 0.46)	0.40 (0.35, 0.46)	0.39 (0.32, 0.45)	0.40 (0.36, 0.44)
2019	0.45 (0.39, 0.52)	0.46 (0.35, 0.57)	0.40 (0.34, 0.46)	0.41 (0.35, 0.49)	0.43 (0.39, 0.47)
2020	0.43 (0.35, 0.50)	0.49 (0.37, 0.64)	0.41 (0.33, 0.50)	0.44 (0.36, 0.53)	0.44 (0.40, 0.49)
2021	0.40 (0.34, 0.48)	0.58 (0.48, 0.64)	0.43 (0.37, 0.49)	0.51 (0.45, 0.53)	0.48 (0.45, 0.51)
2022	0.41 (0.34, 0.48)	0.41 (0.30, 0.52)	0.41 (0.36, 0.47)	0.39 (0.33, 0.45)	0.41 (0.37, 0.45)
Mean	0.46 (0.44, 0.47)	0.41 (0.39, 0.44)	0.40 (0.39, 0.42)	0.40 (0.38, 0.41)	0.42 (0.41, 0.43)

Table C.3: Posterior means (95% credible intervals) for male lesser prairie-chicken annual survival split by ecoregion and year. Posterior means derived from integrated population model fit to aerial, ground and demographic surveys. SOPR = Shinnery Oak Prairie Ecoregion, SSPR = Sand Sagebrush Prairie Ecoregion, MGPR = Mixed-Grass Prairie Ecoregion, and SGPR = Short Grass Prairie/Conservation Reserve Program Mosaic Ecoregion.

Year	SOPR	SSPR	MGPR	SGPR	Mean
2005	0.38 (0.30, 0.49)	0.48 (0.34, 0.61)	0.49 (0.39, 0.59)	0.50 (0.40, 0.59)	0.46 (0.41, 0.52)
2006	0.61 (0.54, 0.68)	0.54 (0.42, 0.65)	0.53 (0.44, 0.61)	0.51 (0.41, 0.60)	0.55 (0.50, 0.59)
2007	0.51 (0.43, 0.58)	0.28 (0.24, 0.36)	0.45 (0.36, 0.54)	0.49 (0.39, 0.58)	0.43 (0.39, 0.47)
2008	0.44 (0.38, 0.51)	0.52 (0.39, 0.64)	0.50 (0.40, 0.60)	0.49 (0.39, 0.58)	0.49 (0.44, 0.54)
2009	0.59 (0.52, 0.67)	0.51 (0.38, 0.63)	0.51 (0.42, 0.60)	0.51 (0.40, 0.60)	0.53 (0.48, 0.58)
2010	0.52 (0.45, 0.59)	0.49 (0.36, 0.62)	0.50 (0.40, 0.59)	0.43 (0.31, 0.54)	0.49 (0.43, 0.54)
2011	0.58 (0.51, 0.65)	0.55 (0.43, 0.66)	0.54 (0.45, 0.62)	0.50 (0.40, 0.60)	0.54 (0.49, 0.59)
2012	0.56 (0.46, 0.65)	0.32 (0.28, 0.42)	0.44 (0.36, 0.54)	0.47 (0.37, 0.56)	0.45 (0.40, 0.49)
2013	0.50 (0.42, 0.58)	0.57 (0.43, 0.70)	0.55 (0.44, 0.64)	0.52 (0.42, 0.62)	0.53 (0.48, 0.59)
2014	0.54 (0.46, 0.63)	0.40 (0.28, 0.52)	0.53 (0.44, 0.62)	0.50 (0.40, 0.59)	0.49 (0.45, 0.54)
2015	0.53 (0.46, 0.60)	0.54 (0.42, 0.65)	0.54 (0.44, 0.62)	0.50 (0.40, 0.59)	0.53 (0.48, 0.57)
2016	0.46 (0.36, 0.57)	0.48 (0.38, 0.58)	0.51 (0.40, 0.62)	0.41 (0.33, 0.48)	0.47 (0.42, 0.51)
2017	0.57 (0.50, 0.66)	0.49 (0.38, 0.61)	0.47 (0.37, 0.57)	0.39 (0.31, 0.47)	0.48 (0.43, 0.53)
2018	0.58 (0.51, 0.65)	0.48 (0.37, 0.59)	0.48 (0.37, 0.58)	0.38 (0.30, 0.46)	0.48 (0.43, 0.52)
2019	0.56 (0.49, 0.63)	0.43 (0.31, 0.54)	0.49 (0.39, 0.58)	0.34 (0.25, 0.43)	0.45 (0.41, 0.50)
2020	0.57 (0.50, 0.64)	0.44 (0.30, 0.57)	0.38 (0.27, 0.50)	0.30 (0.23, 0.41)	0.42 (0.37, 0.48)
2021	0.52 (0.44, 0.60)	0.27 (0.27, 0.28)	0.37 (0.33, 0.46)	0.27 (0.27, 0.27)	0.36 (0.33, 0.39)
2022	0.49 (0.43, 0.57)	0.53 (0.41, 0.65)	0.54 (0.45, 0.63)	0.52 (0.42, 0.60)	0.52 (0.47, 0.57)
Mean	0.53 (0.51, 0.55)	0.46 (0.43, 0.49)	0.49 (0.47, 0.51)	0.45 (0.42, 0.47)	0.48 (0.47, 0.49)

Table C.4: Posterior means (95% credible intervals) for second-year lesser prairie-chicken productivity split by ecoregion and year. Productivity is the expected number of individuals produced per female that survive to sexual maturity. Posterior means derived from integrated population model fit to aerial, ground and demographic surveys. SOPR = Shinnery Oak Prairie Ecoregion, SSPR = Sand Sagebrush Prairie Ecoregion, MGPR = Mixed-Grass Prairie Ecoregion, and SGPR = Short Grass Prairie/Conservation Reserve Program Mosaic Ecoregion.

Year	SOPR	SSPR	MGPR	SGPR	Mean
2005	1.30 (0.65, 2.00)	1.10 (0.35, 2.10)	1.10 (0.46, 1.90)	0.92 (0.40, 1.50)	1.10 (0.78, 1.50)
2006	1.10 (1.10, 1.10)	1.40 (0.63, 2.20)	0.68 (0.32, 1.10)	0.78 (0.39, 1.20)	1.00 (0.77, 1.20)
2007	0.57 (0.26, 0.92)	0.14 (0.06, 0.30)	0.33 (0.11, 0.64)	1.00 (0.45, 1.60)	0.52 (0.34, 0.71)
2008	0.30 (0.12, 0.52)	0.93 (0.21, 1.90)	0.98 (0.37, 1.80)	1.10 (0.60, 1.60)	0.83 (0.54, 1.20)
2009	0.68 (0.37, 1.10)	0.88 (0.32, 1.50)	1.30 (0.71, 1.90)	1.60 (1.00, 2.20)	1.10 (0.85, 1.40)
2010	0.53 (0.22, 0.86)	1.10 (0.34, 1.90)	0.89 (0.44, 1.40)	0.46 (0.05, 0.89)	0.74 (0.48, 1.00)
2011	0.62 (0.34, 0.98)	1.50 (0.63, 2.40)	1.10 (0.45, 1.80)	0.80 (0.35, 1.30)	1.00 (0.70, 1.30)
2012	0.34 (0.16, 0.57)	0.11 (0.01, 0.27)	0.26 (0.09, 0.50)	0.50 (0.18, 0.87)	0.30 (0.19, 0.43)
2013	0.33 (0.15, 0.56)	0.61 (0.09, 1.50)	0.74 (0.26, 1.40)	0.58 (0.23, 1.00)	0.57 (0.34, 0.85)
2014	0.48 (0.24, 0.76)	0.17 (0.03, 0.44)	0.93 (0.39, 1.60)	0.71 (0.30, 1.10)	0.57 (0.38, 0.79)
2015	1.30 (0.72, 1.80)	1.30 (0.36, 2.40)	1.70 (0.82, 2.60)	1.20 (0.62, 1.80)	1.30 (0.97, 1.80)
2016	1.40 (1.00, 1.80)	0.06 (0.05, 0.07)	2.40 (1.60, 3.10)	1.70 (1.10, 2.20)	1.40 (1.10, 1.60)
2017	1.50 (1.40, 1.50)	1.10 (0.30, 2.20)	0.62 (0.29, 0.97)	1.40 (0.89, 1.80)	1.20 (0.89, 1.50)
2018	1.10 (0.88, 1.20)	1.70 (0.92, 2.40)	0.54 (0.21, 0.98)	1.30 (0.79, 1.70)	1.20 (0.92, 1.40)
2019	1.00 (0.69, 1.40)	1.20 (0.55, 1.90)	1.20 (0.47, 2.10)	3.00 (2.00, 3.70)	1.60 (1.20, 2.00)
2020	1.10 (0.74, 1.50)	2.10 (1.20, 2.60)	1.00 (0.50, 1.60)	0.88 (0.58, 1.20)	1.30 (0.98, 1.50)
2021	0.27 (0.10, 0.46)	0.29 (0.08, 0.57)	1.40 (0.62, 2.30)	0.96 (0.44, 1.50)	0.74 (0.48, 1.00)
2022	0.29 (0.12, 0.51)	0.71 (0.13, 1.50)	0.69 (0.27, 1.30)	0.60 (0.25, 1.00)	0.57 (0.35, 0.84)
Mean	0.79 (0.71, 0.87)	0.92 (0.75, 1.10)	1.00 (0.86, 1.10)	1.10 (0.96, 1.20)	0.95 (0.88, 1.00)

Table C.5: Posterior means (95% credible intervals) for after-second-year lesser prairie-chicken productivity split by ecoregion and year. Productivity is the expected number of individuals produced per female that survive to sexual maturity. Posterior means derived from integrated population model fit to aerial, ground and demographic surveys. SOPR = Shinnery Oak Prairie Ecoregion, SSPR = Sand Sagebrush Prairie Ecoregion, MGPR = Mixed-Grass Prairie Ecoregion, and SGPR = Short Grass Prairie/Conservation Reserve Program Mosaic Ecoregion.

Year	SOPR	SSPR	MGPR	SGPR	Mean
2005	1.50 (0.73, 2.20)	1.30 (0.45, 2.40)	1.30 (0.56, 2.20)	1.10 (0.51, 1.70)	1.30 (0.92, 1.70)
2006	1.30 (1.10, 1.30)	1.40 (0.43, 2.40)	0.82 (0.34, 1.40)	0.98 (0.49, 1.50)	1.10 (0.81, 1.40)
2007	0.74 (0.32, 1.20)	0.26 (0.05, 0.61)	0.33 (0.10, 0.62)	1.20 (0.53, 1.90)	0.63 (0.41, 0.86)
2008	0.26 (0.11, 0.46)	1.90 (1.30, 2.60)	1.40 (0.96, 1.90)	1.30 (0.65, 1.90)	1.20 (0.95, 1.50)
2009	1.30 (1.20, 1.40)	1.10 (0.30, 2.00)	1.40 (0.60, 2.30)	1.80 (0.96, 2.60)	1.40 (1.00, 1.80)
2010	0.68 (0.29, 1.10)	1.30 (0.44, 2.10)	1.10 (0.45, 1.80)	0.99 (0.14, 1.90)	1.00 (0.66, 1.40)
2011	1.00 (0.76, 1.20)	1.50 (0.53, 2.50)	1.30 (0.59, 2.10)	1.00 (0.53, 1.50)	1.20 (0.88, 1.60)
2012	0.46 (0.22, 0.73)	0.23 (0.03, 0.60)	0.38 (0.12, 0.73)	0.63 (0.21, 1.10)	0.42 (0.27, 0.60)
2013	0.34 (0.16, 0.57)	1.50 (0.89, 2.20)	1.10 (0.68, 1.60)	0.79 (0.41, 1.20)	0.93 (0.71, 1.20)
2014	0.64 (0.36, 0.94)	0.31 (0.05, 0.78)	1.20 (0.53, 1.90)	0.95 (0.51, 1.40)	0.77 (0.54, 1.00)
2015	1.70 (1.20, 2.20)	2.40 (1.70, 3.20)	1.80 (0.88, 2.90)	1.60 (0.96, 2.20)	1.90 (1.50, 2.30)
2016	1.50 (1.00, 2.00)	0.06 (0.05, 0.15)	1.80 (0.80, 3.10)	1.70 (0.97, 2.60)	1.30 (0.93, 1.70)
2017	1.70 (1.40, 1.80)	1.40 (0.74, 2.20)	1.10 (0.39, 2.00)	1.40 (0.65, 2.20)	1.40 (1.10, 1.80)
2018	1.00 (0.72, 1.30)	1.30 (0.37, 2.50)	0.65 (0.25, 1.10)	1.40 (0.74, 2.30)	1.10 (0.78, 1.50)
2019	1.30 (0.85, 1.70)	1.40 (0.45, 2.60)	1.40 (0.68, 2.10)	2.20 (0.93, 3.70)	1.60 (1.10, 2.10)
2020	1.30 (0.88, 1.70)	2.20 (1.00, 2.90)	1.20 (0.48, 2.00)	1.00 (0.40, 1.80)	1.40 (1.00, 1.80)
2021	0.38 (0.16, 0.65)	0.57 (0.14, 1.20)	1.70 (0.86, 2.70)	1.20 (0.66, 1.80)	0.97 (0.68, 1.30)
2022	0.24 (0.10, 0.42)	1.00 (0.36, 1.90)	0.81 (0.31, 1.50)	0.80 (0.37, 1.30)	0.72 (0.47, 1.00)
Mean	0.96 (0.88, 1.00)	1.20 (1.00, 1.30)	1.20 (0.99, 1.30)	1.20 (1.1, 1.4)	1.10 (1.10, 1.20)

C.6 Submodel Posterior Inference

Mean monthly survival rates for females in the non-breeding season were 0.946, 0.942, 0.943, and 0.939 in the SOPR, SSPR, MGPR, and SGPR, respectively. On average, females had 5% lower monthly survival during the breeding season. Male survival did not decrease during the breeding season.

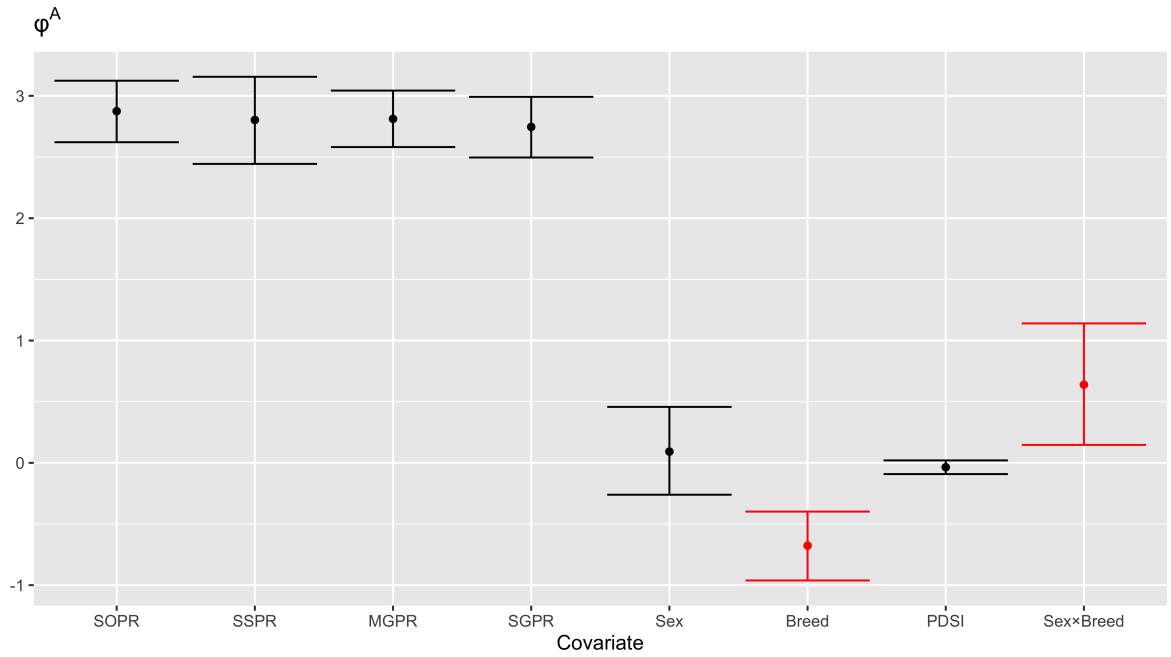

Figure C.2: Posterior means and 95% credible intervals for ecoregion intercepts and covariate associations in lesser prairie-chicken survival submodel. Red indicates the credible interval for the covariate association excluded 0. The parameter describing heterogeneity in monthly adult survival is ϕ^A. Sex$\in \{0, 1\}$ indicates if the individual is male. Breed$\in \{0, 1\}$ indicates if the month is in the breeding season defined as March-June [6].

The density of lesser prairie-chicken groups was highest in the Short-Grass Prairie/Conservation Reserve Program Mosaic Ecoregion (SGPR) and lowest in the Sand Sagebrush Prairie Ecoregion (SSPR) (Figure C.3, top). Fewer lesser prairie-chicken groups were observed in blocks with a higher percentage of anthropogenic development and woodlands and lower percentage of CRP enrollment and shrublands. The density of lesser prairie-chicken groups was also positively associated with larger grassland patches and breeding seasons in the previous year with greater PDSI.

In the aerial distance sampling submodel (ADSM), mean lek sizes were 4.7, 6.7, 9.2, and 11.7 individuals in the Shinnery Oak Prairie Ecoregion (SOPR), SSPR, Mixed-Grass Prairie Ecoregion (MGPR), and SGPR, respectively (Figure C.3, middle). Lek sizes tended to be smaller in regions with more anthropogenic development and larger in shrublands. In the N-mixture submodel, mean lek sizes were 12.1, 3.1, 11.8, and 12.4 individuals in the SOPR, SSPR, MGPR, and SGPR, respectively (Figure C.3, bottom). Leks were smaller, on average, in shrublands and larger following breeding seasons with greater PDSI. The covariate associations for lek sizes in the count submodels were largely similar with the exception of the association for shrubland. On average, the ground sites had 3 times the percentage of shrubland as the aerial blocks, which could explain differences in the observed association across submodels.

Clutch sizes, hatchability, and daily nesting survival rates were all positive associated with PDSI (Figure C.4). On average, after-second-year females were more productive than second-year females, although all credible intervals included 0. Mean clutch sizes were 8.3, 8.5, 10.1, and 9.9 in the SOPR, SSPR, MGPR, and SGPR, respectively. Mean hatchability was 0.71, 0.79, 0.80, and 0.73 and daily nesting survival rates were 0.963, 0.964, 0.964, and 0.965. Daily brood survival rates were 0.954 for the first 14 days post hatch and 0.997 thereafter.

Mean monthly survival rates for females in the non-breeding season were 0.946, 0.942, 0.943, and 0.939 in the SOPR, SSPR, MGPR, and SGPR, respectively. On average, females had 5% lower monthly survival during the breeding season. Male survival did not decrease during the breeding season.

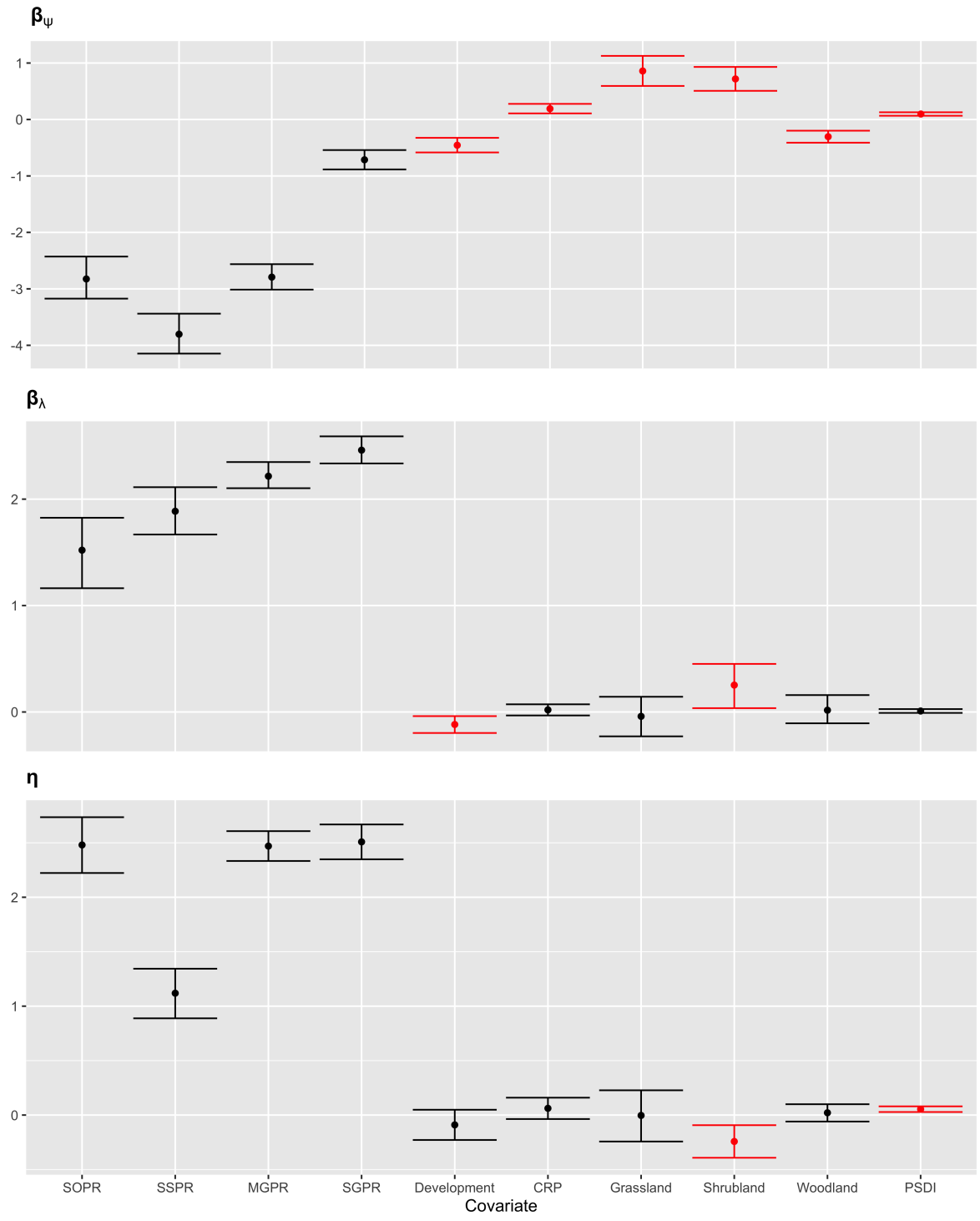

Figure C.3: Posterior means and 95% credible intervals for ecoregion intercepts and covariate associations in lesser prairie-chicken aerial distance sampling and N-mixture submodels. Red indicates the credible interval for the covariate association excludes 0. Parameters describing heterogeneity in lesser prairie-chicken lek sizes and the number of lesser prairie-chicken groups in the aerial distance sampling submodel are given by $\boldsymbol{\beta}_\lambda$ and $\boldsymbol{\beta}_\psi$. Heterogeneity in lesser prairie-chicken lek sizes in the N-mixture submodel is described by $\boldsymbol{\eta}$.

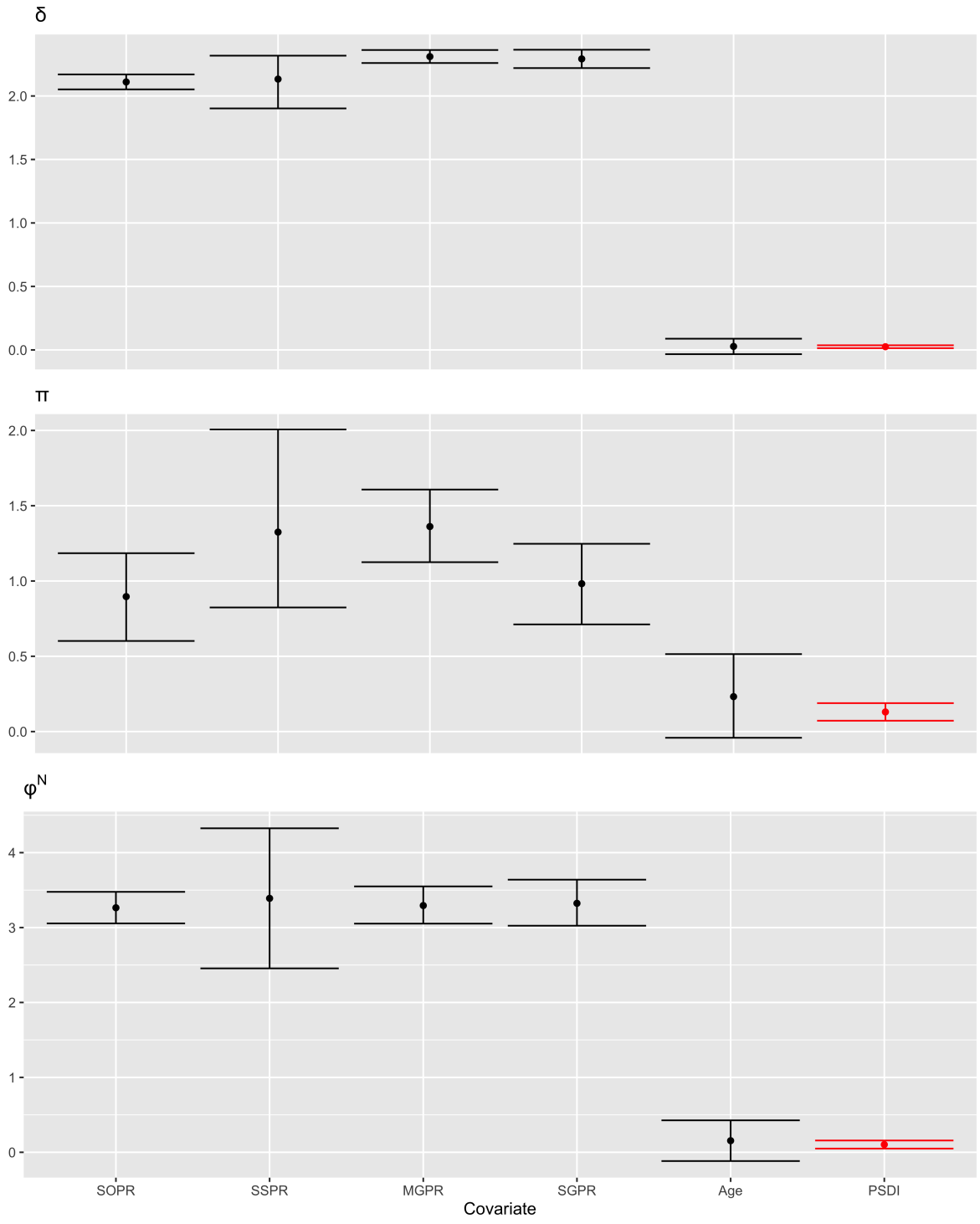

Figure C.4: Posterior means and 95% credible intervals for ecoregion intercepts and covariate associations in lesser prairie-chicken productivity submodels. Red indicates the credible interval for the covariate association excluded 0. Parameters describing heterogeneity in clutch sizes, hatchability, and daily nesting survival rates given by δ, π, and ϕ^N, respectively.

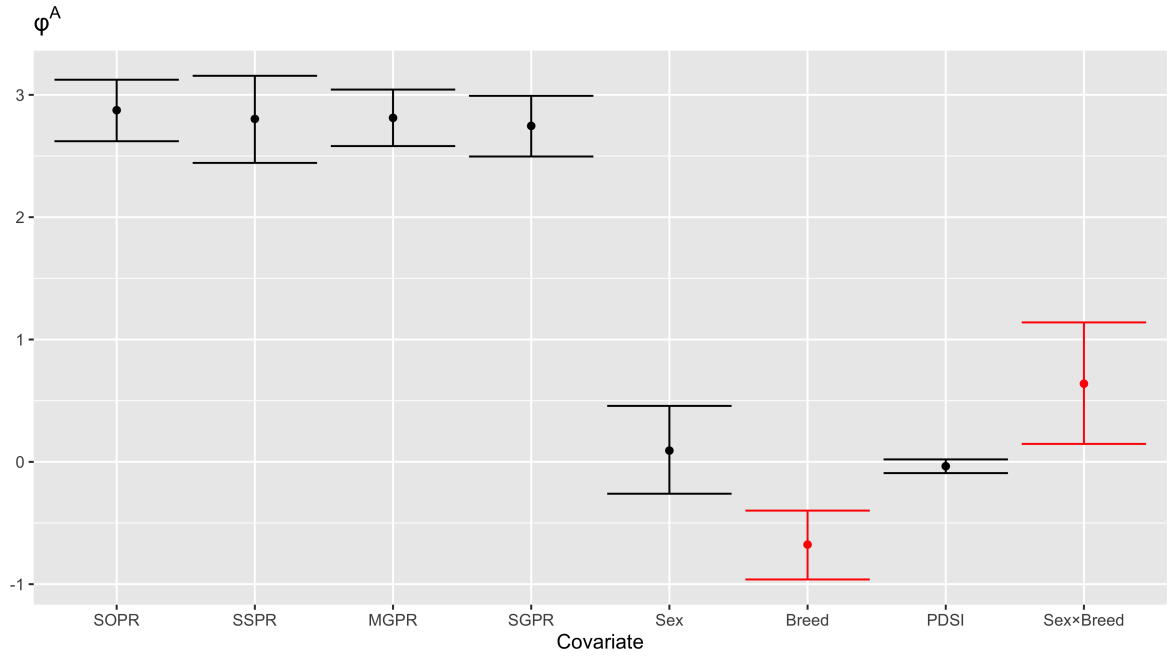

Figure C.5: Posterior means and 95% credible intervals for ecoregion intercepts and covariate associations in lesser prairie-chicken survival submodel. Red indicates the credible interval for the covariate association excluded 0. The parameter describing heterogeneity in monthly adult survival is ϕ^A. Sex$\in \{0, 1\}$ indicates if the individual is male. Breed$\in \{0, 1\}$ indicates if the month is in the breeding season defined as March-June [6].